SIMPLIFIED CHARACTERISATION OF

STRUCTURE-BORNE SOUND SOURCES WITH

MULTI-POINT CONNECTIONS

Thesis submitted in accordance with the requirements of the University of Liverpool

for the degree of Doctor in Philosophy

by

SU JIAN XIN

September 2003

ABSTRACT

A complete characterisation for structure borne sound source contains many elements (or parameters) and is not convenient for practical use. Thus, in this thesis the problem of providing a simplified characterisation for structure-borne sound source has been addressed. The starting point is that the purpose of the characterisation is to predict the vibrational power transmitted from the source into its support (the receiver) when installed. A 'single figure' characterisation has been proposed. i.e. the many elements needed for a full characterisation are contracted into two frequency dependent parameters, one representing the 'active' properties of the source (called 's_1') and the other representing its dynamic properties (called 's_2'.). The average point mobility magnitude was chosen as dynamic property parameter, while three alternative forms for the active property parameter have been investigated. The power cannot be predicted exactly from these simplified characterisations, so whether the chosen pair 's_1'and 's_2' is good or not good, depends on the range of uncertainty in the predicted power.

A major part of the work is concerned with calculating % confidence limits for the three chosen parameters. Real structures cannot provide sufficient data to construct these bands, so one of the main novelties is to introduce the idea of 'generic' structures. Here different types of structural behaviour (for example rigid mass, strongly resonant behaviour etc.) are characterised by certain 'rules'. The elements of the source characterisation are then varied randomly, but in accordance with these rules so as to produce data representing a large number of abstract, but plausible sources. When combined with similar 'generic' receiver structures the statistical

variance in the predicted power is found. These probability bands will provide insight into the global behaviour of the source after knowing the two parameters (s_1 and s_2).

Using the probability bands the active power emission from practical machines into various plate receiver structures was then calculated. The results show that the 'single figure' characterisations give better accuracy than some other methods which use more data. For low mobility receivers, the active parameter based on blocked force gives the best results, and can even be used on its own as a 'source strength' parameter to rank sources. This has practical application for example for machines installed on concrete floors. For matched cases (sources and receiver mobility of comparable magnitude), the active parameters based on the Characteristic Power of the source are most successful.

It was also found that, except for the case of rigid mass sources on stiffness receivers, the Characteristic Power of the source provides practical upper bound to the emission. This has potential application in many practical cases.

To my family and,

in memory of my father and mother

ACKNOWLEDGEMENTS

CONTENTS

ABSTRACT

ACKNOWLEDGEMENTS

CHAPTER 1

INTRODUCTION

Introduction

All machines generate vibration when run to achieve a specified task. The types of machines considered here are generally a combination of components which can perform the specified function, e.g. a fan used in building services includes the fan impeller, motor, fan belt, and frame etc., a washing machine includes motor, drum, and frame, and an engine on a ship could similarly be broken down into components. However, the components themselves are not usually of interest to the purchaser who buys the machine as a single unit. Rather it is the net effect of the machine that is important, and an increasingly important (usually unwanted) effect of machines is the noise they transmit to their surroundings. Vibrational energy from machines is transmitted into the media surrounding the machine, into the air, and into supporting structures, which are hence called 'receiver structures', e.g. the structure of a ship or a concrete floor supporting a fan. The vibrational energy subsequently propagates through the medium, from one medium into another (especially from solid structures into the air), and finally arrives in a human environment, e.g. a place of work or study, in the form of noise. Since it is almost always people who receive the noise, the main frequencies of interest are those defining the audible range for humans, i.e. 20Hz~20kHz.

The noise emitted can be classified broadly as airborne, structure–borne, or fluid-borne. The concepts of airborne and structure-borne sound sources will now be clarified. Referring to figure (1-a): we assume that A is a machine that connects with nothing except air. If the noise at point B is due only to machine A then we can call the noise at point B 'airborne' noise. Correspondingly, machine A is defined as an 'airborne sound source'.

Referring to fig(1-b): here machine A contacts with a solid structure C as well as the air. If the noise at point B is due to only machine A there is now not only airborne noise but also structure borne noise at point B. Machine A is not only an airborne sound source, but also a 'structure-borne' sound source.

The definitions 'airborne' and 'structure-borne' therefore correspond to the medium into which vibration energy is transmitted from the machine at the point of origin. This thesis is concerned with structure-borne sound.

Having defined noise at an arbitrary receiver point as airborne or structure-borne noise, the concept of 'source' must also be clarified. In figure (1-2), A is a motor, and C is a connected solid medium. If A is determined as a 'source', then the noise at B is called the sum of airborne and structure-borne noise. However, if A and C are considered as a whole, and this larger structure is considered to be the 'source', then it is an airborne noise source only. Hence, whether the sound is considered to be airborne or structure-borne in origin depends on how the source is 'separated' from its surroundings.

The acoustic consultant or noise control Engineer often needs to address noise problems at the design stage and make a prediction of sound levels in noise sensitive spaces, so 'noise sources' are naturally of interest. When considering the noise source the questions arises of which parameters of the source influence the resulting noise levels, in other words what kind of parameters 'characterise' the machine as a source of sound.

In the case of air-borne sound, the influence of the source on the 'noise level' can be represented by one parameter, i. e the sound power. Hence, in the case of the air - borne noise, the sound power is a suitable physical parameter to characterise the noise source. However, since the paper 'Urgent need for structure-borne sound source data' [1] was published twenty five years ago, the problem of characterisation for structure –borne sound sources still remains. There are several national and international working groups (e.g. In 1980 the International Organisation for Standardisation (ISO) established the working group (ISO TC 43 SC 1/WG 22) concerned with the formation for standards for characterisation of structure–borne sound sources. Various approaches have been tried as now described.

Free velocity has been developed to an ISO standard [2]. Velocity is measured at the contact points of the yet to be installed machine while it is resiliently suspended and while it is operating normally. It is clear that two sources with the same free velocity at any contact point could give very different noise levels when installed, because the noise level is not only dependent on the 'active' properties (free velocity) but also on the dynamic properties (e.g. mobility) of the source. Even when two sources look the same or similar they may have very different dynamic properties as shown for example by Bernhard [3,4]. Another problem is that too much data is required for practical use when the source has many contact points.

The blocked force theoretically offers similar advantages in terms of simplicity, but has the same problems as above, i.e. two sources with the same blocked force could potentially give very different noise levels when installed. Both the free velocity and

blocked force methods could be described as 'activity' methods, in that the parameter measured describes just the vibrational 'activity' of the source but not the dynamic properties. (In this context 'dynamic' properties are those of the inactive source, for example mechanical mobility, as distinct from 'active' properties which relate to the source in operation). An equivalent force was proposed [5-7], and can be understood as another activity method, but there are still the same problems as above.

The reception plate method [8] is to attach the vibrational source under test, through the proposed contacts and supports, to a passive structure such as a thin plate, the average response of which is then measured. However, even if the average response of the plate can be accepted as directly related to the radiated noise level, the average response itself is dependent strongly on the dynamic properties of both source and receiver, which could vary considerably in the general case [9].

Ohlrich proposed an equivalent power [10], i.e. surface source power. Based on his investigation this power value is insensitive to the receiver structure. However, this finding by itself does not prove that the surface source power is a good characterisation of the structure–borne sound source, for example the consumption of electric power of a source is insensitive to the installed environment, but is at best only weakly related to structure-borne sound.

In theory, the source mobility matrix and free velocity vector (or blocked force) at the contact points can be given as a complete characterisation. We can describe approaches based on this data set under the general heading of 'mobility methods'. Mobility methods can be seen as an extension of the free velocity (or blocked force)

methods in that the free velocity (or blocked force) vector is supplemented by a dynamic description of the source through (usually) the mobility matrix. When these parameters are determined, the properties of the structure-borne sound source are determined. For example when a source is installed on the floor, the force at the connection points applied to the floor can be determined after knowing the floor mobility matrix, and finally, the sound pressure magnitude $|p|$ can be determined [11].

However, there is a practical problem in that the source mobility matrix and free velocity (or blocked force) vector for characterising structure-borne sound sources contain too many elements (each of which represents a physical parameter that must be determined). It is not convenient for practical use. Therefore, there is a need for a simplified characterisation of structure–borne sound sources. According to the above logical steps (source characterisation → interface force → sound pressure) it looks difficult to simplify the characterisation, because the 'interface parameter' is a complex force vector. However, there is one phenomenon that helps us to simplify: this is that the vibrational power transmitted from the machine into the supporting structure is a good indication of the seriousness of the structure–borne sound problem. Mathematically we can say that the structure-borne sound pressure magnitude can be expressed as:

$$|p| = f(R, P) \tag{1-1}$$

where P is the active power from the source into the supporting structure, while R is a set of parameters which depend on the surroundings of the installed source, and f is a monotonically increasing function with P.

Even though equation (1-1) is not always strictly correct, it is still accepted in most studies [12-15]. Therefore, in this thesis, the problem of simplified characterisation of structure–borne sound sources is based on the principle that the active power emission is considered the 'target quantity'. Consequently, a source characterisation is defined as a set of data that allows the emission to be predicted when combined with appropriate data to describe the receiver.

The mobility methods described above fulfil the requirement for a source characterisation and so will be the basic approach adopted. However, the search is not over, because the active power is still a function of the mobility matrix and free velocity vector, and the problem of how to contract so many elements still remains.

If the active power from the source into the receiver is insensitive to the receiver (as is usually the case for airborne sound sources), then the many elements can be contracted into one parameter for characterisation of the source. i.e. the active power emission from the source into a reference receiver (in the airborne case the 'reference receiver' is air at standard temperature and pressure, and the power is the sound power). However, unfortunately, it is generally found that for structure-borne sound sources the active power into the receiver is strongly dependent on both source and receiver.

Therefore, there is a theoretical problem in using one physical parameter to characterise the source. As discussed in chapter 2 even for idealised cases with one contact point and one dimension, we can still not characterise a structure-borne sound source by a single physical parameter. For example the free velocity strongly

influences the active power emission, but it cannot be the only parameter to characterise the source, since two sources with the same free velocity could give completely different power emission when installed, if they have different dynamic properties at the contact point. If we construct a new physical parameter by using free velocity and mobility, for example using the parameter $S = f(\hat{V}_{sf}, Y_s) = \left| \hat{V}_{sf} \right|^2 / \left| Y_s \right|$, again two sources with the same S will in general give different active power emission when installed, because their dynamic properties differ. So, if free velocity is not adequate as a single parameter to characterise a source then by the same logic neither is 'S'. It seems that it is necessary to keep the dynamic property parameters. For the case of single point and one dimension, it may be practical to keep all active and dynamic property parameters. However, for multiple-point cases (practical cases) the active and dynamic property parameters are too numerous for practical use. The work to contract or reduce these elements (characterisation data) is therefore important for practical cases.

It is obvious that reducing the characterisation data implies a 'cost' in terms of uncertainty in the predicted emission. One might think that the greater the reduction in the characterisation data the greater the 'cost' in accuracy. However, this is not necessarily the case: some 'small' data sets may be less 'costly' than other larger sets. Hence, it has practical meaning to find a set of characterisation parameters containing less data, while the 'cost' in terms of uncertainty is kept to a minimum. This thesis is therefore concerned with simplified characterisation of structure–borne sound sources with multiple contact points. The objective is to investigate the cost (in terms of uncertainty) of simplified source characterisations, in particular those consisting of a single 'active' and a single 'passive' parameter.

Chapter 2 reviews some basic concepts and gives a broad definition of source characterisation and source strength. Based on the definition, three alternative possible forms of source characterisation data are proposed. In Chapter 3, the case of multiple point contact is considered. The 'single figure' method for characterising the source is proposed, i.e. the many elements needed to fully characterise a source are collapsed into two parameters, one 'active' property (containing 'strength' information about the source) and one 'dynamic' property. This simplification inevitably implies a range of uncertainty in the predicted power, and the following chapters are dedicated to investigating this range. In Chapter 4, the concept of 'generic' structures is proposed as a tool to investigate the range of uncertainty. Here, the properties of the mobility matrices and free velocity vectors for four types of source are derived together with the mobility matrices for four types of receiver. In Chapter 5, these 'generic' sources and receivers are combined and probability bands for the predicted power are evaluated. Three sets of results are produced, corresponding to the three alternative forms of source descriptor proposed. Chapter 6 studies the prediction of active power from typical practical machines into various receiver types in order to validate this approach. Overall conclusions are given in Chapter 7.
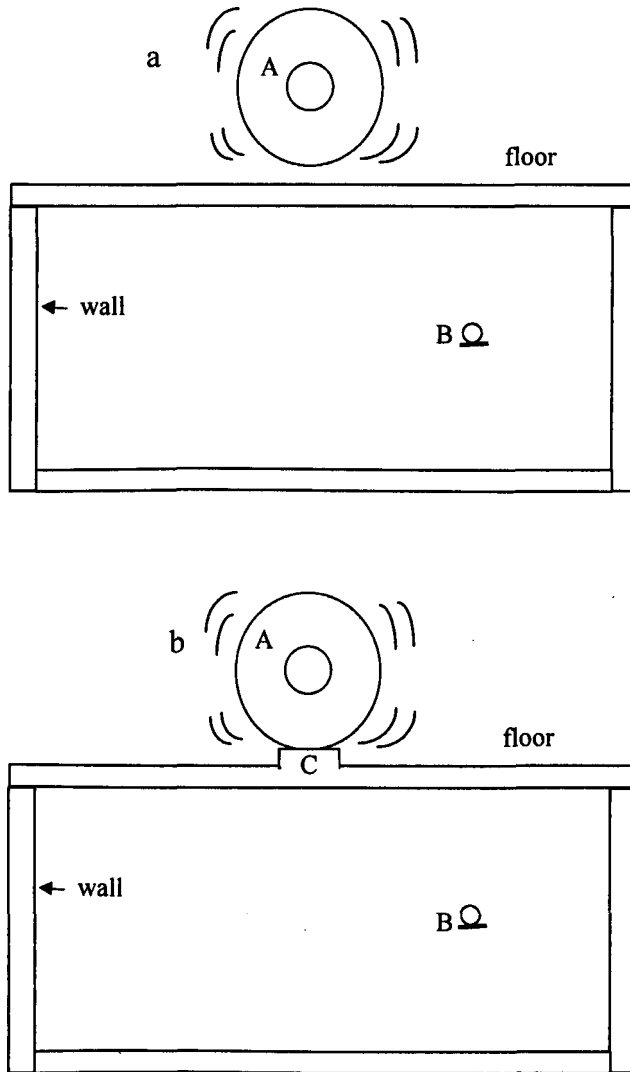
Figure 1-1 a: Air-borne noise source. b: Air-borne and structure-borne noise source.
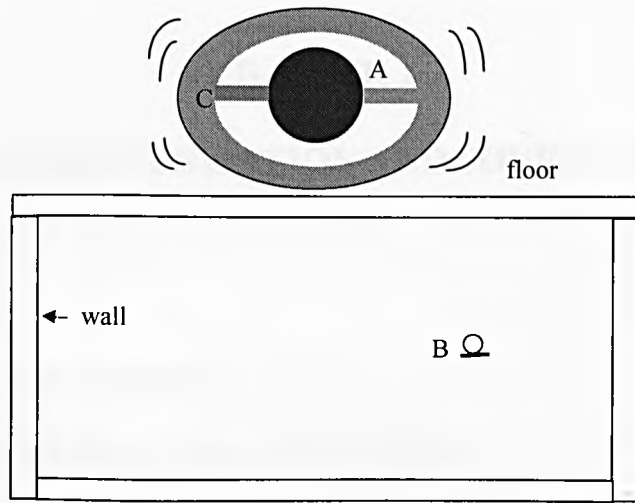
Figure1-2 The noise at B is called air-borne noise, if A and C are considered as a whole source. It is a sum of air-borne and structure-borne noises when motor A is only the noise source.

CHAPTER 2

SOURCE CHARACTERISATION AND SOURCE STRENGTH

2.1 Introduction

2.2 The vibration power emission

2.3 Single point unidirectional source-receiver system

2.4 Remarks and discussion

2.5 Conclusion

2.1 Introduction

The first objective of this chapter is to review some basic concepts. Secondly, since there is some confusion generally about characterising structure-borne sources, the concepts of 'source strength' and 'source characterisation' are presented and compared.

The starting point for this chapter is that the vibration power emission from a source into a receiver is the quantity that best describes structure-borne excitation. This premise has been justified in Chapter 1, and has formed the basis for enough studies that it does not need further justification here.

2.2 The vibration power emission

The instantaneous vibrational power at a point and the ith direction is defined as the product of the instantaneous force and velocity vectors at that point (and direction)

$$P_i = F(t)V(t) \qquad \text{(2-1a)}$$

The average over time can be written in the form of an integration over time:

$$P = \frac{1}{T} \int_0^T F(t)V(t)dt \qquad \text{(2-1b)}$$

If the force and velocity are assumed to have a harmonic time dependence

$$
\begin{aligned}
F(t) &= F_0 \cos(\omega t + \phi_F) = \text{Re}\left\{ F_0 e^{j\phi_F} e^{j\omega t} \right\} \\
V(t) &= V_0 \cos(\omega t + \phi_V) = \text{Re}\left\{ V_0 e^{j\phi_v} e^{j\omega t} \right\}
\end{aligned}
\qquad \text{(2-2)}
$$

then the average power over a period can be written in two basic forms using either the cosine of the relative phase or the real part of the product:

$$P = \frac{1}{2} F_0 V_0 \cos(\phi_F - \phi_v) = \frac{1}{2} \text{Re}(\overline{F}.\overline{V}^*) = \text{Re}(\hat{F}.\hat{V}^*) \qquad \text{(2-3)}$$

where $\overline{F} \equiv F_0 e^{j\phi_F} = \sqrt{2}\hat{F}$ and $\overline{V} \equiv V_0 e^{j\phi_v} = \sqrt{2}\hat{V}$ are complex force and velocity, and

* denotes complex conjugate. The magnitude of $\hat{F}$ is the rms value of force $F(t)$,

and the magnitude of $\hat{V}$ the rms value of velocity $V(t)$. The product of the complex

force ($\hat{F}$) and complex conjugate of the velocity($\hat{V}^*$) is called the complex power

emission. The real part of the complex power is the average active power over a

period. Physically the real part represents power which propagates away from a point

whilst the reactive power represents power which oscillates at the point with no time

averaged net flow.

2.2.1 Single point drive

If the passive structure is driven only at one point and in one direction then the

velocity can be expressed as:

$$\overline{V} = \overline{F}Y = \overline{F}/Z$$

where Y is the mobility and Z the impedance of the structure, which are dynamic

properties of the structure and independent of the driving force. After introducing the

mobility or impedance, equation (2-3) can be rewritten as (2-4)

$$P = \frac{1}{2}|\overline{F}|^2 \operatorname{Re}(Y) \quad (2\text{-}4a)$$

or

$$P = \frac{1}{2}|\overline{V}|^2 \operatorname{Re}(Z) \quad (2\text{-}4b)$$

Since mobility and impedance are structural descriptors these equations highlight that

the vibrational power is dependent on both the exciting structure as well as the

'activity' of the source.

2.2.2 Multiple point drive

Consider a passive structure driven at N points and in J directions. The velocity can be expressed as:

$$\bar{V}_i^n = \sum_n \sum_j Y_{ij}^{nm} \bar{F}_j^m \qquad (2\text{-}5)$$

where $[Y_{ij}^{nm}]$ is defined as follows

$$Y_{ij}^{nm} = \left. \frac{\bar{V}_i^n}{\bar{F}_j^m} \right|_{\bar{F}_s^l = 0} \quad s \neq j \; l \neq n \qquad (2\text{-}6)$$

If the two vectors coincide in both point and direction the above is termed a point mobility, whilst if the two vectors coincide in point only the mobility is termed a cross mobility. If the vectors are of different points but of the same direction it is called a transfer mobility and if both point and direction are different the mobility is termed a cross-transfer mobility

In general a mobility is complex and frequency dependent and is a function of the structure's material properties as well as its geometry and boundary conditions. Analytical expressions for mobilities exist only for simple structures such as plates, beams and cylinders with classically described boundary conditions ie. free, simply-supported, clamped, guided [16-17]. For more complicated structures mobility must be obtained either experimentally [18] or using 'numerical methods'[19].

The total power into the structure can be given by (2-7)

$$P = \frac{1}{2} \text{Re}[\bar{F}]^{*T}[Y_{ij}^{nm}]^{*T}[\bar{F}] \qquad (2\text{-}7)$$

where $[\bar{F}]$ is a column vector with N×J element, $[Y_{ij}^{nm}]$ is a matrix with N×J rows and N×J columns. T is the transverse.

Analogous to mobility functions are impedance functions. In general they are defined as the ratio of a resulting force to an applied velocity.

$$Z_{ij}^{nm} = \frac{\overline{F}_i^n}{\overline{V}_j^m}\bigg|_{\overline{V}_s^l=0} \quad s \neq j \; l \neq n \quad (2\text{-}8)$$

It should be noted that the dynamic condition prescribed for a mobility measurement is that the other points are free (see equation 2-6) whilst for an impedance it is that the other points are blocked (see equation 2-8). So Z_{ij}^{nm} is not the inverse of Y_{ij}^{nm} but the mobility matrix is the inverse of the impedance matrix i.e. $[Y_{ij}^{nm}]^{-1} = [Z_{ij}^{nm}]$. Therefore, the total power can be rewritten as the following:

$$P = \frac{1}{2}\mathrm{Re}[\overline{V}]^{*T}[Z_{ij}^{nm}]^{*T}[\overline{V}] \quad (2\text{-}9)$$

For experimental studies the mobility functions are therefore more convenient. Hence, to facilitate the use of experimental data the concept of mobility rather than impedance is used.

2.3 Single point unidirectional source-receiver system

When a machine source is put onto the supporting receiver, vibrational power flows through the contact points into the receiver structure. The power can be estimated by using Equation (2-3) or (2-4), but the force and the velocity are dependent on both source and receiver structures. For prediction of the power, enough information about the source and receiver is therefore needed. Machines generate vibration when in operation due to internal unbalance and other mechanisms which are complicated and generally unknown. Even if they were known, knowledge of the structure of the machine is still required. So in most practical cases, the whole source is considered as a 'black box' (this is widely accepted, see for example[8]), the inside details of which

are not of interest, while the activity and dynamics of the feet (proposed contact point(s)) only are considered.

The measure proposed for the source activity is the free velocity. It is defined as the velocity measured at the point of interest whilst the source is run under normal operating conditions but suspended in free space. In some practical cases a good and convenient approximation to free space can be used [20-21].

2.3.1 Vibrational power into the receiver

It is known that the power at the source–receiver interface is obtained from the velocity and force at that point. From the point of view of the source, the velocity at the interface of the source and receiver, $v_{s,}$, can be written as the sum of the free velocity due to internal vibration of the source v_{fs} and the velocity due to the force from receiver applied to the source F_s

$$V_s = \overline{V}_{sf} + Y_s \overline{F}_s \qquad (2\text{-}10)$$

and from the point of view of the receiver

$$V_r = Y_r \overline{F}_r \qquad (2\text{-}11)$$

where Y_s is the point mobility of the source at the contact point, Y_r is the point mobility of the receiver, and $\overline{F}_r$ is the force from the source applied to the receiver. From continuity, $\overline{V}_r = \overline{V}_s$, and according to Newton's principle $\overline{F}_s = -\overline{F}_r$.

From equation (2-10) and (2-11), expressions for the force applied to the receiver

$$\overline{F}_r = \frac{\overline{V}_{sf}}{Y_r + Y_s} \qquad (2\text{-}12)$$

and for the velocity,

$$\bar{V}_r = \frac{\bar{V}_{sf}}{Y_r + Y_s} Y_r \qquad (2\text{-}13)$$

are obtained.

The complex power at the interface is obtained by substituting into Equation 2-3:

$$Q = \frac{1}{2} \frac{Y_r}{|Y_r + Y_s|^2} |\bar{V}_{sf}|^2 = |\hat{V}_{sf}|^2 \frac{Y_r}{|Y_r + Y_s|^2} \qquad (2\text{-}14a)$$

The active power emission is the real part of the above:

$$P = \mathrm{Re}(Q) = |\hat{V}_{sf}|^2 \frac{\mathrm{Re}(Y_r)}{|Y_r + Y_s|^2} \qquad (2\text{-}14b)$$

Therefore the power transmission can be predicted from the velocity of the free source and the mobilities of the source and receiver.

From equation (2.14) the maximum power is imparted when the source and receiver mobilities have equal magnitude and are out of phase ie.;

$$Y_s = -Y_r \qquad (2\text{-}15)$$

In this case the power will be theoretically infinite, but in practice the real part of the mobility is always positive so expression (2-15) is not satisfied. For a given source the maximum active power transmission from source to receiver can be imparted when the receiver mobility is just the complex conjugate of the source mobility ie.;

$$Y_r = Y_s^{*T}$$

This can be proved as follows.

Let $Y_r = x_r + jy_r$, $Y_s = x_s + jy_s$ where x_r, y_r are the real and imaginary parts of the receiver mobility, and x_s, y_s are real and imaginary parts of the source mobility. Equation (2-14b) can be rewritten as

$$\mathrm{Re}(Q) = \frac{1}{2} \frac{x_r}{(x_s + x_r)^2 + (y_s + y_r)^2} |\bar{V}_{sf}|^2 \qquad (2\text{-}15)$$

$$\frac{\partial \text{Re}(Q)}{\partial x_r} = \frac{1}{2}\left|\overline{V}_{sf}\right|^2 \frac{(x_s + x_r)^2 + (y_s + y_r)^2 - 2(x_r + x_s)x_r}{((x_s + x_r)^2 + (y_s + y_r)^2)^2} \qquad (2\text{-}16a)$$

$$\frac{\partial \text{Re}(Q)}{\partial y_r} = \frac{1}{2}\left|\overline{V}_{sf}\right|^2 \frac{x_r(y_s + y_r)^2}{((x_s + x_r)^2 + (y_s + y_r)^2)^2} \qquad (2\text{-}16b)$$

when $x_r = x_s$ and $y_r = -y_s$ the right hand side of equation (2-16) equals zero, so the active power transmission has reached a turning point, and from equation 2-14 this clearly corresponds to a maximum value.

2.3.2 Source characterisation and source strength

To be clear, first we will give a broad definition for source characterisation and source strength (here not limited to structure-borne sound source). If the physical parameter L is considered (L is called a 'target quantity'), and it can be expressed as the following function.

$$L = f(R, S) = f(r_1, r_2, \ldots r_m, s_1, s_2, s_3, \ldots s_n) \qquad (2\text{-}17)$$

where $r_1, r_2, \ldots r_m$ are physical parameters dependent on the surroundings of the installed source, $s_1, s_2, \ldots s_n$ are physical parameters independent of the surroundings of the installed source that can be determined before the receiver is known. We can call the physical parameters $s_1, s_2, \ldots s_n$ a 'full source characterisation' in relation to the target quantity L. For example, to calculate the cost of running an electrical appliance the electrical energy used per day is of interest. It can be expressed as:

$$L = tW \qquad (2\text{-}18)$$

where L is the electric energy, W is the electric power of the source, and t is the time for which it is used. The physical parameter W is called a full source characterisation with reference to the electric energy used. In this example the target parameter and source characterisation are different kinds of physical parameter: they have different

units, even though the electric power of the source is related to the electric energy consumption.

If equation (2-17) can be written in the following form;

$$L = f(r_1, r_2, ... r_m, S_c) \qquad (2\text{-}19)$$

where S_c is a physical property of the source, and if the function is monotonically increasing with S_c, then the physical parameter S_c is a quantity describing the 'strength' of the source.

In airborne sound a parameter of frequent interest is the power radiated from the surface of a source into the air. The power radiated can be written as;

$$P_s = f(r_1, r_2, ... r_m, s_1, s_2, ... s_i, ... s_n) \qquad (2\text{-}20)$$

where $r_1, r_2, ... r_m$ are physical parameters dependent on the environment surrounding the installed source, such as the density of air, the temperature of air and so on. In practice, the sound power radiated is insensitive to $r_1, r_2, ... r_m$, or in another words, the physical parameters $r_1, r_2, ... r_m$ can be considered as constant. Therefore, in practical cases, expression (2-20) can be rewritten as;

$$P_s \approx f(a, b, c ... s_1, s_2, ... s_i, ... s_n) \qquad (2\text{-}21a)$$

The right side of expression (2-21) is a function of the source. The value of the function is denoted W_c, which can be measured without reference to any particular installation (this kind of data is called 'available data'). So W_c can be considered as a strength characteristic. In this case equation (2-21a) can be rewritten as:

$$P_s \approx W_c \qquad (2\text{-}21b)$$

Equation (2-21b) is a special case of equation (2-19). Now, if we consider as a target quantity the noise level at some position inside a room rather than the sound power inside the room, this problem will be more complex. However, it can be still written in the following form:

$$L_P = f(r_1, r_2 .. r_m, P_s) \approx f(r_1, r_2 .. r_m, W_c) \qquad (2\text{-}22)$$

where $r_1, r_2, ... r_m$ are parameters which are strongly dependent on the surroundings of the installed source. So, the sound pressure at the position of interest is not only dependent on the source but also strongly dependent on 'receiver' parameters, such as the thickness of walls, the position of source, the distance between the source and 'receiver', and absorption factor of the walls, and so on. Nevertheless W_c is still a 'source strength' parameter with respect to the noise level at any position. It is also a quantity suitable for comparison of sources from an acoustic point of view, the best one having the lowest W_c, since by comparing sources it is assumed that they will work in the same surroundings. From the above example, it is shown that a quantity for describing a source by means of a 'source strength' can have different units to the target quantity. Whether a physical property of the source can be considered as the source strength is not a question of whether it has the same units as the target quantity, rather it depends on whether the relationship between the target quantity and the physical parameter of the source satisfies expression (2-19).

Now we return to the case of structure-borne sound. Here, the active power transmission from source to receiver is taken as the target quantity. Equation (2-14) illustrates that the target quantity is not dependent only on the source but is sensitive to the receiver. It cannot therefore be written in the form of equation (2-21) in general. This sensitivity to the receiver is an inevitable consequence of accepting the active

power as the target quantity. It is completely futile to try to seek a physical parameter which is independent of the receiver in order to reduce this 'sensitivity'. For example, consider a machine source 'A' on two different receivers where the active power from source 'A' into receiver 'R1' is P_{AR1}, while the active power from source 'A' into receiver 'R2' is P_{AR2}. Let the power P_{AR1} be 'x' times the power P_{AR2}. This factor 'x' is not changed no matter how we chose the physical parameters (independent of the receiver) characterising the source.

Mondot [22] rearranges the expression (2-14) into the following form;

$$P = \text{Re}(Q) = \text{Re}(S.C_f) \qquad (2\text{-}23)$$

where S depends only on source data, and has the following form:

$$S = \frac{\left|\hat{V}_{sf}\right|^2}{Y_s^*}. \qquad (2\text{-}24)$$

C_f describes the dynamic properties of the contact point between the source and receiver and is a function of the source and receiver mobility at the interface,

$$C_f = \frac{Y_s^* Y_r}{\left|Y_s + Y_r\right|^2} \qquad (2\text{-}25)$$

or in another form:

$$C_f = \frac{\alpha}{\left|1+\alpha\right|^2} \qquad (2\text{-}26)$$

where

$$\alpha = \frac{Y_r}{Y_s} \equiv |\alpha| e^{j\Delta\phi}. \qquad (2\text{-}27)$$

S is called the 'source descriptor' and C_f the 'coupling function'.

Mondot has conducted several simple experiments based on (equation2-23) and various other authors have discussed this formulation.

In the author's opinion, from the point of view of estimating the power transmission, the introduction of the source descriptor and the coupling function cannot give any new content. Firstly, in order to estimate the transmission three sets of data are needed, (the variable α cannot be provided as an independent variable):

I)   source descriptor S

II)   source mobility at the proposed point Y_s

III)   receiver mobility at the proposed point Y_r.

Secondly, the source descriptor S is obtained based on the free velocity and source mobility, so the results of estimating the transmission by using equation (2-23) are exactly the same as with equation (2-14b), but using equation (2-23) is more complicated than using equation (2-14) (one more multiplication and one more division). Therefore, calculation of the power transmission cannot be simplified by the concepts of source descriptor and coupling function. It does not give a good reason for the introduction of the concepts of source descriptor and coupling function no matter how good is the agreement between the measured and estimated transmission by using equation (2-23).

The results of estimating the transmission based on equation (2-23) cannot indicate that the source descriptor S in equation (2-23) is a better quantity to describe the source structure than the square of free velocity. If we define the first item on the right hand side of equation (2-14) as a 'source descriptor' and the second as a 'coupling function' then equation (2-14) can be written in the form of equation (2-23), i.e.

$$P = \mathrm{Re}(S.C_f) \qquad (2\text{-}28)$$

S still depends only on source data in equation (2-28), C_f still describes the dynamic

properties of the contact point between the source and receiver and is a function of the

source and receiver mobility at the interface. The result of estimating the transmission

using (2-28) is the same as with equation (2-23) without any assumption about the

interface.

The results of estimating the transmission based on equation (2-23) cannot indicate

that the source descriptor S in equation (2-23) can be considered a 'source strength'

characteristic. In equation (2-23) the coupling function is not only a function of the

receiver mobility, but also concerns another physical parameter of the source.

Therefore, the power transmission cannot be written in the form of equation (2-19).

However, the source descriptor S has some value in that it has the same units (power)

as power emission, so it can give an idea of the relative importance of different

components of excitation, for example forces and moments. Also, it will be seen later

that in some cases the source descriptor S is more reliable than the free velocity or

other parameters as a source strength parameter.

It is of interest to establish which of the 'source descriptors' in equation (2-23) or

equation (2-28) (square of free velocity), or another parameter is better as a source

strength characteristic.

In a similar manner to above it is possible to define various combinations of source

descriptor, S and coupling function in which S depends only on source data and the

coupling function is a function of the source and receiver mobility at the interface. Some alternative forms will now be considered.

The power transmission can be rewritten in different forms:

$$P = \text{Re}(Q) = \text{Re} \frac{Y_R}{|Y_R + Y_s|^2} |\hat{V}_{fs}|^2 = \frac{\text{Re}(Y_R)}{|Y_R|^2} \frac{|\alpha|^2}{|1+\alpha|^2} |\hat{V}_{fs}|^2 \qquad (2\text{-}29)$$

$$P = \text{Re}(Q) = \text{Re} \frac{Y_R |Y_s|^2}{|Y_R + Y_s|^2} \frac{|\hat{V}_{fs}|^2}{|Y_s|^2} = \text{Re}(Y_R) \frac{1}{|1+\alpha|^2} |\hat{F}_{sb}|^2 \qquad (2\text{-}30)$$

$$P = \text{Re}(Q) = \text{Re}\left(\frac{Y_R Y_s{}^*}{|Y_R + Y_s|^2} \frac{|\hat{V}_{fs}|^2}{Y_s{}^*}\right) = \frac{\text{Re}(Y_R)}{|Y_R|} \frac{|\alpha|}{|1+\alpha|^2} \left|\frac{|\hat{V}_{fs}|^2}{Y_s{}^*}\right| \qquad (2\text{-}31)$$

where the blocked force, $\hat{F}_{sb} = \hat{V}_{fs}/Y_s$, has been introduced.

Equation (2-29), (2-30), and (2-31) can all be written in the following form:

$$P = \text{Re}(S_g . C_{gf}) \qquad (2\text{-}32)$$

where Sg can be called a 'general source descriptor' and C_{gf} a 'general coupling function':

$$S_g = |\hat{V}_{sf}|^2, C_{gf} = Y_R /|Y_R + Y_s|^2 \qquad \text{for expression (2-29)}$$

$$S_{gf} = |\hat{F}_{sb}|^2, C_f = Y_R |Y_s|^2 /|Y_R + Y_S|^2 \qquad \text{for expression (2-30)}$$

$$S_{gf} = |\hat{V}_{sf}|^2 / Y_S^*, C_{gf} = Y_R Y_S^* /|Y_R + Y_S|^2 \qquad \text{for expression (2-31)}$$

Alternatively, we can write:

$$P = R.l|S_g| \qquad (2\text{-}32)$$

$$R = \frac{\mathrm{Re}(Y_R)}{\left|Y_R\right|^2}, \quad l = \frac{\left|\alpha\right|^2}{\left|1+\alpha\right|^2}, \quad \left|S_g\right| = \left|\hat{V}_{fs}\right|^2 \qquad \text{For expression (2-29)}$$

$$R = \mathrm{Re}(Y_R), \quad l = \frac{1}{\left|1+\alpha\right|^2}, \quad \left|S_g\right| = \left|f_0\right|^2 \qquad \text{For expression (2-30)}$$

$$R = \frac{\mathrm{Re}(Y_R)}{\left|Y_R\right|}, \quad l = \frac{\left|\alpha\right|}{\left|1+\alpha\right|^2}, \quad \left|S_g\right| = \frac{\left|\hat{V}_{fs}\right|^2}{\left|Y_s^*\right|} \qquad \text{For expression (2-31)}$$

Expression (2-32) means the power transmission from source into the receiver can be expressed as the product of three terms. The first is dependent only on the receiver structure, and indicates the ability of the receiver structure to 'absorb' power. The third indicates the 'ability' of the source to deliver power, while the second item is here called a 'link function' and depends on both source and receiver. A general form, which includes the above definitions of S_g C_{gf} is as follows:

$$S_g = \frac{\left|\hat{V}_{fs}\right|^2}{\left|Y_s\right|^{2-x}}, \quad C_{gf} = \frac{Y_R}{\left|Y_R\right|^x} \frac{\left|\alpha\right|^x}{\left|1+\alpha\right|^2}, \quad R = \frac{\mathrm{Re}(Y_R)}{\left|Y_R\right|^x}, \quad l = \frac{\left|\alpha\right|^x}{\left|1+\alpha\right|^2}, \qquad (2-34)$$

where x can be any number.

If the link function l is not sensitive to the variable α, in another words if the curve $l(\alpha)$ is flat and approximately equal to a constant γ, then the emitted power can be rewritten as:

$$P = R\gamma S \quad (2-35)$$

in which case S can be considered a source 'strength' characteristic since equation (2-35) has the same form as equation (2-19).

If the ratio of the receiver to source mobility is small, then the link function can be approximated:

$$l_1 = \frac{|\alpha|^2}{|1+\alpha|^2} \approx |\alpha|^2 \quad \text{for expression (2-29)}$$

$$l_2 = \frac{1}{|1+\alpha|^2} \approx 1 \quad \text{for expression (2-30)}$$

$$l_3 = \frac{|\alpha|}{|1+\alpha|^2} \approx |\alpha| \quad \text{for expression (2-31)}$$

This shows that l_1 is highly sensitive to α, and l_3 is proportional to α. Only the link function l_2 is not sensitive to α. Therefore, only $S_g = \left|\hat{F}_{sb}\right|^2$ is a valid 'source strength' characteristic for this case.

Consider the example of two sources, A and A1, whose mobility is much greater than that of the receiver (this is very common in practice). If the magnitude of the blocked force for source A is greater than that of source A1, then the power transmission from source A into the receiver will be greater that of source A1, i.e. a rank ordering of sources based on blocked force will correspond correctly to the emitted power when installed. However, if another source descriptor is used, for example $|S_g|_A = \left\|\hat{V}_{fsA}\right\|^2 / Y_A^* > |S_g|_{A1} = \left\|\hat{V}_{fsA1}\right\|^2 / Y_{A1}^*$, it is possible that the power transmission from source A into the receiver will be less than that of source A1 and an incorrect rank ordering could be obtained. Therefore, in this case the source descriptor in equation (2-30) (square of blocked force) is a more proper representation of the ability of the source to deliver power than the source descriptor in equation (2-31).

Similarly, if α is much less than unity, the link functions are as follows:

$$l_1 = \frac{|\alpha|^2}{|1+\alpha|^2} \approx 1 \qquad \text{for expression (2-29)}$$

$$l_2 = \frac{1}{|1+\alpha|^2} \approx \frac{1}{|\alpha|^2} \qquad \text{for expression (2-30)}$$

$$l_3 = \frac{|\alpha|}{|1+\alpha|^2} \approx \frac{1}{\alpha} \qquad \text{for expression (2-31)}$$

l_2 and l_3 are sensitive to α, but l_1 is not. Therefore, only $S_g = \left|\hat{V}_{sf}\right|^2$ is a valid 'source strength' characteristic for high mobility receivers.

Shown in Figure 2-1 is the 'normalized active power', (defined as the ratio of active power to the magnitude of the general source descriptor), plotted against $|\alpha|$. Figure 2-1a corresponds to equation (2-29) where the 'source descriptor' is taken as the square of free velocity, figure 2-1b correspond to equation (2-30), where the 'source descriptor' is the square of the blocked force, and figure 2-1c corresponds to equation (2-31) where the source descriptor has units of power. It can be seen from figure2-1a that in the range of $|\alpha| > 10$ the coupling function curve is very flat, the eight lines for various relative phase angles of the source and receiver are virtually indistinguishable. This means that if the magnitude of the receiver mobility is over ten times that of the source mobility then two sources with the same free velocity will give the same power transmission from source to receiver irrespective of the source mobility. Over the same range, the normalized power in figure2-1c has a slope, such that if two sources have the same source descriptor $\left|\hat{V}_{sf}\right|^2 \Big/ \left|Y_s^*\right|$, the power transmission will be different, when they have different mobility. This confirms the previous conclusion that the square of the free velocity is a more proper 'source strength' parameter that $\left|\hat{V}_{sf}\right| / Y_s^*$.

The square of the blocked force is the worst of the three parameters for comparison of source 'strength' in this range ($|\alpha|>10$) because the coupling function in figure 2-1b has the steepest slope.

For the case $|\alpha|<0.1$ the opposite results are obtained, i.e. the square of the blocked force is the best and free velocity the worst parameter for comparison of sources. In the range of $0.1<|\alpha|<10$, the problem will be more complex, since none of the curves are flat.

Consider the points D and D1 on figures 2-1, which again represent two sources with different mobility. Their normalized active power is about 1dB different in figure 2-1a while in figure 2-1c the difference is about 5dB and in figure 2-1b it is about 10dB. So here, the square of free velocity is still the closest parameter to being a valid source strength characteristic. The points A and A1 represent another two sources with different mobility. Their normalized active power differs by 2dB, 7dB and 10dB in figures 2-1a-c respectively. So here, the square of the blocked force is the best parameter to use as a source strength. Points B and B1 represent two sources which are well matched to the receiver. In figure2-1c the differences in normalized active power are 5dB, 2dB and 6dB, indicating that the source descriptor $|\hat{V}_{sf}|/Y_s^{\bullet}$ is the best one in this region.

By comparing a group of sources the receiver is considered fixed so the shape of the link function curve is the same as that of the coupling function.

Any number of rearrangements of equation (2-14) can be made in theory, but not all of these are of practical use. For example, if we let x=4 in equation (2-34) then the corresponding general source descriptor will be written as :

$$S = \frac{\left|v_{fs}\right|^2}{\left|Y_s\right|^{2-4}} = \left|Y_s\right|^2 \left|\hat{V}_{sf}\right|^2 \quad (2\text{-}36)$$

and the coupling function will be

$$C_{gf} = \frac{Y_R}{\left|Y_R\right|^4} \frac{\left|\alpha\right|^x}{\left|1+\alpha\right|^2}, \quad (2\text{-}37)$$

Again, here the source descriptor depends only on source data and the coupling function is a function of the source and receiver mobility at the interface. The power transmission can still written as the product of the source descriptor (equation (2-36)) and coupling function (equation (2-37)), without any assumption about the interface. The results of estimating power transmission based on the source descriptor (equation2-35) and coupling function (equation 2-36) is exactly the same as using equation (2-31). However, the definition in equation 2-36 cannot be used as a source strength because the corresponding 'normalized power' is sensitive to the variable α. Furthermore, its physical meaning is not clear so it does not give any new insight. Therefore, equation 2-36 is a valid, but not particularly useful form for the source descriptor.

2.4 Remarks and discussion

It has been argued that rearrangement of equation (2-14) so as to introduce the source descriptor and coupling function does not help in estimating the power transmission. Some authors [23] have taken good agreement between measured and predicted power as proof that a particular form of equation (2-14) is valid. This is a mistake

however, since if the linearity assumption is satisfied then any combination of the same data will produce the same answer. It is argued above that it is the sensitivity of the 'general normalized function' (or link function) to α that determines whether a particular form of source descriptor are useful.

2.5 Conclusion

A broad definition of source characterisation and source strength been introduced. The active power emission from the source into the receiver is considered the 'target quantity' i.e. the required solution to the structure borne-sound transmission problem. The characterisation of structure–borne sound sources, and the more restricted concept of source strength were discussed for the single point unidirectional case.

It has been shown that the active power emission can be expressed as the product of the 'general source descriptor' and the 'general coupling function' (or coupling function). The former depends only on source data and the latter is a function of the source and receiver mobility at the interface. Therefore, the general source descriptor cannot fully describe the source. It can be used neither as a source strength parameter to rank order sources, nor for predicting the power transmission without introducing assumptions, because the general coupling function involves another physical parameter of the source, namely its mobility. To predict the power emission, two source parameters are required. i.e. a full characterisation needs two quantities to describe the source. For convenience and clear physical meaning it is proposed that one of the two quantities is the source mobility, the other can then be one of three physical parameters: the blocked force squared, free velocity squared or magnitude of

the source descriptor $\left|\hat{V}_{sf}\right|^2/Y^*$. These three quantities can be understood as the physical parameters that contain information about the 'strength' of the source.

A so-called 'normalized active power' was introduced which, when plotted against $|\alpha|$, shows whether the corresponding general source descriptor can be used as a source strength characteristic or not. These curves may be helpful to establish the most suitable form of general source descriptor in a given situation.

In the range $\alpha < 0.1$ the blocked force $S_g = \left|\hat{F}_{sb}\right|^2$ is the best form of general source descriptor to use as a source strength characteristic, while in the range of $\alpha > 10$ the free velocity is most suited, $S = \left|\hat{V}_{sf}\right|^2$. The magnitude of the source descriptor in equation (2-31), $S = \left|\hat{V}_{sf}\right|^2 / \left|Y_s^*\right|$ is relative good parameter to use as a source strength characteristic when the magnitude of the source mobility is similar to that of the receiver.
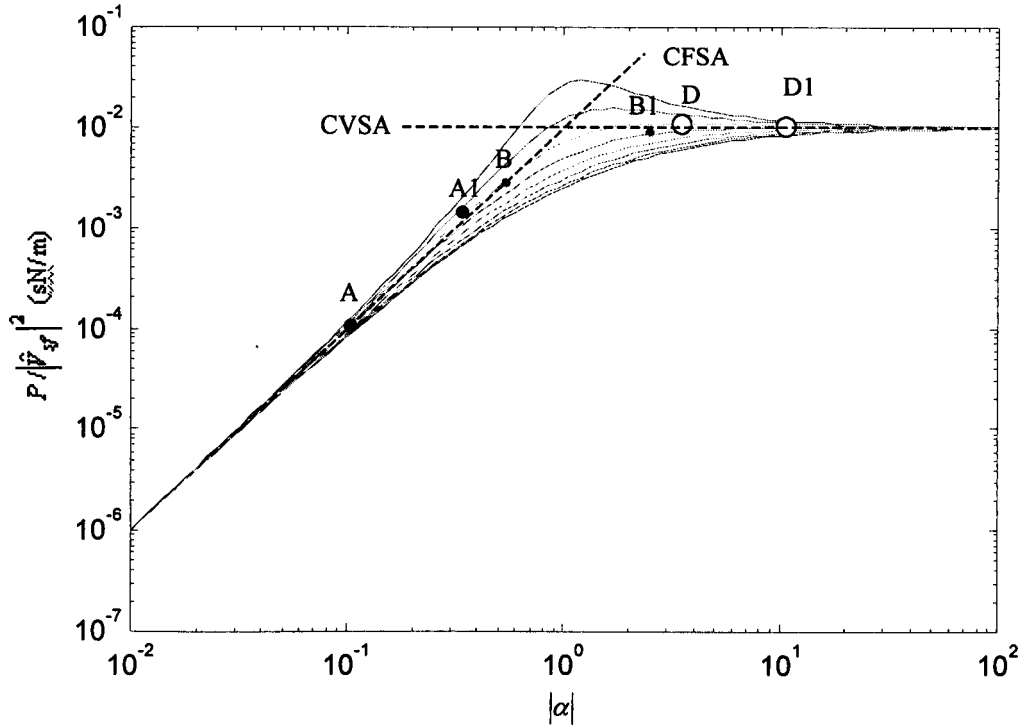
Figure 2-1a General normalised active power (for free velocity square) against $|\alpha|$ for various $\Delta\phi$, $\mathrm{Re}(Y_R)/|Y_R|^2 = 0.01$ (sN/m) from top to bottom curve:$0.8\pi, 0.7\pi, 0.6\pi, 0.5\pi, 0.4\pi, 0.3\pi, 0.2\pi, 0.1\pi$.
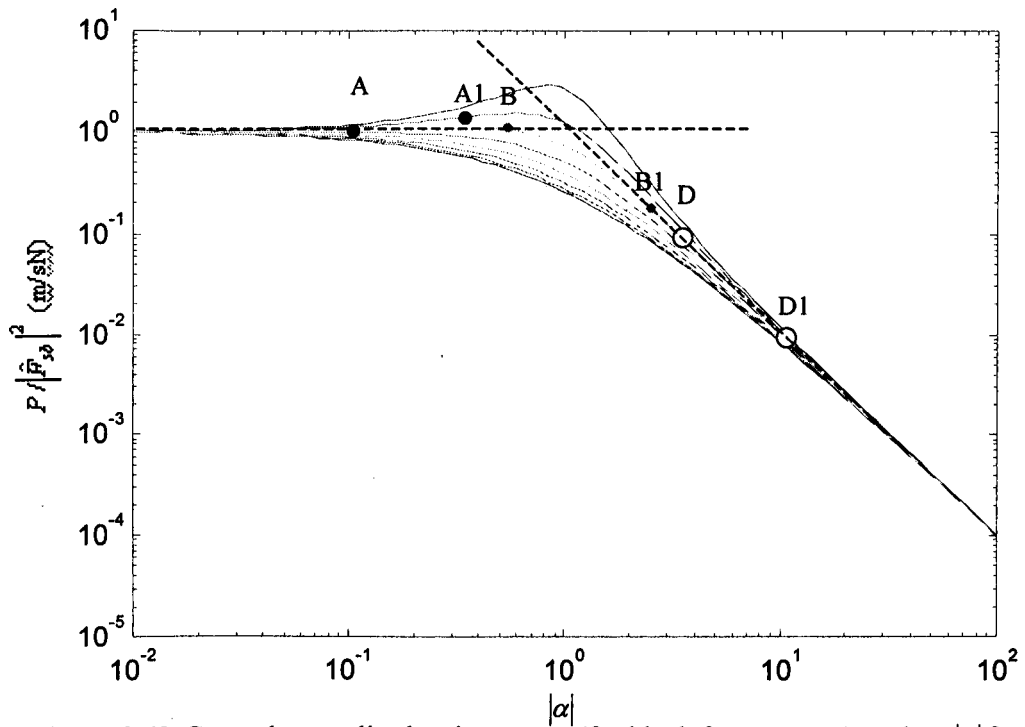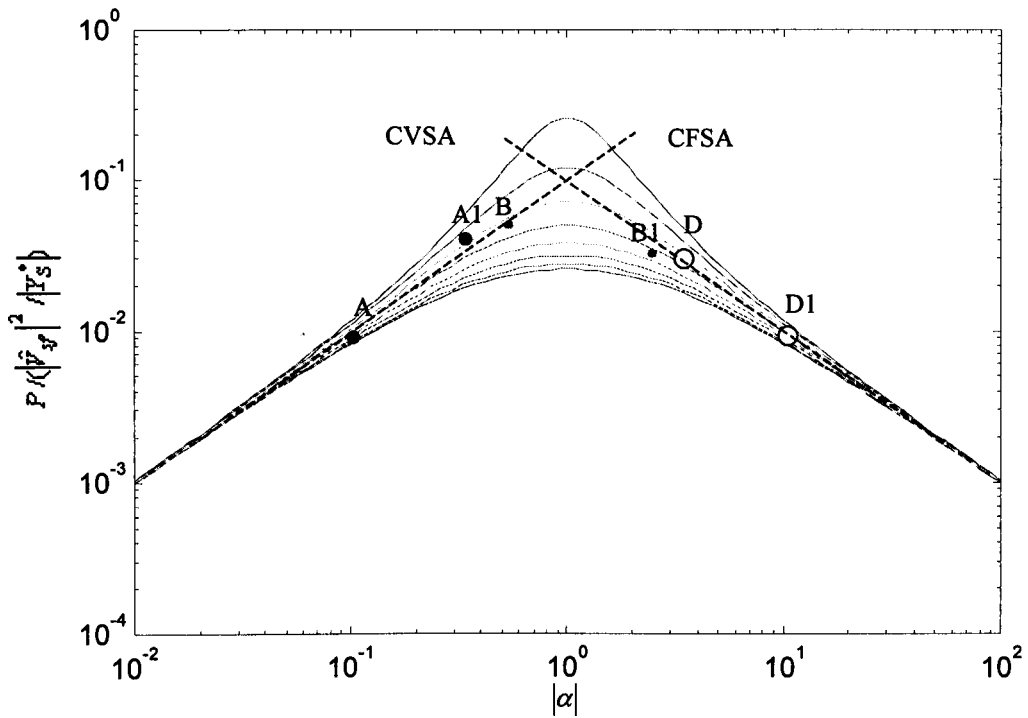

Figure 2-1b General normalised active power (for block force square) against $|\alpha|$ for various $\Delta\phi$, $\mathrm{Re}(Y_R)=1$ (m/sN) from top to bottom curve:$0.8\pi, 0.7\pi, 0.6\pi, 0.5\pi, 0.4\pi, 0.3\pi, 0.2\pi, 0.1\pi$.

Figure 2-1c Normalised active power against $|\alpha|$ for various $\Delta\phi$, $\mathrm{Re}(Y_R)/|Y_R|$ =0.1 ;
from top to bottom curve:$0.8\pi,0.7\pi,0.6\pi,0.5\pi,0.4\pi,0.3\pi,0.2\pi,0.1\pi$.

CHAPTER3

SIMPLIFIED CHARACTERISATION OF MULTI-POINT SOURCES

3.1   Introduction

3.2   The concept of simplification

3.3   'Single figure' characterisation of sources

3.4   Mobility matrix eigenvalues

3.5   The choosing of ' s_1 ' and ' s_2 '

3.6   Conclusion

3.1 Introduction

Having dealt with single point contact in chapter 2, we now consider practical cases where the sources have multiple point connections with up to six degrees of excitation per point. For multi-component and multi-point connections the general equation for complex power from source into the receiver is:

$$Q = [\hat{V}_{sf}]^{*T}([Y_R]+[Y_S])^{-1*T}[Y_R]^{*T}([Y_R]+[Y_S])^{-1}[\hat{V}_{sf}] \qquad (3\text{-}1a)$$

and the active power is

$$P = \text{Re}([\hat{V}_{sf}]^{*T}([Y_R]+[Y_S])^{-1*T}[Y_R]^{*T}([Y_R]+[Y_S])^{-1}[\hat{V}_{sf}]$$
$$= [\hat{V}_{sf}]^{*T}([Y_R]+[Y_S])^{-1*T}(\text{Re}[Y_R])([Y_R]+[Y_S])^{-1}[\hat{V}_{sf}] \qquad (3\text{-}1b)$$

where $[\hat{V}_{sf}]$ is the free velocity vector, $[Y_R]$ and $[Y_S]$ are the complex mobility matrices of the source and receiver respectively. If the machine has N contact points and six degrees of freedom, then 6N frequency dependent free velocity spectra and $(6N)^2$ source mobility spectra are required. When reciprocity is considered, the mobility matrix is symmetrical about the diagonal, and the total number of spectra of the source mobility reduces to 3N(6N+1). Therefore, a total of (3N(6N+1) +6N) data elements are needed to fully characteristic the source, and likewise the full characterisation of the receiving structure requires 3N(6N+1) mobility spectra. For the common case of N=4: the total spectra required for the source will be 300 mobility and 24 free velocity spectra and for the receiver it will be 300 mobility spectra.

In most real cases it is impractical to obtain this amount of data. A common simplifying assumption [24-27] is the limitation of the analysis to one degree of freedom i.e. it is assumed that one degree of freedom dominates vibration. In this case the calculation of power requires N(N+1)/2 mobility matrices for the source, N free velocity spectra and N(N+1)/2 mobility matrices for the receiver. However, this is

still more than can realistically be handled in the majority of cases, so further simplification is needed.

In this chapter we first review some approaches to simplified characterisation of the source, with the aim of clarifying the concept of simplification, and of comparing these approaches to that introduced in later chapters. The second objective is to introduce the 'single figure' method for simplified characterisation of sources.

3.2 The concept of simplification

If the target quantity (equation2-17) can be approximately expressed by a reduced set of source parameters as:

$$L \approx f(r'_1, r'_2, \dots r'_l, s'_1, s'_2, s'_3, \dots s'_r) \tag{3-2a}$$

or if it can be bounded as

$$f_1(r'_1, r'_2, \dots r'_l, s'_1, s'_2, s'_3, \dots s'_r) < L < f_2(r'_1, r'_2, \dots r'_l, s'_1, s'_2, s'_3, \dots s'_r) \tag{3-2b}$$

where $s'_1, s'_2, \dots s'_r$ $(r < n)$ is the reduced set of source parameters, then this set can be considered a simplified characterisation of the source in relation to the target quantity.

3.2.1 Simplified source characterisation based on eigenvalues and eigenvectors

This approach was first suggested in [28], and was later developed in [29]. The main points are recapitulated below in the context of 'simplified characterisation' as outlined above.

For N contacts and a single degree of freedom the active power can be rewritten as

$$P = [\hat{V}_{sf}]^{*T}([Y_R]+[Y_S])^{-1*T}(\text{Re}[Y_R])([Y_R]+[Y_S])^{-1}[\hat{V}_{sf}] \\ = \phi^{*T} D \phi \tag{3-3}$$

where D is the diagonal matrix

$$D = \begin{bmatrix} \eta_1 & & \\ & \ddots & \\ & & \eta_n \end{bmatrix} \qquad (3\text{-}4)$$

and η_i are the eigenvalues of Hermitian matrix $\quad H = ([Y_R]+[Y_S])^{-1*T}(\mathrm{Re}[Y_R])([Y_R]+[Y_S])^{-1}$

with units of mechanical impedance. ϕ is an equivalent velocity vector, which can be expressed as:

$$[\phi] = [p]^{T*}[\hat{V}_{sf}] \qquad (3\text{-}5)$$

in which $[p]$ is a unitary matrix ($[p][p]^{T*} = I$), the ith columns of which corresponded to the ith eigenvector of Hermitian matrix H (assumed to be normalized).

Expanding the right side of equation (3-3) one obtains

$$P = \sum_{i=1}^{n} \eta_i |\phi_i|^2 \qquad (3\text{-}6)$$

Equation (3-6) maybe conceptually helpful, but it does not provide any practical advantages over the first relationship in equation (3-3), since all the complex free velocities must be known as well as the complete mobility matrix of the source and receiver in order to the calculate the eigenvalues and eigenvector. Therefore, equation (3-6) cannot be understood as more simple than the relationship in equation (3-3). Since $[p]$ is a unitary matrix, the following relationship is seen to exist between the equivalent vector and the free velocity:

$$\sum_{i=1}^{n} |\hat{V}_i|^2 = \sum_{i=1}^{n} |\phi_i|^2 \qquad (3\text{-}7)$$

By using equation (3-7) in equation (3-6) and remembering that the eigenvalues are all real and non-negative the power is seen to be bounded as follows

$$\eta_{\min} \left(\sum_{i=1}^{n} |\hat{V}_i|^2 \right) \le P \le \eta_{\max} \left(\sum_{i=1}^{n} |\hat{V}_i|^2 \right) \qquad (3\text{-}8)$$

Note that η_{min} and η_{max} still concern the mobility matrix of the source and receiver, so if N(N+1)/2 +1 source data and N(N+1)/2 receiver data are provided, a unique value for the active power cannot be obtained, only a range of possible values. So the result of the simplification is that the data needed for characterising the source is reduced (N-1 complex spectra are reduced) and the 'cost' is obtaining an uncertain estimate of active power.

We can further reduce the data for describing the source, although the 'cost' may be more: consider that the active power can be rewritten as:

$$P = \hat{F}^{T*} \text{Re}(Y_R) \hat{F} \qquad (3\text{-}9)$$

where $\hat{F}$ is the interface force vector caused by the interaction between the source and the receiver. This is given by

$$\hat{F} = ([Y_R] + [Y_S])^{-1} \hat{V}_{sf} \qquad (3\text{-}10)$$

Similarly to equation (3-8) a strict lower bound for the transmitted power of equation (3-10) can be expressed as

$$P \geq \lambda_{min} \left(\sum_{i=1}^{n} \left| \hat{F}_i \right|^2 \right) \qquad (3\text{-}11)$$

where λ_{min} is the minimum eigenvalue of $\text{Re}(Y_R)$ with units of mobility. By using equation (3-10) it follows that

$$\sum_{i=1}^{n} \left| \hat{F}_i \right|^2 = [\hat{V}_{sf}]^{T*} [Y_{RS}]^{-1} [\hat{V}_{sf}] \qquad (3\text{-}12)$$

where

$$Y_{RS} = ([Y_R] + [Y_S])([Y_R] + [Y_S])^{*T} \qquad (3\text{-}13)$$

It is seen that Y_{RS} is still a Hermitian matrix with non-negative eigenvalues, so we have the following relationship

$$\sum_{i=1}^{n}\left|\hat{F}_i\right|^2 \geq \sum_{i=1}^{n}\left|\hat{V}_i\right|^2 \frac{1}{\lambda_{\max}^{RS}} \quad (3\text{-}14)$$

where $\lambda_{\max}^{RS}$ is the maximum eigenvalue of matrix Y_{RS} and satisfies:

$$\sqrt{\lambda_{\max}^{RS}} \leq \max\left|Y_{R,ii}+Y_{S,ii}\right| + \sqrt{\sum_{i \neq j}\sum\left|Y_{R,ij}+Y_{S,ij}\right|^2} \quad (3\text{-}15)$$

Combining equation (3-11), (3-14)and (3-15) we have

$$P \geq \frac{\lambda_{\min}\sum_{i=1}^{n}\left|\hat{V}_i\right|^2}{(\max\left|Y_{R,ii}+Y_{S,ii}\right| + \sqrt{\sum_{i \neq j}\sum\left|Y_{R,ij}+Y_{S,ij}\right|^2})^2} \quad (3\text{-}16a)$$

Equation (3-16) was derived by L Ji [18], but this equation still needs N(N+1)/2 +1 spectra for characterising the source, which is the same as needed for equation (3-8). A modification will now be made to (3-16). Equation (3-15) can be rewritten as:

$$\sqrt{\lambda_{\max}^{RS}} \leq \max\left|Y_{R,ii}+Y_{S,ii}\right| + \sqrt{\sum_{i \neq j}\sum\left|Y_{R,ij}+Y_{S,ij}\right|^2}$$
$$\leq \max\left|Y_{R,ii}\right| + \max\left|Y_{S,ii}\right| + \sqrt{2(\sum_{i \neq j}\sum\left|Y_{R,ij}\right|^2 + \sum_{i \neq j}\sum\left|Y_{S,ij}\right|^2)} \quad (3\text{-}16b)$$

so Equation (3-16) can be rewritten as

$$P \geq \frac{\lambda_{\min}\sum_{i=1}^{n}\left|\hat{V}_i\right|^2}{(\max\left|Y_{R,ii}+Y_{S,ii}\right| + \sqrt{\sum_{i \neq j}\sum\left|Y_{R,ij}+Y_{S,ij}\right|^2})^2} \geq$$
$$\frac{\lambda_{\min}\sum_{i=1}^{n}\left|\hat{V}_i\right|^2}{\{\max\left|Y_{R,ii}\right| + \max\left|Y_{S,ii}\right| + \sqrt{2\sum_{i \neq j}\sum\left|Y_{R,ij}\right|^2 + 2\sum_{i \neq j}\sum\left|Y_{S,ij}\right|^2}\}^2} \quad (3\text{-}16c)$$

In equation (3-16c) the source is characterised by three real numbers:

i) $\max\left|Y_{S,ii}\right|$

ii) $\sum_{i \neq j} \sum \left| Y_{S,ij} \right|^2$

iii) $\sum_{i=1}^{n} \left| \hat{V}_i \right|^2$

and the passive receiver structure by only three real numbers:

i) $\lambda_{\min}$

ii) $\max \left| Y_{R,ii} \right|$

iii) $\sum_{i \neq j} \sum \left| Y_{R,ij} \right|^2$

The 'cost' of the simplification is that only the lower bound of the active power is obtained.

Using the general relationship $\sqrt{a^2 + b^2} < a + b \quad (a > 0, b > 0)$, then Equation (3-16c) can be rewritten as

$$P \geq \frac{\lambda_{\min} \sum_{i=1}^{n} \left| \hat{V}_i \right|^2}{\left\{ \max \left| Y_{R,ii} \right| + \max \left| Y_{S,ii} \right| + \sqrt{2 \sum_{i \neq j} \sum \left| Y_{R,ij} \right|^2} + \sqrt{2 \sum_{i \neq j} \sum \left| Y_{S,ij} \right|^2} \right\}^2} \qquad (3-17)$$

Now only two data need to be provided for a simplified characterisation of the source

i) $\sum_{i=1}^{n} \left| \hat{V}_i \right|^2$

ii) $\max \left| Y_{S,ii} \right| + \sqrt{2 \sum_{i \neq j} \sum \left| Y_{S,ij} \right|^2}$

Of course the 'cost' is more: the lower bound on the active power is more conservative.

3.2.2 Simplified characterisation based on effective mobility

Introducing the effective mobility the active power equation can be rewritten as[30-

$$P = \text{Re}(\sum_{n=1}^{N} \frac{Y_{R,nn}^{\Sigma}}{\left| Y_{R,nn}^{\Sigma} + Y_{S,nn}^{\Sigma} \right|^2} \left| \hat{V}_{sf,n} \right|^2) \qquad (3\text{-}18)$$

where $Y_{S,nn}^{\Sigma}$ is the source effective point mobility and $Y_{R,nn}^{\Sigma}$ the receiver effective point

mobility and can be expressed as :

$$Y_{nn}^{\Sigma} = Y_{nn} + \sum_{n \neq m}^{N} Y_{nm} \frac{F_m}{F_n} \qquad (3\text{-}19)$$

The first term gives the direct contribution; the second term is the contribution from

the other points. F_i is the interface force vector caused by the interaction between the

source and the receiver. Equation (3-18) does not provide any practical advantages

over equation (3-3), since the effective mobility is unavailable without full knowledge

of the forces. Obtaining the effective mobility is therefore no easier than obtaining

active power directly, unless some simplifying assumption can be introduced. It must

be clear that any assumption must be independent of the receiver, otherwise the

effective mobility is unavailable data. Some possible assumptions are now examined.

a: Unit magnitude and zero phase.[32-33]

Based on this assumption the effective mobility is given by;

$$Y_{nn}^{\Sigma} = Y_{nn} + \sum_{n \neq m}^{N} Y_{nm} \qquad (3\text{-}20)$$

The advantages of this assumption are: i) it is simple and ii) the effective point

mobility can be measured in a single test by using a special arrangement (see figure.

3-1).

b: An alternative assumption is that, the contributions from the N-1 contact points cancel . In this case the effective point mobility will simply reduce to the ordinary point mobility:

$$Y_{nn}^{\Sigma} = Y_{nn} \qquad (3\text{-}21)$$

This is equivalent to assuming that the contact points are uncoupled [23]. This assumption is called the 'point mobility only' assumption.

c: Another estimate takes into account both the excitation of the system and its structural characteristics. The simplest assumption is that the force at a contact point is then given by;

$$F_n = b \frac{V_{sf,n}}{Y_{S,n}} \qquad (3\text{-}22)$$

where b is a constant (Fulford [34] used this form with b=1). In this case the effective point mobility is then given by;

$$Y_{nn}^{\Sigma} = Y_{nn} + \sum_{m \neq n}^{N} Y_{nn} \frac{V_{sf,m}}{Y_{S,mm}} \frac{Y_{S,nn}}{V_{sf}^{n}}. \qquad (3\text{-}23)$$

There is a significant difference between the last assumption (equation3-21) and the previous two. In the first two assumptions N free velocity and N effective point mobility spectra are required, i.e a total of 2N spectra for characterisation of source. However, in the last case 3N-1 spectra are required.

3.2.3 Simplified characterization of structure-borne sound sources based on poles of vibration

The concept of decomposing force, velocity and mobility onto a base of vibration 'poles' was first introduced by Pinnington and Pearce [35-36]. As above, this work will be reviewed from the point view of simplification of the source characterisation.

The active power for $N=2^P$ contact points can be expressed as

$$P = [\hat{U}_{sf}]^{*T}([M_R^P]+[M_S^P])^{-1*T}(\text{Re}[M_R^P])([M_R^P]+[M_S^P])^{-1}[\hat{U}_{sf}] \quad (3\text{-}24)$$

where $[\hat{U}_{sf}]$ is the so-called polar free velocity vector, $[M_S^P]$ is the polar mobility matrix of source and $[M_R^P]$ the polar mobility matrix of receiver. For example, for the case of N=4 (see figure3-2a) the polar free velocity vector $[\hat{U}_{sf}]$ is written as follows.

$$[\hat{U}_{sf}] = \begin{bmatrix} \hat{U}_{sf,1} \\ \hat{U}_{sf,2} \\ \hat{U}_{sf,3} \\ \hat{U}_{sf,4} \end{bmatrix} = \frac{1}{4} \begin{bmatrix} \hat{V}_{sf,1} + \hat{V}_{sf,2} + \hat{V}_{sf,3} + \hat{V}_{sf,4} \\ \hat{V}_{sf,1} + \hat{V}_{sf,2} - \hat{V}_{sf,3} - \hat{V}_{sf,4} \\ \hat{V}_{sf,1} - \hat{V}_{sf,2} + \hat{V}_{sf,3} - \hat{V}_{sf,4} \\ \hat{V}_{sf,1} - \hat{V}_{sf,2} - \hat{V}_{sf,3} + \hat{V}_{sf,4} \end{bmatrix} \quad (3\text{-}25)$$

$\hat{U}_{sf,1}$ is a 'monopole' free velocity, $\hat{U}_{sf,2}$ and $\hat{U}_{sf,3}$ are 'dipole' free velocities, and $\hat{U}_{sf,4}$ is a 'quadrupole' free velocity. These names are based on the arrangement of the contact points of figure 3-2a and the obvious analogy to simple acoustic sources. The polar mobility matrix is:

$$[M^P] = \frac{1}{4^2}[\Phi][Y][\Phi] \quad (3\text{-}26)$$

where $[\Phi]$ is a 'Hadamard matrix':

$$[\Phi] = \begin{bmatrix} 1 & 1 & 1 & 1 \\ 1 & 1 & -1 & -1 \\ 1 & -1 & 1 & -1 \\ 1 & -1 & -1 & 1 \end{bmatrix} \quad (3\text{-}27)$$

The polar mobility matrix is, in general, an N×N square matrix, and for geometrically symmetrical arrangements of the contact points it is diagonal. All field variables can be expressed on the polar basis, so force and velocity vectors, as well as mobility matrices all have equivalent polar forms. There follows a physical interpretation of the polar mobility matrix, which was not given in Pinnington and Pearce's original paper, but is considered to be conceptually useful.

Consider simultaneous excitation at four points with the four different phase arrangements shown in figure 3-2b. The magnitude of the four excitation forces are the same, F_1 and F_4 are in phase, F_2 and F_3 are in phase, but F_1 and F_2 are anti – phase. Consider the ratio:

$$R = \frac{V_1 - V_2 + V_3 - V_4}{16F} \quad (3\text{-}28)$$

where V_1, V_2, V_3, V_4 are the velocity responses at the four points of the excited structure. They can be expressed in terms of the ordinary mobility

$$V_1 = Y_{11}F + Y_{12}(-F) + Y_{13}(-F) + Y_{14}F \quad (3\text{-}29a)$$

$$V_2 = Y_{21}F + Y_{22}(-F) + Y_{23}(-F) + Y_{24}F \quad (3\text{-}29b)$$

$$V_3 = Y_{31}F + Y_{32}(-F) + Y_{33}(-F) + Y_{34}F \quad (3\text{-}29c)$$

$$V_4 = Y_{41}F + Y_{42}(-F) + Y_{43}(-F) + Y_{44}F \quad (3\text{-}29d)$$

Substituting (3-29a,b,c,d,) into (3-28)

$$R = \frac{1}{16}((Y_{11} - Y_{12} - Y_{13} + Y_{14}) - (Y_{11} - Y_{22} - Y_{13} + Y_{14}) + (Y_{31} - Y_{32} - Y_{33} + Y_{44}) - (Y_{41} - Y_{42} - Y_{43} + Y_{44}))$$

$$(3\text{-}30)$$

According to the relationship (3-26), R is simply equal to the element M_{34}^P of the polar mobility . But from another point of view the four polar forces applied to the structure are as follows

$$P_1 = F_1 + F_2 + F_3 + F_4 = 0 \quad \text{(monopole term)}$$

$$P_2 = F_1 + F_2 - F_3 - F_4 = 0 \quad \text{(dipole term)} \qquad \text{(3-31 a,b,c,d)}$$

$$P_3 = F_1 - F_2 + F_3 - F_4 = 0 \quad \text{(dipole term)}$$

$$P_4 = F_1 - F_2 - F_3 + F_4 = 4F \quad \text{(quadrupole term)}$$

and the four corresponding polar velocity responses are:

$$U_1 = \frac{1}{4}(V_1 + V_2 + V_3 + V_4) \quad \text{(monopole term)}$$

$$U_2 = \frac{1}{4}V_1 + V_2 - V_3 - V_4 \quad \text{(dipole term)} \qquad \text{(3-32,a,b,c,d)}$$

$$U_3 = \frac{1}{4}(V_1 - V_2 + V_3 - V_4) \quad \text{(dipole term)}$$

$$U_4 = \frac{1}{4}(V_1 - V_2 - V_3 + V_4) \quad \text{(quadrupole term)}$$

Therefore, R can be rewritten as

$$R = \frac{V_1 - V_2 + V_3 - V_4}{16F} = \left.\frac{U_3}{P_4}\right|_{other\ polar\ forces=0} \qquad \text{(3-33)}$$

Therefore, the element of the polar mobility matrix M_{34}^p can be interpreted as the dipole velocity response to a quadrupole force excitation, with all other polar forces being zero. Here, the author calls M_{34}^p the transfer polar mobility, in this case from quadrupole to dipole. Other elements have similar meaning, (see figure 3.2b). In symmetrical cases the polar mobility matrix remains diagonal and each element M_{nn}^P can be measured in a single measurement by another method (see figure3-1). For example $M_{11}^P = (\hat{V}_1 + \hat{V}_2 + \hat{V}_3 + \hat{V}_4)/(\hat{F}_1 + \hat{F}_2 + \hat{F}_3 + \hat{F}_4)$. In this case the polar mobilities can be obtained by applying point forces independently, i.e. without the need for a special arrangement.

As with the effective mobility described in the previous subsection, use of the polar mobility matrix has no advantages over the normal N×N mobility matrix in terms of simplification unless some simplifying assumptions are introduced. The simplest assumption is that the transfer polar mobility elements can be ignored. Based on this

assumption the active power can be rewritten in terms of the diagonal elements only

as :

$$P = \text{Re}(\sum_{n=1}^{4} \frac{M_{R,nn}^{P}}{\left| M_{R,nn}^{P} + M_{S,nn}^{P} \right|^2} \left| \hat{U}_{sf,n} \right|^2)$$ (3-34)

So the simplification afforded in this case is that the data for characterising (describing) the source is reduced (now only 4 complex and 4 real spectra are needed). The 'cost' is obtaining an approximate active power, although in the case of symmetric source and receiver, Equation 3-34 is exact.

3.3 'Single figure' characterisation of sources

The simplified characterisations of sources in section 3.2 result in formulations either that still require much data or give a large a range of uncertainty in the active power or both. The approaches in sections 3.2.2 and 3.2.3 require assumptions to be introduced, but these cannot be satisfied in many practical cases [34]. Perhaps more importantly it is difficult to know whether the assumptions are satisfied or not. Despite these simplifications, the amount of data required to characterise the source is still too much for many practical purposes, and furthermore does not provide insight into the global behaviour of the source, specifically, the 'strength' information of the source is obscured. For this reason it is hoped to be able to find a simpler formulation.

An alternative approach is here suggested called the 'single figure' approach, i.e. like the single point case, using one physical parameter s_1 as a source 'strength'. Here s_1 contains information about the strength of the source but it is not a true strength parameter (as discussed in Chapter 2, see for example equations (2-19)), rather it is

the active part of a source characterisation. We also need another physical parameter s_2 to describe the structural dynamic properties of the source. Using s_2 and a corresponding parameter r_2 which describes the structural dynamic properties of the receiver we define a new parameter α^Σ. Like the single point case, the normalised power emission due to s_1 can be plotted against α^Σ. Since some detail is lost in the reduction to an equivalent single point, the emission from source into the receiver will be a range, i.e. a plot of normalised emission versus α^Σ is a 'band' rather than a single curve. This means that different sources with the same s_1 and s_2 attached to a given receiver may not give the same emission. Here this band will be called the 'General normalised active power band'. If the 'General normalised active power band' is narrow, it means two sources with the same s_1 and s_2 will emit approximately the same power into a given receiver, expressed as $P \approx f(R, s_1, s_2)$. Then, a rank ordering based on prediction is likely to be a good approximation to the true rank ordering when installed. Thus, we can say that the chosen parameters s_1 and s_2 are 'good' parameters for characterising the source. If the band is not only narrow but also 'flat', then, by analogy with the single point case in Chapter 2, s_1 can considered as a good parameter to characterise source strength. In this case a rank ordering based purely on the source parameter s_1 is likely to be a good approximation to the installed rank ordering based on emission.

In the single point case, it was shown in Chapter 2 that the blocked force squared, source descriptor magnitude $\left| \hat{V}_{sf}^{~2} / Y^* \right|$ or free velocity squared can be used as s_1, and the point mobility was chosen as s_2. The focus of this thesis is on 'force' sources, that is sources whose mobility is much greater than that of the receiver, and on 'matched'

sources, that is those whose mobility is comparable in magnitude to that of the receiver. In the former case, the blocked force squared proved to be a good strength characterisation for the single point case studied in Chapter 2. In the latter case, the parameter $\left| \hat{V}_{sf}^{\ 2}/Y^* \right|$ was a relatively good strength characterisation of source. It is reasonable that in the multiple point case we should choose corresponding parameters for s_1.

Because of the above discussion it is necessary to know what is the range of uncertainty in the target value when using a single figure source characterisation. Hence, the following sections, (and indeed a large part of this thesis) are devoted to an examination of 'uncertainty limits' in the predicted power.

Consider again the power absorbed by a structure when excited by N applied forces. The power is given by equation (3-9) which can be rewritten as follows :

$$P = \sum_{i=1}^{N} \lambda_i \left| \hat{\psi}_i \right|^2 \equiv \lambda \left| \hat{F} \right|^2 \qquad (3\text{-}35a)$$

where

$$\lambda = \frac{P}{\left| \hat{F} \right|^2} = \lambda_1 x_1^2 + \lambda_2 x_2^2 + \cdots \lambda_N x_n^2 , \qquad (3\text{-}36a)$$

$$x_1^2 + x_2^2 + \cdots x_n^2 = 1 \qquad (3\text{-}36\ b)$$

here $x_i = \sqrt{\left| \psi_i \right|^2 / \left| \hat{F} \right|^2}$, and λ is the 'generalised normalised power', (which may also be viewed as an equivalent point mobility that accounts for excitation at all points [37]). It can be seen that λ is bounded:

$$0 \leq \lambda_{\min} \leq \lambda \leq \lambda_{\max} \qquad (3\text{-}37)$$

which means that the power into the receiver is between the band of maximum and minimum eigenvalues for a given unit total force (not knowing the force pattern). Thus, the maximum and minimum eigenvalues determine the upper and lower bound of the power, or the '100% probability bands'. Thus, we can gain insight into the width of the generalised active power band by examining the eigenvalues of the receiver mobility matrix, as described in the next subsection.

3.4. Mobility matrix eigenvalues

Figure 3-3 shows the four eigenvalues of the mobility matrix of a plate. They correspond to four eigenvectors, (for symmetrical cases, the four eigenvectors correspond to four poles: one monopole, two dipoles and one quadrupole, and each eigenvalue corresponds to the active power emission per unit polar force). One of them corresponds to the 'maximum' active power emission, i.e. if the applied force is proportional to the eigenvector ,then the active power emission per unit total force has the maximum value λ_{max} Similarly, one of the four eigenvectors, corresponds to the 'minimum' active power emission with value λ_{min} (the remaining two eigenvalues have intermediate values). The four eigenvectors describe an ortho-normal basis.

Several regimes are illustrated in Fig 3-3. At high frequency (when the model overlap is less than unity [38]) the eigenvalues are relatively close (the higher frequency indicates that the 'wavelength size' of the plate is greater. For very high frequency, the point mobility tends to one constant value, i.e. characteristic point mobility[39] and the transfer mobility tends to zero, so the eigenvalues converge to one value). This

indicates a relatively well-conditioned system which is not highly sensitive to small changes in force pattern. Similar behaviour is expected for shells at high frequencies.

At low frequencies (below first resonant frequency), it is usually considered that the point mobility approximately equals the transfer mobility, i.e $Y_{ii} \approx Y_{ij}$. If this condition is met, all except one of the eigenvalues are small (in the case of exact equality only one eigenvalue is non zero), and the ratio of maximum to minimum eigenvalue (the condition number) will approach infinity. This means the accuracy obtained from a single figure descriptor will be poor. However, this is not always correct, for example for many cases the receiver displays stiffness behaviour, where the condition number can be relatively low (see Chapter 4) no matter how low the frequency. Another factor influencing the condition number is the distribution of the points, for example when the points are close together, this ratio will be larger [40].

In the region of well-separated modes, the resonance peaks will be sharp. At frequencies close to resonance the mobility is dominated by the contribution of one mode so there is one dominant eigenvalue, and all others are significantly lower. The range between maximum and minimum will then be wide.

From the above we may remark that different types of behaviour are associated with wider or narrower ranges in the emission, and this is discussed at more length in Chapter 5.

However, by intuition, λ cannot be a uniform distribution between λ_{max} and λ_{min}, so it is of interest to investigate its statistical distribution. In order to do so we need to

make some assumptions about the forces, the obvious choice is to assume random force patterns, which is considered in the next section.

3.4.1 Random forces

Consider the simplest case of two contact points, illustrated in figure3-4. The normalised equivalent forces are subject to the restriction $x_1^2 + x_2^2 = 1$ which describes a unit circle as shown, and which represents all possible spatial patterns of the applied forces. It is assumed that the probability distribution around this circle is uniform, i.e. that all spatial patterns are equally likely. The structure itself, and the position of the applied forces is assumed fixed, so the eigenvalues in equation 3-36 are assumed known. Equation 3-36 then describes an ellipse of constant shape, but of a size that varies with λ. The probability that λ is less than a given value λ_0 is the proportion of the unit circle circumference that fits inside the ellipse, that is:

$$Probability(\lambda < \lambda_0) = \frac{4\phi}{2\pi}, \text{ where } \tan\phi = \sqrt{\frac{\lambda_0 - \lambda_1}{\lambda_2 - \lambda_0}} \quad (3\text{-}38)$$

For example, the probability is 100% for the ellipse that just encloses the circle, and 0% for that which just fits inside the circle. This result can be extended to three and more dimensions. For n contact point the normalised equivalent forces are subject to the restriction $x_1^2 + x_2^2 + \cdots x_n^2 = 1$ which describes a unit n dimensional super-sphere. Any set of forces corresponds to a point $q(x_1, x_2, \cdots x_n)$ on this super-sphere. It is still assumed that the probability distribution on this super-sphere is uniform. To calculate the probability distribution, the following co-ordinate transforms were used:

$x_1 = \cos\theta_1$

$x_2 = \sin\theta_1\cos\theta_2$

$$x_3 = \sin_1 \sin\theta_2 \cos\theta_3$$
$$\vdots$$

$$x_{n-1} = \sin\theta_1 \sin\theta_2 \cdots \sin\theta_{n-2} \cos\theta_{n-1} \qquad (3\text{-}39)$$

$$x_n = \sin\theta_1 \sin\theta_2 \cdots \sin\theta_{n-2} \sin\theta_{n-1}$$

$\theta_1, \theta_2 \cdots \theta_{n-1}$ are the co-ordinates of the point q in the super-sphere co-ordinate system, although for more than 2 dimensions a numerical evaluation is required.

In figure 3-5 is shown an example of the probability bands calculated in this way for the plate featured in figure 3-3. The 90% probability band is defined to exclude the highest 5% and lowest 5% of estimates, and similarly for other values. It is seen that at high frequency the band is only 3-4dB wide.

Within the band λ has a distribution with long tails (on a linear scale), so that the bands become much narrower as the probability is decreased. For example, at lower frequencies the 68% band (which excludes the highest and lowest 16% of estimates, and is equivalent to one standard deviation for a normal distribution [41]) has only one fifteenth the width of the 100% probability band (i.e. $\lambda_{max}/\lambda_{min} = 15\,\lambda_{1-16}/\lambda_{1-84}$).

3.4.2 Force Patterns due to connection with other structures

In real cases, the applied forces do not display a uniform random distribution, but arise due to contact with other structures. The exciting structure will have its own characteristics, and we imagine that these will result in certain force patterns being preferred over others. In this section we investigate probability distributions for structures excited by other structures. The investigation is carried out using simulations with idealised structures for which analytical solutions exist.

Examples are given in figures 3-6 and 3-7, of a beam and plate, excited by another beam.[1] One of the causes of uncertainty is the position at which the 'source' beam is itself excited. This can be examined statistically by solving the system many times, with the position of the initial excitation gradually moved from one end to the other. Each solution gives a different force pattern, and therefore different power transmission. However, all these force patterns are expected to be conditioned to some extent by the characteristics of the beams and therefore likely to show less variation than a uniform random choice.

Results confirm this speculation. Figure 3-6 shows 90% probability bands for an infinite beam excited by a finite source beam. As before, the 90% band is defined to exclude the 5% highest and 5% lowest of estimates. The 90% band is significantly narrower than the range of λ_{max} and λ_{min}. It is also seen that the average eigenvalue provides a reasonable estimate of the centre of the band.

Shown in figure 3-7 are results for another system. Here the receiver is a simply supported plate. It is still seen that the 90% band is significantly narrower than the range of λ_{max} and λ_{min}.

A further difference between figures 3-6 and 3-7 is that the overall level of power transmitted into the finite plateis significantly less than that into the infinite beam.

---

[1] Note that although analytical solutions for the mobility of beams are found in the literature, these tend to be given as an infinite series of modal functions[42], which is not convenient for computation when the series converges slowly. In other cases, the solutions are not suitable for arbitrary forcing and response points. In order to avoid these problems the author has derived a full set of closed form solutions for beams with typical classical boundary conditions which are given in appendix A.

This is because the infinite beam receiver has a higher average point mobility real part.

3.5 The choice of 's_1' and 's_2'

The examples in the above section show that for the given total force $\sum \left|\hat{F}_i\right|^2$ the active power into the receiver is still uncertain. Especially in the case of high condition number, the range of uncertainty of the power is large. However, the probability that the power achieves the minimum and maximum limits, ($\lambda_{\min} \sum \left|\hat{F}_i\right|^2$ and $\lambda_{\max} \sum \left|\hat{F}_i\right|^2$, respectively), tends to zero. In most cases, the variation range of λ is much narrower than the range $[\lambda_{\min}, \lambda_{\max}]$. Therefore, it is logical to choose the total blocked force, defined as

$$CF = \sum \left|\hat{F}_{bf,i}\right|^2 \qquad (3\text{-}40)$$

as the physical parameter s_1 in the multi-point case, .i.e. to let CF play the role of blocked force squared $\left|\hat{F}_{bf}\right|^2$ in the single point case.

The ratio of average point mobility magnitude is chosen as α^{Σ}:

$$\alpha^{\Sigma} = \left(\frac{1}{N}\sum \left|Y_{R,ii}\right|\right) \Big/ \left(\frac{1}{N}\sum \left|Y_{S,ii}\right|\right) \qquad (3\text{-}41)$$

i.e. average point mobility magnitude of source is chosen as s_2 and that of the receiver as r_2.

As for the physical parameters which play the role of the magnitude of the source descriptor $\left|\hat{V}_{sf}\right|^2 / Y^*$ in the single point case, two parameters have been chosen. The first is the Characteristic Power as proposed by Moorhouse [43] which is defined as :

$$CP1 = \left| [\hat{V}_{sf}]^{*T}[Y_s]^{-1*T}[\hat{V}_{sf}] \right| \qquad (3\text{-}42)$$

It can be understood as the extension of Mondot and Petersson's source descriptor to the multiple point case. For a single point the source descriptor $\left|\hat{V}_{sf}\right|^2 / Y^*$ can be understood as four times the power from the source into a 'mirror' receiver (a passive receiver identical to the source), while equation (3-32) has the same physical meaning for the multiple-point case.

The second parameter is defined as :

$$CP2 = \sqrt{\sum_i \left|\hat{F}_{bf,i}\right|^2 \sum_i \left|\hat{V}_{sf,i}\right|^2} \qquad (3\text{-}43)$$

Although the physical interpretation is unclear, it collapses to the source descriptor for a single point, because the magnitude of $\left|\hat{V}_{sf}\right|^2 / Y^*$ can be written as :

$$\left| \left|\hat{V}_{sf}\right|^2 / Y^* \right| = \sqrt{\left|\hat{F}_{bf,i}\right|^2 \left|\hat{V}_{fs,i}\right|^2} \qquad (3\text{-}44)$$

The complimentary parameter, α^Σ is chosen as above.

Once the physical parameters s_1, α^Σ have been chosen, it remains to study the corresponding properties of the 'General normalised active power band'. This will be conducted in the following chapter.

3.6 Conclusion

Several approaches for simplifying the characterisation of sources have been considered.The eigenvalue approach, although conceptually useful, results in either too much data to characterise the source or too large a range of uncertainty of the active power or both. The effective mobility approach and the polar approach allow

some simplification which will inevitably result in some loss of accuracy. It remains to be seen what level of 'cost' is expected in practical cases.

The 'single figure' method for characterising the source has been proposed. This method can be thought of as representing the source and receiver contact as a kind of single equivalent point. This analogy is not exact because the mobilities and field variables for a single point are complex quantities, while only real data is used in the single figure method. Three alternative physical parameters: CF (net blocked force), CP1 (characteristic power) and CP2 (another descriptor with units of power) defined by equation (3-40), (3-42), and (3-43) have been chosen as s_1 which contains source strength information. α^Σ, which corresponds to the mobility ratio α in the single point case, is defined as the ratio of mean point mobility magnitude of receiver and source, as given by equation (3-41).

The 'single figure' representation has the conceptual advantage that the parameters 'sum up' the global behaviour of the source. Such an approach is attractive to practitioners who currently lack any method for calculating structure-borne sound. Some range of uncertainty is likely to be accepted in return for a simple, workable framework that gives some engineering insight. However, it is important that the range of uncertainty be quantified, which is the objective of the following chapters.
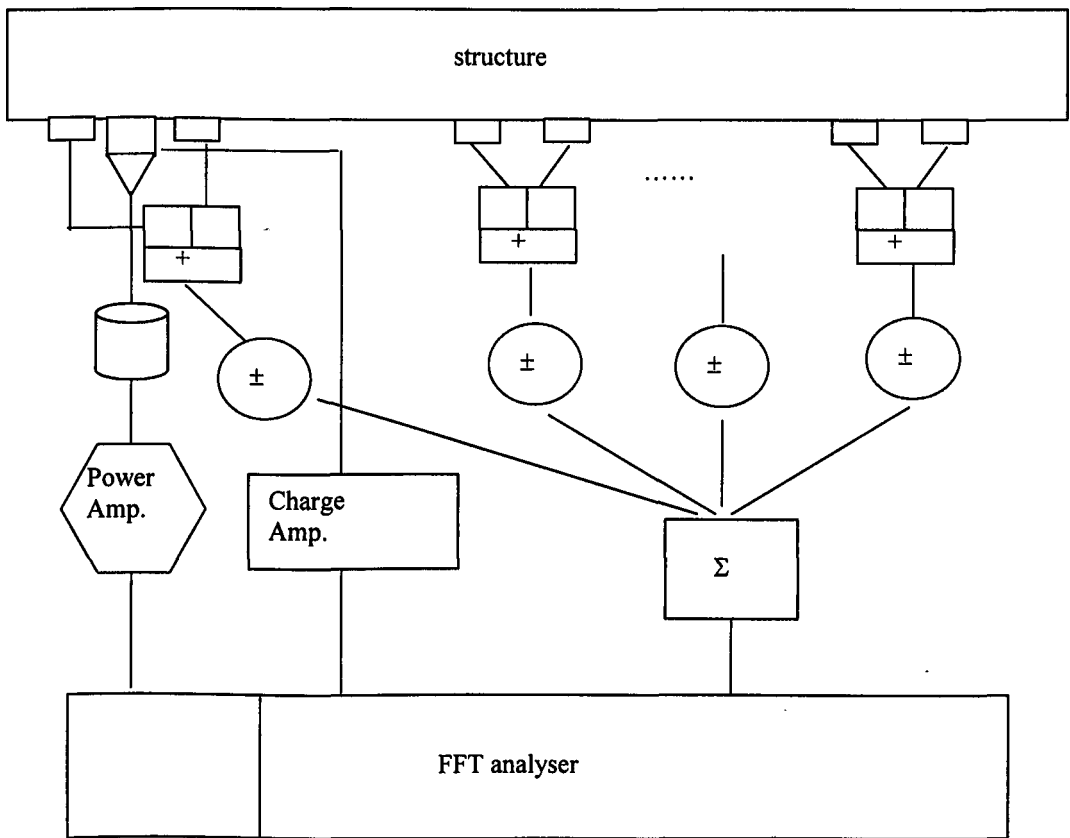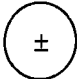
Figure 3-1 Measurement set up for effective mobility (unit magnitude, zero phase force ratios) and polar mobility (symmetric case)
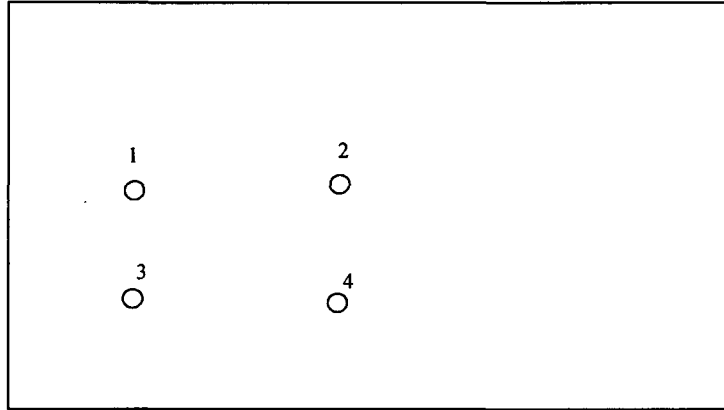
Figure 3-2a A structure excited at four points

$$M_{11}^P = U_1 / P_1 = (\hat{V}_1 + \hat{V}_2 + \hat{V}_3 + \hat{V}_4)/16F$$
$$M_{21}^P = U_2 / P_1 = (\hat{V}_1 + \hat{V}_2 - \hat{V}_3 - \hat{V}_4)/16F$$
$$M_{31}^P = U_3 / P_1 = (\hat{V}_1 - \hat{V}_2 + \hat{V}_3 - \hat{V}_4)/16F$$
$$M_{41}^P = U_4 / P_1 = (\hat{V}_1 - \hat{V}_2 - \hat{V}_3 + \hat{V}_4)/16F$$

$$M_{12}^P = U_1 / P_2 = (\hat{V}_1 + \hat{V}_2 + \hat{V}_3 + \hat{V}_4)/16F$$
$$M_{22}^P = U_2 / P_2 = (\hat{V}_1 + \hat{V}_2 - \hat{V}_3 - \hat{V}_4)/16F$$
$$M_{31}^P = U_3 / P_2 = (\hat{V}_1 - \hat{V}_2 + \hat{V}_3 - \hat{V}_4)/16F$$
$$M_{41}^P = U_4 / P_2 = (\hat{V}_1 - \hat{V}_2 - \hat{V}_3 + \hat{V}_4)/16F$$

$$M_{13}^P = U_1 / P_3 = (\hat{V}_1 + \hat{V}_2 + \hat{V}_3 + \hat{V}_4)/16F$$
$$M_{23}^P = U_2 / P_3 = (\hat{V}_1 + \hat{V}_2 - \hat{V}_3 - \hat{V}_4)/16F$$
$$M_{33}^P = U_3 / P_3 = (\hat{V}_1 - \hat{V}_2 + \hat{V}_3 - \hat{V}_4)/16F$$
$$M_{43}^P = U_4 / P_3 = (\hat{V}_1 - \hat{V}_2 - \hat{V}_3 + \hat{V}_4)/16F$$

$$M_{14}^P = U_1 / P_4 = (\hat{V}_1 + \hat{V}_2 + \hat{V}_3 + \hat{V}_4)/16F$$
$$M_{24}^P = U_2 / P_4 = (\hat{V}_1 + \hat{V}_2 - \hat{V}_3 - \hat{V}_4)/16F$$
$$M_{34}^P = U_3 / P_4 = (\hat{V}_1 - \hat{V}_2 + \hat{V}_3 - \hat{V}_4)/16F$$
$$M_{44}^P = U_3 / P_4 = (\hat{V}_1 - \hat{V}_2 + \hat{V}_3 + \hat{V}_4)/16F$$

Figure 3-2b Force arrangement to obtain the polar mobility matrix
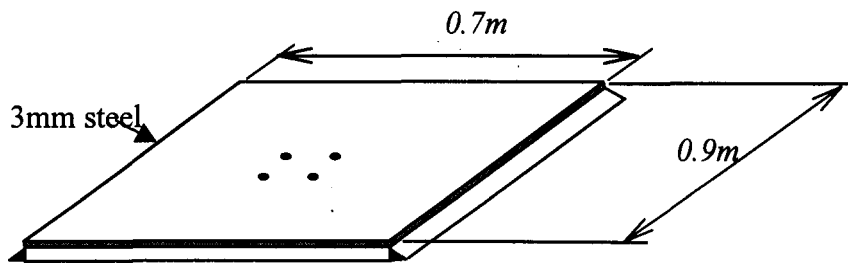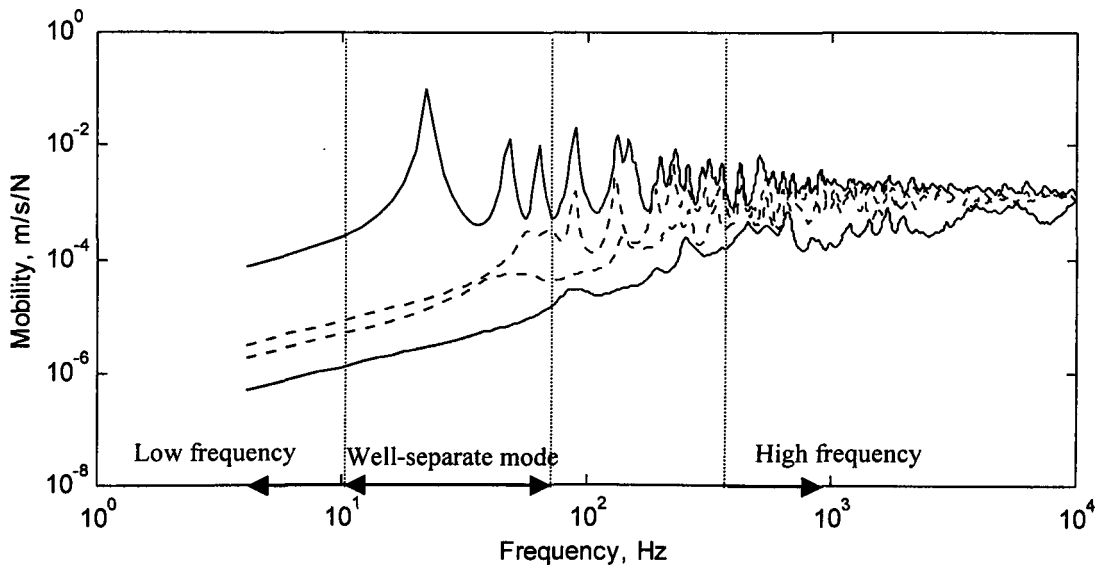
Figure 3-3 Mobility matrix eigenvalues for a simply supported plate
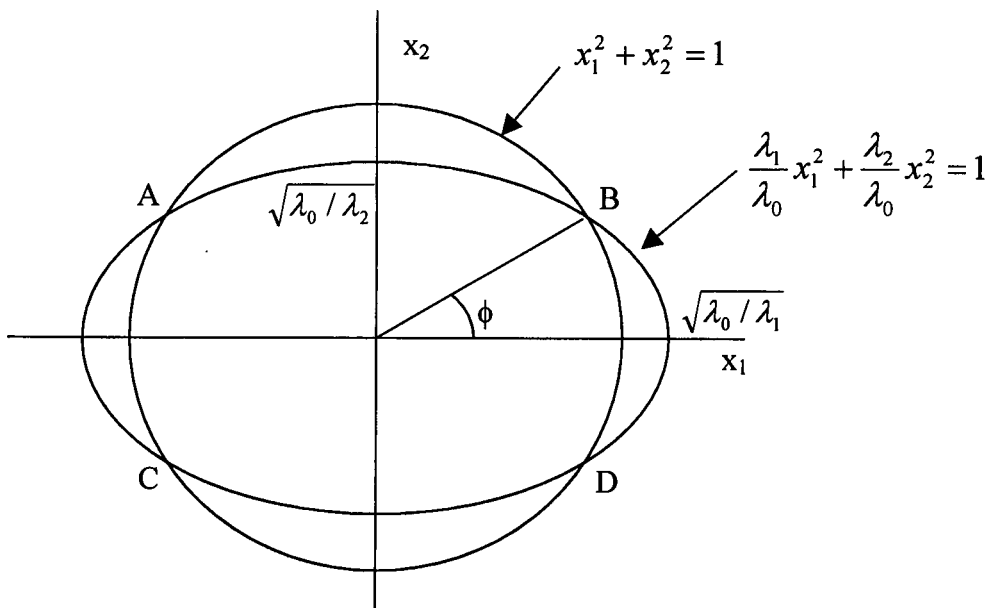
Figure 3-4 Representation of equation 3-36 for 2 contact points
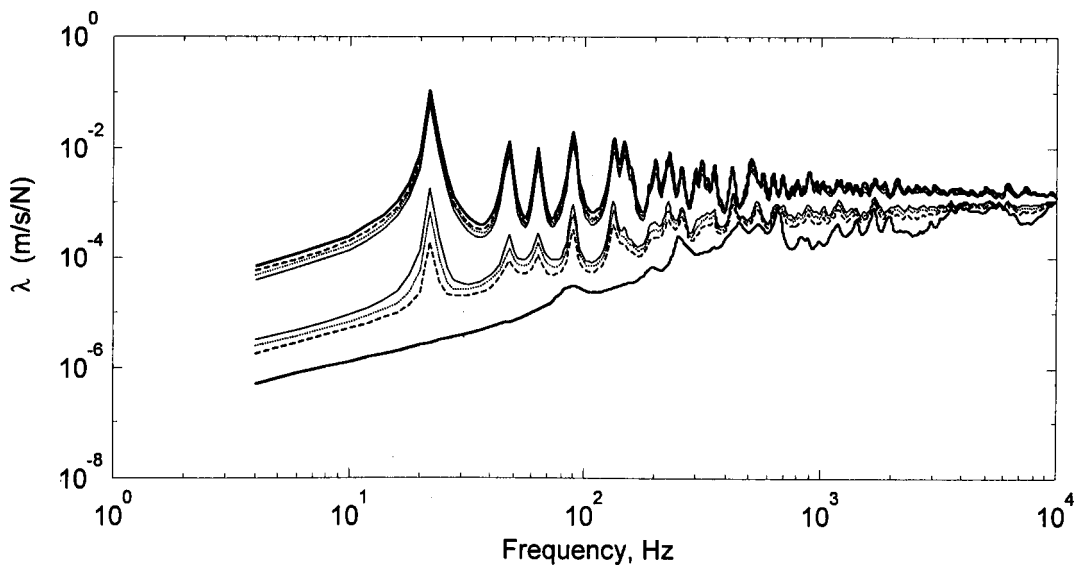
Figure 3-5 Probability bands for the plate illustrated in figure 3-3: ⎯ (dark), max. and min. eigenvalue; --- ,90%; ⎯⎯ , 80%; ⎯ 68%.
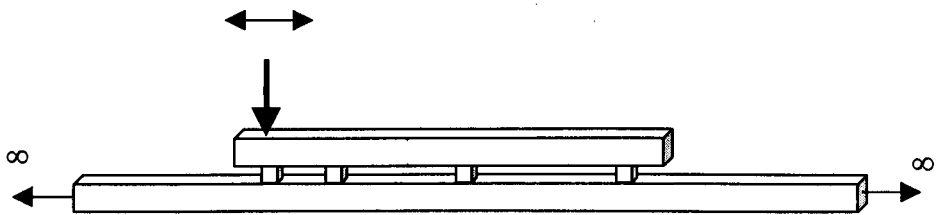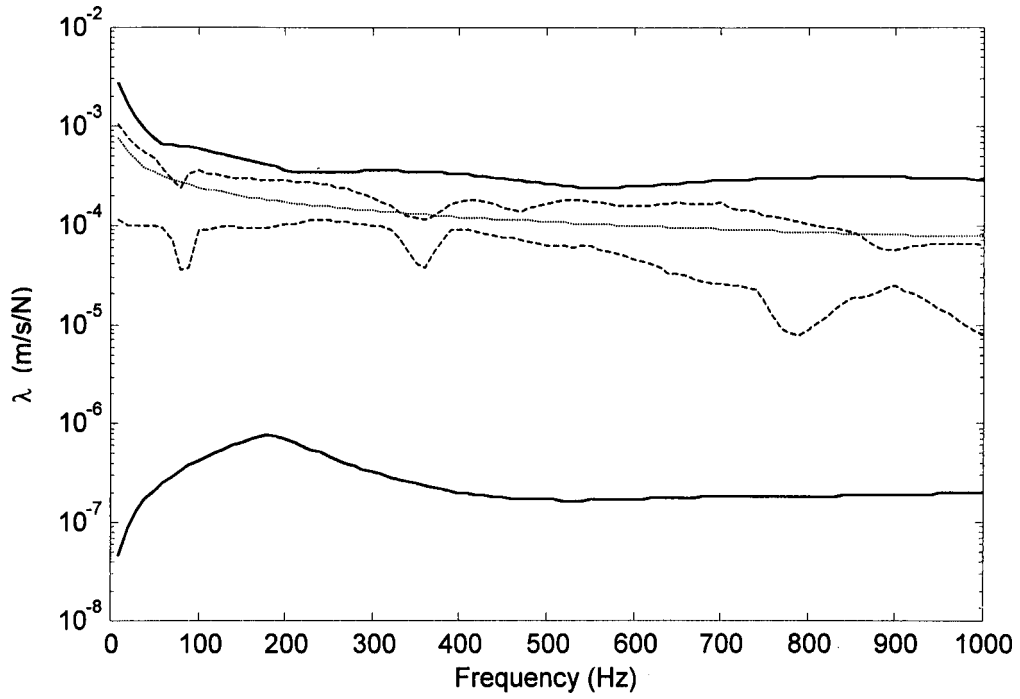
Figure 3- 6 Probability bands for a infinite beam excited by a source beam:----,90%;
·······,mean eigenvalue; —— max. and min. eigenvalue for the infinite beam
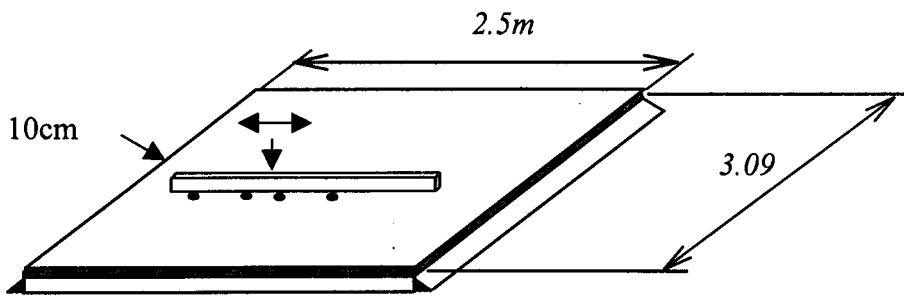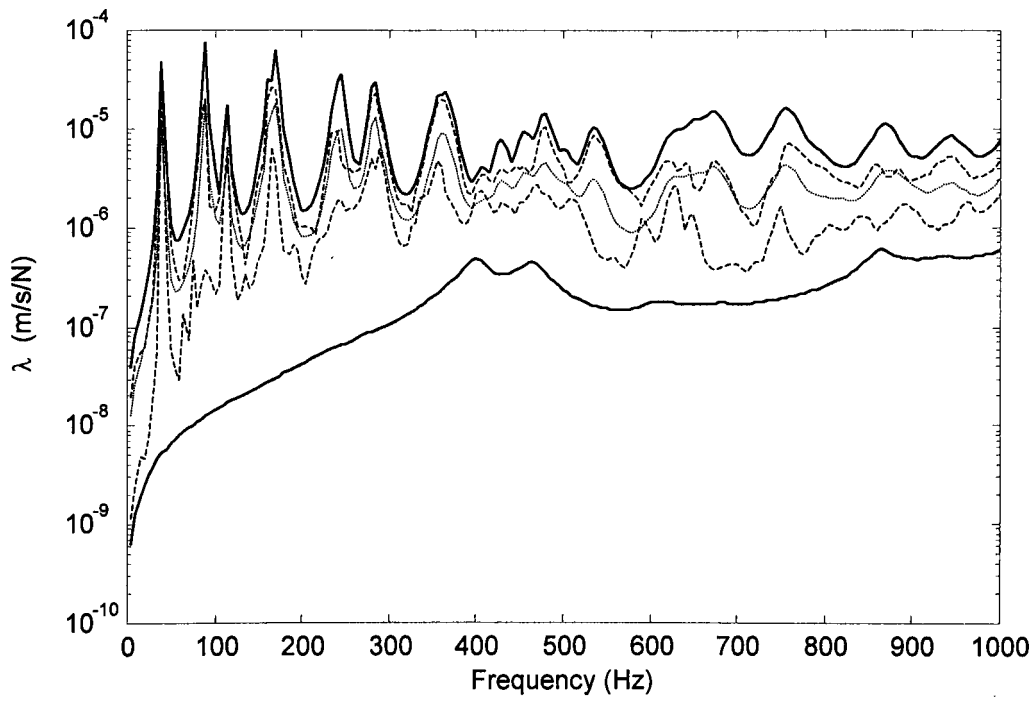
Figure 3-7 Probability bands for a simply supported plate when excited by a source beam: ---- ,90% ; ⋯⋯; meaneigenvalue; — max. and min. eigenvalue for the simply supported plate.

CHAPTER 4

CONSTRUCTION OF GENERIC SOURCES AND RECEIVERS

4.1 Introduction

To obtain the 'general normalised active power band' it is necessary to obtain estimates of emission for a statistically significant number of different sources on a given receiver. A range of source mobilities is required, such that α^Σ covers the required range (from low to high mobility sources), and for each given value of α^Σ enough cases are required to allow the statistical confidence bands to be evaluated. To find a sufficient quantity of data using practical examples is not practicable. A more efficient method of building up the required data is required, so an alternative, non-classical method is proposed here which is now described.

The proposed method is to generate a large quantity of mobility matrices and free velocity vectors at random, and then to select only those which could legitimately belong to a practical structure. For example, the real parts of the diagonal elements of all mobility matrices are positive, so matrices not conforming to this 'rule' are rejected as 'unphysical'. Thus, 'random' is not pure random, since there are inherent properties of practical structures which place constraints on the value that a particular element may take. Five fundamental types of behaviour have been identified for which appropriate constraints (rules) can be developed. These are mass-like, stiffness-like, single mode resonant, off-resonant and quasi infinite (beams or plates). This approach allows us to generate a large number of data sets to represent each of these fundamental types of behaviour. The resulting data sets can be described as 'generic', since if sufficient samples are taken then they represent all possible sources (or receivers) of that type.

It should be appreciated that any structure can be viewed as a combination of these behaviour types occurring over different frequency ranges. Indeed, the idea of 'generic' does not here mean generic to a class of machines, like fans, motors etc, but rather is taken to apply to any machine operating in a frequency range where the behaviour conforms to one of the above types.

Figure 4-1 shows the parameter s_2 (average point mobility magnitude) of a structure illustrating the above five types of behaviour with increasing frequency. f_a is the frequency of the first trough, and for $f < f_a / 2$, the structure can be considered a mass − like structure. f_b is first peak, and for $f_a / 2 < f < f_b / 2$ the structure can be approximately considered stiffness−like. If the peak point is 'sharp' the structure can be considered to approximate a single mode resonant structure. There is no precise definition of 'sharp', but experience suggests that such behaviour is rare in real structures, and a reasonable guide is that the peak should be at least a factor 10^2 greater than the next trough point. f_c is a point at which fluctuations in s_2 due to resonance become insignificant. The usual criterion for the onset of quasi-infinite behaviour is the frequency at which the modal overlap equals unity, but this cannot easily be applied to a measured mobility curve. A practical working measure of this point is when the resonant fluctuations reduce to below approximately 1.0dB. Above this frequency the structure is considered as an infinite (plate) structure. For other frequency ranges not covered above, the structure is considered 'off-resonant'.

In the first part of this chapter we consider the inherent properties of the different types of source and receiver, and derive 'rules' for constructing generic matrices. In the latter part we consider how to construct generic sets of data for source mobility, source free velocity and receiver mobility

4.2 Mass controlled region

At lower frequencies, elements of the mobility matrix for free structures are either in phase or anti-phase, and their magnitude reduces with frequency by $1/\omega$. The behaviour of a source in this frequency region is like a rigid mass, so this type of source is called here a 'mass-like' source. This section does not generally apply to receivers since they are generally fixed rather than free, so a region of mass-like behaviour is not seen.

It is noted for mass-like sources that if one point mobility reduces with frequency by $1/\omega$ then other points must show the same decrease. For example figure 4-2a shows a rigid mass structure, the mobility magnitude at point 1 is different with that at point 2, but they display the same reduction with increasing frequency. Figure 4-2b shows another structure, which is constructed of a rigid body and a thin beam. The mobility magnitude at point 1 reduces with frequency by $1/\omega$, but the relationship of mobility magnitude with frequency at point 2 is not the same. Therefore, figure 4-2b cannot be called a mass-like source. If the proposed contact point 2 be removed to point 2' then it can still be called a mass-like source. For example, figure 4-3b, c shows the mobility of the structure from figure 4-3a at point B and A. The mobility at point B and at point A is given by:

$$y_B = [y_{fb}(B,C1) \quad y_{fb}(B,C2) \quad y_{fb}(B,B)] \left[[Y_{fb} + Y_{rigid}]^{-1} \begin{bmatrix} y_{fb}(B,C1) \\ y_{fb}(B,C2) \\ 1 \end{bmatrix} \right] \quad (4\text{-}1a)$$

$$y_A = [y_{rigid}(A,C1) \quad y_{rigid}(A,C2) \quad y_{rigid}(A,A)] \left[[Y_{fb} + Y_{rigid}]^{-1} \begin{bmatrix} y_{rigid}(B,C1) \\ y_{rigid}(B,C2) \\ 1 \end{bmatrix} \right] \quad (4\text{-}1b)$$

where $y_{fb}(B,C1)$ $y_{fb}(B,C2)$ are the transfer mobilities of the free beam from the drive

point B to C1, C2, and $y_{fb}(B,B)$ is the point mobility of the beam at point B. The

corresponding mobilities for the rigid body are $y_{rigid}(A,C1)$ $y_{rigid}(A,C2)$ $y_{rigid}(A,A)$. Y_{fb} is

the mobility matrix of the free beam for points C1 and C2, and Y_{rigid} the corresponding

matrix of the rigid body. Figure 4-3b, c shows that the structure can be considered mass-

like only up to 3Hz, even though the point mobility at point A has rigid body behaviour

over the whole frequency range. In most cases, real structure–borne sound sources can be

idealised as rigid masses in the lower frequency range.

4.2.1 Generic mobility matrix of a mass-like source

The elements of the mobility matrix of a mass-like source can be given by [44]:

$$Y_{ij} = \frac{1}{j\omega m} (1 + \frac{x_i x_j}{I_{yy}} + \frac{y_i y_j}{I_{xx}}) \quad (4\text{-}2)$$

where Y_{ij} is the point mobility (for $i = j$), and the transfer mobility from the ith point to

the jth point (for $i \neq j$), ω is the excitation frequency, x_i and y_i are the position of ith

point with respect to the centre of gravity and I_{xx} I_{yy} are the moments of inertia around

the x and y axis, respectively.

Introducing the radii of inertia,

$$p_x^2 \equiv \frac{I_{yy}}{m} \qquad (4\text{-}3)$$

$$p_y^2 \equiv \frac{I_{xx}}{m} \qquad (4.\text{-}4)$$

equation (4-2) is rewritten as (4-5)

$$Y_{ij} = \frac{-j}{\omega m}(1 + \frac{x_i x_j}{p_x^2} + \frac{y_i y_j}{p_y^2}). \qquad (4\text{-}5)$$

For the single point case the mobility has no positive imaginary part. For the multi-point

case the mobility still has 'no positive imaginary part', in the sense that every eigenvalue

of the imaginary part of the mobility matrix is non positive. (This result can be used to

check measurement results to determine the frequency range over which the rigid mass

idealisation applies.) This can be proved as follows: for the N point case the mobility

matrix is given by:

$$Y == \frac{-j}{\omega m} A = \frac{-j}{\omega m}(A_1 + A_2 + A_3) \qquad (4\text{-}6)$$

where

$$A_1 = \begin{bmatrix} 1 & \cdots & 1 \\ \vdots & \ddots & \vdots \\ 1 & \cdots & 1 \end{bmatrix} \qquad (4\text{-}7)$$

$$A_2 = \begin{bmatrix} \dfrac{x_1 x_1}{p_x^2} & \cdots & \dfrac{x_1 x_n}{p_x^2} \\ \vdots & \ddots & \vdots \\ \dfrac{x_n x_1}{p_x^2} & \cdots & \dfrac{x_n x_n}{p_x^2} \end{bmatrix} \qquad (4\text{-}8)$$

$$A_3 = \begin{bmatrix} \dfrac{y_1 y_1}{p_y^2} & \cdots & \dfrac{y_1 y_n}{p_y^2} \\ \vdots & \ddots & \vdots \\ \dfrac{y_n y_1}{p_y^2} & \cdots & \dfrac{y_n y_n}{p_y^2} \end{bmatrix} \qquad (4\text{-}9)$$

Equation (4-6) indicates that matrix A is the sum of three matrices, each having unit rank.

The eigenvalues can given by

$$\lambda_1^{A_1} = n \quad \lambda_2^{A_1} = \cdots \lambda_n^{A_1} = 0 \text{ for matrix } A_1 \qquad (4\text{-}10)$$

$$\lambda_1^{A_2} = \frac{x_1 x_1}{p_x^2} + \frac{x_2 x_2}{p_x^2} + \cdots \frac{x_n x_n}{p_x^2} > 0 \quad \lambda_2^{A_2} = \cdots \lambda_3^{A_2} = 0 \text{ for matrix } A_2 \qquad (4\text{-}11)$$

$$\lambda_1^{A_3} = \frac{y_1 y_1}{p_y^2} + \frac{y_2 y_2}{p_y^2} + \cdots \frac{y_n y_n}{p_y^2} > 0 \quad \lambda_2^{A_3} = \cdots \lambda_3^{A_3} = 0 \text{ for matrix } A_3 \qquad (4\text{-}12)$$

This means that for any vector $\phi = (\phi_1, \phi_2, \phi_3)$ the following equation is satisfied:

$$\phi A \phi^T = \lambda_1^{A_1} \left| \varphi_1^{A_1} \right|^2 + \lambda_2^{A_1} \left| \varphi_1^{A_1} \right|^2 + \cdots \lambda_n^{A_1} \left| \varphi_1^{A_1} \right|^2 + \lambda_1^{A_2} \left| \varphi_1^{A_2} \right|^2 + \lambda_2^{A_2} \left| \varphi_1^{A_2} \right|^2 + \cdots \lambda_n^{A_2} \left| \varphi_1^{A_2} \right|^2$$
$$+ \lambda_1^{A_3} \left| \varphi_1^{A_3} \right|^2 + \lambda_2^{A_3} \left| \varphi_1^{A_3} \right|^2 + \cdots \lambda_n^{A_3} \left| \varphi_1^{A_3} \right|^2 \geq 0$$

$$(4\text{-}13)$$

Equation (4-13) indicates that every eigenvalue of matrix A is positive, i.e. the eigenvalues of the imaginary part of the mobility matrix Y (equation 4-5) are non positive in general.

For three points, matrix A is full rank, unless the points are on the same line. The determinant of matrix A will be zero for three collinear points. This result will be used in chapter 5. To prove it here a physical method is considered. Let three forces be applied at the three points. The corresponding velocity at these three points can be given by

$$\begin{pmatrix} v_1 \\ v_2 \\ v_3 \end{pmatrix} = \frac{-j}{\omega m} A \begin{pmatrix} f_1 \\ f_2 \\ f_3 \end{pmatrix} \qquad (4\text{-}14)$$

The net force and moments due to the three forces is given by

$$\begin{aligned}
f_1 + f_2 + f_3 &= F \\
-(f_1 x_1 + f_2 x_2 + f_3 x_3) &= M_y \qquad (4\text{-}15) \\
(f_1 y_1 + f_2 y_2 + f_3 y_3) &= M_x
\end{aligned}$$

and the area of the triangle enclosed by the three points is given by:

$$\Delta = \begin{Vmatrix} 1 & 1 & 1 \\ x_1 & x_2 & x_3 \\ y_1 & y_2 & y_3 \end{Vmatrix} \qquad (4\text{-}16)$$

The area will be zero when the three points lie on one line. In this case there is a non zero solution f_1, f_2, f_3 in equation (4-12) which satisfies:

$$\begin{aligned}
f_1 + f_2 + f_3 &= 0 \\
-(f_1 x_1 + f_2 x_2 + f_3 x_3) &= 0 \qquad (4\text{-}17) \\
(f_1 y_1 + f_2 y_2 + f_3 y_3) &= 0
\end{aligned}$$

This means that the velocity at any point of the rigid body is zero, i.e. the non trivial solution f_1, f_2, f_3 makes the left of equation (4-14) to be zero, so the determinant of A must be zero.

For four points, which is most common, the determinant of A will be zero, i.e at least one of the four eigenvalues will be zero. This result will be used as a check on measurement results: there are always errors in practical measurements, and the minimum eigenvalue of A is likely to be negative even with a very small error, but if more than one eigenvalue is negative, it could be that the error is too large, or that it is unreasonable that the source be idealised as a rigid mass.

4.2.2 Relationships between elements of the matrix (phase and magnitude)

The phase of the point mobility of a rigid body is always $\pi/2$ and the transfer mobility is either $\pi/2$ or $-\pi/2$. The relationship between the magnitudes of the elements is more complex, being dependent on the position and the radius of gyration p_x p_y. Now we introduce two new variables α_i β_i, defined as

$$\alpha_i \equiv \frac{x_i}{p_x} \qquad (4\text{-}18)$$

$$\beta_i \equiv \frac{y_i}{p_y} \qquad (4\text{-}19)$$

For a rigid rectangular body, I_{xx} and I_{yy} are given by

$$I_{xx} = I_{yy} = \frac{m}{12}(L^2 + H^2) \qquad (4\text{-}20)$$

where the L defines the base length and H the height of the body. So p_x and p_y are given by

$$p_x^2 = p_y^2 = \frac{1}{12}(L^2 + H^2) \qquad (4\text{-}21)$$

The point and transfer mobility normalised by $1/j\omega m$ are then given by

$$y_{ij} = 1 + \frac{x_i x_j}{(L^2 + H^2)/12} + \frac{y_i y_j}{(L^2 + H^2)/12} \equiv 1 + \alpha_i \alpha_j + \beta_i \beta_j \qquad (4\text{-}22)$$

where

$$\alpha_i \equiv \frac{x_i}{\sqrt{(L^2 + H^2)/12}} \qquad (4\text{-}23\text{a})$$

$$\alpha_j \equiv \frac{x_j}{\sqrt{(L^2 + H^2)/12}} \qquad (4\text{-}23\text{b})$$

$$\beta_i \equiv \frac{y_i}{\sqrt{(L^2 + H^2)/12}} \qquad (4\text{-}23\text{c})$$

$$\beta_j \equiv \frac{y_j}{\sqrt{(L^2 + H^2)/12}} \qquad (4\text{-}23\text{d})$$

In theory the x_i, x_j, y_i, and y_j can vary in the range of (-L/2~L/2), but in practical cases the centre of gravity is within the area of the polygon enclosed by the contact points.

Consider as an example a four point case (see figure 4-4) where the contact points are located within the following ranges

x_1, x_4	(0 ~L/2)	y_1, y_2	(0~L/2)
x_2, x_3	(0 ~-L/2)	y_3, y_4	(0~-L/2)

Then, α_1 lies within the range $0 \sim \dfrac{\sqrt{3}L}{\sqrt{L^2 + H^2}}$

Setting H=L, α_1 varies in the range $0 \sim \sqrt{3/2}$, and the other parameters can be similarly obtained.

Though the above results are obtained in the case of a rigid rectangular body, the range of the parameter α_i for the other shapes is likely to be similar in practical cases. Consider a practical motor. Here a cylinder or shell model is used to represent the motor.(see figure4-5). The moment of inertia around x and y axes should be somewhere between a solid cylinder and a thin shell. For the cylinder case the moment of inertia around x and y is given by

$$I_{xx} = \frac{1}{2} mR^2 \qquad (4.24)$$

$$I_{yy} = \frac{1}{12} ml^2 + \frac{1}{16} mD^2 \qquad (4\text{-}25)$$

where R are radii , l the length and D the diameter of the cylinder. For the shell model the moment of inertia around x and y is given by

$$I_{xx} = mR^2 \qquad (4\text{-}26)$$

$$I_{yy} = \frac{1}{12} ml^2 + \frac{1}{8} mD^2 . \qquad (4\text{-}27)$$

So we have for the cylinder model

$$\alpha_1 \equiv \frac{x_1}{\sqrt{\frac{1}{12}l^2 + \frac{1}{16}D^2}}$$

$$\beta_1 \equiv \frac{y_1}{\sqrt{\frac{1}{2}R^2}} \qquad (4\text{-}28)$$

For $x_1 \approx 70mm$ $y_1 \approx 60$ $R \approx 60mm$ $l \approx 140mm$ $D = 2R = 120mm$ we get for the cylinder model $\alpha_1 \approx 1.4$, and for the shell model $\alpha_1 \approx 1$ $\beta_1 \approx 1.2$. Similarly we get for the cylinder model $\alpha_2 \approx -1.4$ $\beta_2 \approx 1.4$ $\alpha_3 \approx -1.4$ $\beta_3 \approx -1.4$ $\alpha_4 \approx 1.4$ $\beta_4 \approx -1.4$, and for the shell model $\alpha_2 \approx -1$ $\beta_2 \approx 1.2$, $\alpha_3 \approx -1$ $\beta_3 \approx -1.2$, $\alpha_4 \approx 1$ $\beta_4 \approx -1.2$. So, although the range of variables α_i and β_i can be very large in theory, only the range of $[0 \sim \pm 1.5]$ will be considered for constructing a 'generic' mass-like source mobility, which represents the most common practical cases.

In practical cases, the polygon constructed by the four points often forms a rectangle, so we can always choose a co-ordinate system whose x axis and y axis is parallel with both edges of this rectangle. In this co-ordinate system we have for a rectangle:

$x_1 = x_4$ $x_2 = x_3$ $y_1 = y_2$ $y_4 = y_3$ or $\alpha_1 = \alpha_4, \alpha_2 = \alpha_3, \beta_1 = \beta_2, \beta_4 = \beta_3$.

Therefore, the mobility matrix of many mass–like bodies with four mount points can be given by following expression

$$Y = \frac{1}{j\omega m}\begin{pmatrix} 1+\alpha_1\alpha_1+\beta_1\beta_1 & 1+\alpha_1\alpha_2+\beta_1\beta_2 & 1+\alpha_1\alpha_3+\beta_1\beta_3 & 1+\alpha_1\alpha_4+\beta_1\beta_4 \\ 1+\alpha_1\alpha_2+\beta_1\beta_2 & 1+\alpha_2\alpha_2+\beta_2\beta_2 & 1+\alpha_2\alpha_3+\beta_2\beta_3 & 1+\alpha_2\alpha_4+\beta_2\beta_4 \\ 1+\alpha_1\alpha_3+\beta_1\beta_3 & 1+\alpha_2\alpha_3+\beta_2\beta_3 & 1+\alpha_3\alpha_3+\beta_3\beta_3 & 1+\alpha_3\alpha_4+\beta_3\beta_4 \\ 1+\alpha_1\alpha_4+\beta_1\beta_4 & 1+\alpha_2\alpha_4+\beta_2\beta_4 & 1+\alpha_3\alpha_4+\beta_3\beta_4 & 1+\alpha_4\alpha_4+\beta_4\beta_4 \end{pmatrix}$$

$$= \frac{1}{j\omega m}\begin{pmatrix} 1+\alpha_1\alpha_1+\beta_1\beta_1 & 1+\alpha_1\alpha_3+\beta_1\beta_1 & 1+\alpha_1\alpha_3+\beta_1\beta_3 & 1+\alpha_1\alpha_1+\beta_1\beta_3 \\ 1+\alpha_1\alpha_3+\beta_1\beta_1 & 1+\alpha_3\alpha_3+\beta_2\beta_2 & 1+\alpha_3\alpha_3+\beta_1\beta_3 & 1+\alpha_3\alpha_1+\beta_1\beta_3 \\ 1+\alpha_1\alpha_3+\beta_1\beta_3 & 1+\alpha_3\alpha_3+\beta_1\beta_3 & 1+\alpha_3\alpha_3+\beta_3\beta_3 & 1+\alpha_3\alpha_1+\beta_3\beta_1 \\ 1+\alpha_1\alpha_1+\beta_1\beta_3 & 1+\alpha_3\alpha_1+\beta_1\beta_3 & 1+\alpha_3\alpha_1+\beta_3\beta_1 & 1+\alpha_1\alpha_1+\beta_3\beta_3 \end{pmatrix}$$

(4-29)

4.3 Stiffness-like structures (source and receiver)

At frequencies above the mass regime the mass-like source model cannot be used. However, if the frequency is still not above the first resonance, the source can be model as 'mass+spring', see figure4-6. In this case, the mobility can be expressed as

$$Y = \frac{1}{j\omega M} + \frac{j\omega}{K} \qquad (4\text{-}30)$$

where M is the mass of the machine and K is the local stiffness of the mount footing

It is clear from this equation that the system will experience an anti-resonance at the frequency

$$\omega_0 = \sqrt{\frac{K}{M}}. \qquad (4\text{-}31)$$

Sufficiently below this frequency the mass is dominant (mass-like source) whilst above, the stiffness term will dominate. The point mobility can then be given by

$$Y \approx j\omega/K \quad \text{if } \omega_0 \ll \omega \qquad (4\text{-}32)$$

In this region of frequency the source can be considered as a 'stiffness-like' source. However, it is not enough simply to describe the mobility matrix of the machine. In order to derive generic matrices later we need to know the relationships between the point and transfer mobility in the stiffness controlled range. Hence, the properties of stiffness-like systems are discussed in the following sections (see also[34] for an analyse of stiffness behaviour).

4.3.1 String

The string is not a practical element of most machines, but it is used here to give insight into stiffness-like behaviour, which will be applied to more practical systems later on. Consider a homogeneous string of length l and rigidly supported at both ends (see figure 4-7a). The differential equation for transverse motion of the string under sinusoidal point excitation of angular frequency ω is

$$\frac{\partial^2 w}{\partial x^2} + \frac{\varepsilon \omega^2}{T} w = \frac{-f_0}{T} \delta(x - x_0) \quad (4\text{-}33)$$

where T is the tension of the string, ε is the mass per unit length, x_0 is the excitation co-ordinate. According to equation (4-33) w must be a solution of the homogeneous equation $\frac{\partial^2 w}{\partial x^2} + \frac{\varepsilon \omega^2}{T} w = 0$ for all appropriate values of x except at the point $x=x_0$, where it must have a discontinuity of the slope of $-f_0/T$. It must also satisfy the boundary conditions at the two ends of the string. So the solution for the equation (4-33) can be given by:

$$w = \begin{cases} w_-(x) = A \cos kx + B \sin kx & 0 < x \le x_0 < l \\ w_+(x) = a \cos kx + b \sin kx & 0 < x_0 \le x < l \end{cases} \quad (4\text{-}34)$$

where $k \equiv \omega / c$ is the wave number and $c \equiv \sqrt{\dfrac{T}{\varepsilon}}$ is the speed of wave propagation.

The four as yet unknown quantities (A, B, a, b) can be determined from the force balance at the point $x = x_0$ and the boundary conditions at the two ends, they are

$$w_-(0) = 0 \qquad (4\text{-}35a)$$

$$w_+(l) = 0 \qquad (4\text{-}35b)$$

$$w_-(x_0) = w_+(x_0) \qquad (4\text{-}35\text{ c})$$

$$\frac{\partial}{\partial x} w_+(x_0) - \frac{\partial}{\partial x} w_-(x_0) = -f_0 / T \qquad (4\text{-}35d)$$

Using equation (4-35a)~ (4-35 d) we get the final solution

$$w = \begin{cases} w_-(x) = \dfrac{f_0 k}{T \sin kl} \sin k(l - x_0) \sin kx & 0 < x \le x_0 < l \\[4mm] w_+(x) = \dfrac{f_0 k}{T \sin kl} \sin kx_0 \sin k(l - x) & 0 < x_0 \le x < l \end{cases} \qquad (4\text{-}36)$$

From the above equation we can get the point mobility and transfer mobility from the drive point x_0 to the response point x . They are

$$Y = j\omega \, w / f_0 = \begin{cases} \dfrac{j\omega k}{T \sin kl} \sin k(l - x_0) \sin kx & 0 < x \le x_0 < l \\[4mm] \dfrac{j\omega k}{T \sin kl} \sin kx_0 \sin k(l - x) & 0 < x_0 \le x < l \end{cases} \qquad (4\text{-}37)$$

If $\dfrac{\omega}{c} \to 0$ equation (4-37) simplifies to Equation (4-38)

$$Y = \begin{cases} \dfrac{j\omega}{T}(l - x_0)\dfrac{x}{l} & 0 < x \le x_0 < l \\[4mm] \dfrac{j\omega}{T}\dfrac{x_0}{l}(l - x) & 0 < x_0 \le x < l \end{cases} \qquad (4\text{-}38)$$

In this case the point mobility of the string is of the form of a stiffness controlled mobility

with stiffness $K = \dfrac{Tl}{(l - x_0)x_0}$ (K is independent of excitation frequency). This result give

us the idea that the mobility in the stiffness range can be obtained by using a force with

angular frequency $\omega=0$, i.e. a static force. The static solution for the same string, (see

figure 4-7b) can be solved based on the force balance to get the displacement of the

string:

$$f_0 = T(\sin\alpha + \sin\beta) \approx T(\tan\alpha + \tan\beta)$$
$$= T(\frac{w(x_0)}{x_0} + \frac{w(x_0)}{l - x_0}) \qquad (4\text{-}39)$$

from (4-39) we have got

$$w(x_0) = \frac{f_0}{T}\frac{x_0}{l}(l - x_0) \qquad (4\text{-}40)$$

Further, we can get the displacement at any point on the string

$$w(x) = x\tan\alpha = \frac{f_0}{T}\frac{x}{l}(l - x_0) \quad 0 < x < x_0 < l \qquad (4\text{-}41\text{a})$$

$$w(x) = (l - x)\tan\beta = \frac{f_0}{T}\frac{x_0}{l}(l - x) \quad 0 < x_0 < x < l \qquad (4\text{-}41\text{b})$$

Therefore, we can get the mobility in the stiffness range from the string displacement

equations (4-41a) and (4-41b)

$$Y = j\omega\, w/f_0 = \begin{cases} \dfrac{j\omega}{T}(l - x_0)\dfrac{x}{l} & 0 < x \le x_0 < l \\[4mm] \dfrac{j\omega}{T}\dfrac{x_0}{l}(l - x) & 0 < x_0 \le x < l \end{cases} \qquad (4\text{-}42)$$

The above solution is the same form as equation (4-38). Of course, we can solve equation

(4-33) with boundary condition (4-35) in the case of letting $\omega=0$, and we will get same

results. This shows that the stiffness-controlled mobility can be obtained by solving the static problem, then multiplying the displacement by jω. This idea is applied to beams and plates in the following sections.

4.3.2 Beams

Now we consider a beam (see figure4-8a) simply-simply supported at both ends. According to the above, the static solution can be used in the stiffness range. The differential equation for transverse motion of the beam under sinusoidal point excitation of angular frequency ω=0 is

$$B\frac{\partial^4 w}{\partial x^4} = f_0 \delta(x - x_0) \qquad (4\text{-}43)$$

where B is the bending stiffness. The boundary conditions at both ends and force balance condition at the excitation point $x=x_0$ is given by following equations:

$$w(0) = w(l) = 0$$
$$\left.\frac{\partial^2 w}{\partial x^2}\right|_{x=0} = \left.\frac{\partial^2 w}{\partial x^2}\right|_{x=l} = 0 \qquad (4\text{-}44)$$

$$w(x_0 + 0) - w(x_0 - 0) = 0 \qquad (4\text{-}45\ a)$$

$$\frac{\partial w(x_0 + 0)}{\partial x} - \frac{\partial w(x_0 - 0)}{\partial x} = 0 \qquad (4\text{-}45\ b)$$

$$\frac{\partial^2 w(x_0 + 0)}{\partial x^2} - \frac{\partial^2 w(x_0 - 0)}{\partial x^2} = 0 \qquad (4\text{-}45\ c)$$

$$\frac{\partial^3 w(x_0 + 0)}{\partial x^3} - \frac{\partial^3 w(x_0 - 0)}{\partial x^3} = \frac{-f_0}{B} \qquad (4\text{-}45d)$$

A closed form solution can be obtained:

$$
w = \begin{cases} \dfrac{1}{6Bl} x(l - x_0)[l^2 - x^2 - (l - x_0)^2] & 0 < x < x_0 < l \\[3mm] \dfrac{1}{6Bl} x_0(l - x)[l^2 - x_0^2 - (l - x)^2] & 0 < x_0 < x < l \end{cases} \quad (4\text{-}46)
$$

$$
= \frac{1}{6Bl} g(x, x_0)
$$

$$
g(x_0, x) \equiv \begin{cases} x\,(l - x_0)[l^2 - x^2 - (l - x_0)^2] & 0 < x < x_0 < l \\[3mm] x_0(l - x)[l^2 - x_0^2 - (l - x)^2] & 0 < x_0 < x < l \end{cases} \quad (4\text{-}47)
$$

and the mobility in the stiffness range is hence given by:

$$
Y = j\omega g(x_0, x)/6Bl \qquad (4\text{-}48)
$$

Now, we give an example to support the statement in section 3.4.1 that the condition number of a stiffness-like structure is low no matter how low the frequency. Consider the ratio of point mobility (where the excitation point is at $x_0 = l/8$) and transfer mobility from x_0 to x ($x = l/8$). From equation (4-46) we can get that the ratio is about 3.16. Therefore, no matter how low the frequency, the point mobility does not approximately equal the transfer mobility. In this case, the ratio of maximum to minimum eigenvalue of the mobility matrix for these two points x_0, x is less than 2, not infinite.

From equation (4-46) we know that the transfer mobilities are in phase with the point mobility because the function $g(x_0, x)$ is always real and positive.

This result is intuitively correct. When a simply-simply supported beam is subject to a static force, the displacement at each point on the beam should have the same sign. However, there are some cases where the phase between the point mobility and transfer

mobility is opposite in the stiffness range (see figure(4-8b)). This is a beam free at both ends and simply supported at two other points P and Q. When a static force is applied between P and Q, the displacement on the free ends should have the opposite sign to that at the drive point. So, by the using static force idea, we get the result that point mobility and transfer mobility are in phase or out of phase.

4.3.3 Plate

In many practical cases, the mobility matrix behaviour of the source or receiver is like that of a plate with different boundary conditions. The specifics of the machine or receiver as a whole need not be considered. Although the dynamics of plates has been considered extensively in the literature, the main concern has been with the natural frequencies of the plate rather than the forced response. In the stiffness region the relationship between the point mobility and transfer mobility cannot be expected to be as simple as for a beam. However, the static force idea can be used to establish some rules. Consider a thin orthotropic plate. It is assumed that the plate motion satisfies the equation of the classical theory of thin plate bending. If the transverse force on the plate is harmonic q(x,y)exp(iωt), this equation is:

$$D_1 \frac{\partial^4 w}{\partial x^4} + 2D_3 \frac{\partial^4 w}{\partial x^2 \partial y^2} + D_2 \frac{\partial^4 w}{\partial y^4} - m\omega^2 w = q \quad (4\text{-}49)$$

where w(x,y)exp(iωt) is the transverse displacement of the plate, m is the surface mass, D_1, D_2, D_3 is the corresponding rigidity of the plate and given by $D_{1,2} = \dfrac{E_{1,2}h^3}{12(1 - v_1 v_2)}$,

$D_3 = D_{12} + 2D_k$, $D_{12} = D_1 v_2 = D_2 v1$ $D_k = Gh^3/12$, in which $E_{1,2}$ is Young 's modulus,

$v_{1,2}$ the Poisson's ratio, h the plate thickness and G the shear modulus.

It is common that the plate is isotropic, so equation (4-49) can be rewritten as equation (4-50)

$$D(\frac{\partial^4 w}{\partial x^4} + 2\frac{\partial^4 w}{\partial x^2 \partial y^2} + \frac{\partial^4 w}{\partial y^4}) - m\omega^2 w = q \qquad (4\text{-}50)$$

A solution for the forced motion of the plate is obtained by both equation (4-51) and the prescribed boundary conditions. For completeness the well-known classical boundary conditions are repeated here: at an edge x=a:

1)clamped

$w = 0$

$$\frac{\partial w}{\partial x} = 0 \qquad (4\text{-}51)$$

2) simply supported

$w = 0$

$$\frac{\partial^2 w}{\partial x^2} = 0 \qquad (4\text{-}52)$$

3)free

$$\frac{\partial^2 w}{\partial x^2} + v\frac{\partial^2 w}{\partial y^2} = 0 \qquad (4\text{-}53)$$

$$\frac{\partial^3 w}{\partial x^3} + (2-v)\frac{\partial^2 w}{\partial y^2} = 0 \qquad (4\text{-}54)$$

An exact solution of the wave equation can only be obtained in a plate where at least one pair of opposite edges is simply supported. Nevertheless, we can obtain useful information about the stiffness region despite this restriction.

The solution for equation (4-50) can be expressed in the following form:

$$Y = \frac{j\omega}{M} \sum_{n=1}^{\infty} \frac{\phi_n(r)\phi_n(r_0)}{\overline{\omega}_n^2 - \omega^2} \quad (4\text{-}55)$$

where ϕ_n is the nth mode function, (a real function), r and r_0 are the drive point and response point respectively, M is the total mass of the plate and $\overline{\omega}_n^2 = \omega_n^2(1 + j\eta)$ is the square of the complex natural frequency for mode n with loss factor η, and ω is the angular frequency of the driving force. Letting $\omega^2 \to 0$ and we can get the mobility in the stiffness range:

$$Y = \frac{j\omega}{M} \sum_{n=1}^{\infty} \frac{\phi_n(r)\phi_n(r_0)}{\overline{\omega}_n^2} = \frac{j\omega}{M(1+j\eta)} \sum_{n=1}^{\infty} \frac{\phi_n(r)\phi_n(r_0)}{\omega_n^2} = \frac{j\omega}{M(1+j\eta)} g(r,r_0) \quad (4\text{-}56)$$

$$g(r,r_0) \equiv \sum_{n=0}^{\infty} \frac{\phi_n(r)\phi_n(r_0)}{\omega_n^2} \quad (4\text{-}57)$$

The function $g(r,r_0)$ cannot be obtained in most cases, but despite this we still can deduce the following useful properties pertaining to the stiffness region.

a. $g(r,r_0)$ is a real function because the mode function and the ω_n are real

b. when $g(r,r_0)$ is positive the transfer mobility will be in phase with the point mobility and if $g(r,r_0)$ is negative, they will be of opposite phase

c. the real part of the mobility matrix is the same as the imaginary part except for a positive constant multiplier

d. every eigenvalue of the real part of the matrix must be positive, so every eigenvalue of the imaginary part of the matrix is positive too. Note that for the single point case the stiffness mobility has a positive imaginary part, and for the multi-point case it also has a 'positive imaginary part', even if some transfer mobilities are negative. This contrasts with the mass case where all eigenvalues were non positive.

We can also deduce that in the following cases the mobility will be inversely proportional with the rigidity of the plate D in the stiffness range:

i) the plate is simply supported on all four edges

ii) the plate is clamped on all four edges

iii) the plate is simply supported on the some edges and clamped on the remaining edges.

This can be shown using the static force idea, from which the mobility in the stiffness region can be given by:

$$Y = j\omega w'$$

where w' is static displacement per unit force which satisfies equation (4-58)

$$D(\frac{\partial^4 w'}{\partial x^4} + 2\frac{\partial^4 w'}{\partial x^2 \partial y^2} + \frac{\partial^4 w'}{\partial y^4}) = \delta(x - x_0)\delta(y - y_0) \quad (4\text{-}58)$$

and boundary conditions i) or ii) or iii). The boundary conditions i) ii) iii) are independent of the rigidity of the plate D, so it is easy to understand from equation (4-56) that the static displacement w' should be inversely proportional to the rigidity of the plate D. This relationship does not strictly apply if some edges are free, because the free boundary condition contains Poisson's ratio v which concerns rigidity of the plate D. However, it

still can be said that the mobility is inversely proportional to the third power of plate thickness and Youngs modulus E. An example is now given

The rectangle OABC (see fig 4.9) is a S-S-F-F plate. When the driving force f_0 is applied at point B, the static displacement at point P (x,y) can be given by [45]

$$w' = \frac{f_0 xy}{2(1-v)D}, \quad (4-59)$$

so the mobility in the stiffness range can be expressed as:

$$Y = \frac{j\omega xy}{2(1-v)D} = \frac{6j\omega xy(1+v)}{Eh^3}. \quad (4-60)$$

When D is increased with an increase of Poisson ratio v, the mobility also increases. Therefore, the mobility is no longer inversely proportional to the rigidity of the plate D.

4.4 Single mode resonant structure (source and receiver)

The mobility of any continuous structure can be given by the modal expansion;

$$Y_{ij} = \frac{j\omega}{M} \sum_{n=1}^{\infty} \frac{\phi_n(x_i)\phi_n(x_j)}{\omega_n^2(1+\eta j) - \omega^2} \quad (4-61)$$

In the case of $\omega = \omega_n$ the system is resonant, and if ω_n is well away from other natural frequencies, is not large and the loss factor η is small, then equation (4-61) can be approximated by equation (4-62)

$$Y_{ij} \approx \frac{1}{M} \frac{\phi_n(x_i)\phi_n(x_j)}{\eta\omega_n} \quad (4-62)$$

The mobility matrix for m points can then be written as:

$$[Y] \approx \frac{1}{M\eta\omega_n} \begin{bmatrix} \phi_n(x_1)\phi_n(x_1) & \phi_n(x_i)\phi_n(x_j) & \cdots & \phi_n(x_1)\phi_n(x_m) \\ \phi_n(x_2)\phi_n(x_1) & \phi_n(x_2)\phi_n(x_2) & \cdots & \phi_n(x_2)\phi_n(x_m) \\ \vdots & & & \\ \phi_n(x_m)\phi_n(x_1) & \phi_n(r_m)\phi_n(x_2) & & \phi_n(x_m)\phi_n(x_m) \end{bmatrix} \quad (4\text{-}63)$$

The mobility matrix in equation (4-61) has a rank of unity. This kind of resonance is here called a 'single mode' (or 'idealised') resonance. For a system with low loss factor, its mobility matrix can be approximated as equation (4-63) at the first few resonant peaks.

4.5 Off-resonant structure (source and receiver)

The above idealised model applies only at, or very close to the resonance peaks. However, most of the frequency range is 'between peaks', where the response is due to several modes, and the simple single mode model described above does not apply. At these frequencies the structure is here called an 'off-resonant' structure. The same label can be used at higher frequencies where individual resonances are no longer distinct. Off-resonant behaviour is characterised by 'weaker' relationships between the elements of the mobility matrix than for all the previous idealised cases. The elements are not limited by particular equations or rules, so have more a random character.

The same can be said to apply in the transition regions between mass-like behaviour, stiffness-like behaviour and the first isolated resonance peaks. Thus, these regions will also be categorised as 'off-resonant'. Hence, within the context of constructing generic mobility matrices, 'off-resonant' behaviour is seen to occupy much of the frequency range.

4.6 Infinite plate receiver

The mobility of an infinite plate is a useful tool for approximate modelling of damped or large building structures. Using polar co-ordinates the infinite plate mobility can be written

$$Y_{ij} = Y_\infty (H_0^{(2)}(kr_{ij}) - H_0^{(2)}(-jkr_{ij})) \qquad (4\text{-}64)$$

where $k = \omega^2 m''/D$ is the wave number, ($D = Eh^3/12(1-v^2)$) is the bending stiffness and m'' is the mass per unit area, $Y_\infty = 8\sqrt{Dm''}$ is the characteristic mobility and H_0^2 is a Hankel function of the second order. The relationship between the Hankel function and the Bessel function of the first and second kind (Neuman) function is :

$$H_0^{(2)}(z) = J_0(z) - jN_0(z)$$

Asymptotic values of the mobility can be used to give:

$$Y_{ij} = Y_\infty (H_0^{(2)}(kr_{ij}) - H_0^{(2)}(-jkr_{ij})$$

$$\rightarrow Y_\infty \sqrt{\frac{2}{\pi kr_{ij}}} e^{-j(kr-\pi/4)} \quad when \quad kr \rightarrow \infty$$

$$\rightarrow Y_\infty \left\{ 1 - \frac{1}{4}(kr_{ij})^2 - \frac{j}{\pi}(kr_{ij})^2 - \frac{j}{\pi}(kr_{ij})^2[\ln kr_{ij} - (\ln 2 - \delta\gamma)] \right\} \quad kr \rightarrow 0$$

where $\delta\gamma$ is the Euler number, given by

$$\delta\gamma = 1 + 1/2 + \cdots + 1/k - \ln k \quad k \rightarrow \infty.$$

The magnitude of the function $(H_0^{(2)}(kr_{ij}) - H_0^{(2)}(-jkr_{ij}))$ is less than unity and decreases with kr_{ij} .(see fig(4.8)), so the mobility matrix for m points can be expressed as:

$$[Y] = \frac{1}{8\sqrt{Dm''}} \begin{bmatrix} 1 & H_0^{(2)}(kr_{12}) - H_0^{(2)}(-jkr_{12}) & \cdots & H_0^{(2)}(kr_{1m}) - H_0^{(2)}(-jkr_{1m}) \\ H_0^{(2)}(kr_{21}) - H_0^{(2)}(-jkr_{21}) & 1 & & \\ \vdots & & \ddots & \\ H_0^{(2)}(kr_{m1}) - H_0^{(2)}(-jkr_{m1}) & & & 1 \end{bmatrix}$$

$$(4\text{-}65)$$

4.7 Semi-infinite plate

The free edge of a semi-infinite plate is an important case to describe sources. However, it was found that the only existing solutions were given in terms of unsolved integrals [46-47]. In order to facilitate development of rules for generic matrices the author has solved some of these integrals and presented a closed form solution for the case of a free edge. This is presented in reference [48] and is given in a more expanded form with some discussion in appendix B. These solutions are not specifically used in the following, although the details are given for reference.

4.8 Source free velocity

Free velocity data is needed to obtain the general normalised active power band. The definition of free velocity was stated in Chapter 2. The free velocity which corresponds to the above types of source structures is addressed in this section.

4.8.1 Free velocity for mass –like source

In the mass controlled region the machine is as a rigid body. The free velocity at mount point i can be written as

$$\hat{V}_{sf,i} = \hat{V}_{sf,i}^1 + \hat{V}_{sf,i}^2 + \hat{V}_{sf,i}^3 \quad (4\text{-}66)$$

where $\hat{V}_{sf,i}^1$ is the contribution of the translation of the rigid body, $\hat{V}_{sf,i}^2$ and $\hat{V}_{sf,i}^3$ are the contributions of rotations about the x and y axis respectively. The phase relationship is (for the four point case considered in figure 4-4)

$$\theta\,(\hat{V}_{sf,1}^1) = \theta\,(\hat{V}_{sf,2}^1) = \theta\,(\hat{V}_{sf,3}^1) = \theta\,(\hat{V}_{sf,4}^1) \quad (4\text{-}67)$$

$$\theta\,(\hat{V}_{sf,1}^2) = \theta\,(\hat{V}_{sf,2}^2) \qquad\qquad (4\text{-}68a)$$

$$\theta\,(\hat{V}_{sf,1}^2) = \theta\,(\hat{V}_{sf,3}^2) \pm \pi \qquad\qquad (4\text{-}68b)$$

$$\theta\,(\hat{V}_{sf,3}^2) = \theta\,(\hat{V}_{sf,4}^2) \qquad\qquad (4\text{-}68c)$$

$$\theta\,(\hat{V}_{sf,1}^3) = \theta\,(\hat{V}_{sf,4}^3) \qquad\qquad (4\text{-}69a)$$

$$\theta\,(\hat{V}_{sf,1}^3) = \theta\,(\hat{V}_{sf,3}^3) \pm \pi \qquad\qquad (4\text{-}69b)$$

$$\theta\,(\hat{V}_{sf,2}^3) = \theta\,(\hat{V}_{sf,3}^3) \qquad\qquad (4\text{-}69c)$$

If the free velocity is only due to an internal force f_0, this can be decomposed into a force f_e, applied at the centre of gravity, a moment about the x axis, m_x and a moment about the y axis, m_y. Here, the force f_e is either in phase with the moment or of opposite phase. In this case the phase of the free velocity between the two mounts is either in phase or opposite phase. However, if the free velocity is due to many internal forces or moments and their phase relationship is complex, then the phase of the free velocity between two mounts may be neither in phase nor anti-phase. This result may be not recognized in some reference literature [34]. Consider a simple example. The force at the drive point is shown in figure 4-10. The phase of these two forces is different and given by:

$$f_1 = f_0 e^{j\omega t}$$

$$f_2 = f_0 e^{j\omega t + \pi/3}$$

The resulting velocities at points 1 and 2 are then

$$\hat{V}_{sf,1} = \frac{f_0}{j\omega M} (2\cos(\pi/6)e^{j\pi/6} + 2\sin(\pi/6)\frac{ab}{I/M}e^{j2\pi/3})e^{j\omega t} \quad (4\text{-}70)$$

$$\hat{V}_{sf,2} = \frac{f_0}{j\omega M} (2\cos(\pi/6)e^{j\pi/6} - 2\sin(\pi/6)\frac{ab}{I/M}e^{j2\pi/3})e^{j\omega t} \quad (4\text{-}71)$$

where M is the mass of the rigid body and I its moment of inertia. The relative phase is

$$\theta(\hat{V}_{sf,1}) - \theta(\hat{V}_{sf,2}) = \tan^{-1}(\frac{\cos(\pi/6)e^{j\pi/6} + \sin(\pi/6)\dfrac{ab}{I/M}e^{j2\pi/3}}{\cos(\pi/6)e^{j\pi/6} - \sin(\pi/6)\dfrac{ab}{I/M}e^{j2\pi/3}}) \quad (4\text{-}72)$$

It is clear, these two points are neither in phase nor opposed phase.

The relationship of the velocity magnitude among the mount points is complicated. It is dependent on the internal force distribution of the machine source, on the structure of the machine and on the position of the mount points. However, there are still some relationships due to the fact that the determinant of the mobility matrix of the four points is zero. This means that one row of the matrix can be linearly expressed by the other three rows. For example, if the fourth row can be expressed as:

$$\begin{pmatrix} Y_{41} & Y_{42} & Y_{43} & Y_{44} \end{pmatrix} = a_1\begin{pmatrix} Y_{11} & Y_{12} & Y_{13} & Y_{14} \end{pmatrix} + a_2\begin{pmatrix} Y_{21} & Y_{22} & Y_{23} & Y_{24} \end{pmatrix} + a_3\begin{pmatrix} Y_{31} & Y_{32} & Y_{33} & Y_{34} \end{pmatrix} \quad , (4\text{-}73)$$

then the free velocity $\hat{V}_{sf,4}$ can be expressed as:

$$\hat{V}_{sf,4} = a_1\hat{V}_{sf,1} + a_2\hat{V}_{sf,2} + a_3\hat{V}_{sf,3} \quad (4\text{-}74)$$

Hence, the free velocity of the four mount points is not independent. A common example is of four points at the corners of a rectangle, then $a_1 = 1 \quad a_2 = -1 \quad a_3 = 1$ i.e.

$$\hat{V}_{sf,4} + \hat{V}_{sf,2} = \hat{V}_{sf,1} + \hat{V}_{sf,3} \qquad (4\text{-}75)$$

4.8.2 Free velocity for stiffness source

In the stiffness controlled region the machine no longer moves as a mass controlled source and wave behaviour çan occur within the machine structure. As such both the magnitude and phase of the free velocity are dependant upon the details of the machine. The magnitude and phase relationships between the elements of the velocity vector cannot be limited by some generic equation or rule.

4.8.3 Free velocity for off-resonant source

Like the stiffness source, the wave behaviour in the off-resonant source dictates that generalised magnitude and phase relationship between the elements of the velocity vector cannot be determined

4.8.4 Free velocity for single mode resonant source

The mobility can be written as

$$Y_{ij} \approx \frac{1}{M} \frac{\phi_n(x_i)\phi_n(x_j)}{\eta\omega_n} \qquad (4\text{-}76)$$

so if the internal forces $F_{0,1}, F_{0,2}, \cdots F_{0,k}$, are applied at the points $x_{0,1}, x_{0,2} \cdots x_{0,k}$ respectively, then the free velocity at point j can be expressed as

$$\hat{V}_{fs,j} \approx \frac{\phi_n(x_j)}{M\eta\omega_n}(\hat{F}_{0,1}\phi_n(x_{0,1}) + \hat{F}_{0,2}\phi_n(x_{0,1}) + \cdots \hat{F}_{0,k}\phi_n(x_{0,1})) \qquad (4\text{-}77)$$

and the free velocity vector can be given by

$$[\hat{V}_{fs}] \approx \frac{1}{M\eta\omega_n}(\hat{F}_{0,1}\phi_n(x_{0,1}) + \hat{F}_{0,2}\phi_n(x_{0,1}) + \cdots \hat{F}_{0,k}\phi_n(x_{0,1}))\begin{bmatrix}\phi_n(x_1)\\\phi_n(x_2)\\\\\phi_n(x_m)\end{bmatrix} \quad (4\text{-}78)$$

4.9 Construction of the generic source and receiver data

Having outlined the different types of behaviour in the source and receiver structures, we are now in a position to construct 'generic' sources and receivers.

4.9.1 Sources

4.9.1.1 Construction of mass-like source mobility

An expression for the mobility matrix of mass-like sources for four points is given by equation 4-29 which can be rewritten as the following expression:

$$Y = A_s\chi[y] \quad\quad (4\text{-}79\ a)$$

where $[y]$ is

$$[y] = (\begin{bmatrix}1\\1\\1\\1\end{bmatrix}\begin{bmatrix}1 & 1 & 1 & 1\end{bmatrix} + \begin{bmatrix}\alpha_1\\\alpha_2\\\alpha_3\\\alpha_4\end{bmatrix}\begin{bmatrix}\alpha_1 & \alpha_2 & \alpha_3 & \alpha_4\end{bmatrix} + \begin{bmatrix}\beta_1\\\beta_2\\\beta_3\\\beta_4\end{bmatrix}\begin{bmatrix}\beta_1 & \beta_2 & \beta_3 & \beta_4\end{bmatrix}) \quad (4\text{-}79b)$$

and is called the basic matrix. $\chi = -j$ is called the 'type factor', because it depends on the type of structure as will be seen later. A_s is a real number (here the author has named it the size factor). α_i and β_i depend upon

i) the positions of the contact points,

ii) the radii of inertia around the x and y axis.

According to the results of section 4.2, for practical cases, the magnitude of α_i, β_i is limited to the range 0~1.5. For a general mass–like source it is simply suggested therefore that a statistical description be made by assuming that the corresponding variables $\alpha_1, \beta_1 \beta_2 \alpha_4$ have a uniform distribution in the range of 0~1.5 and, α_2, $\alpha_3, \beta_3, \beta_4$ have a uniform distribution in the range of $0 \sim -1.5$.

Furthermore, if the polygon constructed by the four contact points is a rectangle, $\alpha_1 = \alpha_4 \; \alpha_2 = \alpha_3 \; \beta_1 = \beta_2 \; \beta_4 = \beta_3$ so there only four independent terms.

4.9.1.2 Off-resonant source mobility

The relationship between the elements of the mobility matrix for an off-resonant source are 'weak'. The mobility matrix can be expressed as

$$[Y] = A_s \chi [y] \qquad (4\text{-}80)$$

where A_s is the mean value of the magnitude of each element of the mobility matrix (here it is still called the size factor). $\chi = 1$ is again called the type factor. $[y]$ is the normalised mobility matrix, here also called the 'basic matrix'. According to the results of Fulford [34], the magnitude distribution of the elements of the mobility matrix is a log10normal distribution, i.e. $z_{ij} = \log 10 |y_{ij}(x_i, x_j)|$ is a normal distribution (z_{ij} is a log10 function of the magnitude of y_{ij}). If so, the following approximation for the standard deviation of z_{ij}, (σ), applies [49]

$$\sigma \approx \frac{z_{max} - z_{min}}{\sqrt{N}} = \log 10 \left| \frac{y_{max}}{y_{min}} \right| / \sqrt{N} \qquad \text{(4-81a)}$$

Figure 4-11 shows the results of σ calculated from measured mobilities of a typical fan. The solid line represents equation (4-81a) and the dashed line is obtained from equation (4-81b)

$$\sigma' = \sqrt{\sum_{j=1}^{N} (z_j - \bar{z})^2 \Big/ N - 1} \,. \qquad \text{(4-81b)}$$

The two lines are close. This result provides some evidence that it is reliable to assume z to have a normal distribution. Secondly, figure 4-11 shows that σ is less than 0.85 for this typical structure. Fulford plotted the value of Y_{max} / Y_{min} (it equals y_{max} / y_{min}) for some practical fans, and found a similar range of the standard deviation. So it is assumed that, for off-resonant sources, $\log 10|y|$ has normal distribution with a mean zero and a standard deviation in the range of 0~0.85, and that the phase has a uniform distribution in the range of $-\pi/2 \sim \pi/2$ for diagonal elements (the real part of diagonal elements must be positive) and 0~2π for off-diagonal elements.

4.9.1. 3 Stiffness source mobility

The mobility of a stiffness like structure is given by equation (4-56). It can be rewritten as the following expression:

$$Y_{ij} = \frac{j}{M\omega(1+\eta j)} \sum_{n=1}^{\infty} \frac{\phi_n(x_i)\phi_n(x_j)}{\omega_n^2 / \omega^2} \qquad \text{(4-82a)}$$
$$= A_s y_{ij}(x_i, x_j) e^{j(\pi/2 - Arctg\eta)}$$

The mobility matrix is now expressed as :

$$[Y] = A_s \chi[y] \qquad (4\text{-}82\text{b})$$

Similar to the off-resonant source, the 'size factor' A_s is the mean value of the magnitude of each element of mobility matrix. $\chi = e^{j(\pi/2 - Arctg\eta)}$ is again the type factor and $[y]$ is the normalised mobility matrix (or 'basic matrix'). It is further assumed that for stiffness sources y_{ij} has zero phase and $\log 10 |y|$ has a normal distribution with a mean zero and a standard deviation in the range of 0~0.85.

4.9.1. 4 Single mode resonant source mobility

The mobility of a resonant structure is given by equation (4-63). It can be rewritten as the following expression:

$$Y \approx A_s \chi[y] \qquad (4\text{-}83\ a)$$

where the basic matrix in this case is

$$[y] = \begin{bmatrix} \phi_n(x_1) \\ \phi_n(x_2) \\ \vdots \\ \phi_n(x_m) \end{bmatrix} [\phi_n(x_1) \quad \phi_n(x_2) \quad \cdots \quad \phi_n(x_m)] \qquad (4\text{-}83\text{b})$$

A_s is a real number (still called size factor) and the type factor $\chi = 1$.

Here it is assumed that the real numbers $\phi_n(x_i)$ have a log10normal magnitude distribution, i.e. $\log 10 |\phi_n|$ has a normal distribution with a mean zero (assumed to have been normalised) and a standard deviation in the range of 0~0.85.

To summarise section 4.8.1, for any type of source the mobility is written as $A_s \chi_s [y_s]$.

$[y_s]$ will be constructed by random functions within certain constraints which have been

defined for each structural type. Two numbers still need to be determined, A_s and, for

stiffness sources, the loss factor η. This will be addressed in chapter5.

4.9.2 Construction of the Free velocity vector

4.9.2.1 Mass source

For mass-like sources the free velocity depends on the internal force distribution. The

free velocity vector can be written as

$$[\hat{V}] = -\frac{j}{\omega M}(\hat{l}_1 \begin{bmatrix} 1 \\ 1 \\ 1 \\ 1 \end{bmatrix} + \hat{l}_2 \begin{bmatrix} \alpha_1 \\ \alpha_2 \\ \alpha_3 \\ \alpha_4 \end{bmatrix} + \hat{l}_3 \begin{bmatrix} \beta_1 \\ \beta_2 \\ \beta_3 \\ \beta_4 \end{bmatrix}) \qquad (4\text{-}84)$$

where

$$\hat{l}_1 = \hat{f}_1 + \hat{f}_2 + \cdots \hat{f}_{ek}, \hat{l}_2 = \hat{f}_1\alpha_{e,1} + \hat{f}_2\alpha_{e,2} + \cdots \hat{f}_k\alpha_{e,k}, \hat{l}_3 = \hat{f}_1\beta_{e,1} + \hat{f}_2\beta_{e,2} + \cdots \hat{f}_k\beta_{e,k}$$

in where $\hat{f}_i$ is the ith internal force , $\alpha_{e,i} = x_{e,i}/p_x$, $\beta_{e,i} = y_{e,i}/p_y$, $x_{e,i}$, $y_{e,i}$ are co-ordinates

of the ith internal force .

Equation (4-84) can be rewritten as (4-85a)

$$[\hat{V}] = -\frac{j}{\omega M}(|\hat{l}_1| + |\hat{l}_1| + |\hat{l}_1|) \ (\hat{k}_1 \begin{bmatrix} 1 \\ 1 \\ 1 \\ 1 \end{bmatrix} + \hat{k}_2 \begin{bmatrix} \alpha_1 \\ \alpha_2 \\ \alpha_3 \\ \alpha_4 \end{bmatrix} + \hat{k}_3 \begin{bmatrix} \beta_1 \\ \beta_2 \\ \beta_3 \\ \beta_4 \end{bmatrix}) = -j|\hat{V}_0|[v] \quad (4\text{-}85a)$$

where $|\hat{V}_0| = \frac{1}{\omega M}(|\hat{l}_1| + |\hat{l}_1| + |\hat{l}_1|)$ is a real number and

$$[v] = (\hat{k}_1 \begin{bmatrix} 1 \\ 1 \\ 1 \\ 1 \end{bmatrix} + \hat{k}_2 \begin{bmatrix} \alpha_1 \\ \alpha_2 \\ \alpha_3 \\ \alpha_4 \end{bmatrix} + \hat{k}_3 \begin{bmatrix} \beta_1 \\ \beta_2 \\ \beta_3 \\ \beta_4 \end{bmatrix}) \qquad (4\text{-}85b)$$

is called the basic free velocity vector. The column vector $[\alpha_1 \quad \alpha_2 \quad \alpha_3 \quad \alpha_4]^T$ and $[\beta_1 \quad \beta_2 \quad \beta_3 \quad \beta_4]^T$ must correspond to the vectors in equation (4-79) used to construct the mobility matrix. The magnitude of the complex number $\hat{k}_1, \hat{k}_2, \hat{k}_3$ is in a range of 0~1 and satisfies:

$$\left|\hat{k}_1\right| + \left|\hat{k}_2\right| + \left|\hat{k}_3\right| = 1. \qquad (4\text{-}86)$$

It is assumed that the phase of these complex numbers $\hat{k}_1, \hat{k}_2, \hat{k}_3$ has a uniform distribution in the range of 0~2π, and that the magnitude is a uniform distribution in the range of 0~1 which is limited by equation (4-86).

4.9.2.2 Construction of free velocity for stiffness source and off-resonant source

The free velocity vector will be written as:

$$\begin{bmatrix} \hat{V}_i \\ \vdots \\ V_m \end{bmatrix} = \left|\hat{V}_0\right| \begin{bmatrix} v_1 \\ \vdots \\ v_m \end{bmatrix} \qquad (4\text{-}87)$$

where $\left|\hat{V}_0\right|$ is the mean magnitude. Like the assumption of source mobility distribution, it is assumed that v_i has a log10normal magnitude distribution. The standard deviation of the corresponding normal distribution is determined still by equation (4-81). Here the standard deviation will be chosen in the range of 0~0.85The phase is not deterministic and a uniform distribution is assumed.

4.9.2.3 Single mode resonant source

For a single mode resonant source the free velocity distribution is determined by the

corresponding single mode resonant source mobility, i.e. the free velocity is given by

$$[\hat{V}] \approx |\hat{V}_0| \begin{bmatrix} \phi_n(x_1) \\ \phi_n(x_2) \\ \vdots \\ \phi_n(x_m) \end{bmatrix} \quad (4\text{-}88)$$

The vector $[\phi_n(x_1)\,\phi_n(x_2)\cdots\phi_n(x_m)]^T$ must be the same as the corresponding vector in equation (4-83b).

4.9.3 Construction of receiver mobility

Similar to the source the receiver mobility matrix can be written as the product of a size factor type factor and basic mobility matrix, i.e. $[Y_r] = A_r \chi_r [y_r]$.

4.9.3.1 Off- resonant, stiffness and single mode resonant receiver mobility

Here the receiver mobility relationships are the same as those for the source. The same statistical descriptions are therefore proposed, i.e. for off-resonant receivers the corresponding y_{ij} have a uniform phase distribution in range of $-\pi/2\sim\pi/2$ for $i = j$ and $0\sim 2\pi$ for $i \neq j$, and $\log 10|y|$ has a normal distribution with a mean zero and a standard deviation in the range of $0\sim 0.85$. For stiffness-like receivers the corresponding y_{ij} have zero phase and a $\log 10|y|$ has a normal distribution with a mean zero and a standard deviation in the range of $0\sim 0.85$. For single mode resonant receivers the corresponding $\log 10|\phi_n|$ has a normal distribution with a mean zero and a standard deviation in the range of $0\sim 0.85$.

As for sources, the determination of A_r and loss factor η, which concerns stiffness receivers will be addressed in chapter5.

4.9.3.2 Infinite plate receiver

For infinite plate receivers the mobility matrix is

$$[Y] = A_r \chi_r [y]$$

where the type factor is $\chi = 1$, and A_r is a real number. The diagonal elements for the basic matrix $[y]$ are unity, and off-diagonal elements depend on the variable kr_{ij}. Here, the variable kr_{ij} is considered only in the range of 0.1~100, and is chosen to be uniform on a log scale.(This range was chosen as it gives condition numbers similar to those found for real structures.) .

However, two restrictions can be introduced which narrows the choice of valid values:

1) for stability reasons, the distances between support points are usually of the same order, so it is here assumed that the distance between two points is not greater than 5 times that between any other two points.

2) there are $N = C^n_{n-3} = n!/((n-3)! \cdot 3!)$ triangles (C^n_r: Combination symbol) for n contact points, and for any triangle the sum of the two sides must be greater than the length of the third side. For example, between any three points there exist three transfer mobilities. Once values for kr are established for any two of these elements then kr for the third element is not fully independent but is bounded because of the above relationships.

4.10 Example: Steps for construction of generic sources and receivers

To be clear, the steps for construction of the mobility matrix for off-resonant structures (four point case) are now described as an example. The input data required is the standard deviation, which from above lies anywhere in the range 0~0.85.

1. A value for the standard deviation σ is chosen at random from within the range 0~0.85 using the 'random' function from Matlab*.

2. Ten numbers z_{ij} are generated at random using a mean value of unity and the above chosen standard deviation σ.

3. Ten matrix elements $|y_{ij}|$ are calculated from the equation $z_{ij} = \log 10 |y_{ij}|$.

4. Ten phase angles θ are generated at random from within the range 0~2π.

5. Ten complex data $y_{ij} = |y_{ij}|(\cos\theta + j\sin\theta)$ are assembled into the lower half of a 4x4 symmetric matrix.

6. The eigenvalues of the real part of the matrix are checked, and if each is positive the matrix is chosen, otherwise it is rejected

7. The above steps are repeated until a sufficient number of valid matrices is obtained.

*Because the standard deviation does not apply to a uniform distribution, the author used the expression $\sigma = 0.15 * (randn(1,1) + 0.45$ and the relationship $0 < \sigma \le 0.85$. $randn(1,1)$ is one random data chosen from a normal distribution with mean zero and variance one.

4.11 Conclusion

In order to obtain the general normalised active power band the 'source replacement

method' will be used in Chapter 5, that is where a number of different sources are combined with a given receiver to produce a statistical distribution for the power emission (normalised to one of the three chosen source parameters). However, before such an analysis can be conducted, appropriate statistical input data is required which has been the focus of this Chapter. The approach adopted has been to construct 'generic' statistical sources and receivers. The 'generic' matrices are based on the inherent properties of the mobility matrices and free velocity vectors for different types of behaviour. Four types of source, i.e. mass-like source, stiffness source, single mode resonant source and off-resonant source and four types of receiver, i. e. stiffness receiver, single mode resonant receiver, off-resonant receiver and infinite plate receiver have been considered.

For any source and receiver the eigenvalues of the real part of the mobility matrix are non-negative. For mass-like sources the mobility matrix has the form of equation (4-79), and the free velocity has the form of equation (4.85). The elements of the vectors $[\alpha_i]$ and $[\beta_i]$ have a uniform distribution in the range of 0~1.5 or 0~ -1.5. For stiffness sources the mobility matrix has the form of equation (4-82), and the elements of the basic mobility matrix have zero phase and a log10normal magnitude distribution. The free velocity has the form of equation (4-87), and the elements of the vector have a log10normal magnitude distribution and uniform phase in range of 0~2π. For single mode resonant sources, the mobility matrix has the form of equation (4-83), and source free velocities have the form of equation (4.88). The elements of the vector $[\phi]$ have a log10normal magnitude distribution and zero or π phase. For off-resonant sources the

mobility matrix has the form of equation (4-80). The elements of the basic mobility matrix have uniform phase distribution in range of $-\pi/2 \sim \pi/2$ for diagonal elements and in the range of $0 \sim 2\pi$ for off-diagonal elements and have a log10normal magnitude distribution. The free velocities have the same distribution as a stiffness source.

For a stiffness receiver, single mode resonant receiver and off-resonant receiver, the mobility matrix has the same properties as the corresponding source. In addition, infinite plate receivers were considered, for which the diagonal elements of the basic matrix $[y]$ are unity and off-diagonal elements depend on the variable kr_{ij}, considered only in the range of $0.1 \sim 100$.
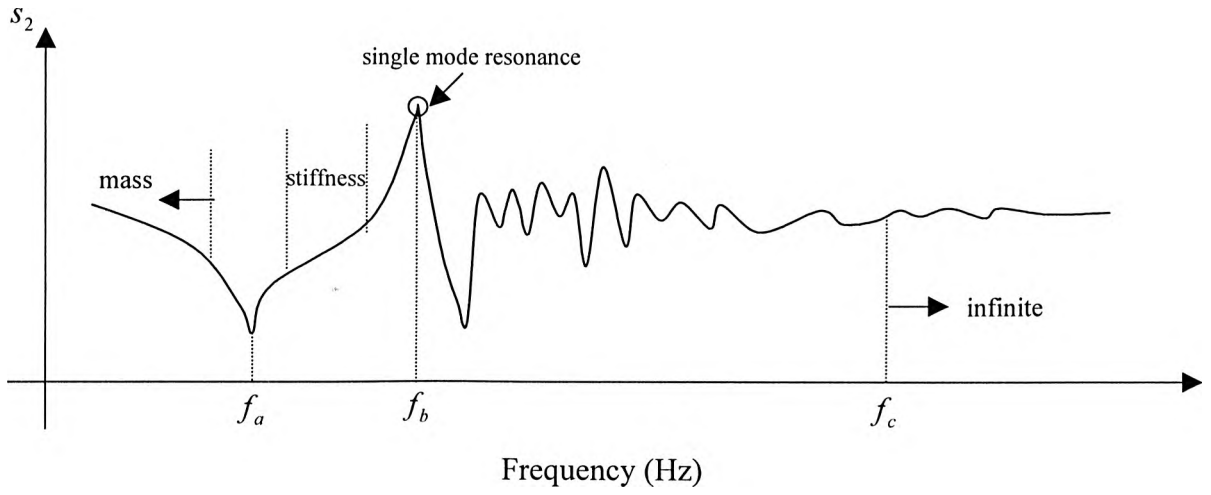
Figure 4-1 Illustrating the five types of behaviour with increasing frequency.
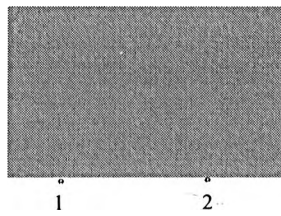
Figure 4-2a A rigid body structure
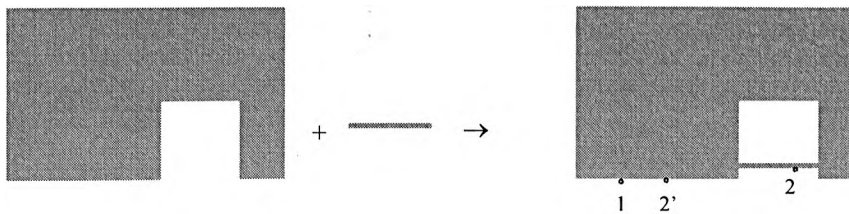
Figure 4-2b A structure constructed of a rigid body and thin beam
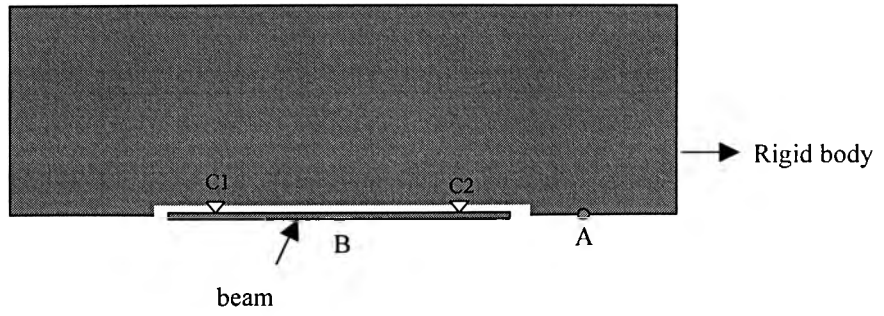
Figure 4-3a A structure constructed of a rigid body and thin beam
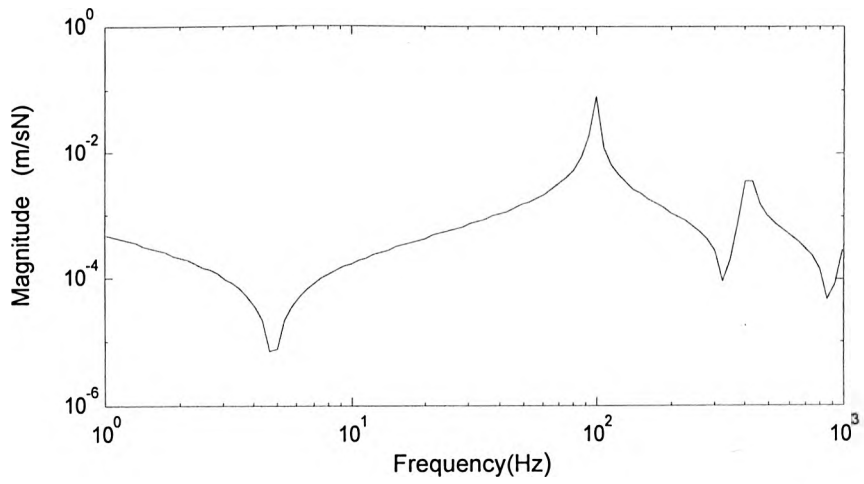
Figure 4-3b Point mobility at position B
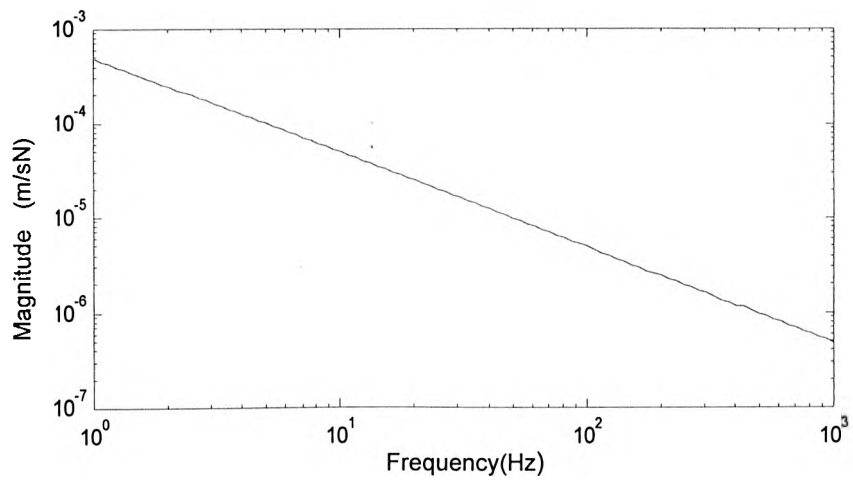
Figure 4-3c Point mobility at position A
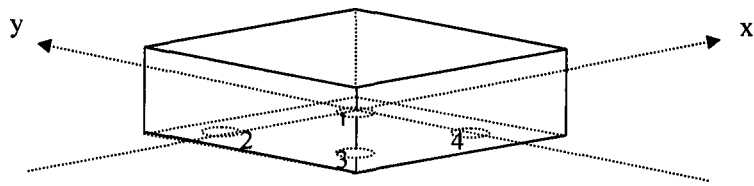
Figure 4-4 A rectangular rigid body with four contact points which are located within the four quadrants respectively
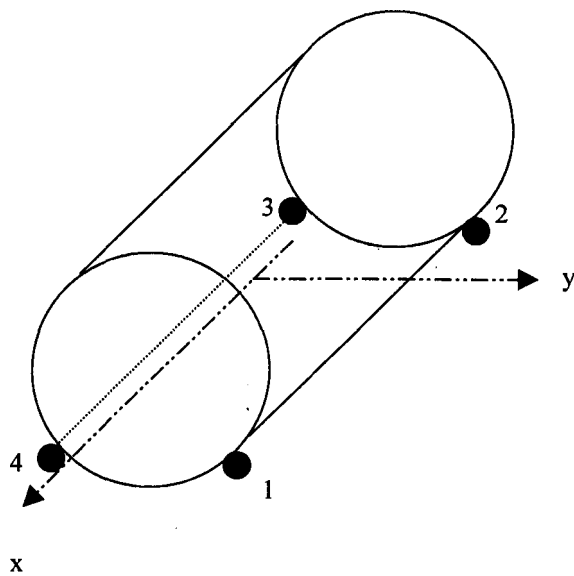
Figure 4-5 A motor modelled as a cylinder or shell
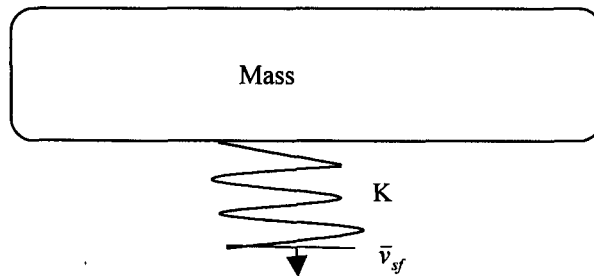
Figure 4-6 A model for a source mount point at low frequency
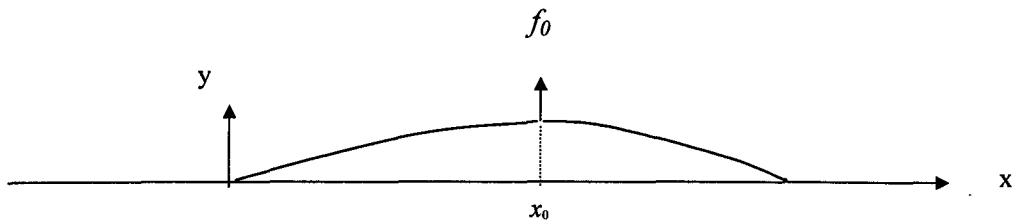
Figure 4-7a A string rigidly supported at both ends
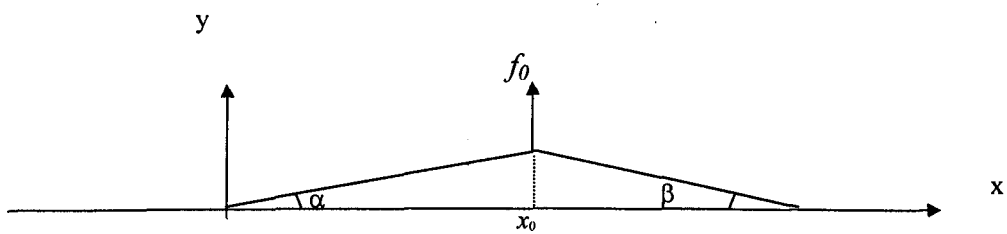
Figure 4-7b Under static force the Shape of a string rigidly supported at both ends
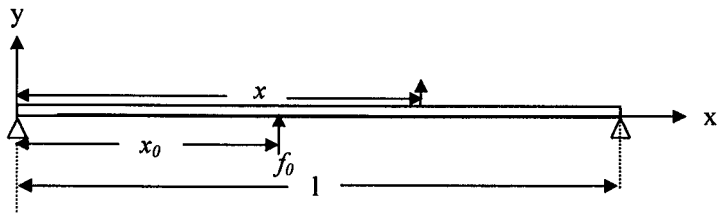
Figure 4-8a A beam simply supported at both ends
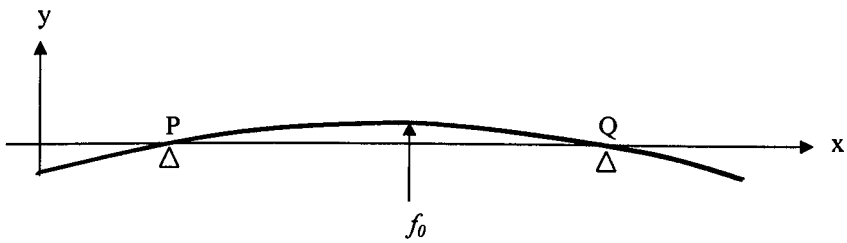
Figure 4-8b Under static force the Shape of a beam rigidly supported at both ends
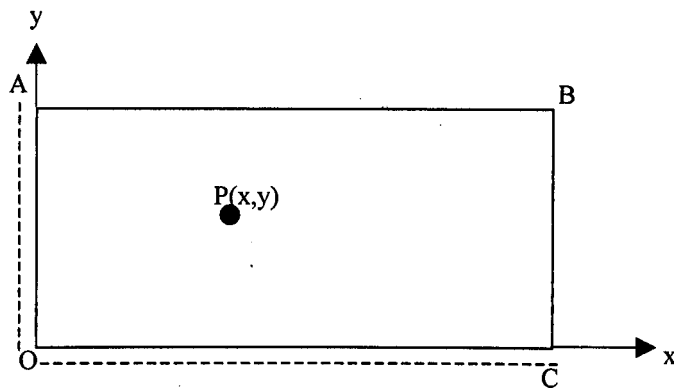
Figure 4-9 A S-S-F-F plate
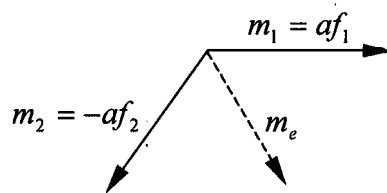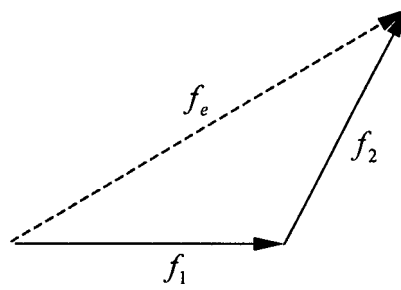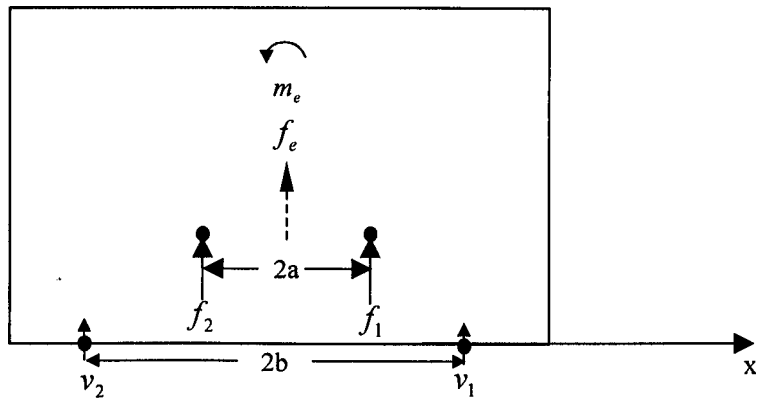
Figure 4-10 A rigid body excited by two internal forces with different phase
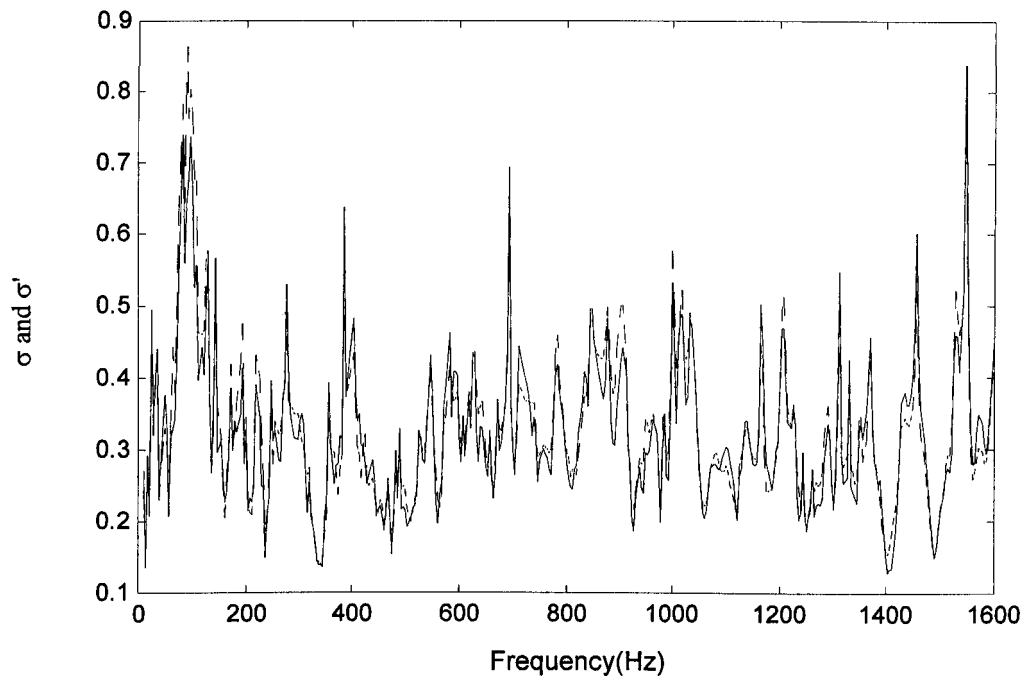
Figure 4-11a Standard deviation for a typical fan .(-,equation 4-81a); (--,equation4-81b).
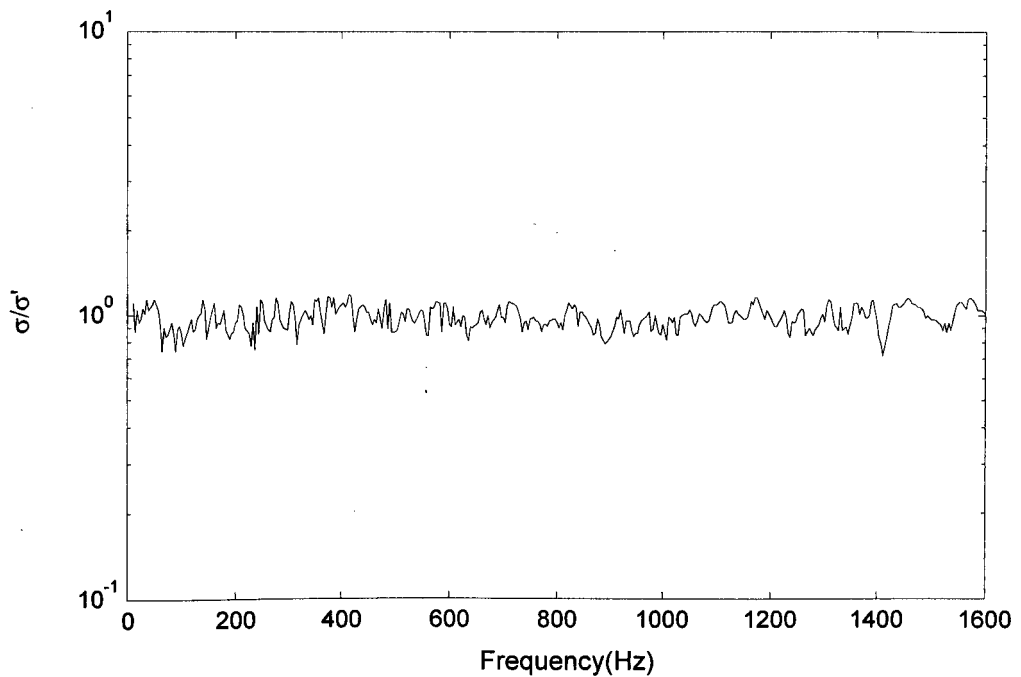
Figure 4-11b Ratio of σ and σ'

CHAPTER 5

GENERAL NORMALISED ACTIVE POWER BANDS FOR COMBINATIONS OF GENERIC SOURCES AND RECEIVERS

5.1 Introduction

5.2   Procedure for getting the general normalized active power band

5.3 Combination of mass-like sources with various receivers

5.4. Combination of stiffness sources with various receivers

5.5 Combination of off-resonant source on various receivers

5.6 Combination of single mode resonant source on various receivers

5.7 Example

5.8 Conclusion

1 Introduction

In this chapter, the general normalised active power band will be calculated and plotted for the various possible combinations of generic mobility matrices and free velocity vectors developed in chapter 4. This is done for different choices of the source descriptor parameters s_1 and s_2, namely: the blocked force parameter, CF, the characteristic power and its approximation, CP1 and CP2 respectively. From the plots of general normalized active power band, we can see if the chosen parameters s_1 and s_2 provide tolerable range, and whether s_1 can be accepted as a source strength parameter. We also develop the method for predicting active power from a source into the receiver which will be used in Chapter 6. Furthermore, the general normalized active power band will give insight into the global behaviour of the source.

5.2 Procedure for getting the general normalized active power band

1. According to chapter 4, a receiver basic matrix $[y_r]$ is constructed by using the Matlab 'random' function. This basic matrix is multiplied by a type factor χ_r and a positive real number A_r, to form the receiver mobility matrix.

2. The source free velocity is formed from a basic free velocity vector, multiplied by an arbitrary positive real number V_0. A group of basic matrices for the source is formed using the same method as above. Each basic matrix, times type factor χ_r and a suitable positive real number A_s, forms a source mobility matrix. Here, a suitable positive real number means that it is chosen so as to make each source mobility matrix have the same α^Σ (see equation (3-42) which is the definition for α^Σ), i.e. A_s satisfies the following relationship:

$$A_s = A_r \Lambda \qquad (5\text{-}1)$$

where

$$\Lambda \equiv \frac{1}{\alpha^\Sigma} \sum |y_{r,ii}| / \sum |y_{s,ii}| \quad (5\text{-}2)$$

α^Σ is considered mainly in the range of $[10^{-3}, 10]$ in this thesis. For a given α^Σ, the general normalized active power from a group of sources into the receiver can be calculated. Similar to the method in chapter3, a statistical description of the general normalized active power band can be expressed in terms of percentage confidence limits. Here the width of the 90% confidence limit is defined as the 'band width' (Note that this is a different concept to frequency bandwidth often used in acoustics). There are still two points needing consideration.

i) The influence of the number A_r on the general normalized active power band.

The active power can be rewritten as

$$\begin{aligned}
P &= [\hat{V}_{sf}]^{*T} ([Y_R] + [Y_S])^{-1*T} (\mathrm{Re}[Y_R])([Y_R] + [Y_S])^{-1} [\hat{V}_{sf}] \\
&= |\hat{V}_0|^2 ([v_{sf}]^{*T} (A_r \chi_r [y_r] + A_s \chi_s [y_s])^{-1*T} (\mathrm{Re}(A_r \chi_r [y_r]))(A_r \chi_r [y_r] + A_s \chi_s [y_s])^{-1} [v_{sf}]) \\
&= A_r^{-1} |\hat{V}_0|^2 ([v_{sf}]^{*T} (\chi_r [y_r] + \Lambda \chi_s [y_s])^{-1*T} (\mathrm{Re}(\chi_r [y_r]))(\chi_r [y_r] + \Lambda \chi_s [y_s])^{-1} [v_{sf}])
\end{aligned}$$
$$(5\text{-}3)$$

and the source parameters $CF, CP1, CP2$ defined in chapter 3 can be rewritten as,

$$CF = A_r^{-2} |\hat{V}_0|^2 ([v_{sf}]^{*T} (\Lambda \chi_s [y_s])^{-1*T} (\Lambda \chi_s [y_s])^{-1} [v_{sf}]) \qquad (5\text{-}4a)$$

$$CP1 = \left| A_r^{-1} |\hat{V}_0|^2 ([v_{sf}]^{*T} (\Lambda \chi_s [y_s])^{-1} [v_{sf}]) \right| \qquad (5\text{-}4b)$$

$$CP2 = A_r^{-1} |\hat{V}_0|^2 \sqrt{([v_{sf}]^{*T} [v_{sf}])([v_{sf}]^{*T} (\Lambda \chi_s [y_s])^{-1*T} (\Lambda \chi_s [y_s])^{-1} [v_{sf}])} \qquad (5\text{-}4c)$$

From the above equations it can be shown that the general normalized active power P/CF is proportional to A_r, in other words the value of A_r influences the 'level' of the general normalized active power band P/CF, while it has no influence on the

general normalized active power $P/CP1$ and $P/CP2$. In this chapter we have more interest in the shape of the general normalized active power band, rather than its 'level'. For convenience, let A_r equal unity. The value of $|\hat{V}_0|$ has no influence on the three general normalized active power bands, so let $|\hat{V}_0|$ equal unity too.

ii) Determination of loss factor η in stiffness source and receiver structures

The loss factor η in stiffness sources and receivers has still not been determined. For stiffness sources the type factor is $\chi_s = e^{j(\pi/2-Arctg\eta)}$, and since many sources are made of metal, which has inherently low damping, so $\chi_s \approx j$ is used. In any case, the loss factor η in stiffness sources has no influence on the general normalized active power. For stiffness receivers the fourth term $(\mathrm{Re}(\chi_r[y_r])$ in equation (5-3) can be expressed as

$$\mathrm{Re}(\chi_r[y_r] = \frac{\eta}{1+\eta^2}[y_r], \qquad (5\text{-}5)$$

therefore, the loss factor has an influence on the 'level' of the three general normalized active power bands. Similarly to above, the shape is of more interest, so here we define the loss factor as an arbitrary realistic value $\eta = 0.1$.

5. 3 Combination of Mass-like sources with various receivers

Four contact points are considered. Here we meet some problems at first since the mobility matrix is not of 'full rank', i.e. the determinant of the matrix is zero. Therefore, CP1 is mathematically meaningless, but in physical terms CP1 for a rigid body is 2ω times kinetic energy. Reference [50] gives an interpretation for it in the case of two points where it is easily understood, because the determinant of the matrix

is non zero. An interpretation is now given for the case of three points on a line for which the determinant of the mobility matrix is also zero.

Consider three points on the x axis (see figure 5-1). CP1 can be expressed as:

$$CP1 = \left| \begin{pmatrix} \hat{V}_{sf,1} & \hat{V}_{sf,2} & \hat{V}_{sf,3} \end{pmatrix}^* \begin{bmatrix} 1+\dfrac{x_1x_1}{p^2} & 1+\dfrac{x_1x_2}{p^2} & 1+\dfrac{x_1x_3}{p^2} \\ 1+\dfrac{x_1x_2}{p^2} & 1+\dfrac{x_2x_2}{p^2} & 1+\dfrac{x_2x_3}{p^2} \\ 1+\dfrac{x_3x_1}{p^2} & 1+\dfrac{x_3x_2}{p^2} & 1+\dfrac{x_3x_3}{p^2} \end{bmatrix}^{-1} \begin{pmatrix} \hat{V}_{sf,1} \\ \hat{V}_{sf,2} \\ \hat{V}_{sf,3} \end{pmatrix} (-j\omega M) \right| \quad (5\text{-}6)$$

where x_1, x_2 and x_3 are the co-ordinates of points 1,2,3 (the reference point is at the centre of the mass). In this case the determinant of the mobility matrix is zero (see chapter 4) but if we rewrite expression 5-6 in the following form, it will be seen to have a close relationship with kinetic energy:

$$CP1 = \left| \begin{pmatrix} \hat{V}_{sf,1} & \hat{V}_{sf,2} & \hat{V}_{sf,3} \end{pmatrix}^* \phi_2\phi_2^{-1} \begin{bmatrix} 1+\dfrac{x_1x_1}{p^2} & 1+\dfrac{x_1x_2}{p^2} & 1+\dfrac{x_1x_3}{p^2} \\ 1+\dfrac{x_1x_2}{p^2} & 1+\dfrac{x_2x_2}{p^2} & 1+\dfrac{x_2x_3}{p^2} \\ 1+\dfrac{x_3x_1}{p^2} & 1+\dfrac{x_3x_2}{p^2} & 1+\dfrac{x_3x_3}{p^2} \end{bmatrix}^{-1} \phi_1^{-1}\phi_1 \begin{pmatrix} \hat{V}_{sf,1} \\ \hat{V}_{sf,2} \\ \hat{V}_{sf,3} \end{pmatrix} (-j\omega M) \right|$$

$$= \left| \begin{pmatrix} \hat{V}_{sf,1} & \hat{V}_{sf,2} & \hat{V}_{sf,3} \end{pmatrix}^* \phi_2 (\phi_1 \begin{bmatrix} 1+\dfrac{x_1x_1}{p^2} & 1+\dfrac{x_1x_2}{p^2} & 1+\dfrac{x_1x_3}{p^2} \\ 1+\dfrac{x_1x_2}{p^2} & 1+\dfrac{x_2x_2}{p^2} & 1+\dfrac{x_2x_3}{p^2} \\ 1+\dfrac{x_3x_1}{p^2} & 1+\dfrac{x_3x_2}{p^2} & 1+\dfrac{x_3x_3}{p^2} \end{bmatrix} \phi_2)^{-1}\phi_1 \begin{pmatrix} \hat{V}_{sf,1} \\ \hat{V}_{sf,2} \\ \hat{V}_{sf,3} \end{pmatrix} (-j\omega M) \right|$$

$$(5\text{-}7)$$

If here ϕ_1 is chosen in the following form:

$$\phi_1 = \begin{bmatrix} \dfrac{x_2}{x_2 - x_1} & \dfrac{-x_1}{x_2 - x_1} & 0 \\ 1 & -1 & 0 \\ \dfrac{x_3 - x_2}{x_2 - x_1} & \dfrac{x_1 - x_2}{x_2 - x_1} & 1 \end{bmatrix} \qquad \phi_2 = \phi_1^{T*}$$

then the expression (5-7) becomes expression (5-8)

$$CP1 = \left| \left(\frac{x_2 \hat{V}_{sf,1} - x_1 \hat{V}_{sf,2}}{x_2 - x_1} \quad \frac{\hat{V}_{sf,2} - \hat{V}_{sf,1}}{1} \quad 0 \right) \begin{bmatrix} 1 & 0 & 0 \\ 0 & \dfrac{(x_2 - x_1)^2}{p^2} & 0 \\ 0 & 0 & 0 \end{bmatrix}^{-1} \omega \left(\begin{array}{c} \dfrac{x_2 \hat{V}_{sf,1} - x_1 \hat{V}_{sf,2}}{x_2 - x_1} \\ \dfrac{\hat{V}_{sf,2} - \hat{V}_{sf,1}}{1} \\ 0 \end{array} \right) (-j\omega M) \right|$$

$$= \left| -j\omega M \left| \frac{x_2 \hat{V}_{sf,1} - x_1 \hat{V}_{sf,2}}{x_2 - x_1} \right|^2 + -j\omega M p^2 \left| \frac{\hat{V}_{sf,2} - \hat{V}_{sf,1}}{x_2 - x_1} \right|^2 + \frac{0 \times 0}{0} \right|$$

$$(5-8)$$

The sum of the first and second terms on the right side of equation (5-8) is simply 2ω times kinetic energy, and the last team is mathematically meaningless, but here can be understood as zero. This result extends to mass-like sources with any number of contact points and degrees of freedom.

The numerical calculation of CP1 (and CF) for the rigid body case can also be treated by using SVD [51] (Singular Value Decomposition).

5.3.1 Combination of mass-like source with stiffness-like receiver

5.3.1.1 General normalized active power band for CF

The stiffness receiver was obtained from the random function of Matlab. The condition number was 28dB (the condition number is the ratio of maximum to minimum eigenvalues of the real part of the mobility matrix). The many different

sources (here referred to as a source group) were 'attached' to the receiver in turn. In the range of $\alpha<0.2$ (see figure 5-2a) the band width is only about 10dB and the band is flat, and in the range of $\alpha>0.2$ the band width is more complex in its variation with α. The band is strongly sloping in this range. There are two peaks at $\alpha=0.5$ and $\alpha=2$ where the corresponding band width is 20dB. The position of these peaks is not like the single point case where a maximum always occurs at $\alpha=1$. This can be explained as follows.

Consider two symmetric connection points for simplicity, where a symmetric mass-like source is placed symmetrically on a symmetric stiffness receiver. The active power emission from source into the receiver is given by:

$$P = \mathrm{Re}\left(\begin{pmatrix} \hat{V}_{sf,1} \\ \hat{V}_{sf,2} \end{pmatrix}^{T*} \begin{pmatrix} Y_{11}^R + Y_{11}^s & Y_{12}^R + Y_{12}^S \\ Y_{12}^R + Y_{12}^S & Y_{11}^R + Y_{11}^S \end{pmatrix}^{-1T*} \begin{pmatrix} Y_{11}^R & Y_{12}^R \\ Y_{12}^R & Y_{11}^R \end{pmatrix} \begin{pmatrix} Y_{11}^R + Y_{11}^S & Y_{12}^R + Y_{12}^S \\ Y_{12}^R + Y_{12}^S & Y_{11}^R + Y_{11}^S \end{pmatrix}^{-1} \begin{pmatrix} \hat{V}_{sf,1} \\ \hat{V}_{sf,2} \end{pmatrix} \right)$$

$$(5-9)$$

where Y_{11}^R Y_{12}^R are the point and transfer mobility of the stiffness receiver, and Y_{11}^S Y_{12}^S are the point mobility and transfer mobility of the mass like source. Equation 5-9 can be simplified by using a Hadamard matrix:

$$P = \mathrm{Re}\left(\frac{Y_{11}^R + Y_{12}^R}{\left| Y_{11}^R + Y_{12}^R + Y_{11}^S + Y_{12}^S \right|^2} \left| \hat{V}_{sf,1} + \hat{V}_{sf,2} \right|^2 + \frac{Y_{11}^R - Y_{12}^R}{\left| Y_{11}^R - Y_{12}^R + Y_{11}^S - Y_{12}^S \right|^2} \left| \hat{V}_{sf,1} - \hat{V}_{sf,2} \right|^2 \right)$$

$$(5-10)$$

Now we consider the first term of the above equation:

$Y_{11}^S + Y_{12}^S$ can be rewritten $Y_{11}^S + Y_{12}^S = -jY_+^S$ where Y_+^S is real and positive and

$Y_{11}^R + Y_{12}^R = \dfrac{j}{(1+\eta j)} Y_+^R$, where Y_+^R is real and positive. Thus, the phase of $Y_{11}^S + Y_{12}^S$ is

opposite to $Y_{11}^R + Y_{12}^R$ when the loss factor is small, so there are large peaks when:

$$\left| Y_{11}^S + Y_{12}^S \right| = \left| Y_{11}^R + Y_{12}^R \right| \qquad (5\text{-}11)$$

Equation (5-11) can be rewritten as (5-12)

$$\left| 1 + \frac{Y_{12}^S}{Y_{11}^S} \right| = \left| \frac{Y_{11}^R}{Y_{11}^R} \right| \left| 1 + \frac{Y_{12}^R}{Y_{11}^R} \right| = \alpha^\Sigma \left| 1 + \frac{Y_{12}^R}{Y_{11}^R} \right| . \quad (5\text{-}12)$$

For mass-like sources the transfer mobility phase is the same or opposite as that of the point mobility, and for a stiffness receiver the transfer mobility phase is the same as the point mobility in most cases. If the transfer mobility phase for the source is opposite to that of the point mobility, then $-1 < \dfrac{Y_{12}^S}{Y_{11}^S} < 0$, so from equation (5-12) we have $\alpha^\Sigma < 1$. If the transfer mobility has the same phase as the point mobility and $\dfrac{Y_{12}^S}{Y_{11}^S} > \dfrac{Y_{12}^R}{Y_{11}^R}$, then from equation (5-12) we have $\alpha^\Sigma > 1$. The second term of equation (5-10) gives similar results, so the position of the peak of the general normalised active power is not at $\alpha^\Sigma = 1$ only.

The results of figure 5-2a indicate that in the range of $\alpha^\Sigma < 0.1$, the active power emission from different sources with the same CF into the receiver is similar. It is effectively the same as the band width. However, when $10 > \alpha^\Sigma > 0.1$ the active power emission from different sources with same CF in to the receiver varies significantly (about 42dB), which is considerably more than the band width.

Figure 5-2b shows the result with a stiffness receiver chosen by the same method as above, but this time with a condition number of about 10dB. The shape of the band is similar to Figure5-1a, but there are three peaks in this figure. In the range of $\alpha^\Sigma < 0.1$ the band is narrower than that in figure5-2a, which is due to the smaller condition number. The presence of three peaks maybe can be explained: for four contact points

there are only three independent modes of vibration. Consider the symmetrical case for simplicity. The active power emission can expressed in the following form:

$$Q = \text{Re}(\hat{C}_1\hat{S}_1 + \hat{C}_2\hat{S}_2 + \hat{C}_3\hat{S}_3 + \hat{C}_4\hat{S}_4) \quad (5\text{-}13)$$

One term in equation (5-13) is zero, and any of the remaining three terms will appear as a peak at some point.

5.3.1.2 General normalized active power band for CP1

See figure 5-3a. The General normalized active power band for CP1, source and receiver are similar to figure 5-2a. The band width is similar to the band for CF (about 11dB) in the range of $\alpha^\Sigma < 0.1$. but is not flat. The range of variation of the general normalized active power is about 33dB in the range of $0.001 < \alpha^\Sigma < 0.1$, which is considerably wider than the band width. The corresponding range is about 35dB in the range of $0.1 < \alpha^\Sigma < 10$.

Figure 5-3 b. shows the General normalized active power band for CP1 with a receiver with a lower condition number. The source and receiver is the same as Figure 5-2b. In the range of $0.001 < \alpha^\Sigma < 0.1$ the band width is smaller (about 6dB) than the above case due to the smaller condition number, but the range of the General normalized active power is still about 28dB in this range. In the range of $0.1 < \alpha^\Sigma < 10$, the range of variation is about 30dB. (The width of the band at lower α is reduced according to the receiver condition number, but the shape and hence overall range is similar to figure 5-2a.)

5.3.1.3 General nomalised active power band for CP2

Figure 5-4 a, b shows the corresponding results for CP2 which are very similar to those for CP1.

5.3.2 Combination of a mass like source with single mode resonant receiver

5.3.2 .1 General normalized active power band for CF

A single mode resonant receiver matrix was constructed by using the rules described in chapter 4. The column vector from which the mobility matrix is constructed was generated at random. A group of mass-like sources was then 'connected' to the single mode resonant receiver. Here the condition number of the receiver is infinite.

Figure 5-5 shows the general normalized active power band for CF. The form of the bands is quite different to the previous plots (and following plots). The most striking point is that the power is very low, in fact it is zero except for 'numerical noise' from the calculation. (These numerical errors caused some negative values which are not plotted). It is not clear physically why the power into an isolated resonance should be zero, after all, it is usually considered that a resonance is an efficient 'absorber' of energy. The author has conjectured an explanation as follows.

Let $[A]$ be an n by n matrix with rank n-1 (representing the mobility matrix of the mass source), and let $[B]$ and $[C]$ be column vectors (where [B] represents the free velocity vector of the source, and [C] represents the mode shape vector of the single mode receiver). If the matrix [A B] has the same rank as matrix $[A]$ (which is the case for the mass sources with four contact points considered in Chapter 4), and the rank of matrix $[A + CC^{T*}]$ is n (where $[CC^{T*}]$ represents the single mode receiver mobility matrix), then we have:

$$[B]^{T*}[A + CC^{T*}]^{-1T*}[CC^{T*}][A + CC^{T*}]^{-1}[B] = 0 \quad (5\text{-}14a)$$

$$[C]^{T*}[A + CC^{T*}]^{-1T*}[CC^{T*}][A + CC^{T*}]^{-1}[C] = 1 \quad (5\text{-}14b)$$

The first equation represents the power into the receiver. (The physical interpretation of the second is not clear, but it is given for mathematical interest.) If the above conjecture (equation 5-14a) is right, the power from a rigid body source with four points into a single mode resonant receiver is zero. However, if the rank of matrix $[A+CC^{T*}]$ is less than n, then equation (5-14a) is meaningless. If here SVD is used to treat the left side of equation (5-14a), then the power from a rigid body source with four contact points into the receiver is non zero as shown in the following example.

Consider a symmetric single mode resonant receiver, for example. Its mobility matrix is given by:

$$Yr = \begin{pmatrix} \phi_1 \\ \phi_1 \\ \phi_1 \\ \phi_1 \end{pmatrix} \begin{pmatrix} \phi_1 & \phi_1 & \phi_1 & \phi_1 \end{pmatrix} = \phi_1^2 \begin{pmatrix} 1 & 1 & 1 & 1 \\ 1 & 1 & 1 & 1 \\ 1 & 1 & 1 & 1 \\ 1 & 1 & 1 & 1 \end{pmatrix} \qquad (5-15)$$

If the matrix of the mass source is symmetric too, then the active power emission from the mass to this receiver can be given by

$$P = \frac{\phi_1 \phi_1}{\left| 4\phi_1 \phi_1 + Y_{11}^S + Y_{12}^S + Y_{13}^S + Y_{14}^S \right|^2} \left| \hat{V}_{sf,1} + \hat{V}_{sf,2} + \hat{V}_{sf,3} + \hat{V}_{sf,4} \right|^2 \quad (5-16)$$

where Y_{ij}^S is the point and transfer mobility, and $\hat{V}_{sf,i}$ is the free velocity of the mass source. Therefore, the active power emission cannot be zero when both source and receiver are exactly symmetrical.

A further example of a system for which the sum of the source and receiver matrices is not full rank is where the receiver is symmetric, but the mass source group is not symmetric. This case was solved numerically and results are given in Figures 5-6 a, b, Again, this shows that the active power emission is not zero.

The single mode resonant receiver model used above suggests that strongly resonant receiver structures may have a lower ability of power absorption when the source is mass-like. This result was not expected on physical grounds. However, single resonances do not occur in real physical cases, so we must consider the possibility that the zero power is due to the idealised model, and would not occur in real cases. To investigate this a real system has been solved and in the following results the receiver data is taken from a plate resonance with low loss factor, rather than the idealised single mode theory.

Figure 5-7 shows a SSSS plate (as a receiver). Its properties are: density $\rho = 2.87 \times 10^3 \, kg \, / \, m^3$ and Poisson's ratio $v = 0.3$, Young's modulus $E = 2 * 10^{10} \, N \, / \, m^2$. For loss factor two cases were considered: case 1, $\eta_1 = 0.0001$, and case 2 $\eta_2 = 0.001$. The mobility matrix was calculated by using thin plate theory. Figure 5-8 shows the maximum and minimum eigenvalues together with the mean eigenvalue (note that the mean eigenvalue is equal to the mean point mobility) for both loss factors.

The general normalized active power band for CF is plotted in figure 5-9. The elements of the real part of the mobility matrix for case one are almost ten times that for case two. It would normally be considered that the less damped receiver has more ability to absorb power, but here the opposite is the case: the sharper the peak, the lower the power, and the absorption of power for case one is only one tenth of that for case two. Because the behaviour of case one is closer to an idealised single mode resonant receiver than that of case two, so the active power emission becomes

smaller. If we assume that this trend continues indefinitely as the damping is reduced, then the trend is towards zero power which agrees with results from the idealised model above.

Figure 5-10a,b shows results for the plate CP1 (results for CP2 were essentially the same and are not shown). The width of the band is similar to the above case, but the band is not flat, and the power increases almost proportionally to α^Σ. In practice, cases with such a condition number are not common. The aim of giving the above example is to indicate that strongly resonant receiver structures may have a lower ability of power absorption when the source is mass-like.

5.3.3 Combination of mass like source with an off-resonant receiver

This system was constructed as before, with a group of mass-like sources attached to an-off-resonant receiver. The off-resonant receiver matrix was constructed by 'random' generation of the elements as described in Chapter 4.

5.3.3.1 General normalized active power band for CF

See figure. 5-11a. The condition number for the receiver matrix was 27dB. Over most of the range, the band width is about 9dB. There is a small peak at $\alpha^\Sigma \approx 1$, so in this range the band is wider, at about 13dB. The band is 'flat' in the range of $\alpha^\Sigma < 0.1$, so that the ratio of maximum to minimum power is the same as the band width. However, in the range of $\alpha^\Sigma > 0.1$ it is no longer flat, and so there is a wide variation from maximum to minimum power of about 30dB for $0.1 < \alpha^\Sigma < 10$.

See Figure 5-11b: the group of sources is the same as above but the receiver has a condition number of 10dB. The shape of the general normalized active power band for CF is similar to the previous case, but the width of the band is narrower due to the smaller condition number. The band width is about 6dB over the whole range. The band is also more flat than the first case in the range of $\alpha^{\Sigma}<1$. There is a range of power of 22dB in the range of $0.1<\alpha^{\Sigma}<10$ for CF.

5.3.3.2 General normalized active power band for CP1 and CP2

Results for CP1 are plotted in figure 5-12. Results for CP2 were very similar and are not shown. Figure 5-12a: the source and receiver are the same as in figure 5-11a. Over the whole range the band width is similar to that for CF, but is not 'flat' in the range of $\alpha^{\Sigma}<0.1$. The ratio of maximum to minimum power in the range of $0.1<\alpha^{\Sigma}<10$ is about 20dB.

For Figure 5-12b the receiver was the same as fig 5-11b. The shape of the coupling function CP1 is similar to figure. 5-12a, but the band width is narrower due to the smaller condition number. The variation range of general normalized active power for CP1 is 15dB in range of $0.1<\alpha^{\Sigma}<10$. This is less by about 7dB than the corresponding figure for CF over the same range, indicating less sensitivity of CP1 to α^{Σ}.

5.3.4 Combination of mass like source with infinite receiver

The infinite receiver matrix was constructed by using the rules developed in chapter 4. A group of mass like sources were combined with this receiver to form the mass-on–infinite receiver system.

5.3.4.1 General normalized active power for CF

Figure 5.13a.The receiver matrix was chosen from the Matlab 'random' function, assuming a condition number of 26dB. In most of the range the width of the coupling function band is about 11dB, the band is very 'flat' in the range of $\alpha^{\Sigma} < 0.5$. In the range of $\alpha^{\Sigma} > 1$ the band is no longer flat. In the range of $\alpha^{\Sigma} < 0.5$ the General normalized active power band for CF is about 11dB, which is about the same as the band width, while the range of the general normalized active power is about 22dB and wider than the band width.

Figure 5-13b. The group of sources is the same as in Figure5-13a and the receiver is another plate for which the condition number is 10dB. The shape of general normalized active power band for CF is similar to Figure5.13a, but the band width is narrower due to smaller condition number, over most of the range it is less than 7dB. The variation range of general normalized active power for CF is less than 6dB in the range of $\alpha^{\Sigma} < 0.3$. while in the range of $0.3 < \alpha^{\Sigma} < 10$. it is 28dB, and larger than the band width due to the slope.

5.3.4.2 General normalized active power band for CP1 and CP2

Fig 5-14a shows results for CP1. Results for CP2 were very similar and are not shown. The receiver is the same as in fig.5-13a. Over the whole range the band width is similar to figure 5-13a, but the band is sloped and the range is 30dB. In the range of $0.3 < \alpha^{\Sigma} < 10$ it is about 14dB.

Figure5-14b.The receiver is same as figure 5-13b, and as before the shape is similar to 5-14a but with a narrower bandwidth due to the smaller condition number. The variation is 14dB in the range of $0.1 < \alpha^{\Sigma} < 10$, which is 13dB less than for CF.

5.4. Combination of stiffness sources with various receivers

In practical cases the condition number for stiffness sources is not large, because the distance between the mount points is usually of the same order as the size of the base plate of the source for stability reasons. For sources with 'flange bases' the condition number in the stiffness range tends to be low because the transfer mobility is low [34]. Figure 5-15b plots the cumulative distribution for the condition number of 215 plate sources operating in a stiffness controlled regime. The plate, a rectangular plate with SSSS supports is shown in figure Figure5-15a, where ABCD was modelled as the base plate of a source, while various positions of the rectangle described by the four mounts points 1, 2, 3, 4 were considered as the contact points to the receiver. It shows that about 99 percent of the condition numbers were less than 25dB. Most condition numbers were between 10 and 15 dB. For this reason, a rule that the condition number is less than 25dB was added when constructing the stiffness sources.

5.4.1 Combination of stiffness source with stiffness receiver

5.4.1.1 General normalized active power band for CF

Figure5-16a. The receiver condition number is 20dB. The band width is about 9dB in the range of $\alpha^{\Sigma} < 10^{-1}$ and quite flat. Above this frequency, the band is not flat and becomes more and more wide. In the range of $10^{-1} < \alpha^{\Sigma} < 10$ the range is about 38dB. This range is partly because the band widens with the increase of α^{Σ}, and partly because the band is more and more sloped.

Figure5-16b The receiver condition number is 13dB, and the source group is the same as above. As expected, the lower condition number for the receiver gives a narrower band with a width less than 7dB in the range of $\alpha^{\Sigma} < 10^{-1}$. The band has a slight slope in the range of $0.5 \times 10^{-1} < \alpha^{\Sigma} < 10^{-1}$. Again, above this frequency the band widens. The range is 8 dB in the range of $\alpha^{\Sigma} < 10^{-1}$. The variation range is about 37dB in the range of $0.1 < \alpha^{\Sigma} < 10$.

5.4.1.2 General normalized active power band for CP1 and CP2

Figure5-17a. The stiffness receiver is the same as for Figure5-16a. The band width varies with α^{Σ}. In the middle range of α^{Σ} the band is narrowest and is flattest. For $\alpha^{\Sigma} < 10^{-1}$ the range for CP1 is 26dB, which is 16 dB larger than that for CF. On the other hand, for $10^{-1} < \alpha^{\Sigma} < 10$ the range for CP1 is 10dB which is 28dB less than for CF over the same range.

Figure5-17b. the stiffness receiver is the same as for figure5-16b. The shape of the band is similar to that in figure5-17a.

Results for CP2 were very similar and are shown in figure5-18.

5.4.1.3 Discussion for stiffness sources

Some important and interesting results arise for the combination of stiffness on stiffness systems. In the case where the average point mobility magnitude of the source is much greater than that of the receiver, the general normalized active power band for CF is not only flatter but also narrower than that for CP1. This result

indicates that CF is better than using CP1 as a source strength characterisation, even when the different sources have the same average point mobility magnitude. However, in the matched region the results are the opposite. This is different from the single point case, where if the different sources have the same mobility, the rank ordering for CF and CP1 are identical.

5.4.2. Combination of stiffness source on single mode resonant receiver

The single mode resonant receiver matrix was constructed by using the same method as in section 5.3. Figure5-19 a, b, c plots the three general normalized active power bands.

5.4.2.1 General normalized active power band for CF

Figure5-19a. In the range of $\alpha^\Sigma < 0.1$ the band width for CF is about 19dB, and the band is flat. In the range of $0.1 < \alpha^\Sigma < 10$ the band is not flat and the band width changes slowly with α^Σ. This phenomenon could be anticipated from figure 5-16 and figure5-20, where the larger the receiver condition number the slower the variation of band width. The range of the General normalized active power is about 50dB, it is much bigger than the band width due to the slope of the band.

5.4.2.2 General normalized active power band for CP1

Figure5-19b. In the range of $0.001 < \alpha^\Sigma < 10$ the band width shows a small change with α^Σ, decreasing from 22dB to 17dB over the range. In range of $0.001 < \alpha^\Sigma < 0.1$ the band is wider than that for CF due to the slope. In the range of $0.1 < \alpha^\Sigma < 10$ the band is a little narrower than General normalized active power band for CF. The band is still

sloped, but less strongly than that for CF. The range in active power is 30dB for $0.1 < \alpha^{\Sigma} < 10$, this range is 20dB less than that for CF.

Conclusions for CP2 are similar, Figure5-19c.

5.4.3 Combination of stiffness source with off-resonant receiver

Figure5-20~5-22 shows three General normalized active power bands where figure a and b correspond to condition numbers for the off-resonant receiver of 27dB and 10dB respectively. These three figures are similar to those for the combination of stiffness source and stiffness receiver shown in Figures 5-16~5-18. The band width for $0.001 < \alpha^{\Sigma} < 0.1$ depends mainly on the condition number of the receiver. In the range of $0.1 < \alpha^{\Sigma} < 10$. the bands for CP1 and CP2 of figure 5-17~5-18 (stiffness case) are slightly narrower and flatter than that of figure 5-21~5-22 (off resonant case).

5.4.4Combination of stiffness source with infinite plate receiver

Similarly, figures 5-23~5-25 show three bands, where Figure a and b correspond to 23dB and 10dB condition number of the infinite plate receiver respectively. The properties of the bands are similar to those for the combination of stiffness source with off-resonant receiver.

5.5 Combination of off-resonant source on various receivers

The off-resonant sources were chosen from random functions of Matlab and the chosen receiver is similar to section 5.4.

Figure5-26~5-35 shows three General normalized active power bands. The properties of the General normalized active power band are similar to those for the combination of stiffness source on any receiver, except that the curves are shifted slightly to the right.

5.6 Combination of single mode resonant source on various receivers

As for the mass like source, the SVD (Singular Value Decomposition) method was used the mobility matrix for the single mode resonant source is not full rank. In this case the relationship between the CF and CP1 and CP2 are simply:

$$CP1 = CF\sum Y_{S,ii} \qquad (5\text{-}17)$$

$$CP1 = CP2 \qquad (5\text{-}18)$$

Therefore, the width of the three General normalized active power bands is the same.

5.6.1 Combination of single resonant source with stiffness receiver

Fig5-36~5-37 shows the general normalised active power band for CF and CP1, The stiffness receiver matrices are the same as those in section 5.5.1. In comparison with the previous section, here the band has 'moved' obviously to the right. (The range of the plot has been extended to $\alpha^{\Sigma} = 100$ to show this).

Figure5-36 shows that the 'flat' part of the band for CF extends to $\alpha^{\Sigma} = 1$ or more, but the band width in the 'flat part' is wider than that for other types of source. Figure5-37 shows that the maximum for CP1 appears in the range of $\alpha^{\Sigma} = 3$~30.

5.6.2 Combination of single resonant source with off-resonant receiver and infinite plate

Figure5-38~5-41 shows the general normalised active power band for CF and CP1. The corresponding receiver matrices are the same as that in section 5.5.1. The properties of the corresponding band are similar to that in Figure5-36~5-37. The shift

to the right seen in Figure5-38~5-39 (off-resonant receiver case) is here not so obvious.

5.7 Example

In this section an example of a real system is presented, which has been arbitrarily chosen to consist of a stiffness source on a stiffness receiver.

Figure5-42a shows a small SSSS plate which is the modelled source and figure5-42b shows another larger SSSS-plate which is the modelled receiver. The small plate is called the source plate and the larger plate the receiver plate. The physical constants for the two plates are the same: density $\rho = 2.87 \times 10^3 \, kg/m^3$,Poisson's ratio $v = 0.3$, Young's modulus $E = 2 \times 10^{10} \, N/m$, loss factor $\eta = 0.05$. The geometrical parameters of the source and receiver plate including the mount positions are shown in Figure5-42a, and Figure5-42b respectively. Now we consider three cases where the source plate is:

1) 5cm,

2) 2cm,

3) 5mm.

The source plate free velocity was obtained by the following method: an excitation force couple was applied to the source plate at a random position. A number of free velocity vectors were then combined with the mobility matrix to describe a source group. When the source is connected to the receiver plate, the General normalised active power can be obtained.

Before showing the numerical results, it can be shown that, when the source plate and the receiver plate are stiffness controlled, the General normalised active power for

CP1 is independent of frequency and for CF it is proportional to frequency. This result can be proved by the following development. The active power emission is given by:

$$P = \text{Re}([\hat{V}_{sf}]^{T*}([Y_R]+[Y_S])^{-1T*}([Y_R])([Y_R]+[Y_S])^{-1}[\hat{V}_{sf}]) \quad (5\text{-}19)$$

where $[\hat{V}_{sf}]$ is the free velocity vector, $[Y_R]$ is the receiver mobility matrix, $[Y_S]$ is the source mobility matrix, and T* indicates complex conjugate.

For stiffness controlled source and receiver, the mobility matrix can be rewritten as follows

$$[Y_R] = \frac{j\omega}{1+j\eta}[y_R] \quad (5\text{-}20a)$$

$$[Y_S] = \frac{j\omega}{1+j\eta}[y_S] \quad (5\text{-}20b)$$

where ω is angular frequency, and $[y_R]$ and $[y_S]$ are functions of position and independent of frequency. The free velocity vector can be rewritten as

$$[\hat{V}_{sf}] = \frac{j\omega}{1+j\eta}\hat{F}(\omega)[v_{sf}] = \Phi[v_{sf}] \quad (5\text{-}21)$$

where $\frac{j\omega}{1+j\eta}\hat{F}(\omega) \equiv \Phi$ is a function of the angular frequency, excitation force and

position while $[v_{sf}]$ is a function of the mount and excitation position, and independent of frequency. Combining the above, the General normalized active power for CP1 can be given:

$$P/|CP1| = \text{Re}([\hat{V}_{sf}]^{T*}([Y_R]+[Y_S])^{-1T*}([Y_R])([Y_R]+[Y_S])^{-1}[\hat{V}_{sf}])/|CP1|$$

$$= \text{Re}([v_{sf}]^{T*}([y_R]+[y_S])^{-1T*}\frac{j}{1+\eta j}([y_R])([y_R]+[y_S])^{-1}[v_{sf}])/\left|[\hat{v}_{sf}]^{T*}\frac{j}{1+\eta j}([y_S])^{-1}[v_{sf}]\right|$$

$$(5\text{-}22)$$

Since frequency does not appear in this equation the general normalized active power for CP1 is independent of the frequency. Similar to the above, the General normalized active power for CF can be given

$$P/|CF| = \text{Re}([\hat{V}_{sf}]^{T^*}([Y_R]+[Y_S])^{-1T^*}([Y_R])([Y_R]+[Y_S])^{-1}[\hat{V}_{sf}])/|CF|$$

$$= \text{Re}([v_{sf}]^{T^*}([y_R]+[y_S])^{-1T^*}\frac{j\omega}{1+\eta j}([y_R])([y_R]+[y_S])^{-1}[v_{sf}])/\left|[v_{sf}]^{T^*}[y_S]^{-1T^*}([y_S])^{-1}[v_{sf}]\right|$$

(5-23)

which is proportional to frequency.

We now consider case 1), where the sum of the point mobility magnitude of the small plate and the receiver plate is plotted in Figure 5-43a. When the frequency is less than 100 Hz, the source plate and receiver plate are stiffness controlled. The ratio of average point mobility magnitude $\alpha^\Sigma \approx 2$.

Figure5-44 gives twenty straight lines, each corresponding to one excitation, or say corresponding to a particular source. Figure5-44a and b are the General normalized active power for CP1 and CF respectively plotted against frequency. Twenty lines for Figure5-44a are in the range of 8dB, while twenty lines for Figure5-44b are in the range of 15dB. These results coincide with figure5-16 and figure5-17, where the General normalized active power band for CP1 is narrower than that for CF when $\alpha^\Sigma \approx 2$.

For case 2), the sum of the point mobility magnitude of the source plate and receiver plate is plotted in Figure5-43b. Again, below 100 Hz the source and receiver plates are stiffness controlled, with $\alpha^\Sigma \approx 0.1$. Similarly to case 1, twenty lines of the General normalized active power for CP1 and for CF are plotted in figure5-45a and 5-45b. Now the range of the twenty lines for CP1 and for CF are comparable. Again, this

result coincides with figure5-16 and figure5-17, where the General normalized active power band for CP1 and CF are comparable when $\alpha^{\Sigma} \approx 0.1$.

Mobilities for case 3) are plotted in Figure5-43c. In the range of frequency below 25Hz both source and receiver plates are stiffness controlled, with $\alpha^{\Sigma} \approx 0.005$. Similarly to the above case, twenty lines of the General normalized active power for CP1 and for CF are plotted in figure5-46 and 5-46b. Now the range for CP1 is wider than that for CF. Again this result agrees with figure5-16 and figure5-17, where the General normalized active power band for CP1 is wider when $\alpha^{\Sigma} \approx 0.005$.

This section shows that although the generic structures used earlier in this Chapter to derive the general normalised active power bands are 'artificial' constructions, the results obtained are in agreement with those from 'real' structures. This goes some way towards validating the approach, and further validation will be reported in Chapter 6.

5.8 Conclusion

Three general normalised active power bands (for CF, CP1 and CP2) have been studied for combinations of different source and receiver types.

In all cases the results for CP1 and CP2 were similar, and it is not necessary to discuss these two parameters separately. Thus, we have two broad approaches in which the active source properties are characterised by blocked force (CF) or characteristic power (CP1/CP2).

Conclusions relating to each source type are as follows.

- For mass–like sources the band widths are similar. The flat range of the band for CF extends to $\alpha^{\Sigma}=0.1$ or more, so in the range of $\alpha^{\Sigma}<0.1$, using CF as a source strength parameter to characterise sources is better than using CP1 (or CP2). For the matched case ($0.1<\alpha^{\Sigma}<10$), the general normalised active power bands are more complicated. In the case of stiffness receivers there are several peaks and the bands are wide. In the case of off-resonant and infinite plate receivers, the bands for CP1, and CP2 are relatively 'flat', so using either as a source strength is better than using CF. However, if the receiver is sharply resonant the band is not flat, in other words the power is still dependent on the mobility ratio.

- For stiffness sources the band width for CF and CP1 (CP2) are no longer similar. In the range of $\alpha^{\Sigma}<0.1$ the band for CF is still flat and narrower than for CP1 and CP2, so in this range using CF as a source strength is better than using CP1 or CP2. However, in the matched region, the bands for CP1 and CP2 are relatively flat and relatively narrow by comparison with CF. Therefore, in the matched region using a power quantity as a source strength is more reasonable than using blocked force.

- For off-resonant sources the band properties are similar with those for stiffness sources, and the conclusions are the same.

- For single mode resonant sources, the band widths are the same. There is a deterministic relationship between CF, CP1, CP2 (given by equation (5-17,18). The 'flat' range of the band for CF extends well into the matching region, to $\alpha^{\Sigma}\approx1$ or more. So, for this case CF may be a better source strength parameter than CP1 (or CP2) even for matched sources and receivers. Overall, the strongly resonant behaviour is less significant in terms of high power flow

than might have been expected. Furthermore, this type of source appears to be uncommon, in fact is almost non-existent in practical cases.

Thus, it is generally found that for low mobility receivers the blocked force approach is favourable, whereas in the matched region the characteristic power approach is usually preferable. This is because the band of uncertainty for CF is relatively narrow for all receiver types below to $\alpha^\Sigma < 0.1$, typically the 90% probability bands are less than 12dB wide in all cases except strongly resonant receivers or sources, and less than about 8dB in many 'typical' cases. Furthermore, since the bands are flat, the power is almost independent of the mobility ratio, and CF can therefore reasonably be considered as a 'source strength' parameter. In the matched region, the situation is more complicated as might be expected, but the band for CP1 or CP2 are as flat or flatter, and as narrow or narrower than for CF in all cases except single mode resonant sources, (and this case is inherently unlikely in that a sharp resonant peak extends over only a very narrow range of frequencies).

For sources commonly used in building services the source mobility is generally one or several decades bigger than that of the supporting floor. Also, concrete floors tend to have relatively high loss factor, so the condition numbers for concrete floors are not high, 10dB is very typical [40]. Therefore, good results should be obtained by using CF to rank machines to be installed on concrete receiver structures.

For receivers of similar material to the source (steel sources on steel receivers is a common example) it is likely that the mobilities will be matched, at least over certain frequency ranges. The power approach is then likely to be most advantageous. Here, a

wider range of uncertainty is expected, although in every case except mass sources and very strong resonant receiver, the band widths do not exceed 13dB. There is also more sensitivity to mobility ratio.

There is one additional potential advantage with the power approach: except for mass-like sources combined with stiffness or off-resonant receivers the 90% probability band never exceeds CP1 or CP2. Thus, CP1 (or CP2) may be considered as practical upper limit for the active power emission. This will be quite reliable unless the source is mass-like. This could be of significant practical value, and provides further grounds to suggest that sources destined for 'matched' sources and receivers should be ranked in terms of characteristic power.

There is no significant difference between CP1 and CP2 therefore since CP2 is much simpler to implement it is preferred over CP1 as a practical working method.
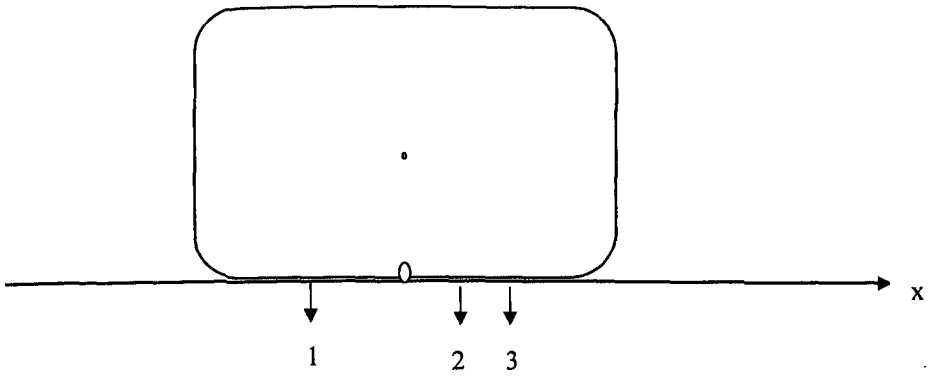
Figure 5-1 Rigid body source with three collinear points
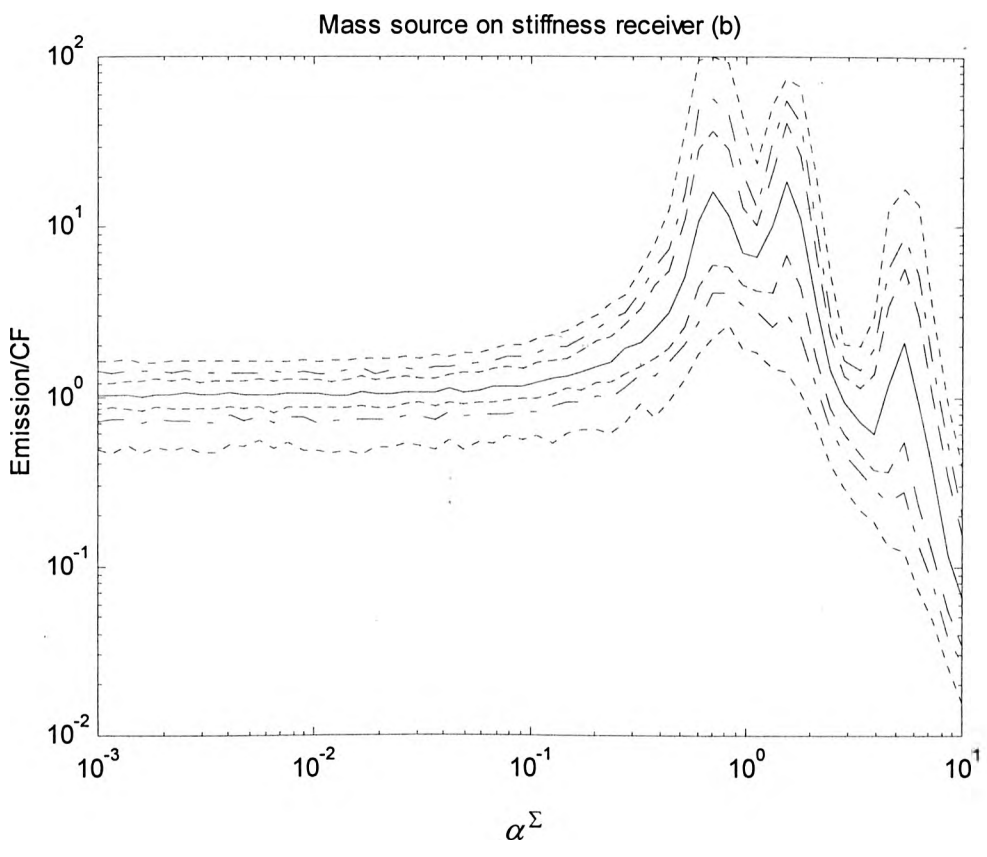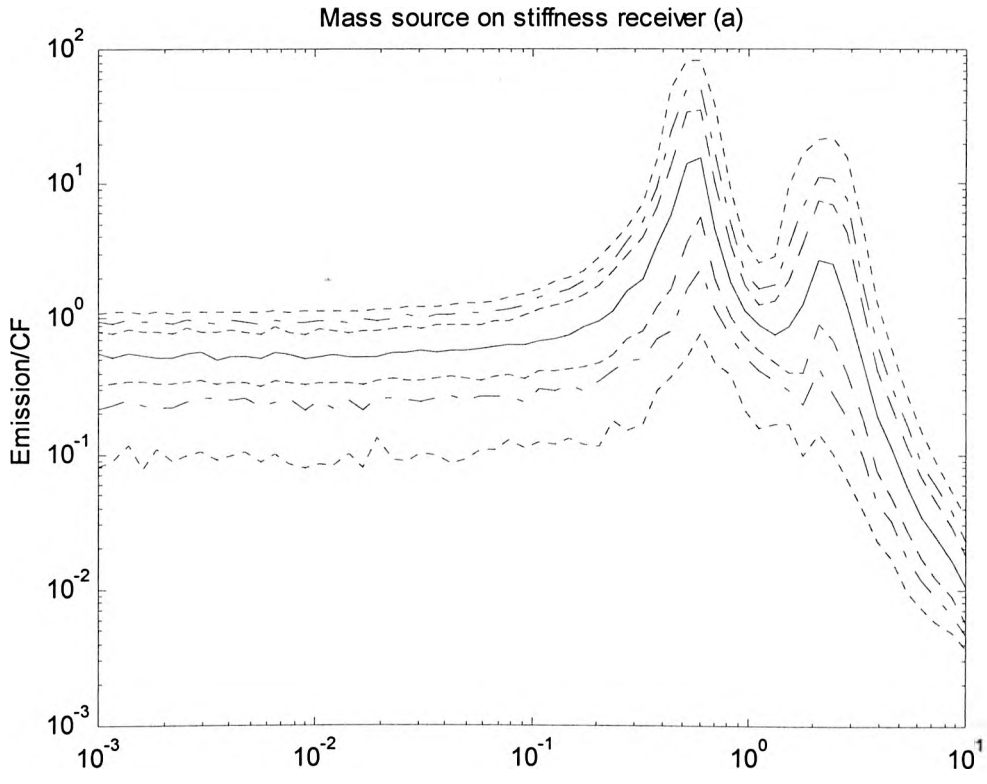
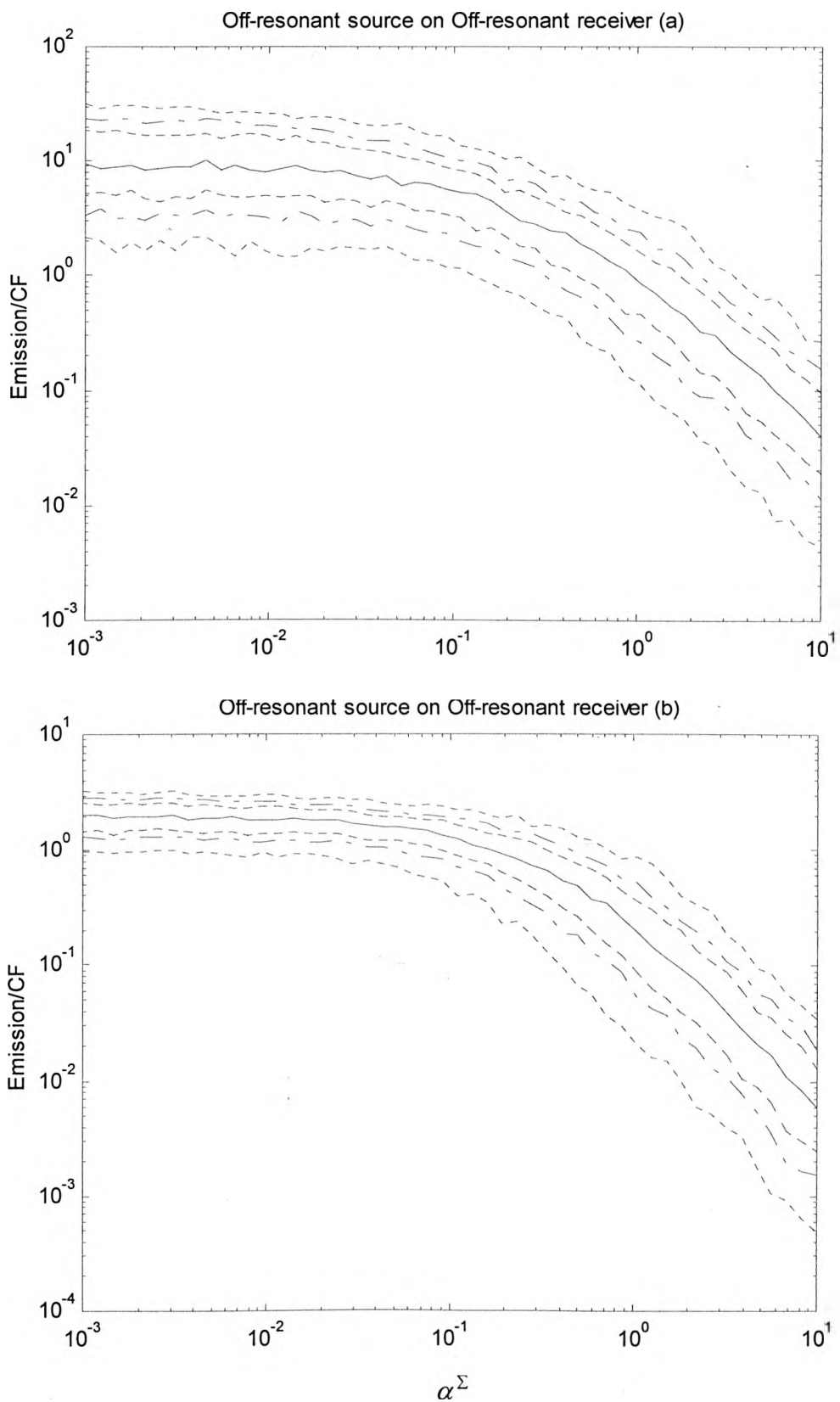**Figure 5-2** General normalised active power bands for CF for a combination of mass source on stiffness receiver. Pairs of curves show probability bands:...90%;-.-.-70%;---50%, solid line is median value Top: condition number 28dB. Bottom: condition number 10dB.
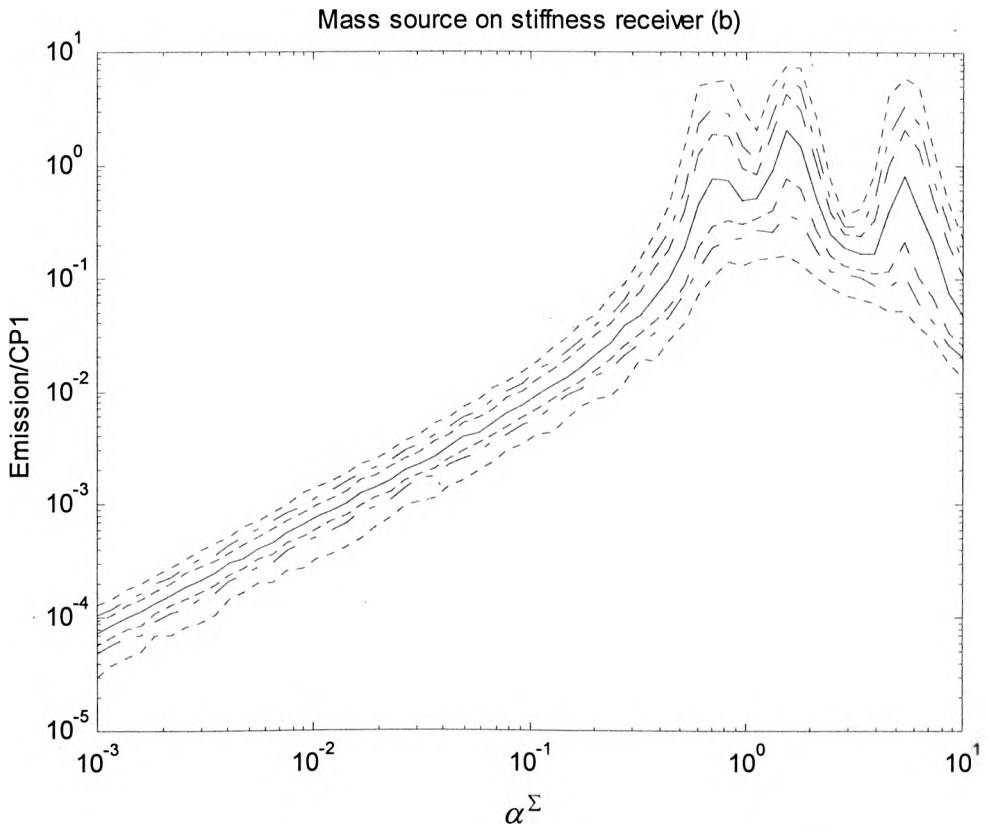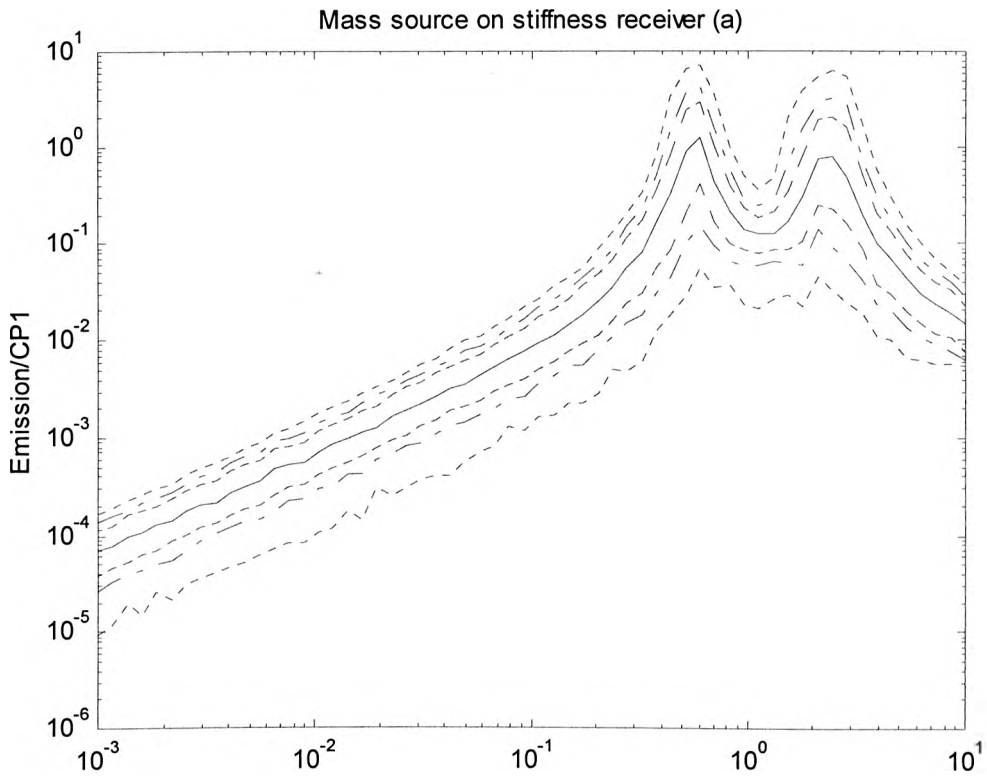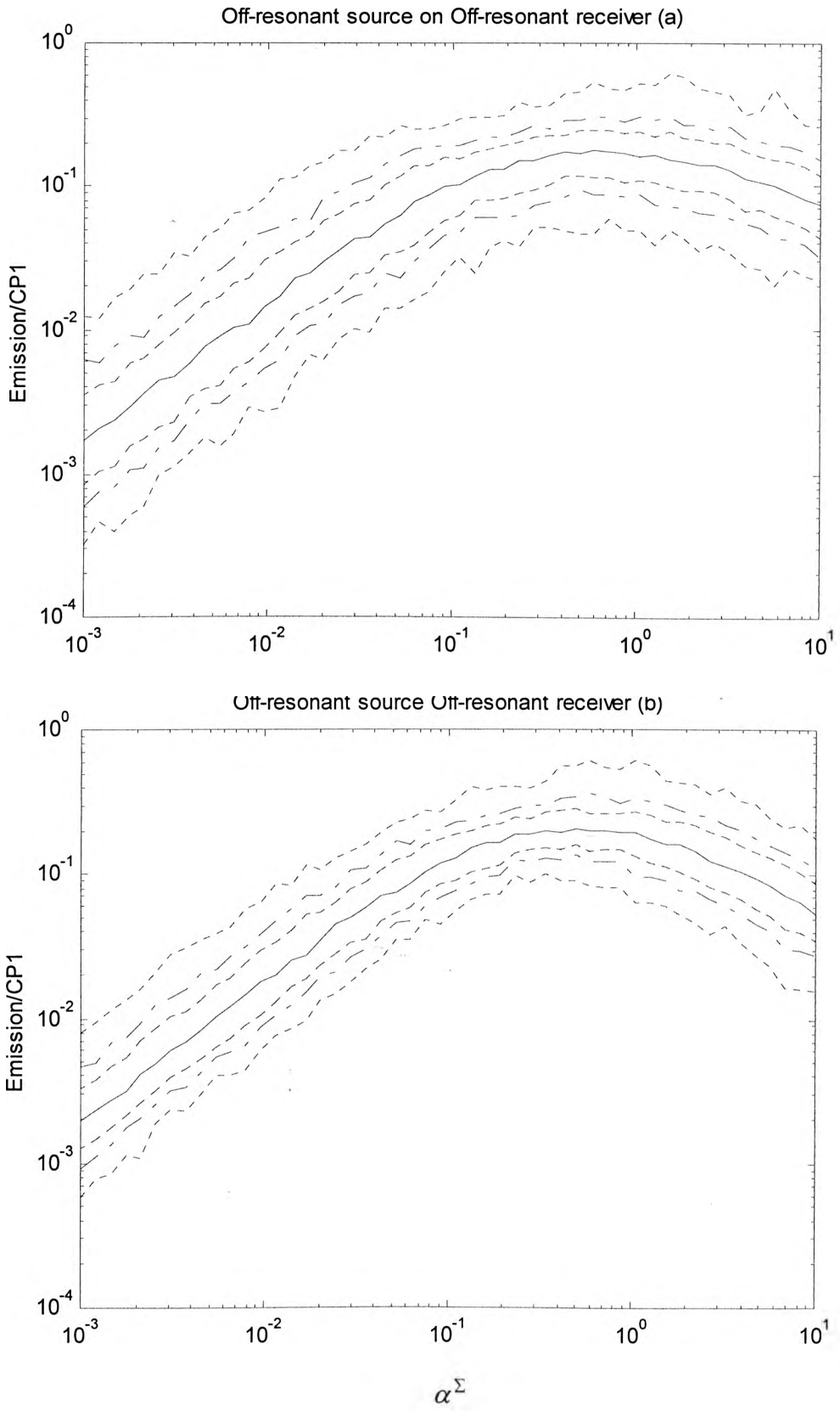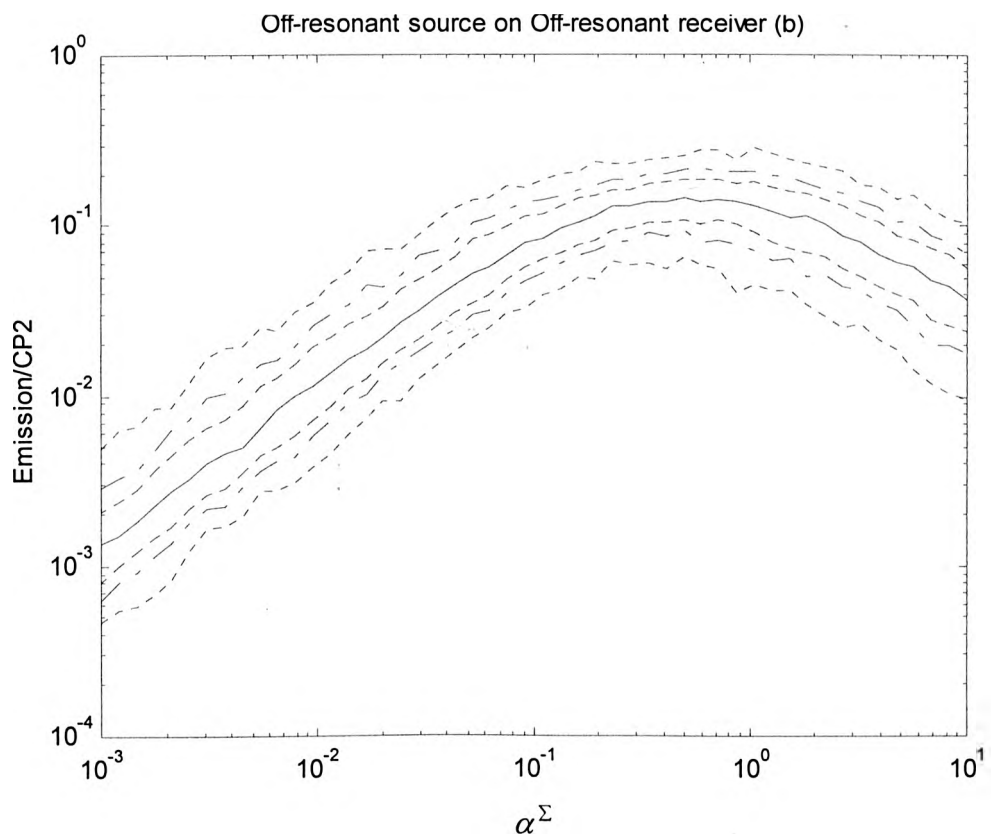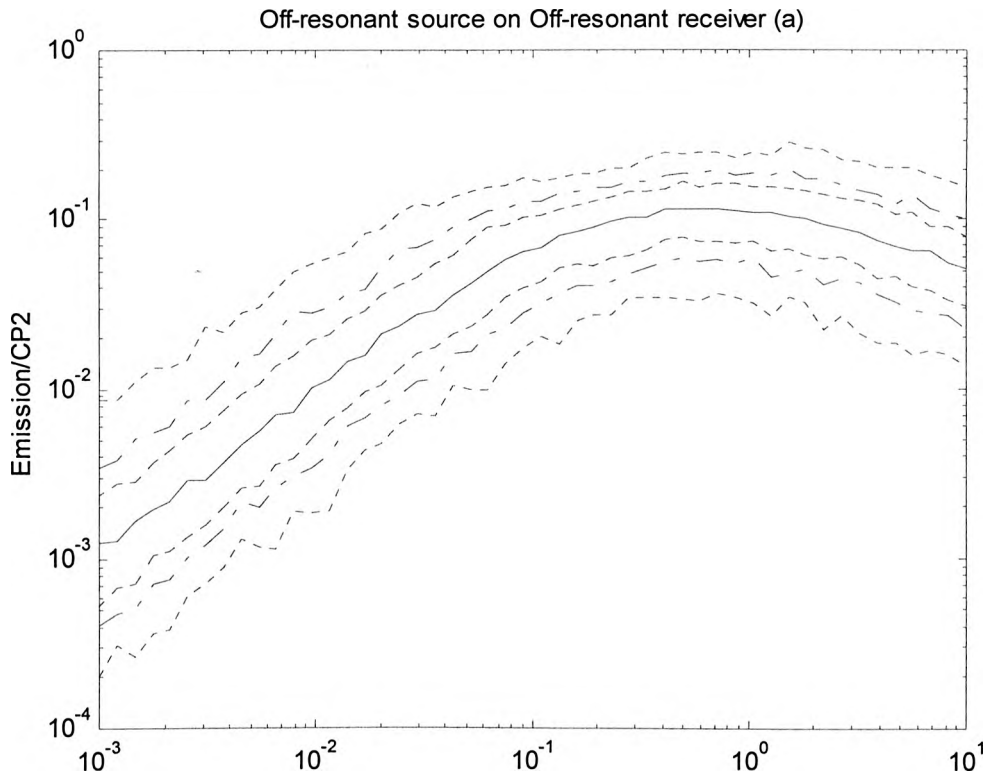
Figure 5-3 General normalised active power bands for CP1 for a combination of mass source on stiffness receiver. Pairs of curves show probability bands:....90%;-.-.-70%;---50%, solid line is median value Top: condition number 28dB. Bottom: condition number 10dB.
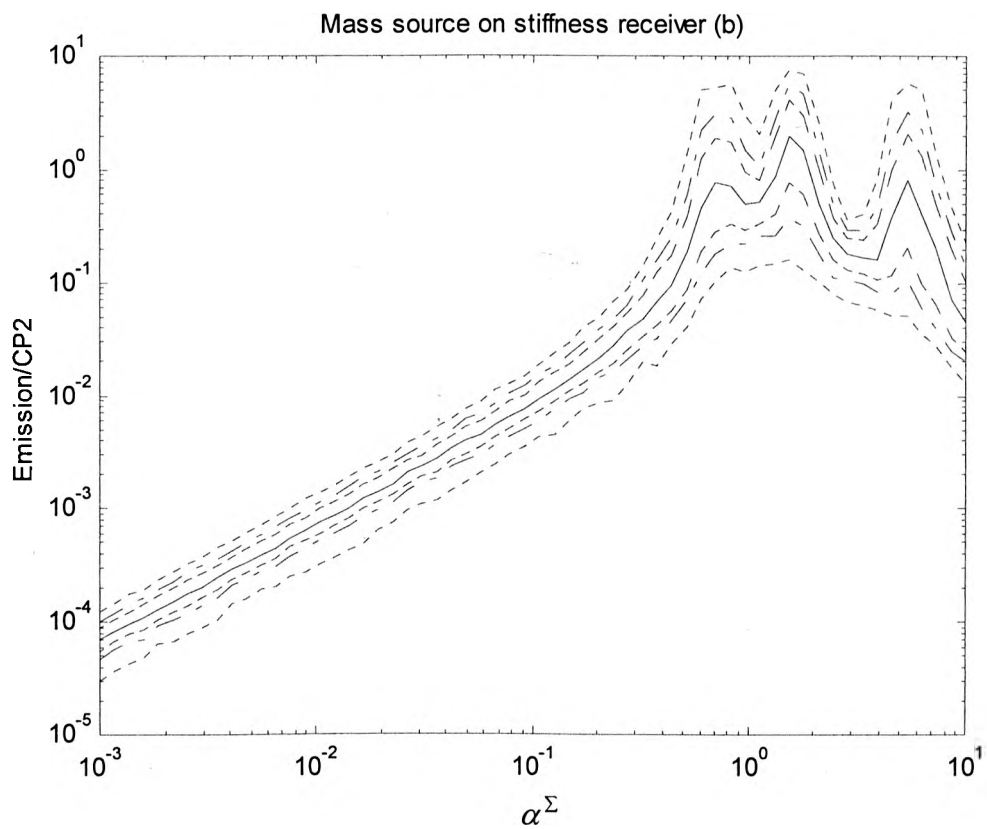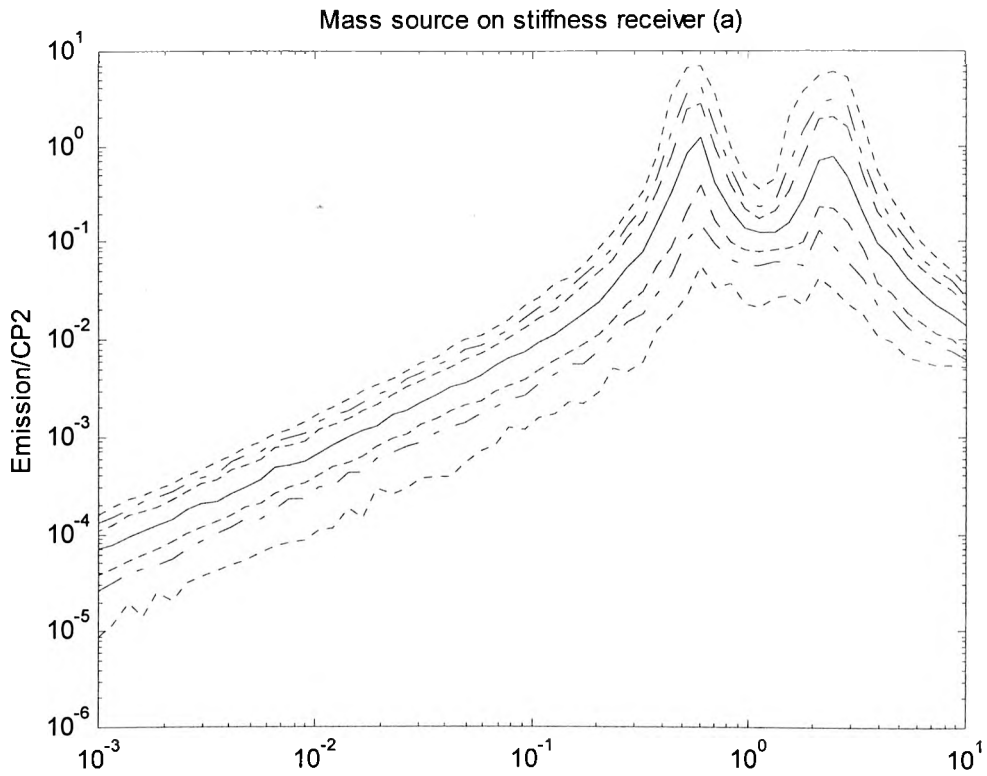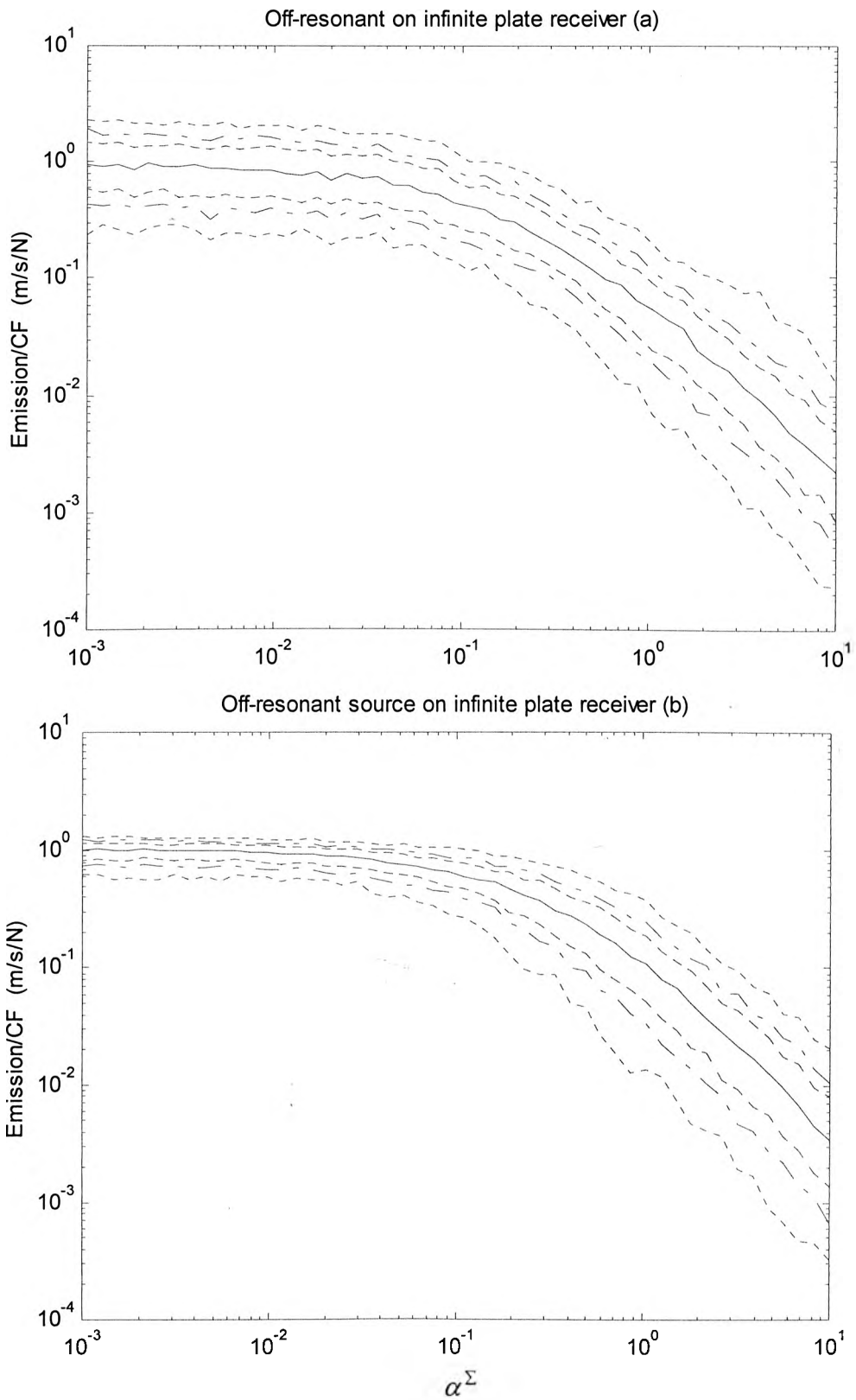
Figure 5-4 General normalised active power bands for CP2 for a combination of mass source on stiffness receiver. Pairs of curves show probability bands:…90%;-.-.-70%;---50%, solid line is median value Top: condition number 28dB. Bottom: condition number 10dB.
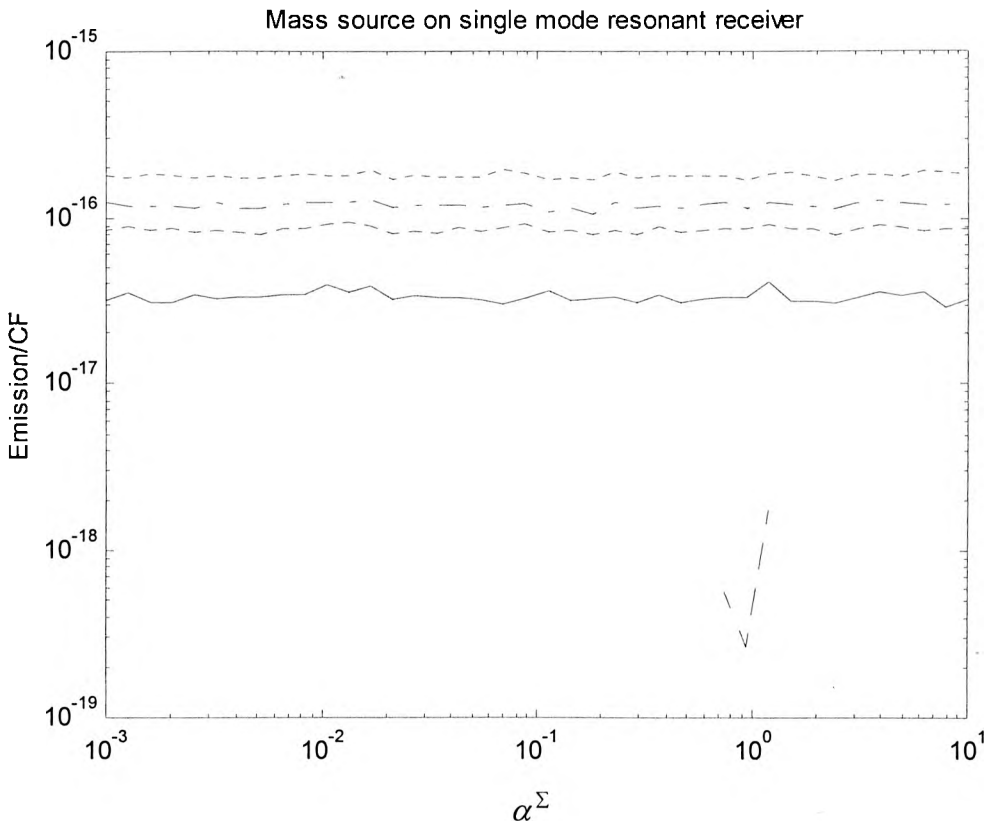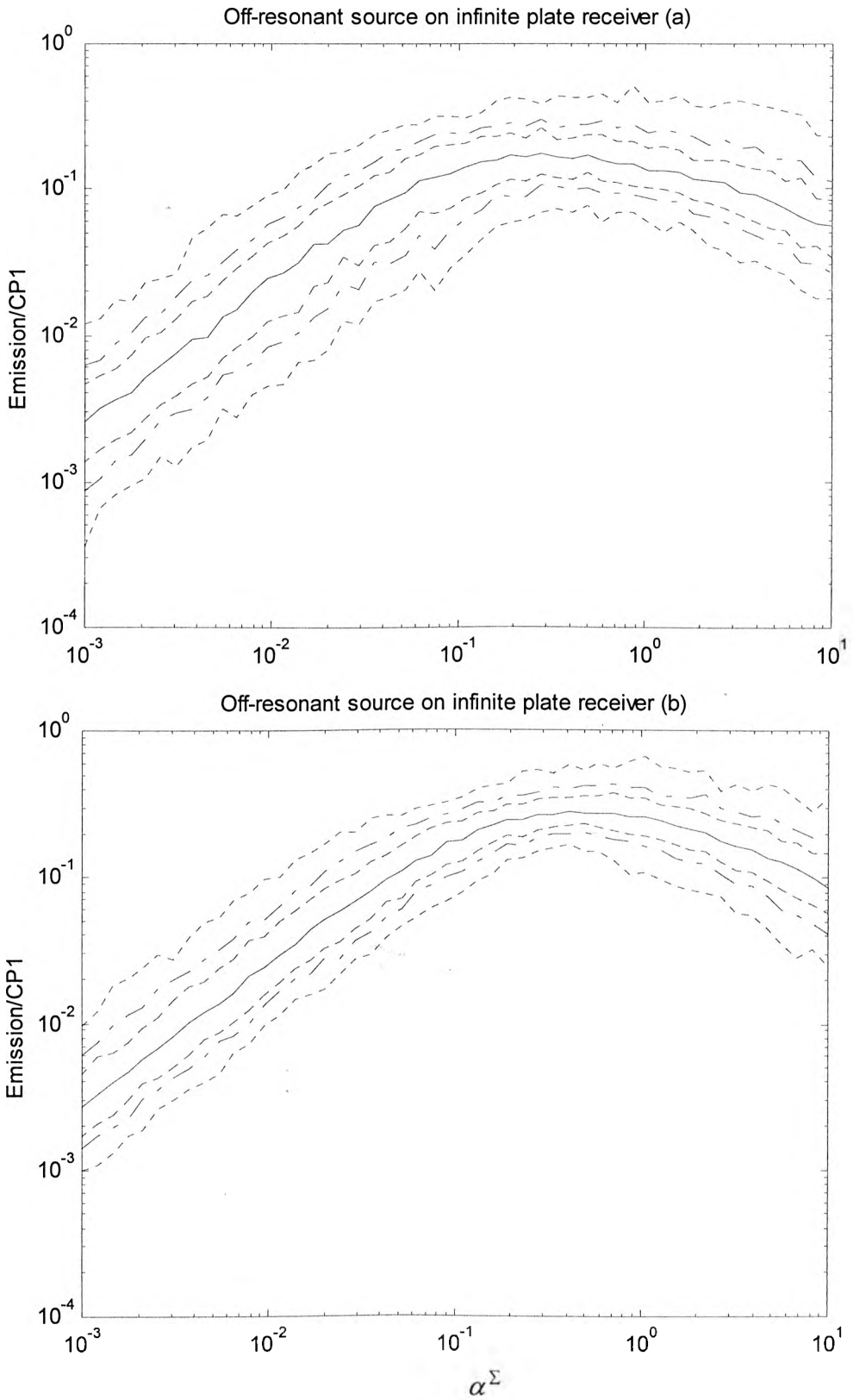
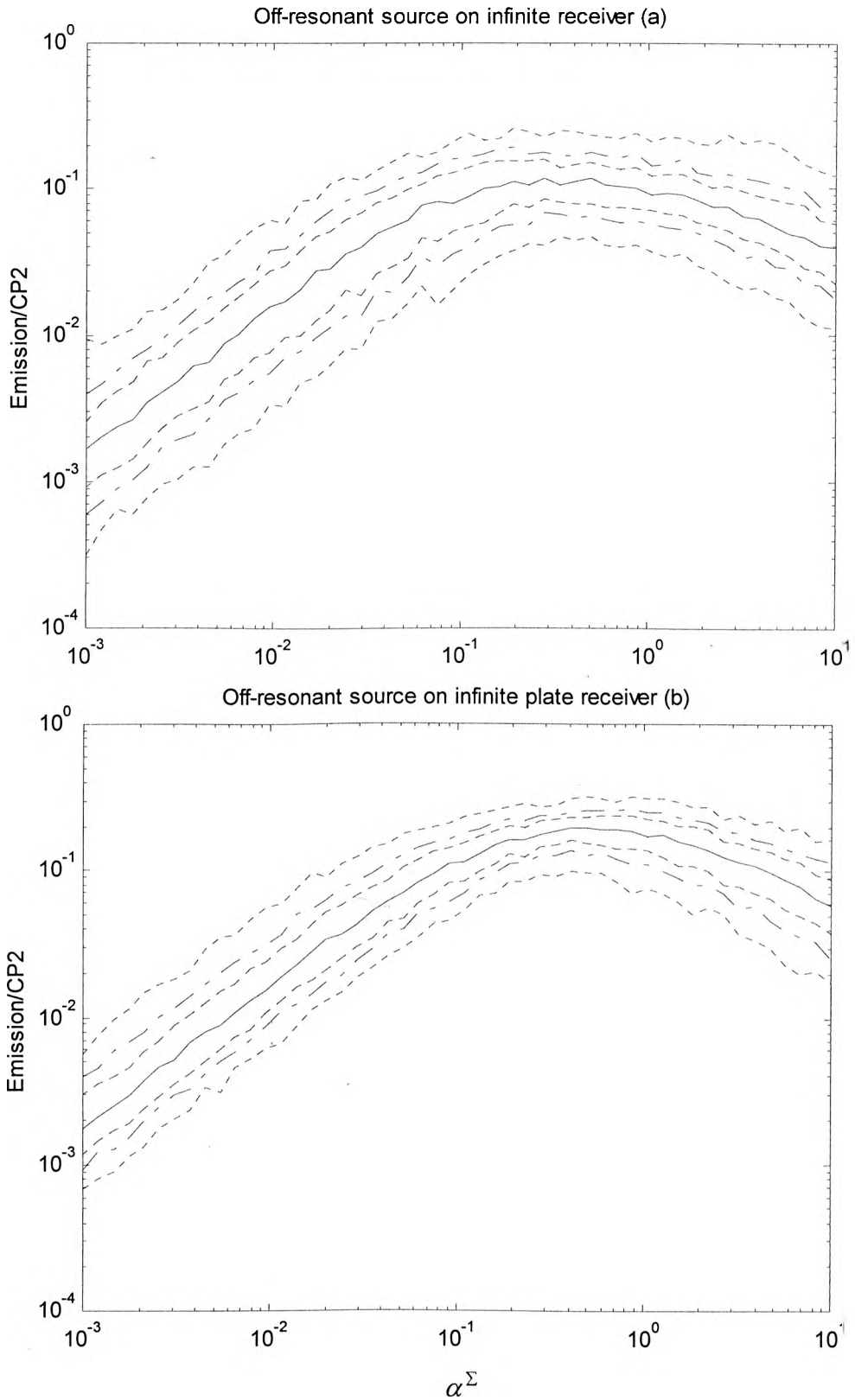**Figure 5-5** General normalised active power bands for CF for a combination of mass source on single mode resonant receiver. Probability bands:…90%;-.-.-70%;---50%, solid line is median value. (Negative values not shown)
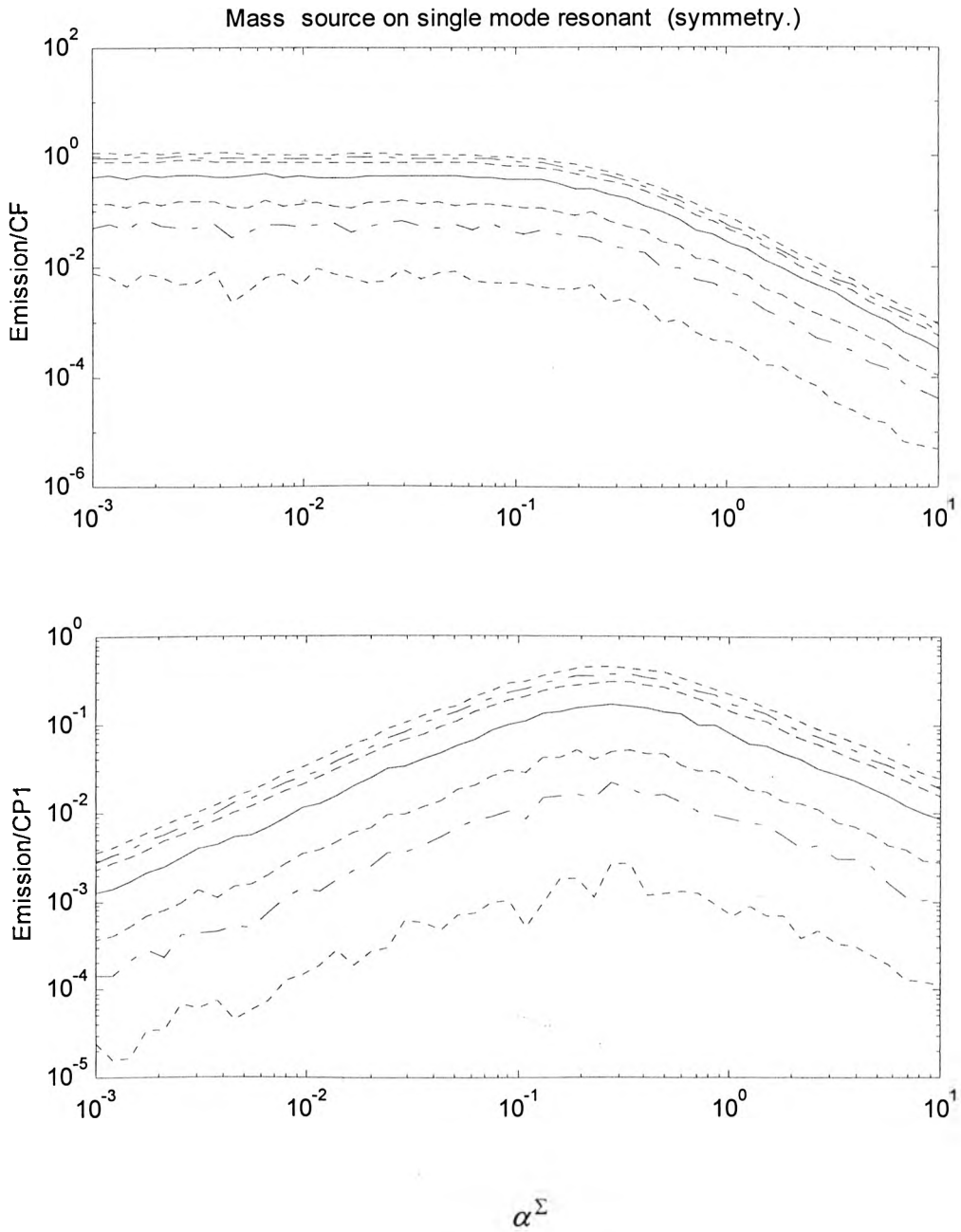
Figure 5-6 General normalised active power bands for CF (top)and CP1(bottom) for a combination of mass source on symmetry single mode resonant receiver. Pairs of curves show probability bands:…90%;-.-.-70%;---50%, solid line is median value.
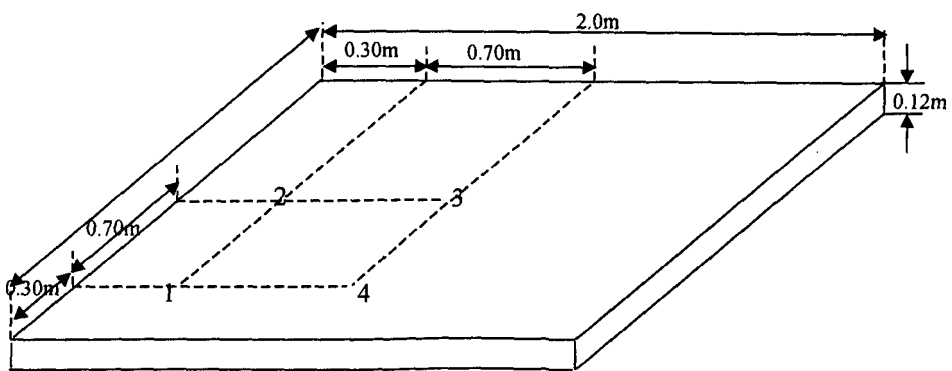
Figure 5-7 SSSS plate
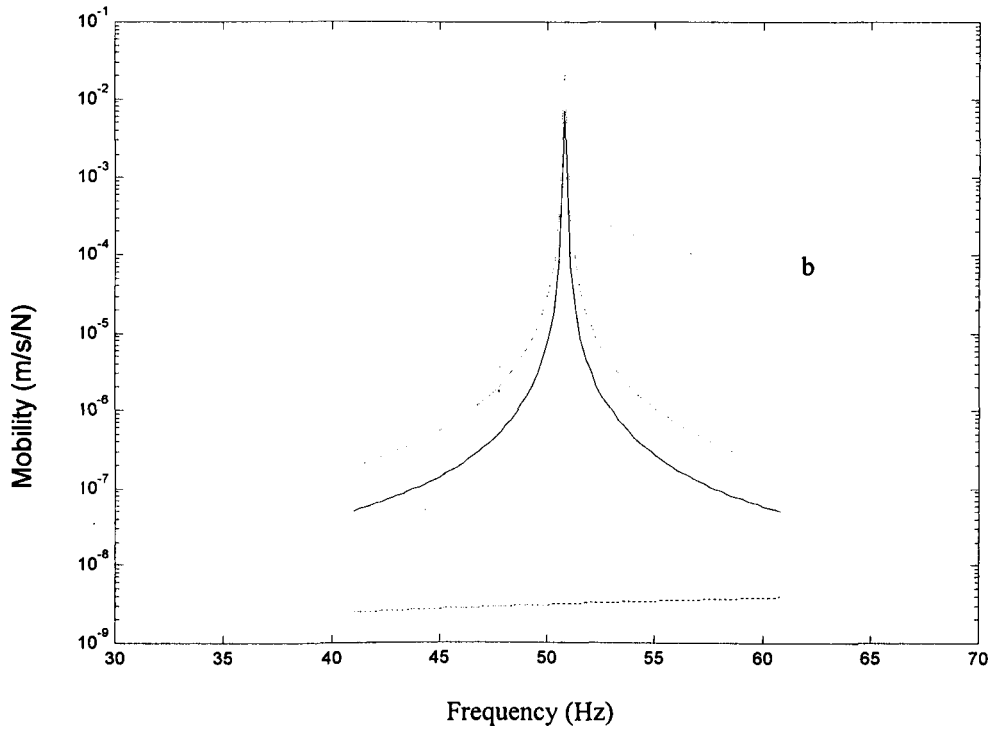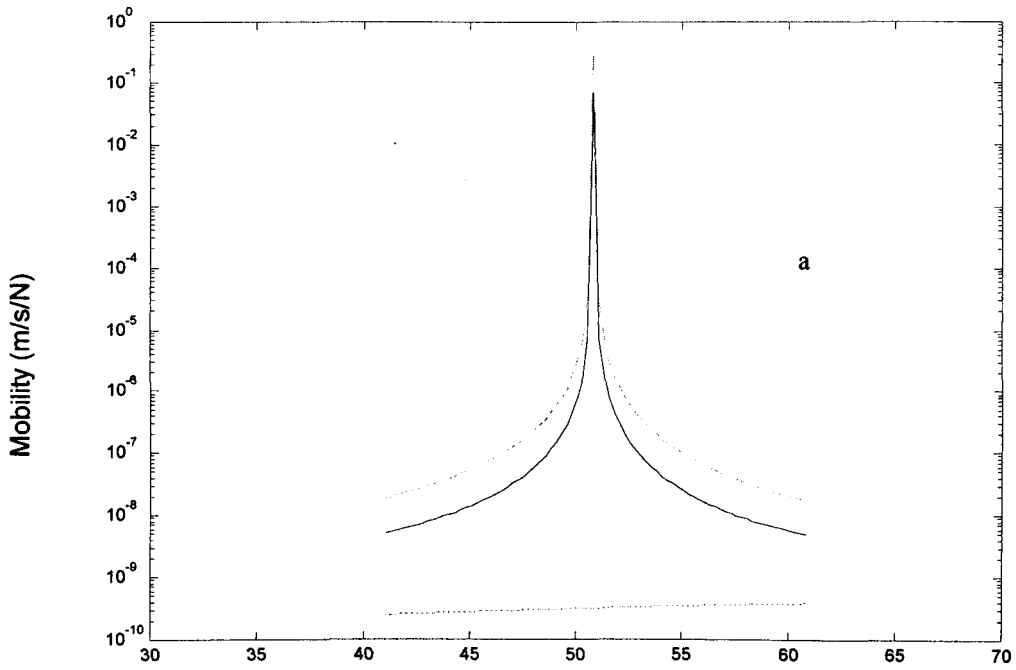
Figure 5-8 Mobility real part eigenvalues for a sharp resonance. a : loss factor η=0.0001;
b: loss factor η=0.001, solid line mean eigenvalue; dashed line max and min.eigenvalue.

Mass source on very sharp resonant receiver (condition number 90dB)

Mass source on very sharp resonant receiver (condition number 70dB)

α^{Σ}
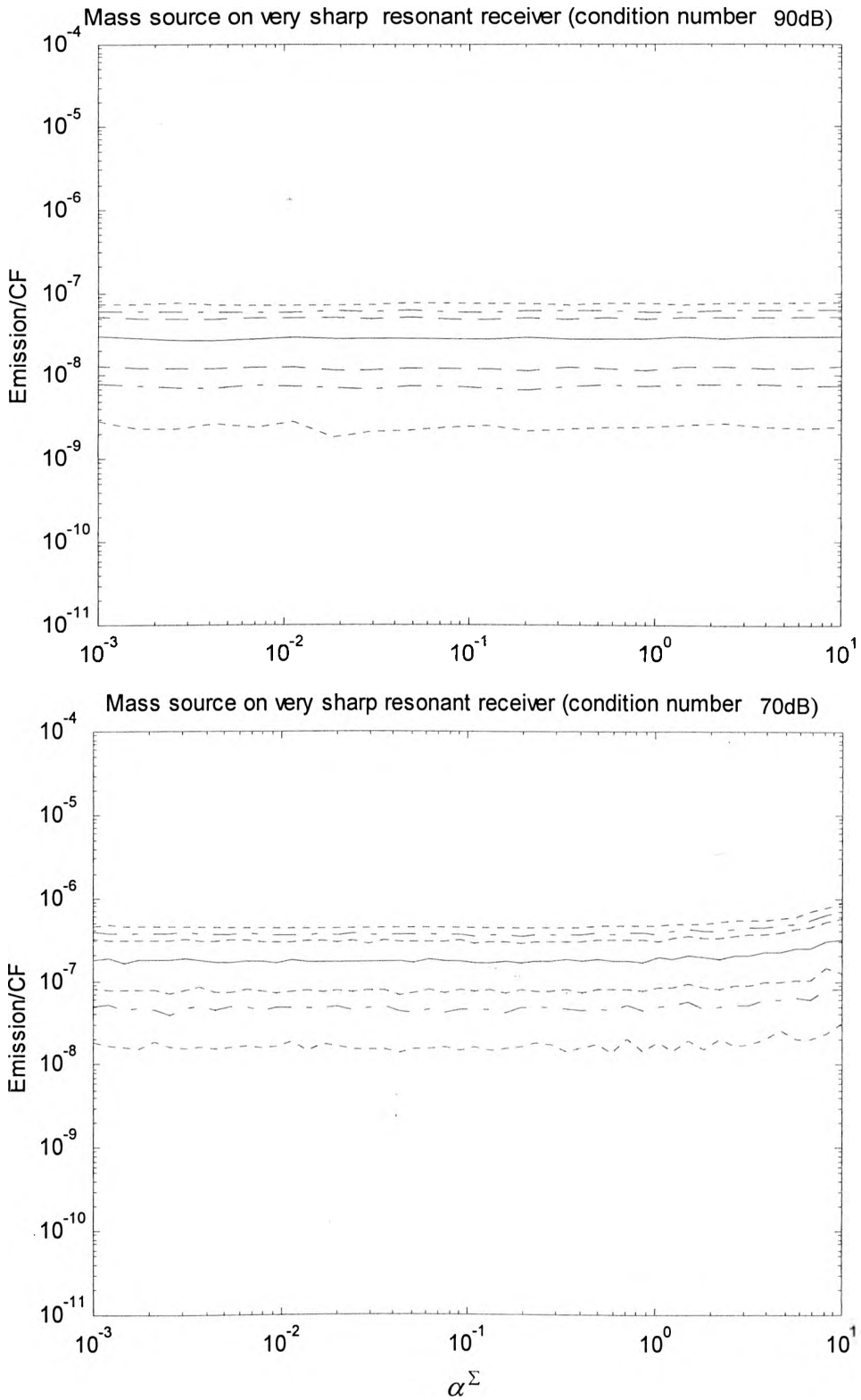
Figure 5-9 General normalised active power bands for CF for a combination of mass source on very sharp resonant receiver. Pairs of curves show probability bands:…90%;-.-.-70%;---50%, solid line is median value Top: condition number 90dB. Bottom: condition number 70dB.
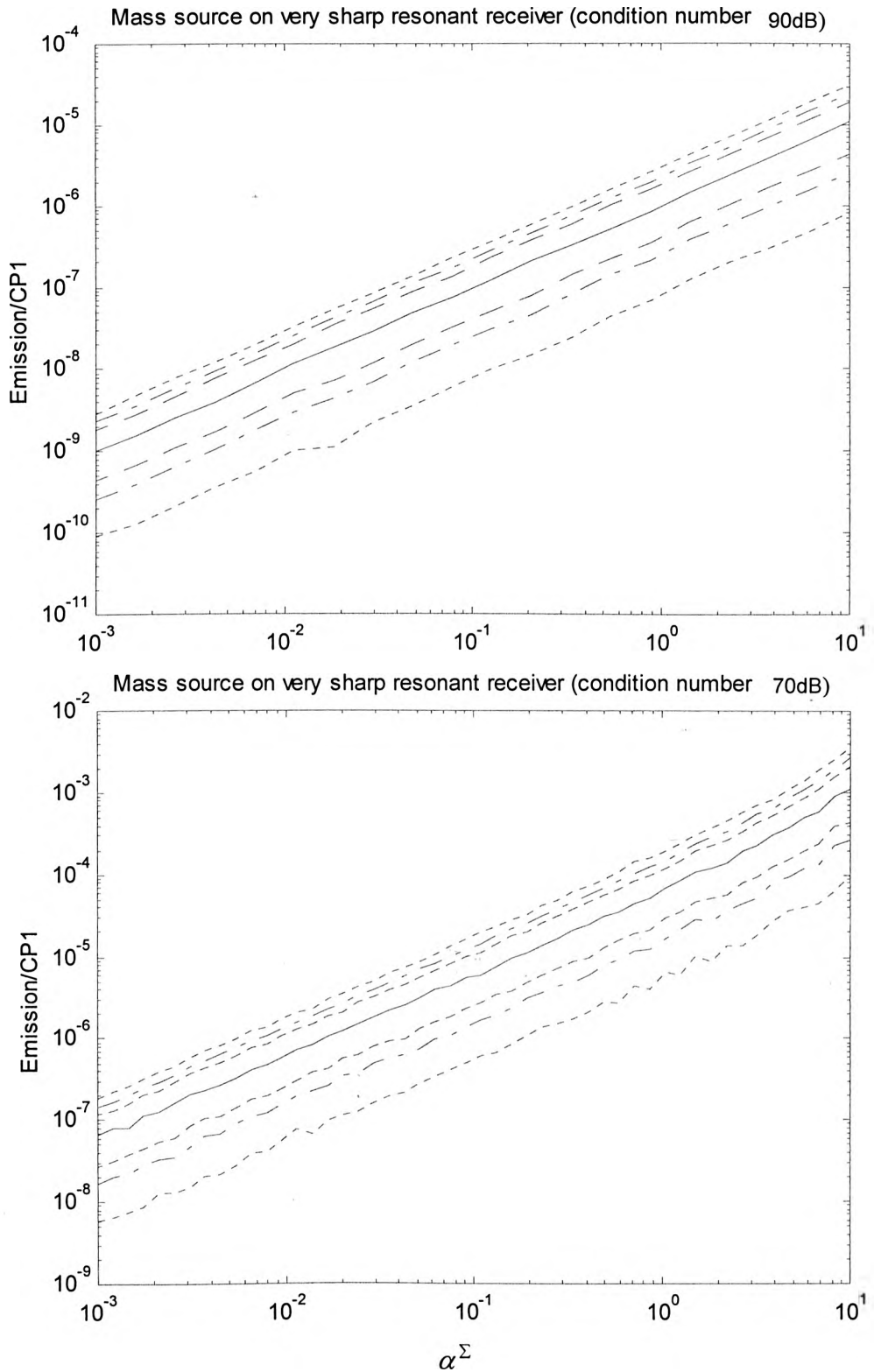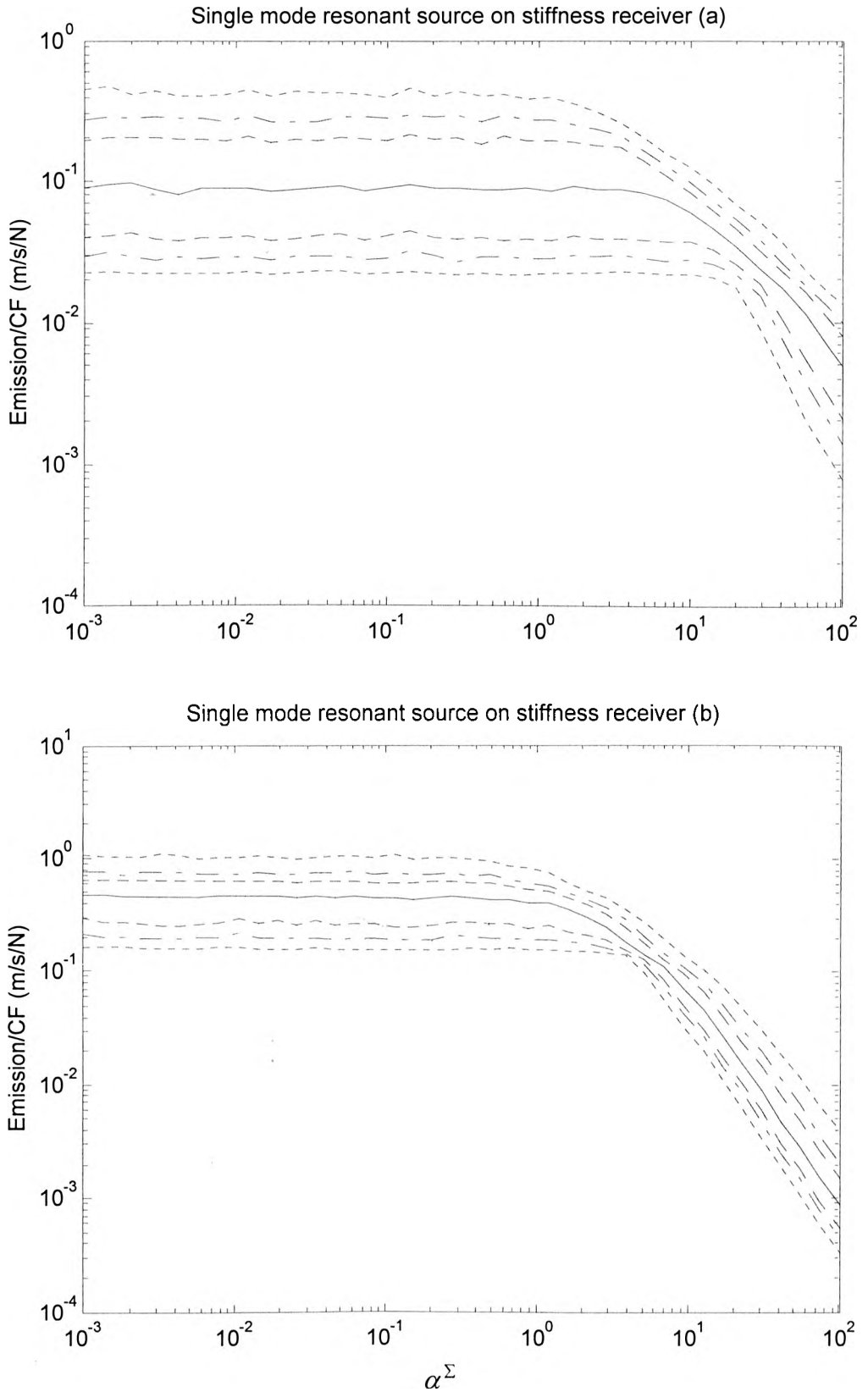
Figure 5-10 General normalised active power bands for CP1 for a combination of mass source on very sharp resonant receiver. Pairs of curves show probability bands:…90%;-.-.-70%;---50%, solid line is median value Top: condition number 90dB. Bottom: condition number 70dB.
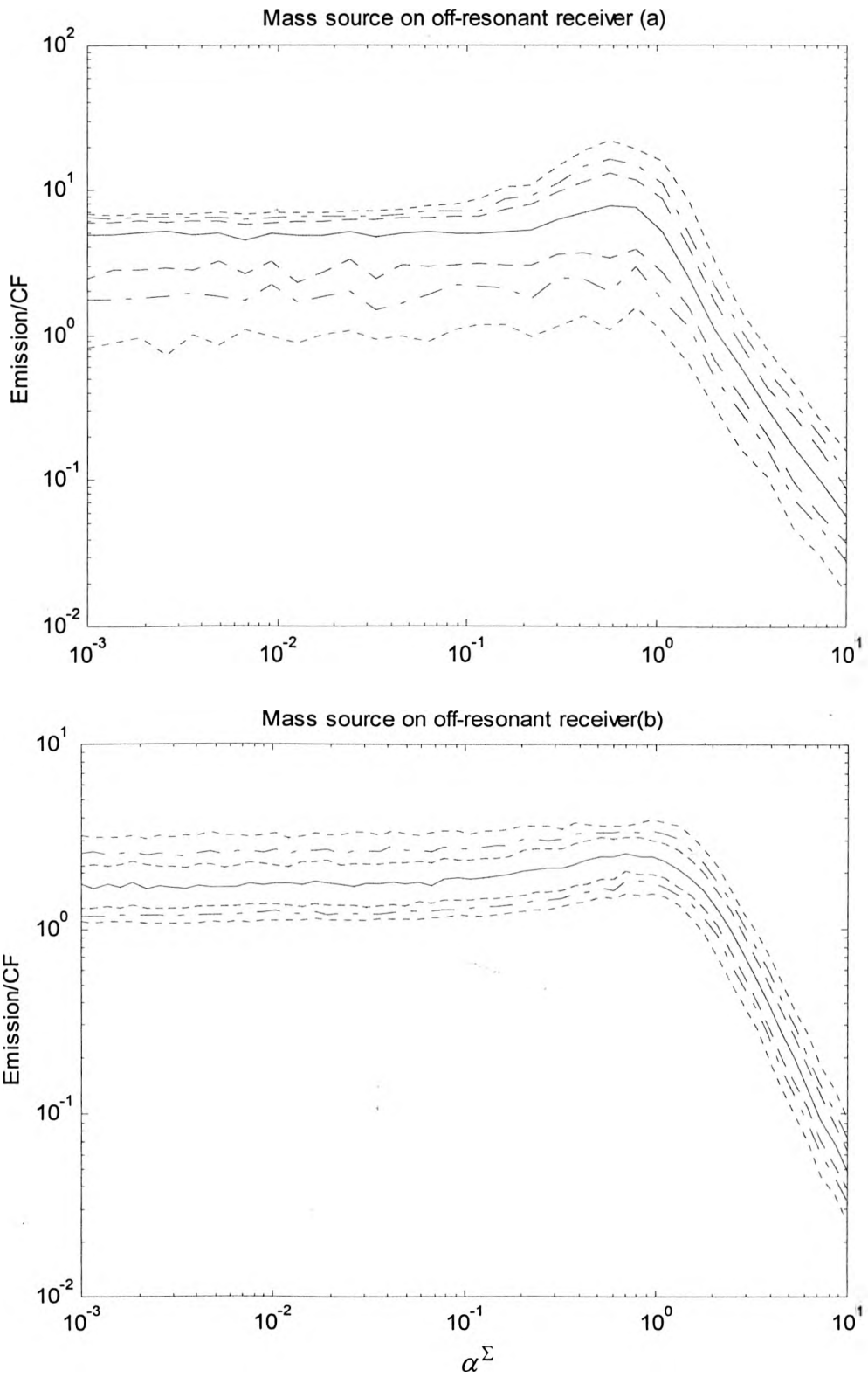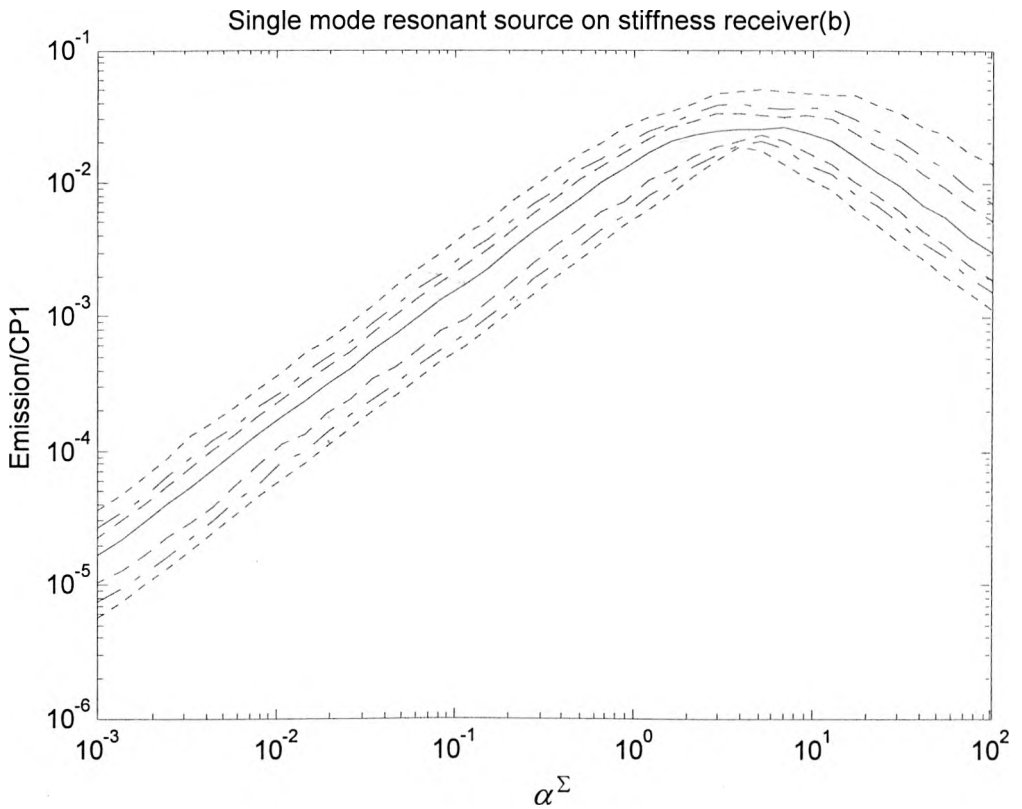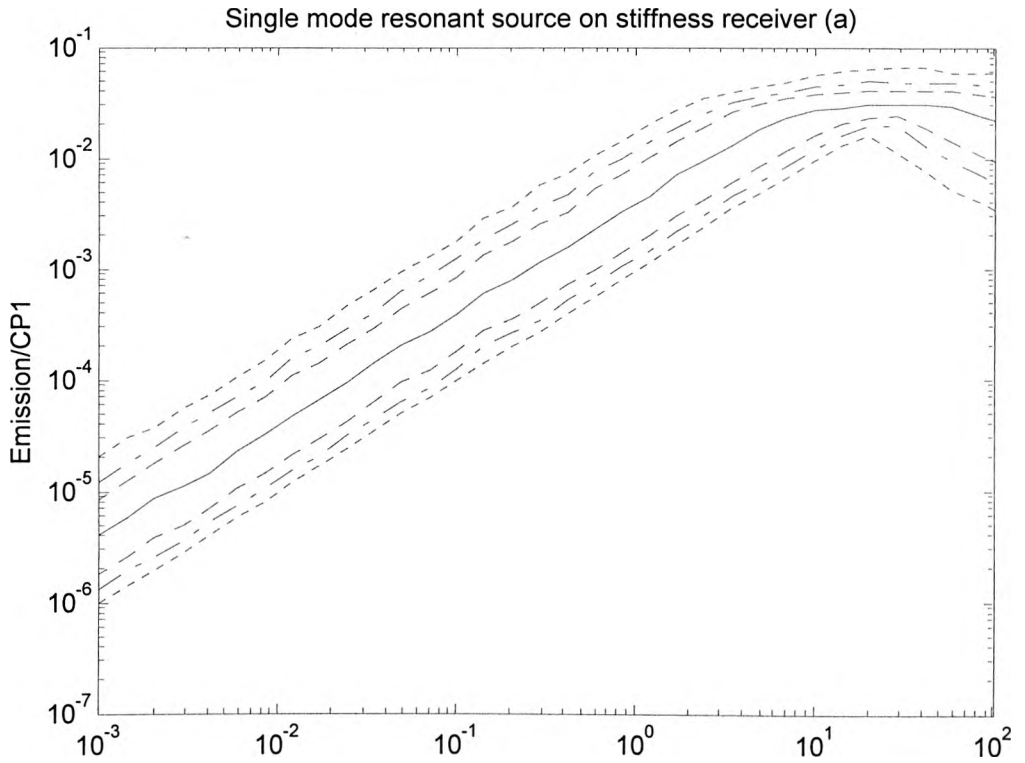
Figure 5-11 General normalised active power bands for CF for a combination of mass source on off-resonant receiver. Pairs of curves show probability bands:…90%;-.-.-70%;---50%, solid line is median value Top: condition number 27dB. Bottom: condition number 10 dB.
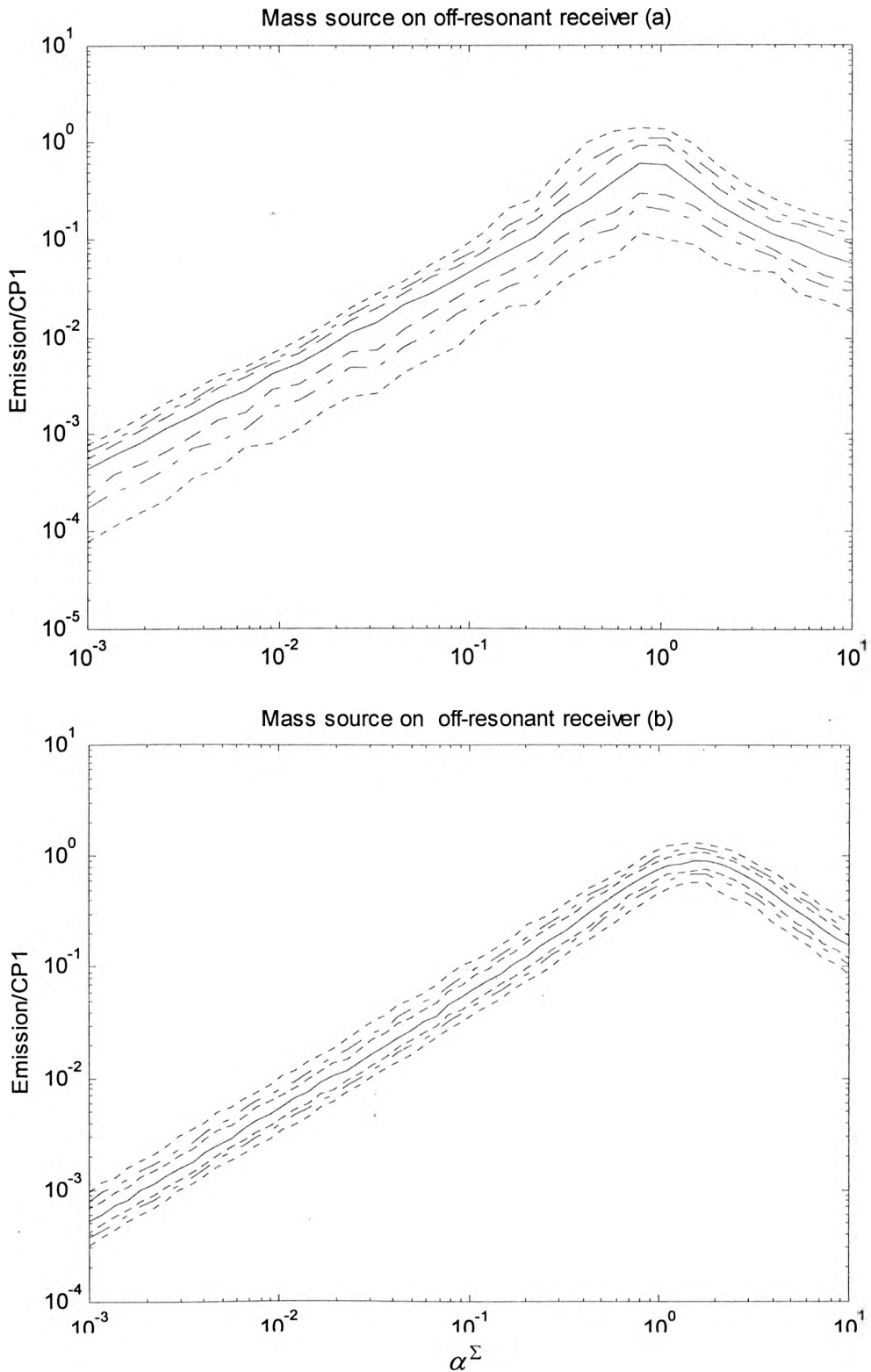
Figure 5-12 General normalised active power bands for CP1 for a combination of mass source on off-resonant receiver. Pairs of curves show probability bands:…90%;-.-.-70%;---50%, solid line is median value Top: condition number 27dB. Bottom: condition number 10 dB.
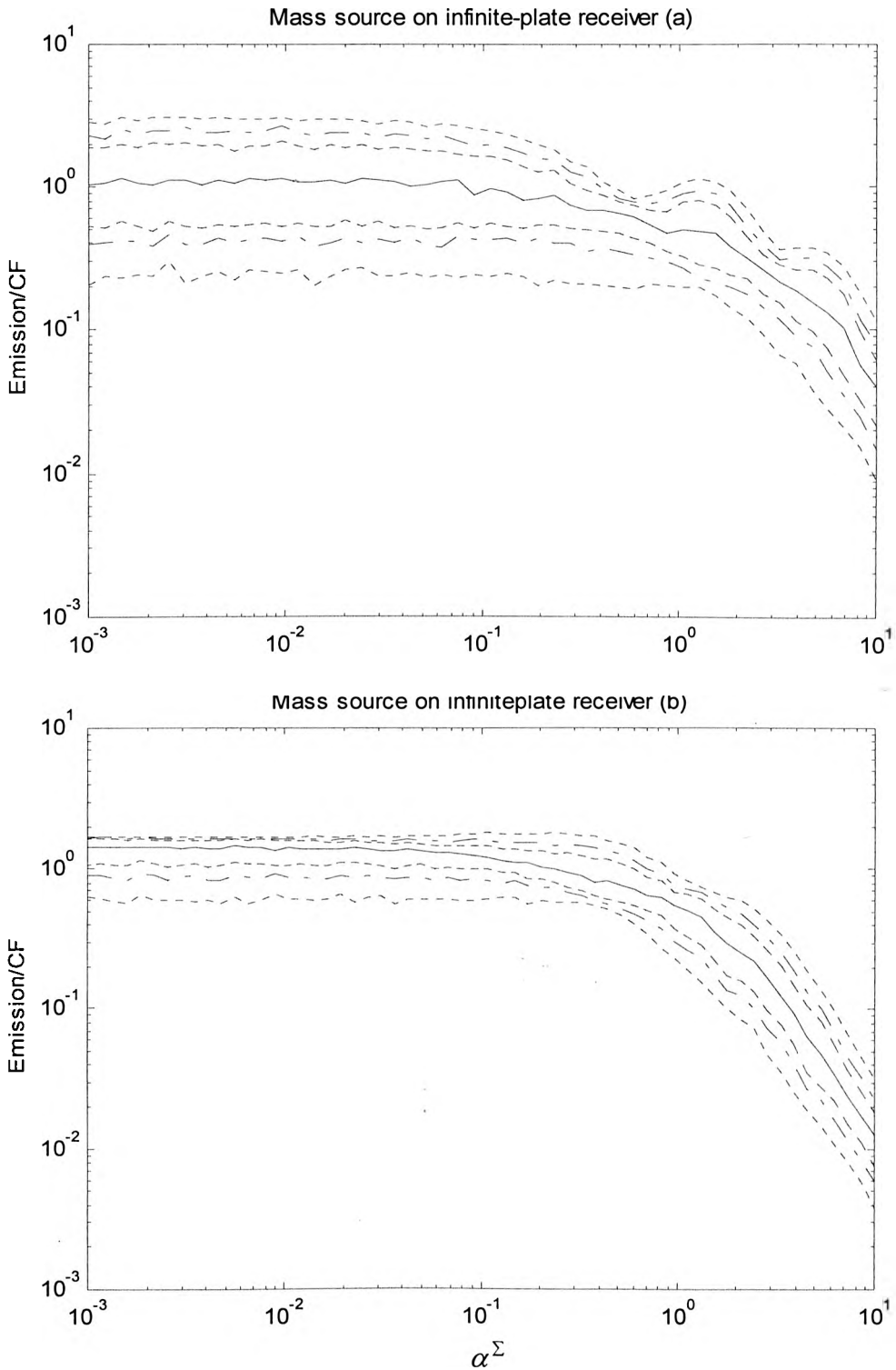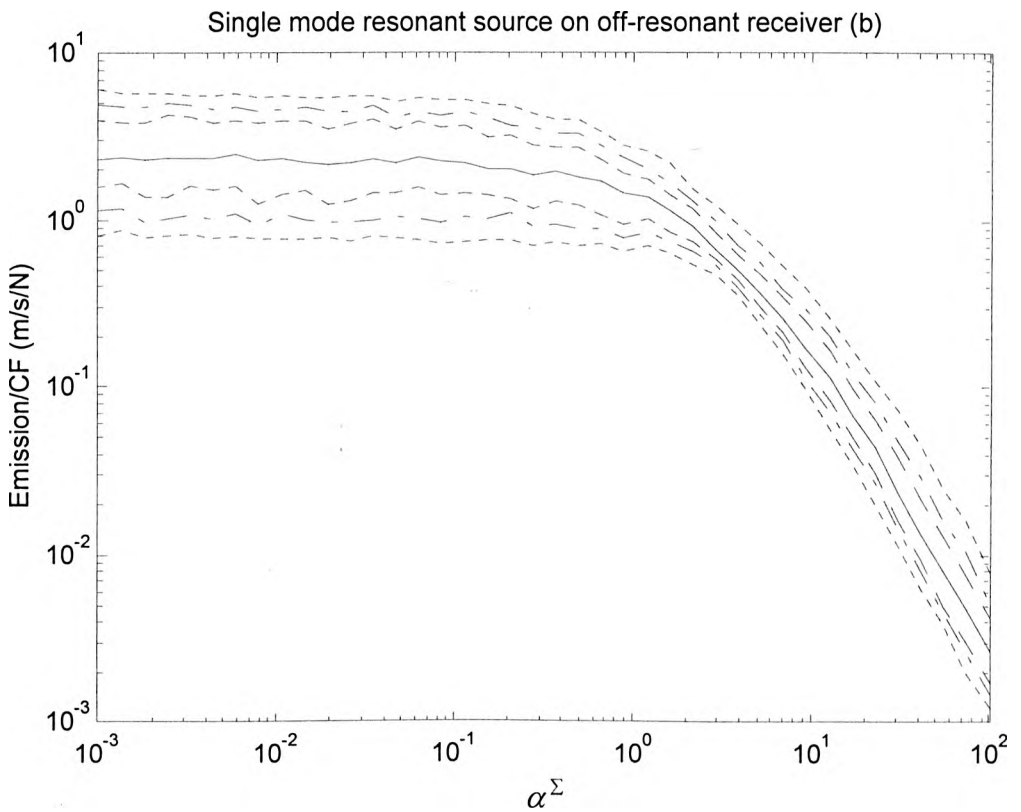
Figure 5-13 General normalised active power bands for CF for a combination of mass source on infinite-plate receiver. Pairs of curves show probability bands:…90%;-.-.-70%;---50%, solid line is median value Top: condition number 26 dB. Bottom: condition number 11 dB.
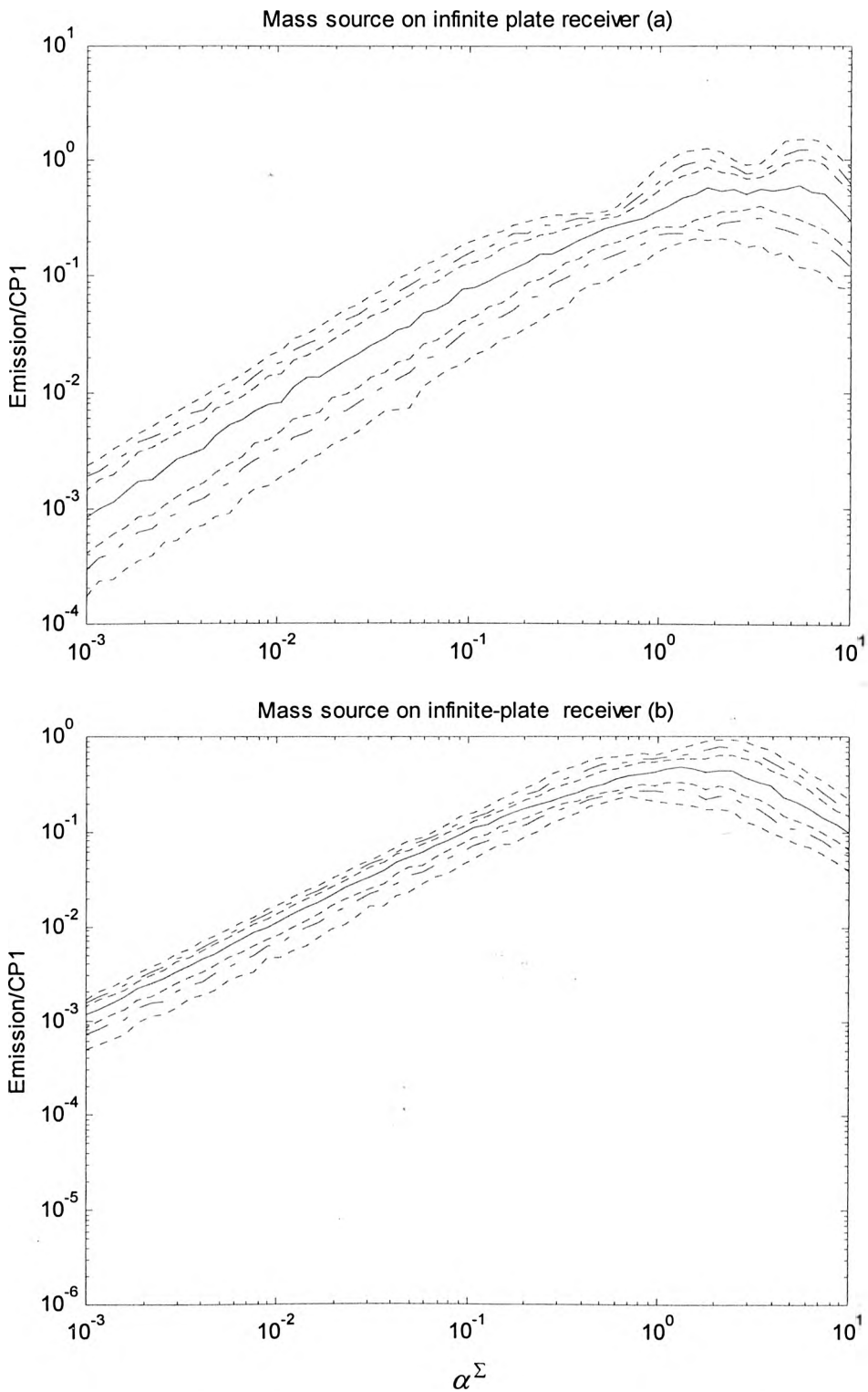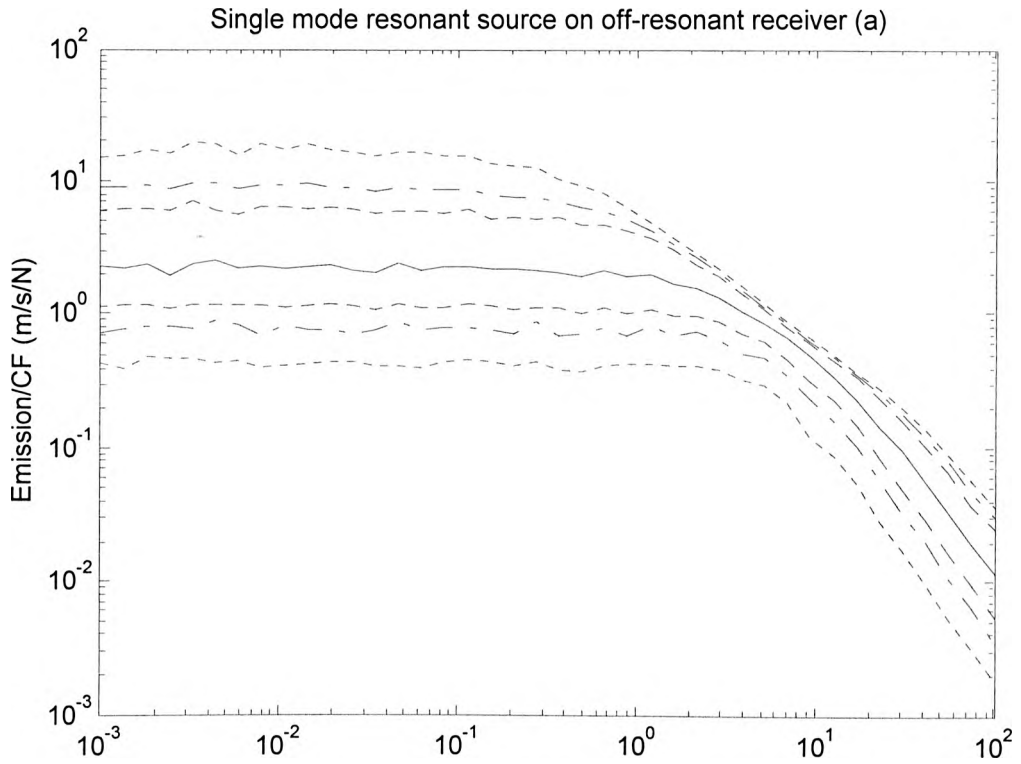
Figure 5-14 General normalised active power bands for CP1 for a combination of mass source on infinite-plate receiver. Pairs of curves show probability bands:…90%;-.-.-70%;---50%, solid line is median value Top: condition number 26 dB. Bottom: condition number 11 dB.
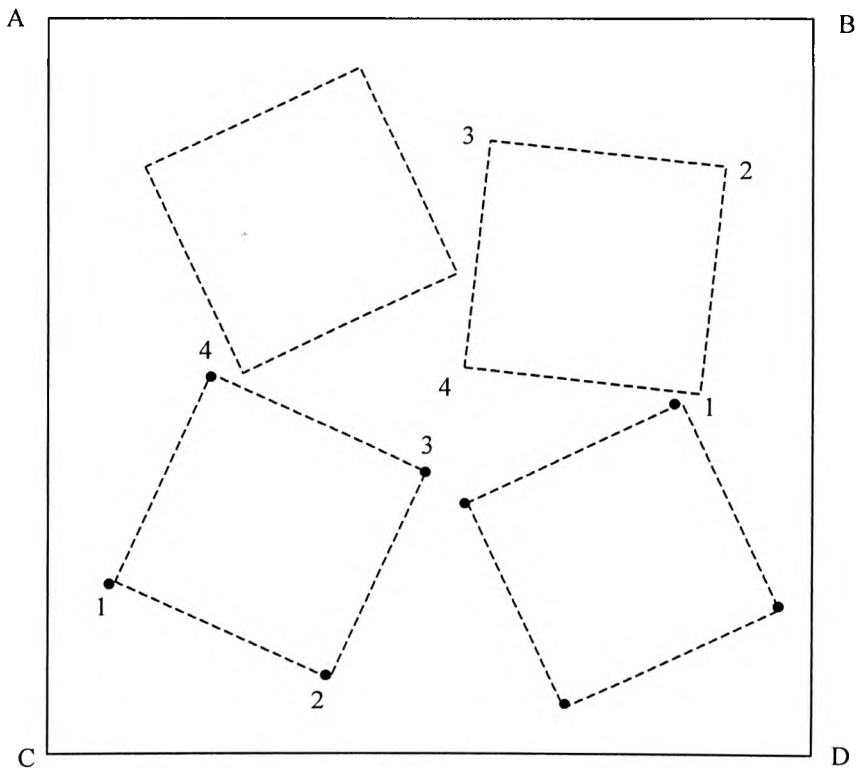
Figure 5-15a Model for a stiffness source with four contact points
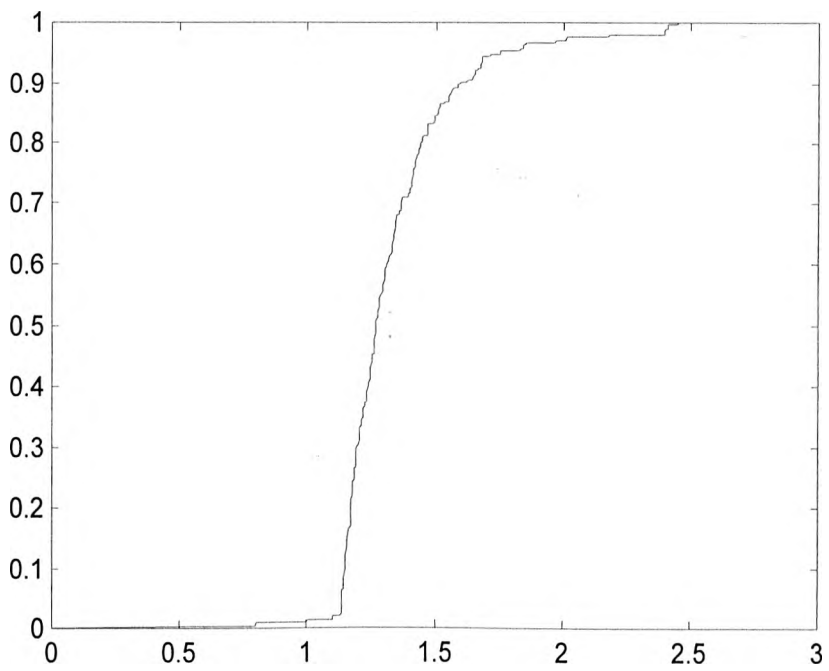
Figure 5-15b Cumulative distribution function for condition number of stiffness source
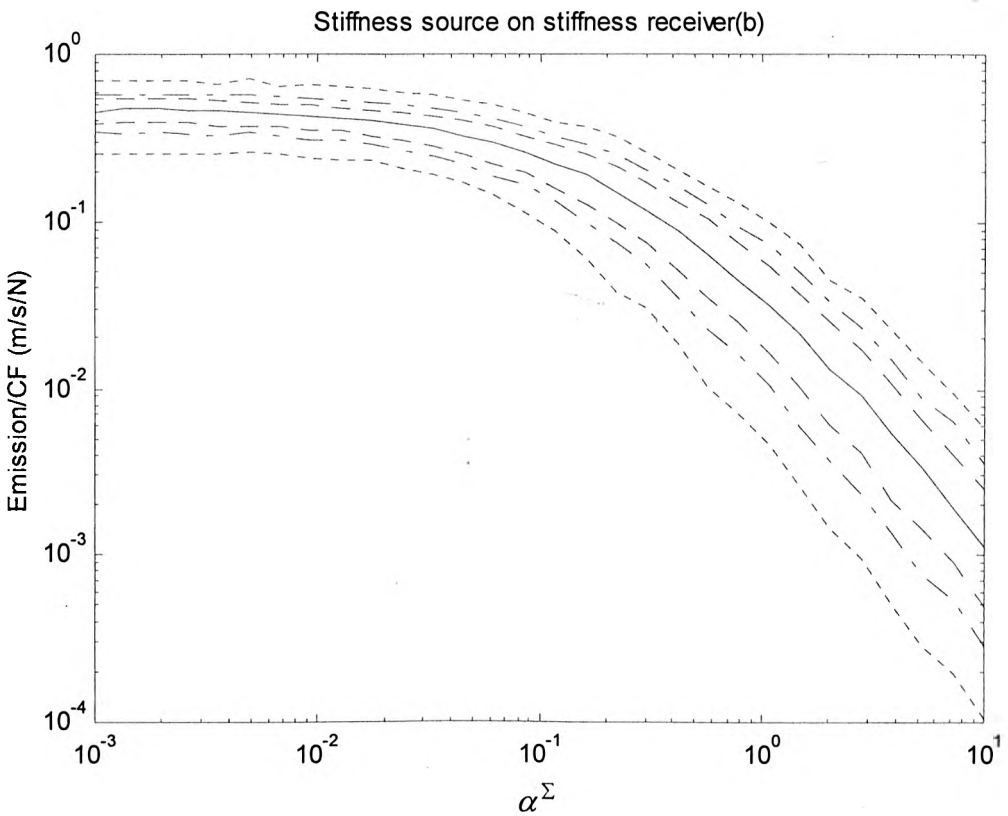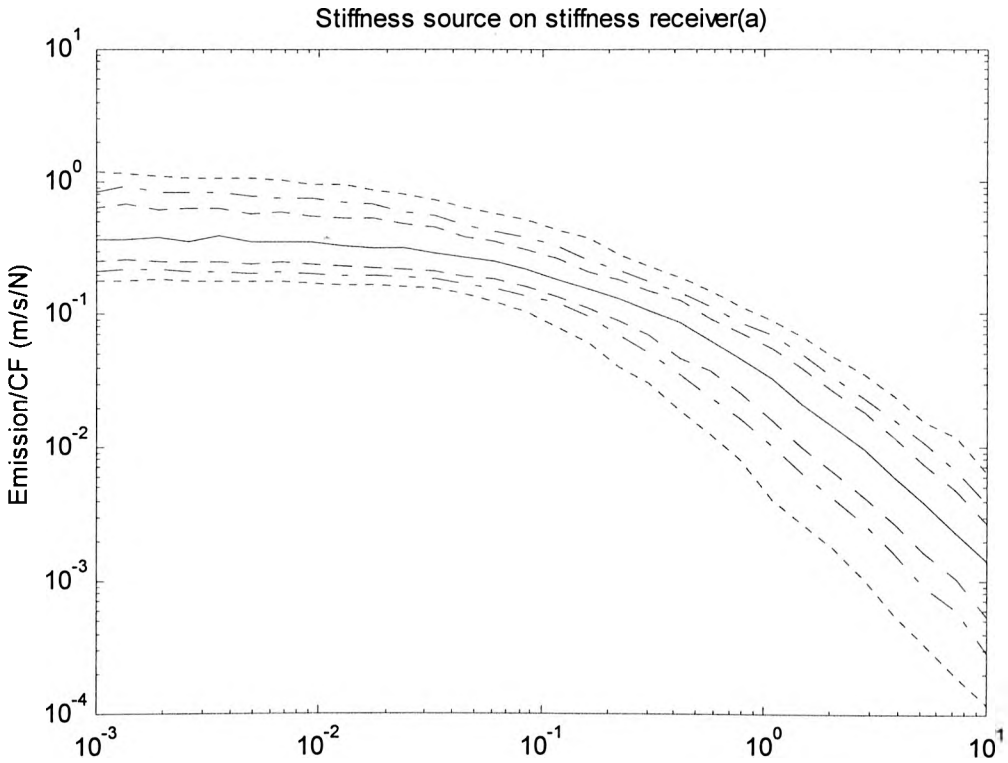
Figure 5-16 General normalised active power bands for CF for a combination of stiffness source on stiffness receiver. Pairs of curves show probability bands:…90%;-.-.-70%;---50%, solid line is median value Top: condition number 20dB. Bottom: condition number 13dB.
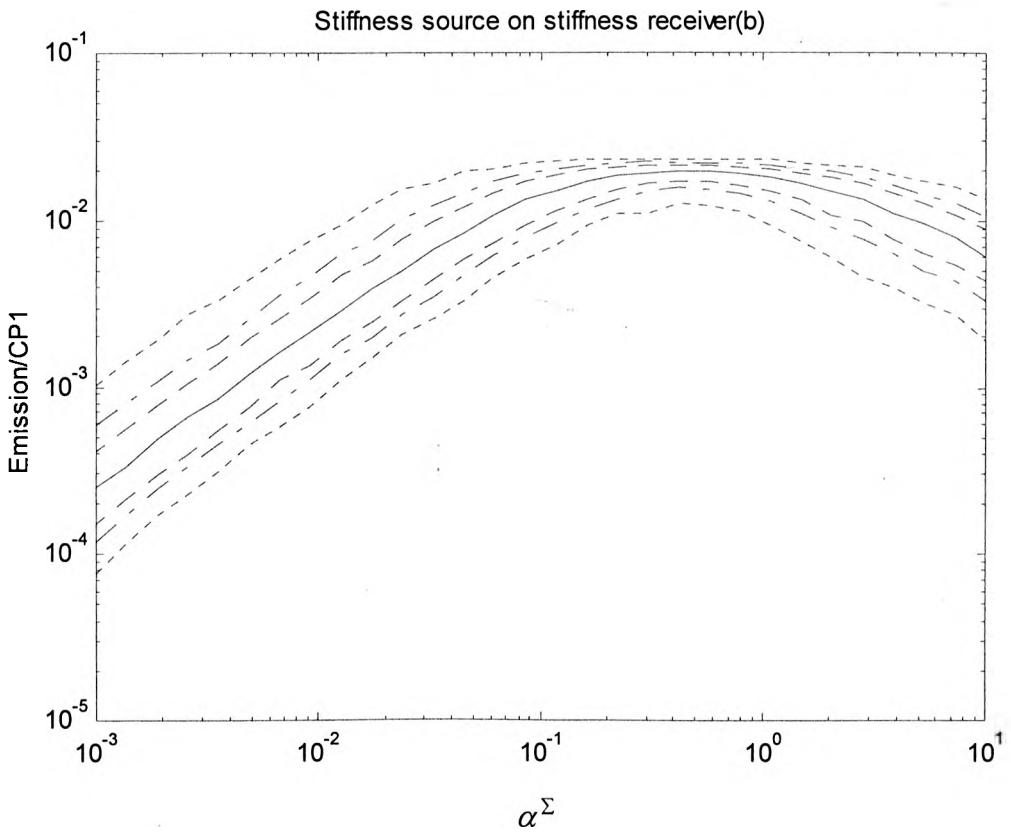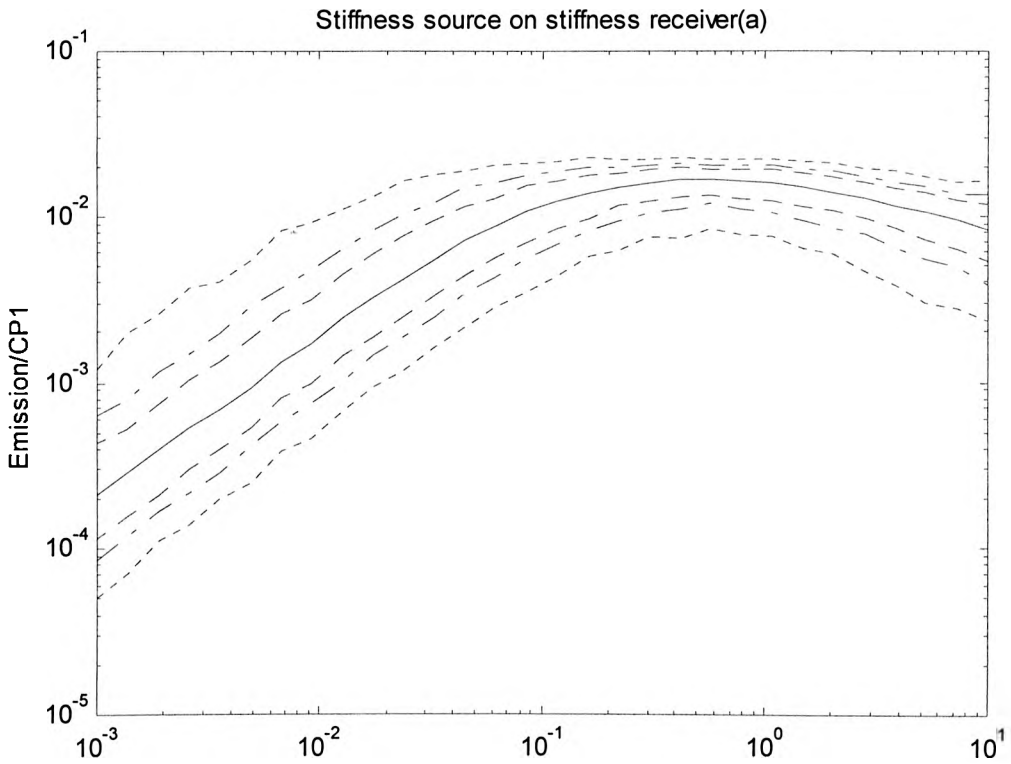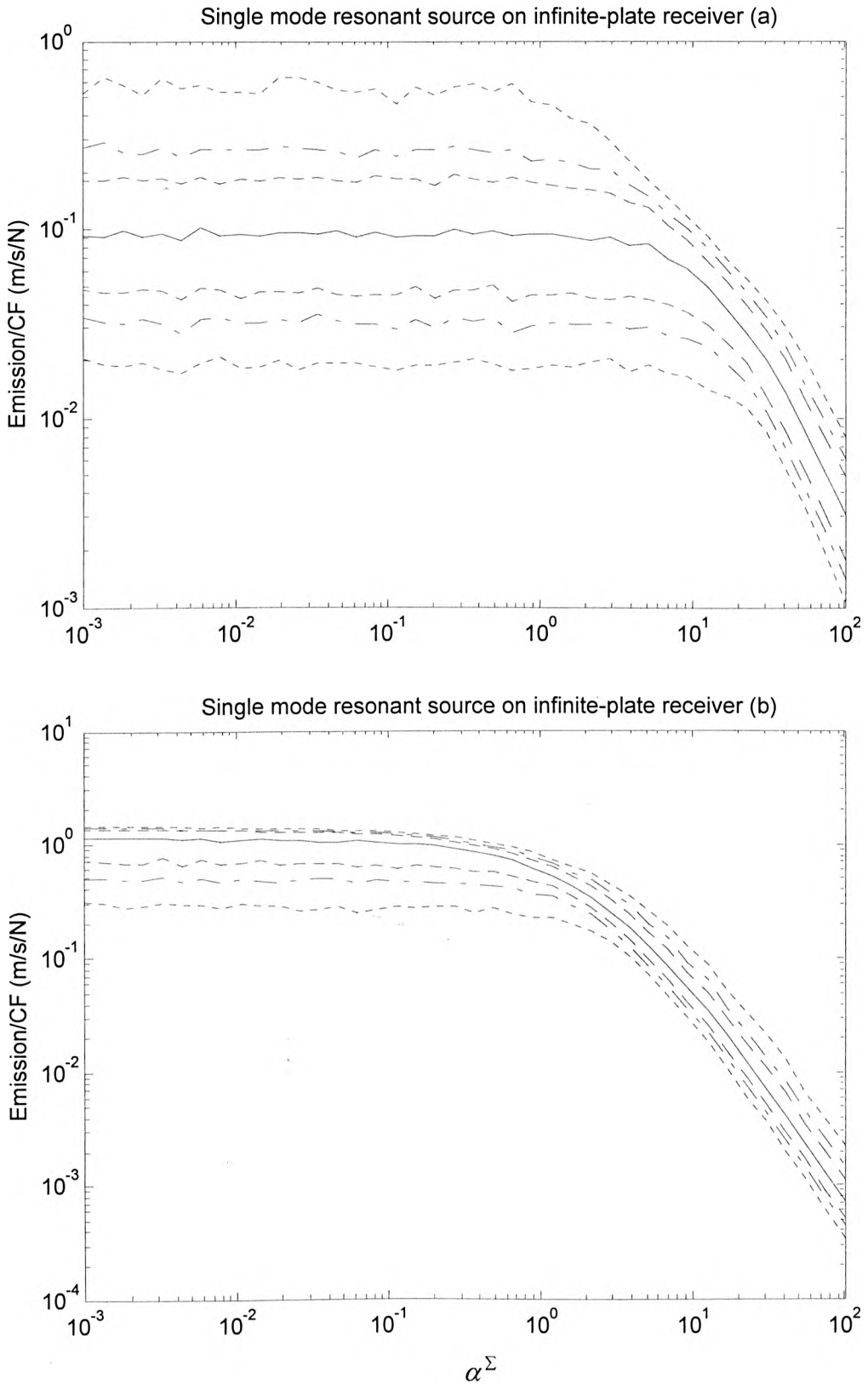
Figure 5-17 General normalised active power bands for CP1 for a combination of stiffness source on stiffness receiver. Pairs of curves show probability bands:…90%;-.-.-70%;---50%, solid line is median value Top: condition number 20dB. Bottom: condition number 13dB.
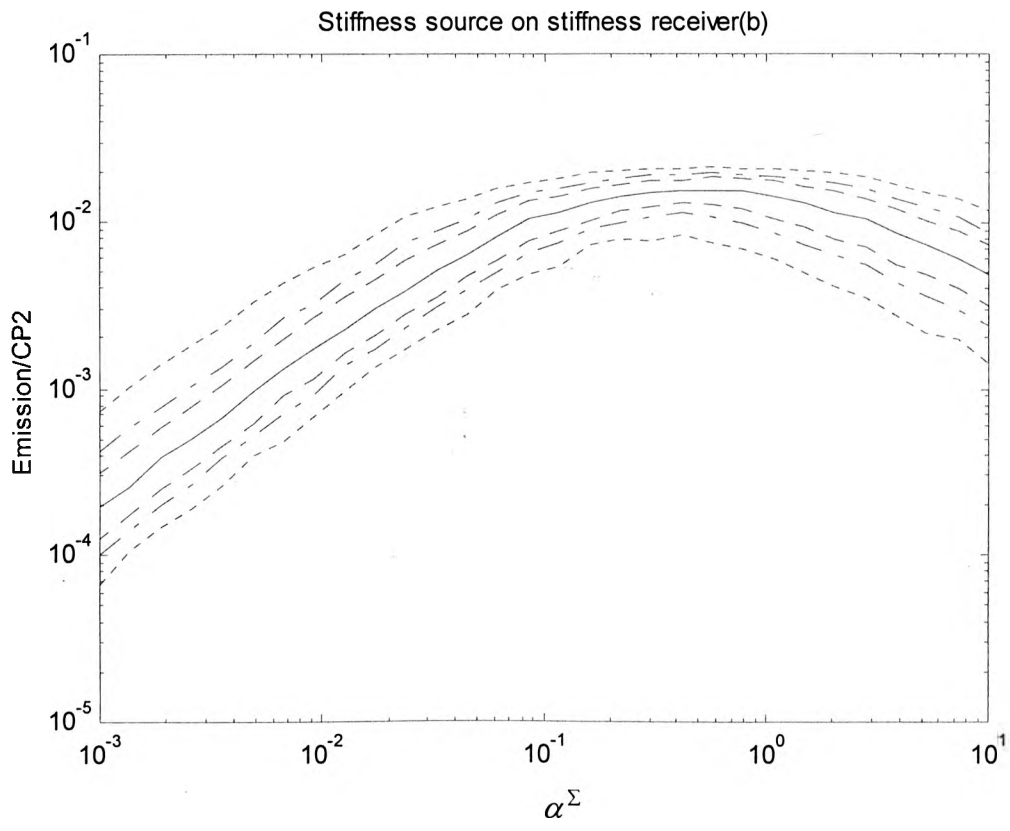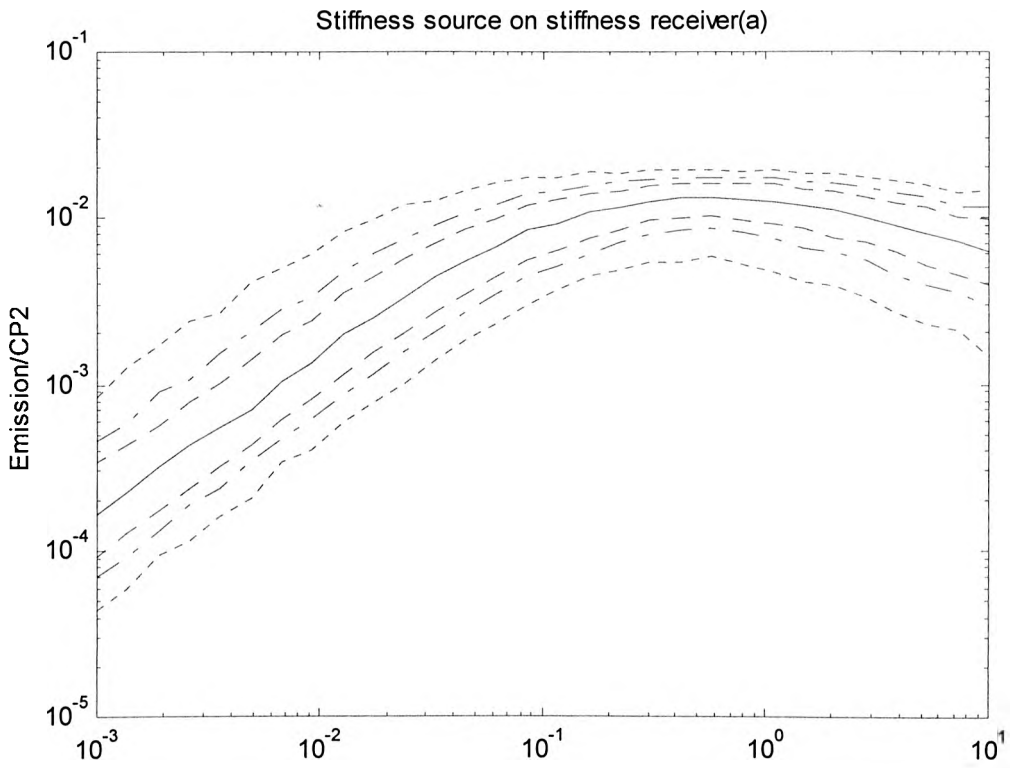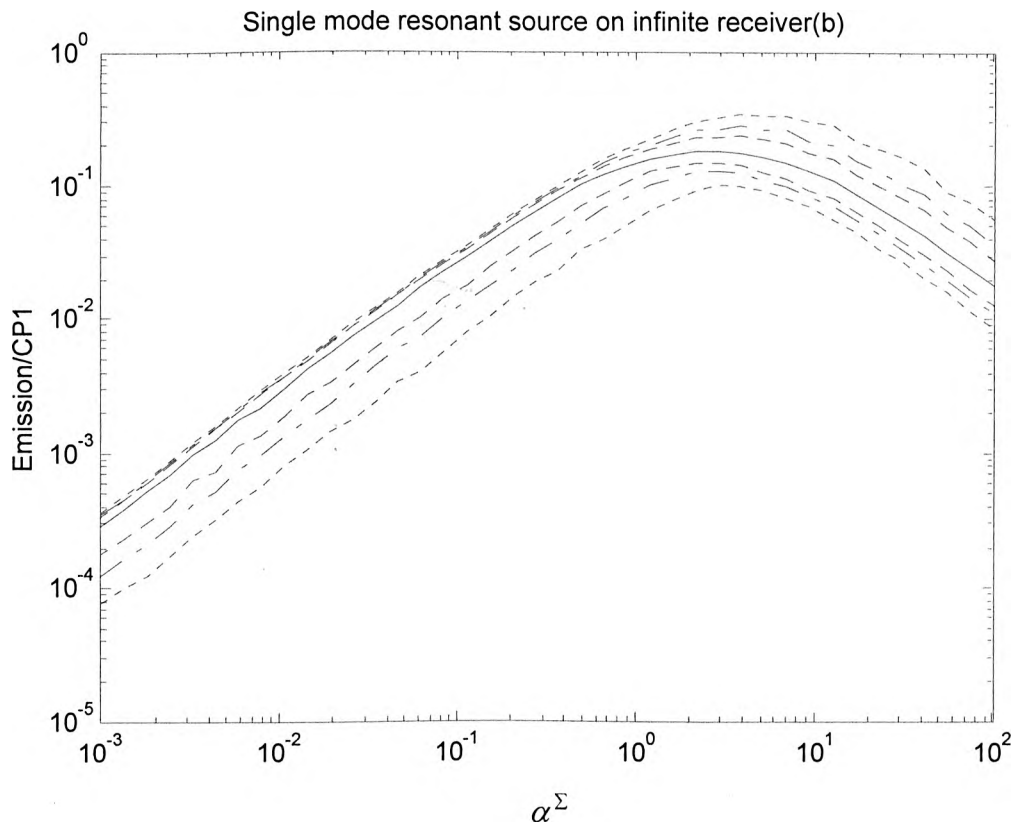
Figure 5-18 General normalised active power bands for CP2 for a combination of stiffness source on stiffness receiver. Pairs of curves show probability bands:…90%;-.-.-70%;---50%, solid line is median value. Top: condition number 20dB. Bottom: condition number 13dB.

155
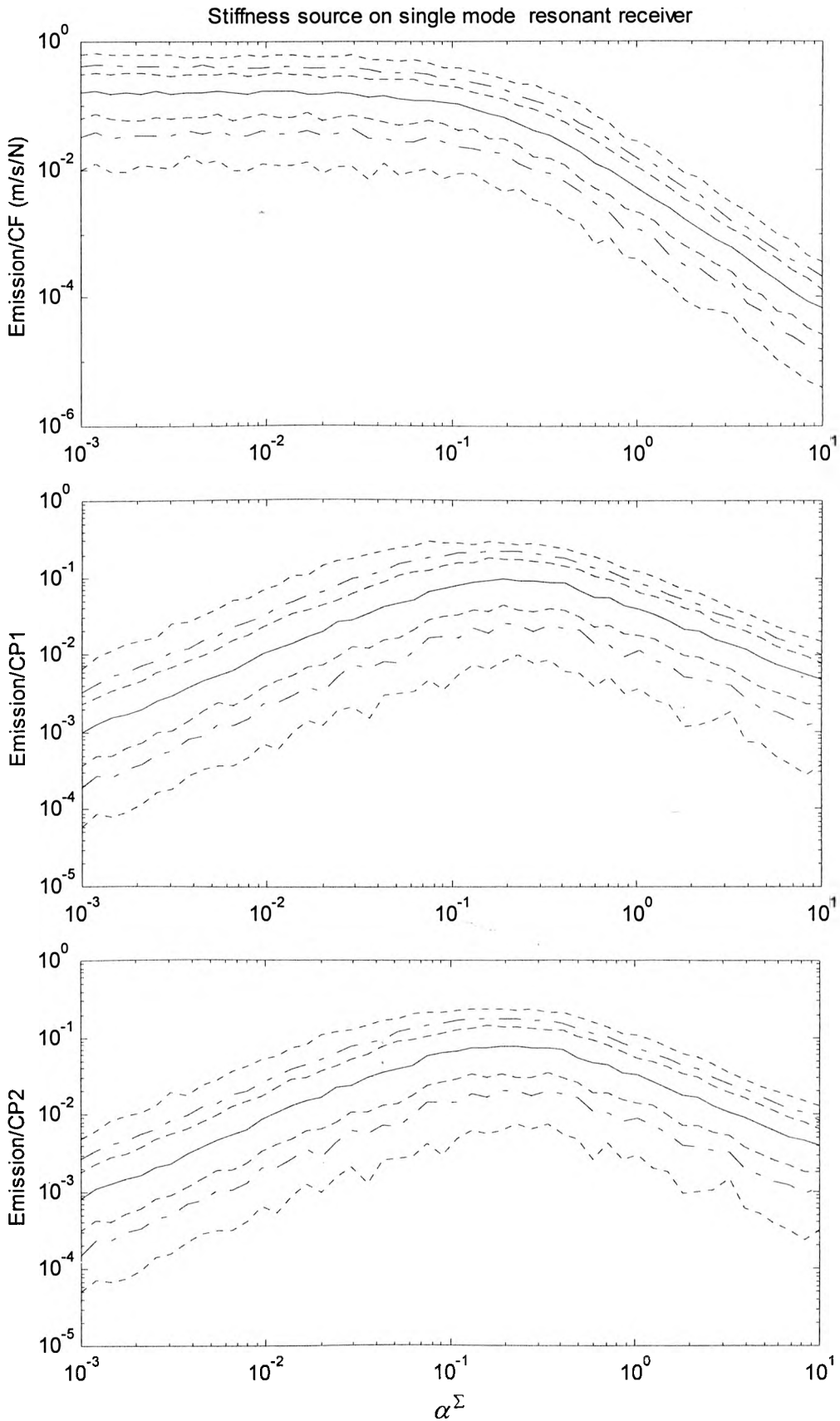
Figure 5-19 General normalised active power bands for CF(top),CP1(middle) andCP2(bottom) for a combination of stiffness source on single mode resonant receiver. Pairs of curves show probability bands:…90%;-.-.-70%;---50%, solid line is median value
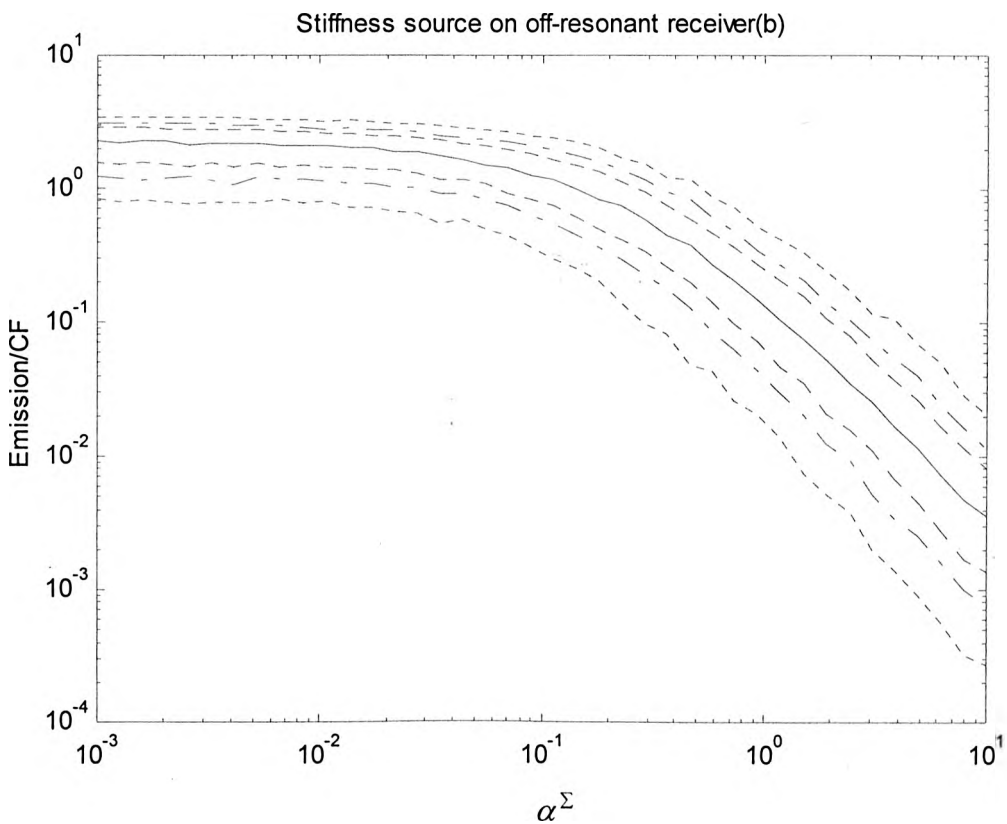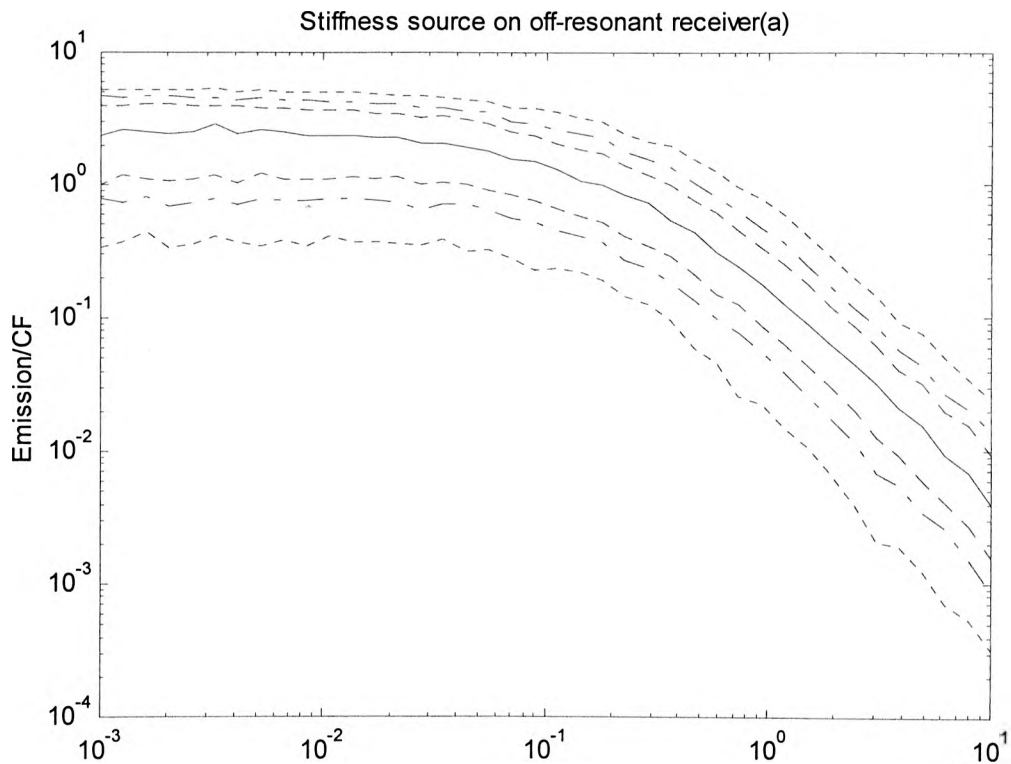
Figure 5-20 General normalised active power bands for CF for a combination of stiffness source on off-resonant receiver. Pairs of curves show probability bands:...90%;-.-.-70%;---50%, solid line is median value Top: condition number 27dB. Bottom: condition number 10dB.
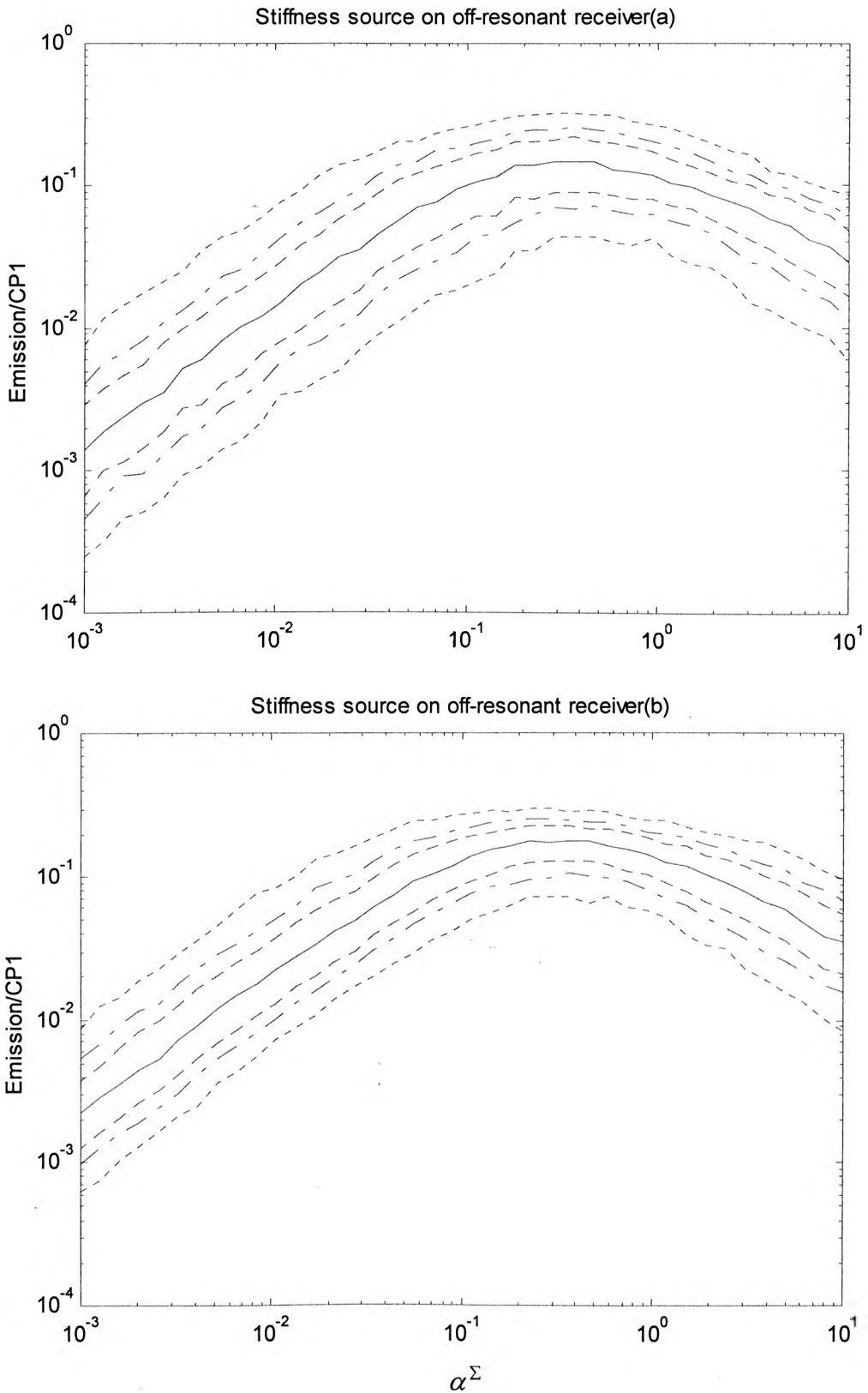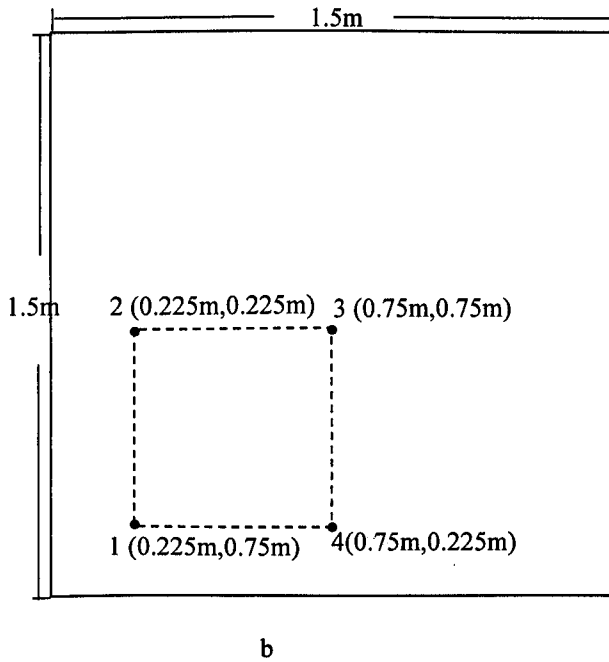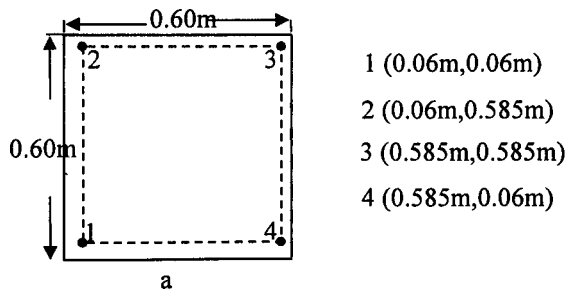
Figure 5-21 General normalised active power bands for CP1 for a combination of stiffness source on off-resonant receiver. Pairs of curves show probability bands:…90%;-.-.-70%;--- 50%, solid line is median value Top: condition number 27dB. Bottom: condition number 10dB.
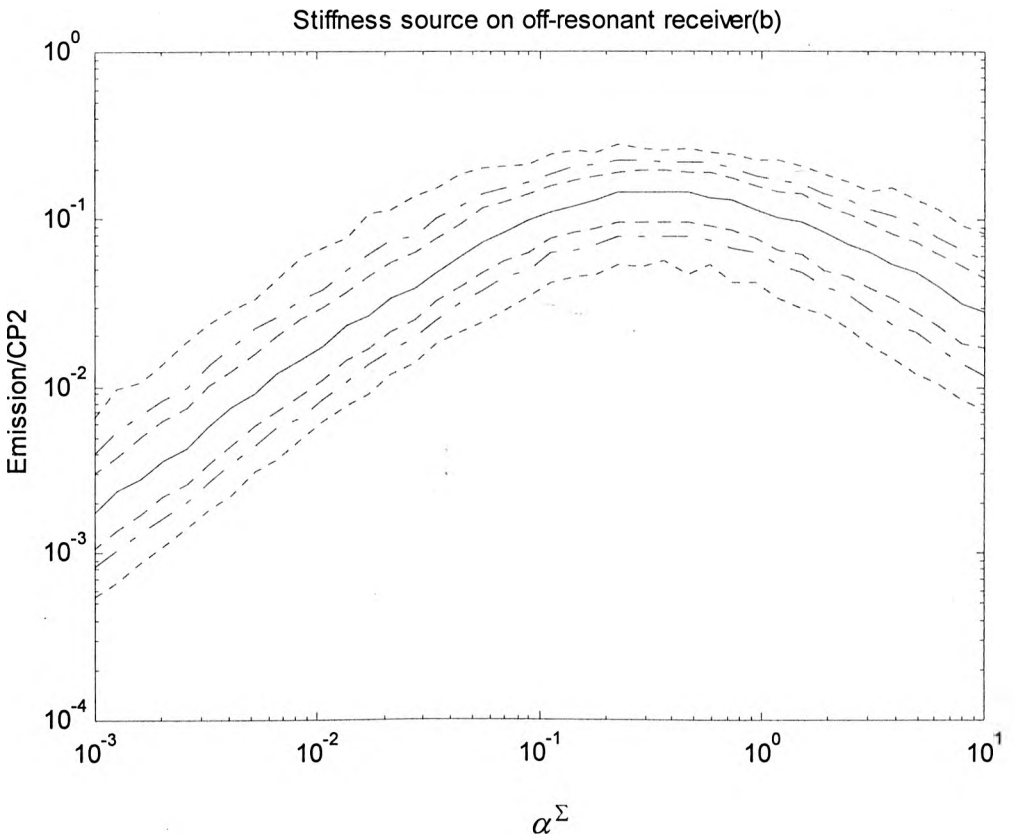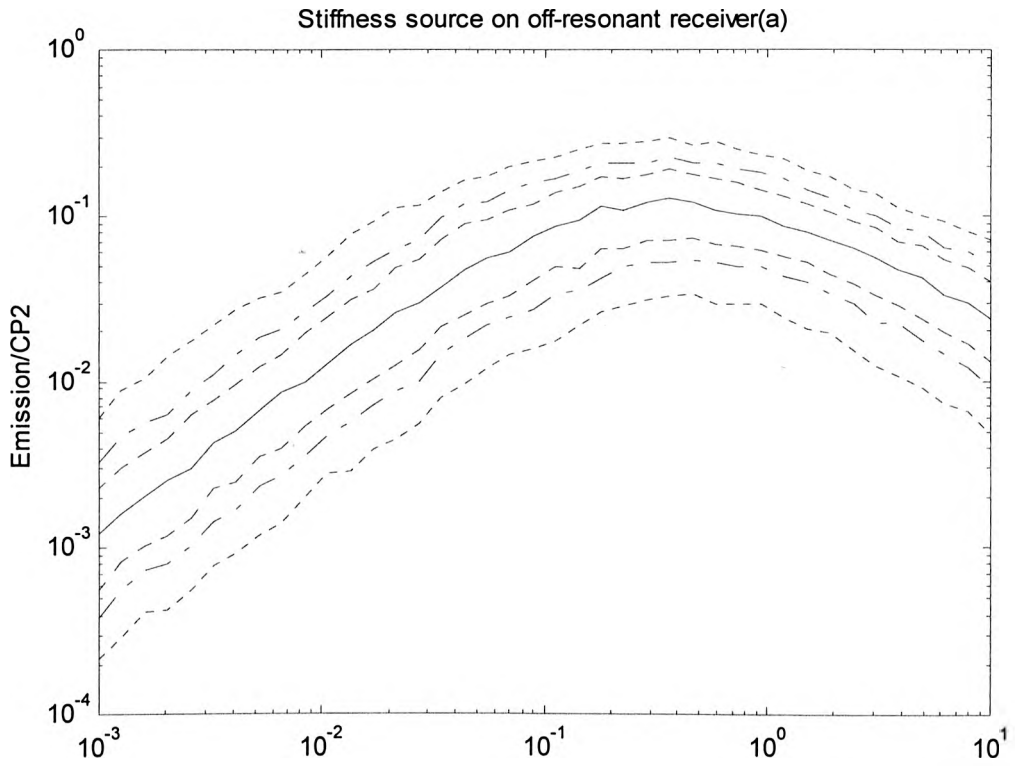
Figure 5-22 General normalised active power bands for CP2 for a combination of stiffness source on off-resonant receiver. Pairs of curves show probability bands:…90%;-.-.-70%;---50%, solid line is median value Top: condition number 27dB. Bottom: condition number 10dB.
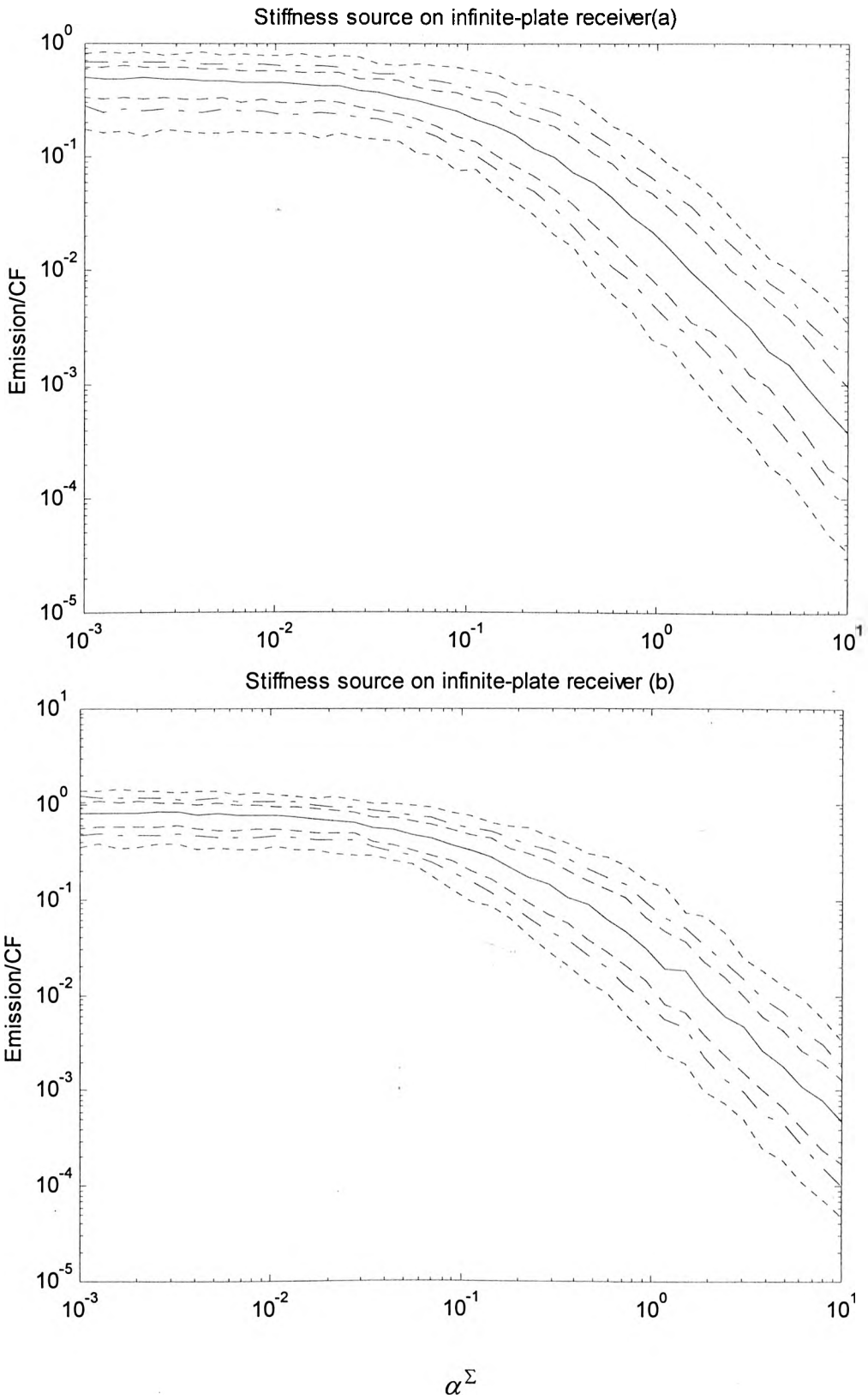
Figure 5-23 General normalised active power bands for CF for a combination of stiffness source on infinite-plate receiver. Pairs of curves show probability bands:…90%;-.-.-70%;---50%, solid line is median value Top: condition number 23dB. Bottom: condition number 10dB.
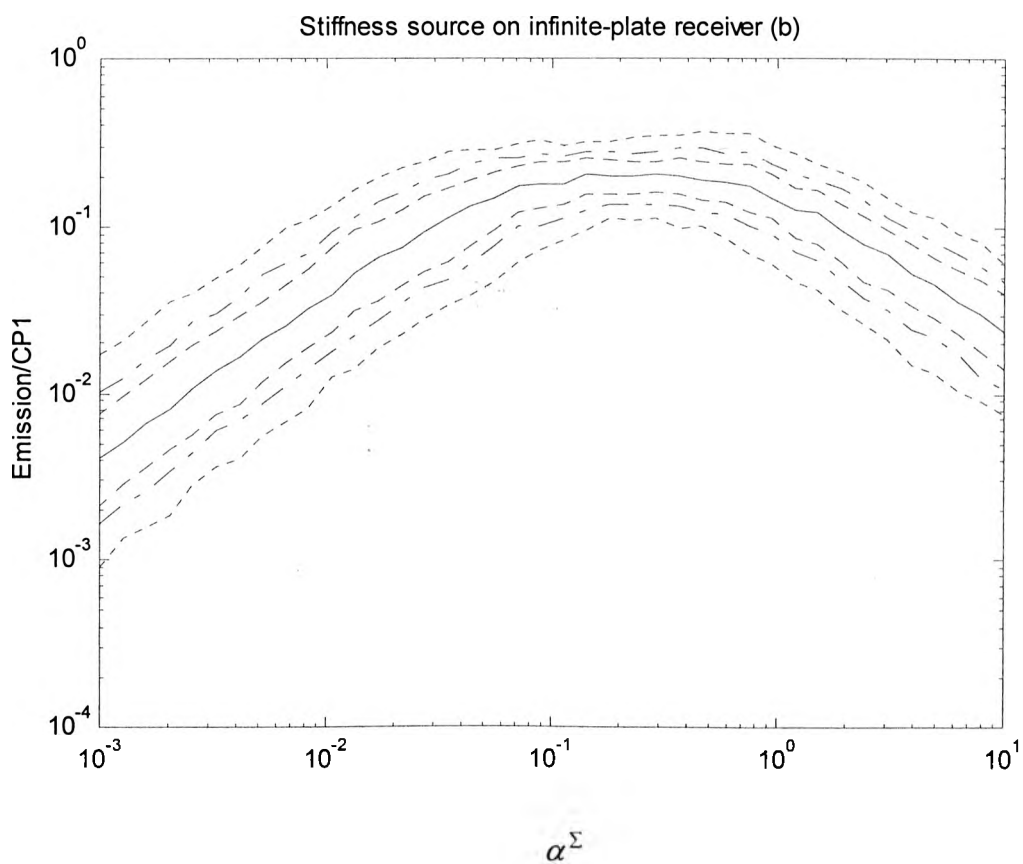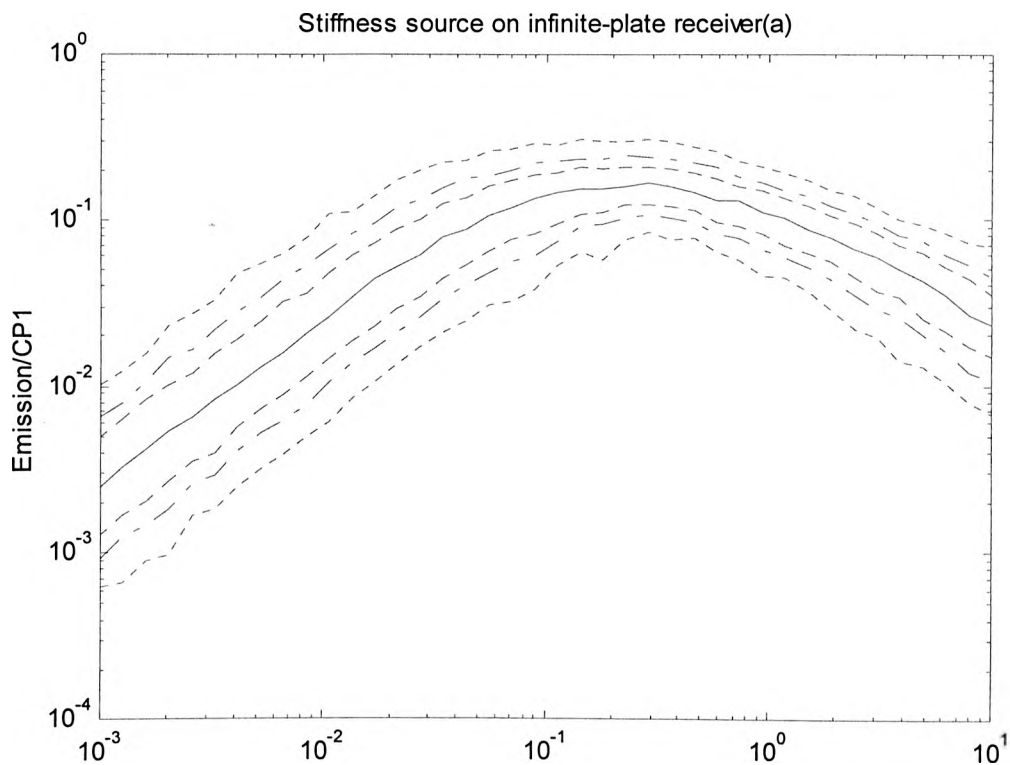
Figure 5-24 General normalised active power bands for CP1 for a combination of stiffness source on infinite-plate receiver. Pairs of curves show probability bands:…90%;-.-.-70%;---50%, solid line is median value Top: condition number 23dB. Bottom: condition number 10dB.
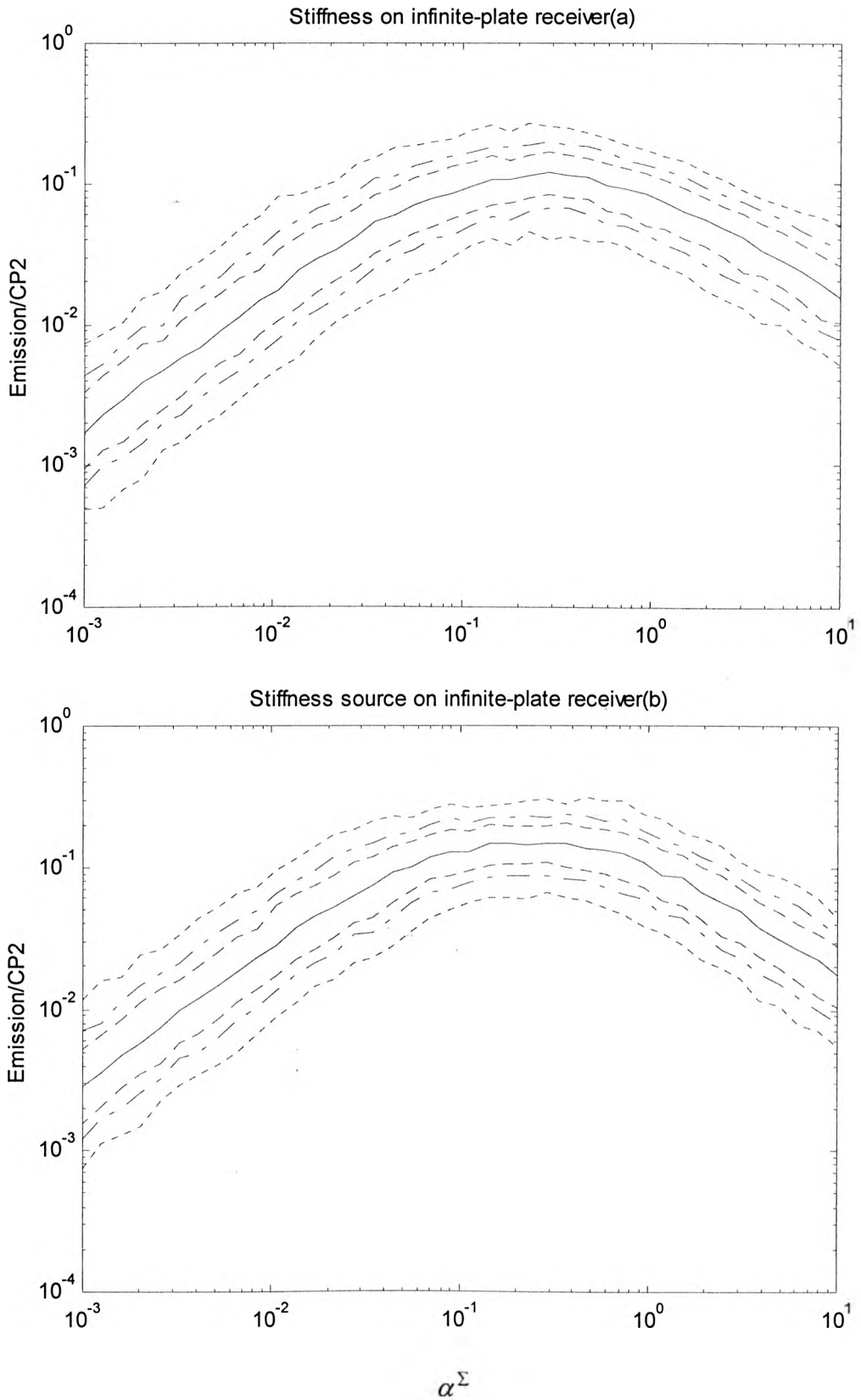
Figure 5-25 General normalised active power bands for CP2 for a combination of stiffness source on infinite-plate receiver. Pairs of curves show probability bands:…90%;-.-.-70%;---50%, solid line is median value Top: condition number 23dB. Bottom: condition number 10dB.

Off-resonant source on stiffness receiver (a)

Off-resonant source on stiffness receiver (b)
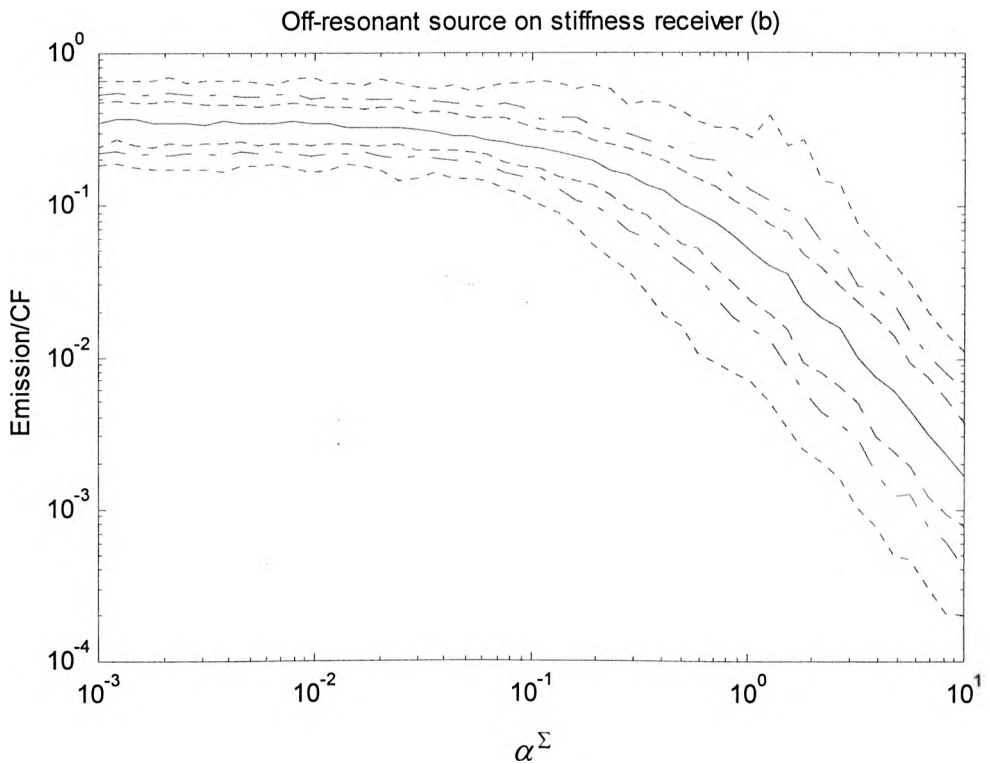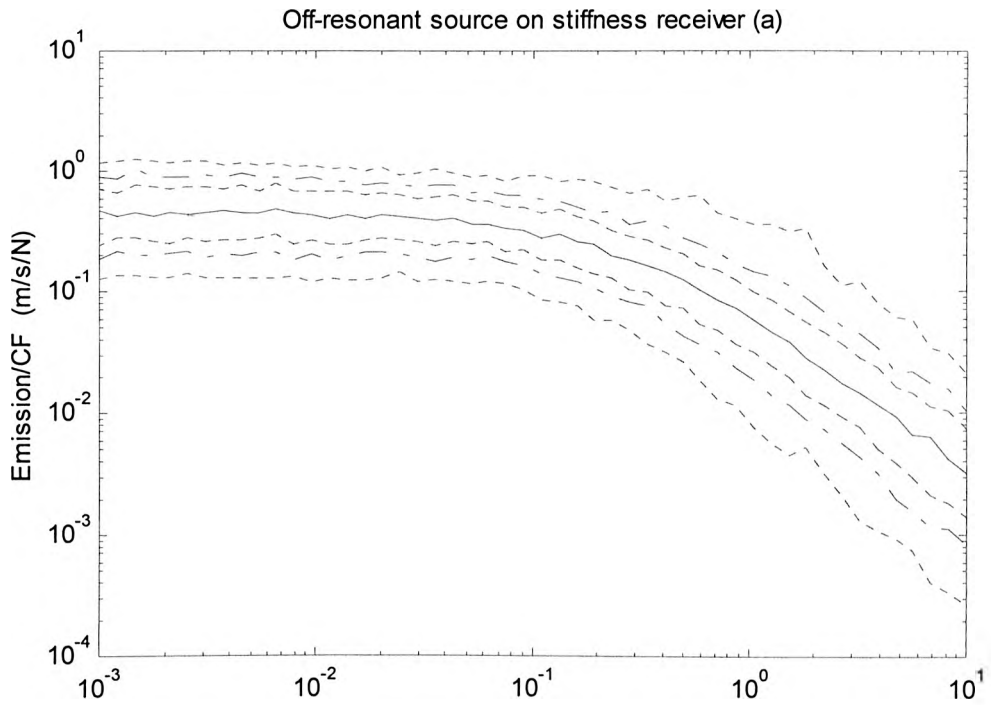
Figure 5-26 General normalised active power bands for CF for a combination of off-resonant source on stiffness receiver. Pairs of curves show probability bands:…90%;-.-.-70%;---50%, solid line is median value Top: condition number 20dB. Bottom: condition number 13dB.
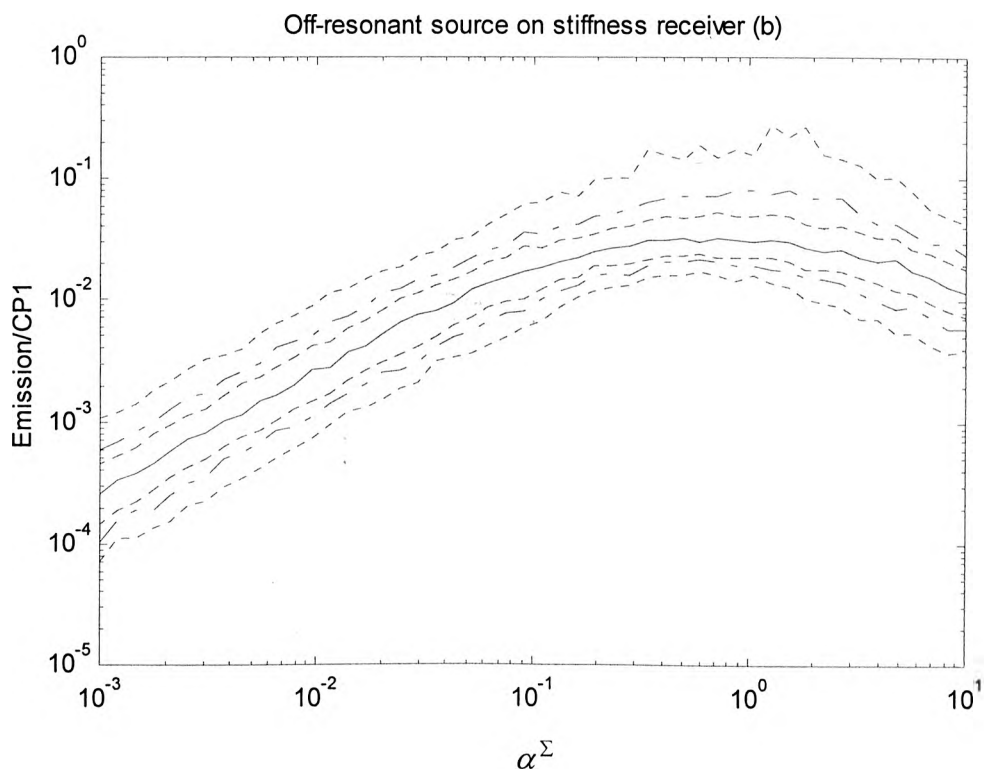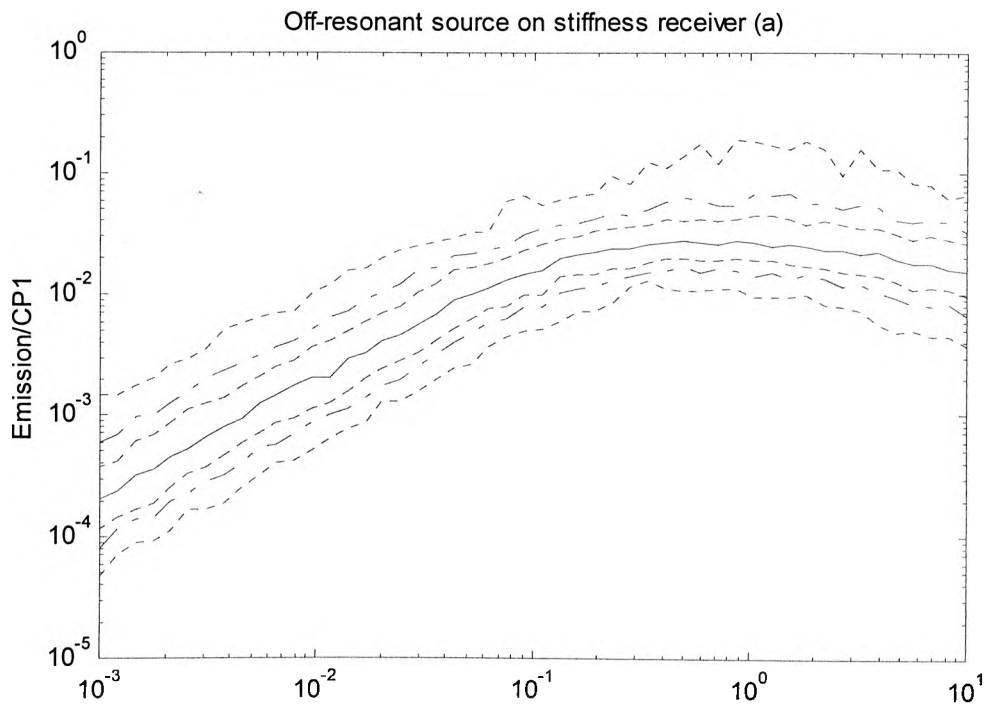
Figure 5-27 General normalised active power bands for CF for a combination of off-resonant source on stiffness receiver. Pairs of curves show probability bands:…90%;-.-.-70%;---50%, solid line is median value Top: condition number 20dB. Bottom: condition number 13dB.
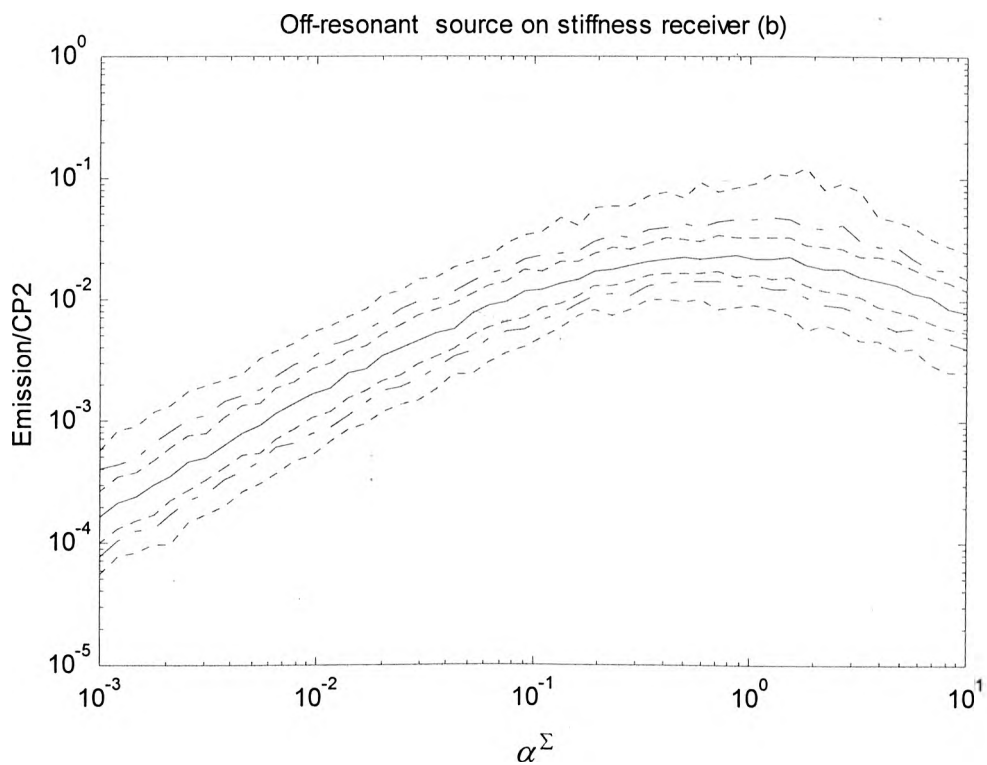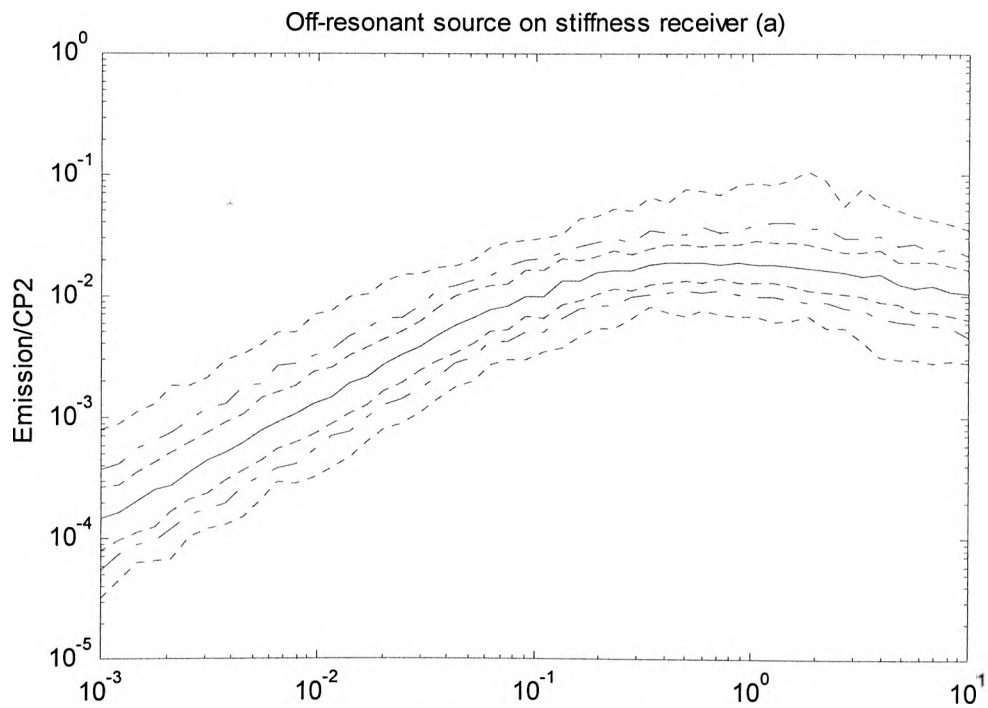
Figure 5-28 General normalised active power bands for CP2 for a combination of off-resonant source on stiffness receiver. Pairs of curves show probability bands:...90%;-.-.-70%;---50%, solid line is median value Top: condition number 20dB. Bottom: condition number 13dB.
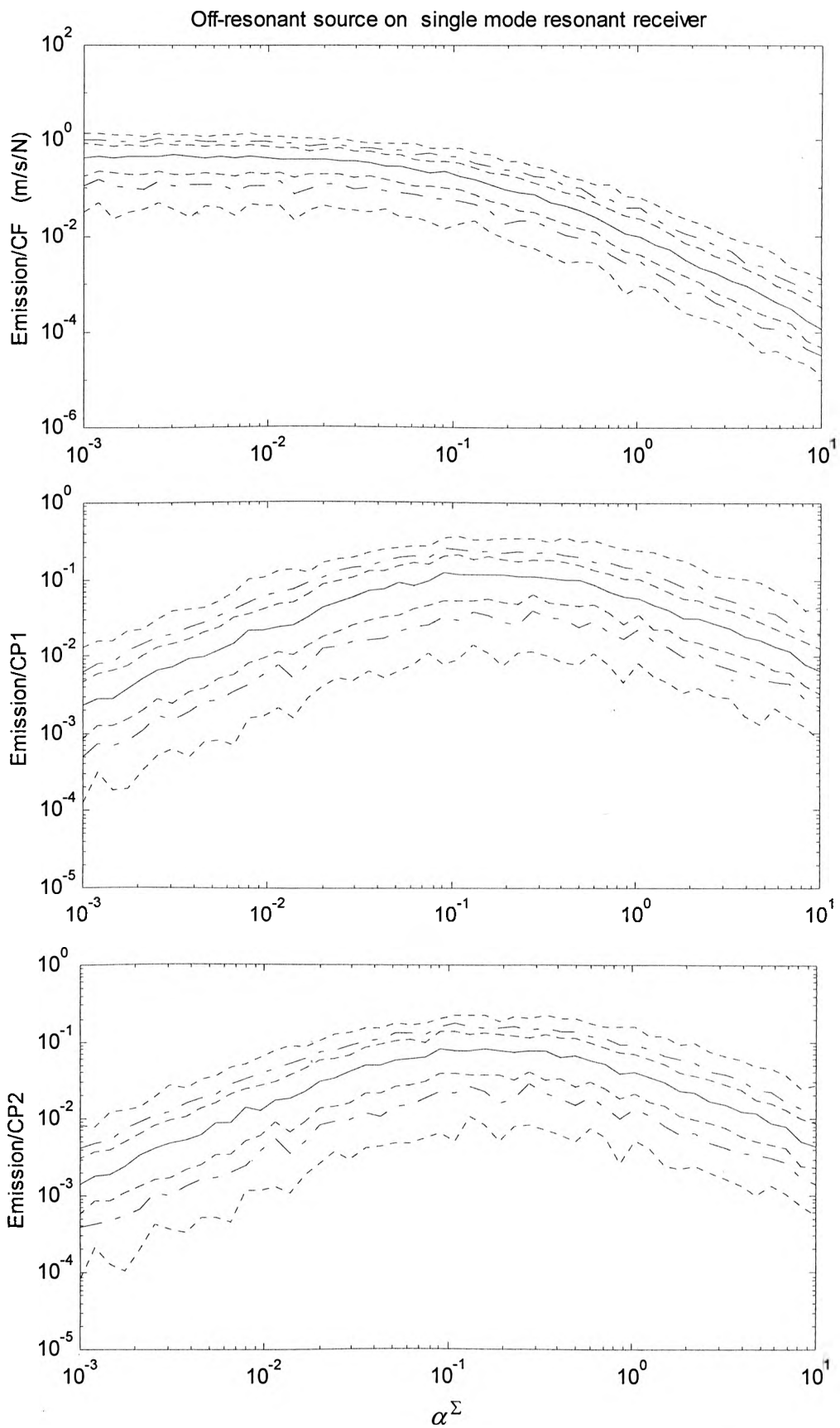
Figure 5-29 General normalised active power bands for CF(top),CP1(middle) andCP2(bottom) for a combination of off-resonant source on single mode resonant receiver. Pairs of curves show probability bands:…90%;-.-.-70%;---50%, solid line is median value

Figure 5-30 General normalised active power bands for CF for a combination of off-resonant source on off-resonant receiver. Pairs of curves show probability bands:…90%;-.-.-70%;---50%, solid line is median value Top: condition number 27dB. Bottom: condition number 10dB.

Figure 5-31 General normalised active power bands for CP1 for a combination of off-resonant source on off-resonant receiver. Pairs of curves show probability bands:…90%;-.-.-70%;---50%, solid line is median value Top: condition number 27dB. Bottom: condition number 10dB.

Figure 5-32 General normalised active power bands for CP2 for a combination of off-resonant source on off-resonant receiver. Pairs of curves show probability bands:…90%;-.-.-70%;---50%, solid line is median value Top: condition number 27dB. Bottom: condition number 10dB.

Figure 5-33 General normalised active power bands for CF for a combination of off-resonant source on infinite-plate receiver. Pairs of curves show probability bands:…90%;-.-.-70%;---50%, solid line is median value Top: condition number 23dB. Bottom: condition number 10dB.

Figure 5-34 General normalised active power bands for CP1 for a combination of off-resonant source on infinite-plate receiver. Pairs of curves show probability bands:…90%;-.-.-70%;---50%, solid line is median value Top: condition number 23dB. Bottom: condition number 10dB.

Figure 5-35 General normalised active power bands for CP2 for a combination of off-resonant source on infinite-plate receiver. Pairs of curves show probability bands:…90%;-.-.-70%;---50%, solid line is median value Top: condition number 23dB. Bottom: condition number 10dB.

Figure 5-36 General normalised active power bands for CF for a combination of single mode resonant source on stiffness receiver. Pairs of curves show probability bands:…90%;-.-.-70%;---50%, solid line is median value. Top: condition number 20dB. Bottom: condition number 13dB.

Figure 5-37 General normalised active power bands for CP1 for a combination of single mode resonant source on stiffness receiver. Pairs of curves show probability bands:…90%;-.-.-70%;---50%, solid line is median value. Top: condition number 20dB. Bottom: condition number 13dB.

Figure 5-38 General normalised active power bands for CF for a combination of single mode resonant source on off-resonant receiver. Pairs of curves show probability bands:…90%;-.-.-70%;---50%, solid line is median value.Top: condition number 27dB. Bottom: condition number 11dB.
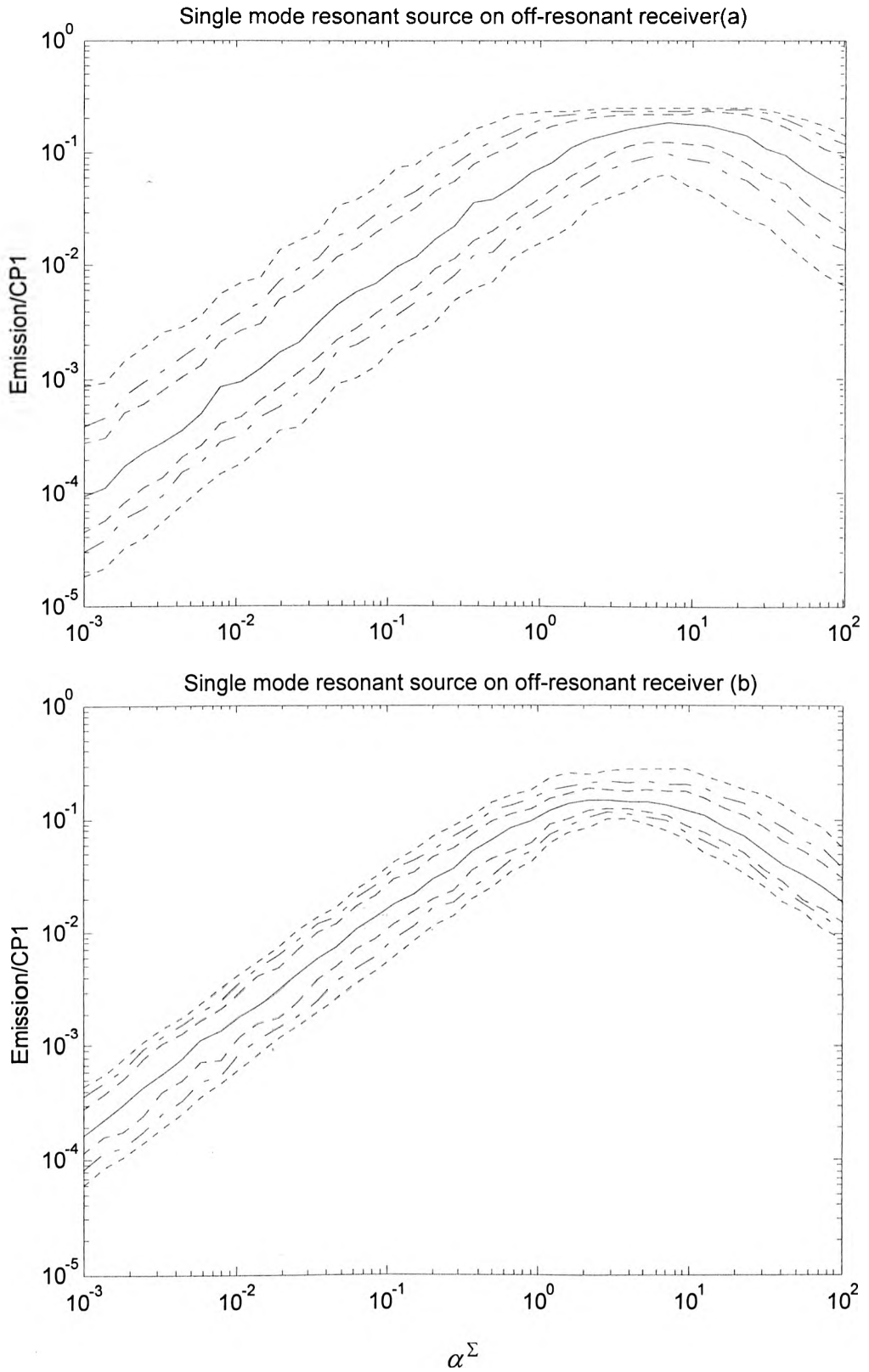
Figure 5-39 General normalised active power bands for CP1 for a combination of single mode resonant source on off-resonant receiver. Pairs of curves show probability bands:...90%;-.-.-70%;---50%, solid line is median value.Top: condition number 27dB. Bottom: condition number 11dB.

Figure 5-40 General normalised active power bands for CF for a combination of single mode resonant source on infinite-plate. Pairs of curves show probability bands:...90%;-.-.-70%;---50%, solid line is median value Top: condition number 25dB. Bottom: condition number 10dB.
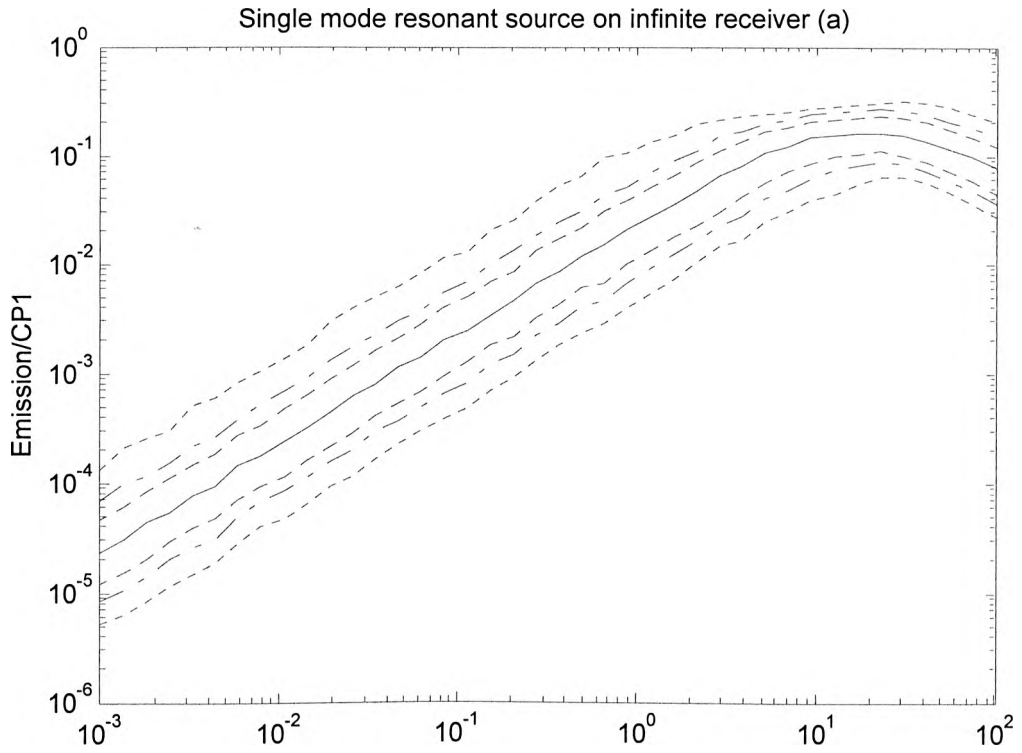
Figure 5-41 General normalised active power bands for CP1 for a combination of single mode resonant source on infinite-plate. Pairs of curves show probability bands:…90%;-.-.-70%;---50%, solid line is median value Top: condition number 25dB. Bottom: condition number 10dB.

1 (0.06m,0.06m)

2 (0.06m,0.585m)

3 (0.585m,0.585m)

4 (0.585m,0.06m)

a

2 (0.225m,0.225m) 3 (0.75m,0.75m)

1 (0.225m,0.75m) 4(0.75m,0.225m)

b

Figure 5-42 a: a SSSS plate as a source, thickness is 5cm for case 1; 2cm for case2, 0.5cm for case 3. b: a SSSS plate as a receiver, thickness is 0.20m
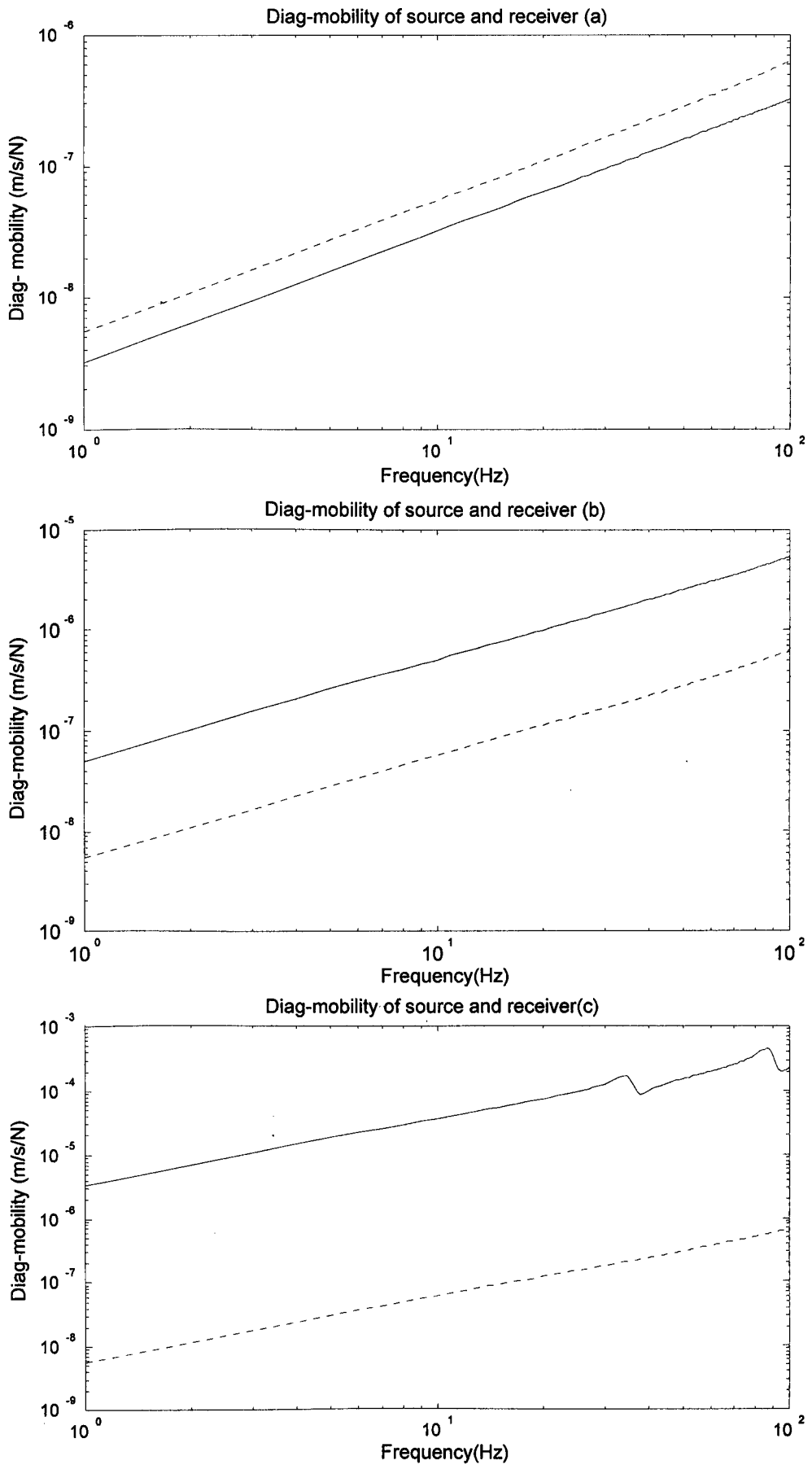
Figure 5-43 Diag-mobility (sum of point mobility magnitude) of source plate (-) and receiver plate(--).Top: the thickness of the source plate is 5cm.Middle: the thickness of the source plate is 2cm.Bottom the thickness of the source plate is 0.5cm
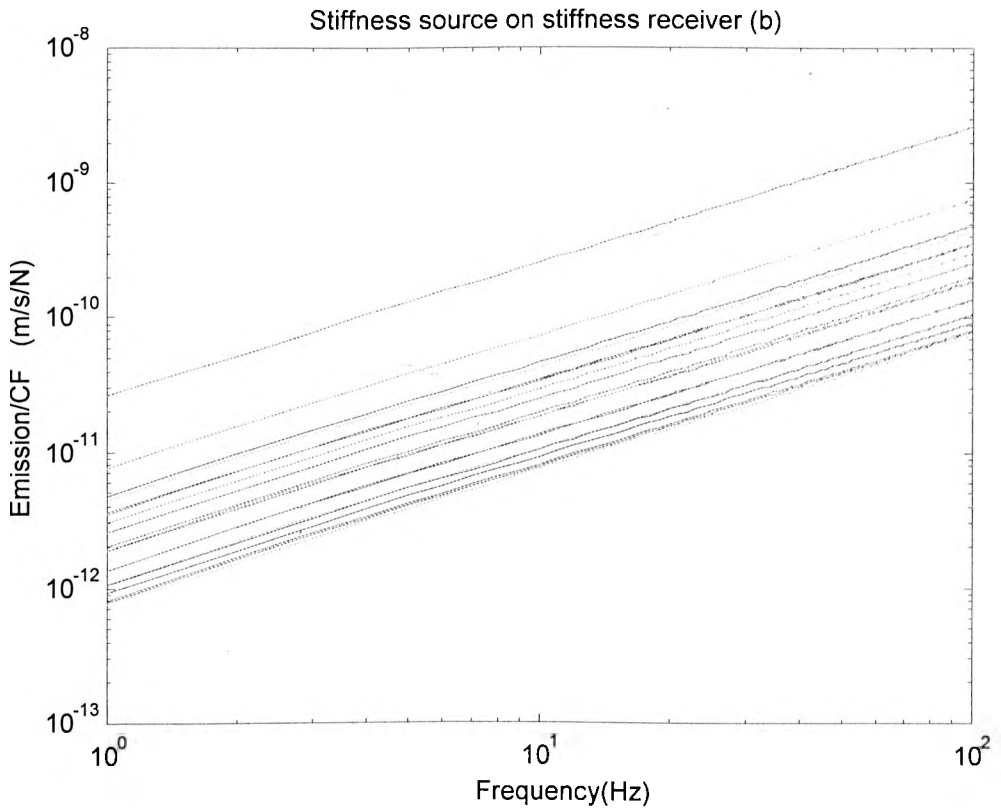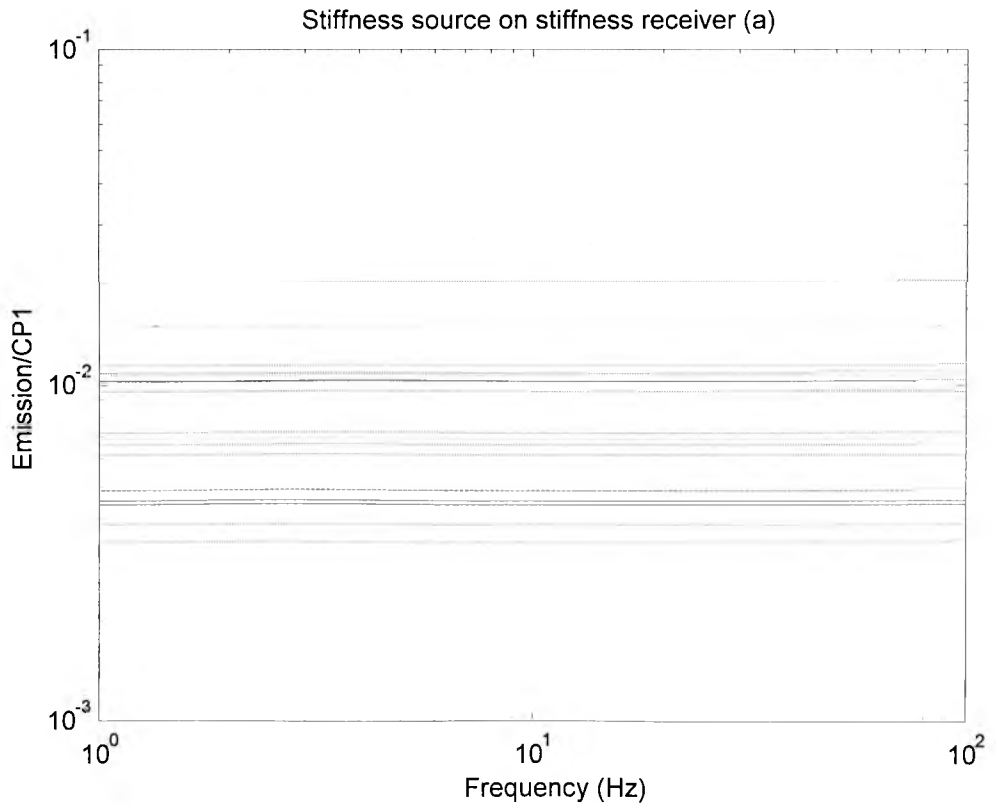
Figure 5-44 General normalised active power for CP1 (top) and CF(bottom) for a combination of a 5cm thickness plate in stiffness frequency range on another plate in stiffness frequency range. Each line correspond to a random excitation position.
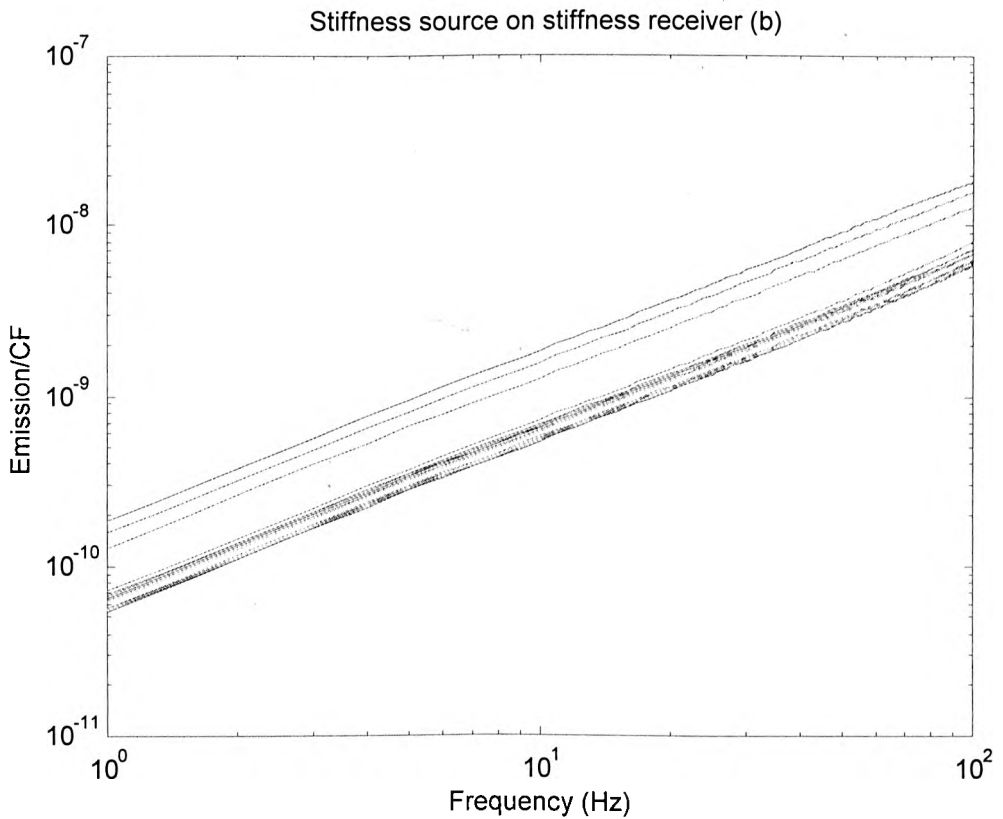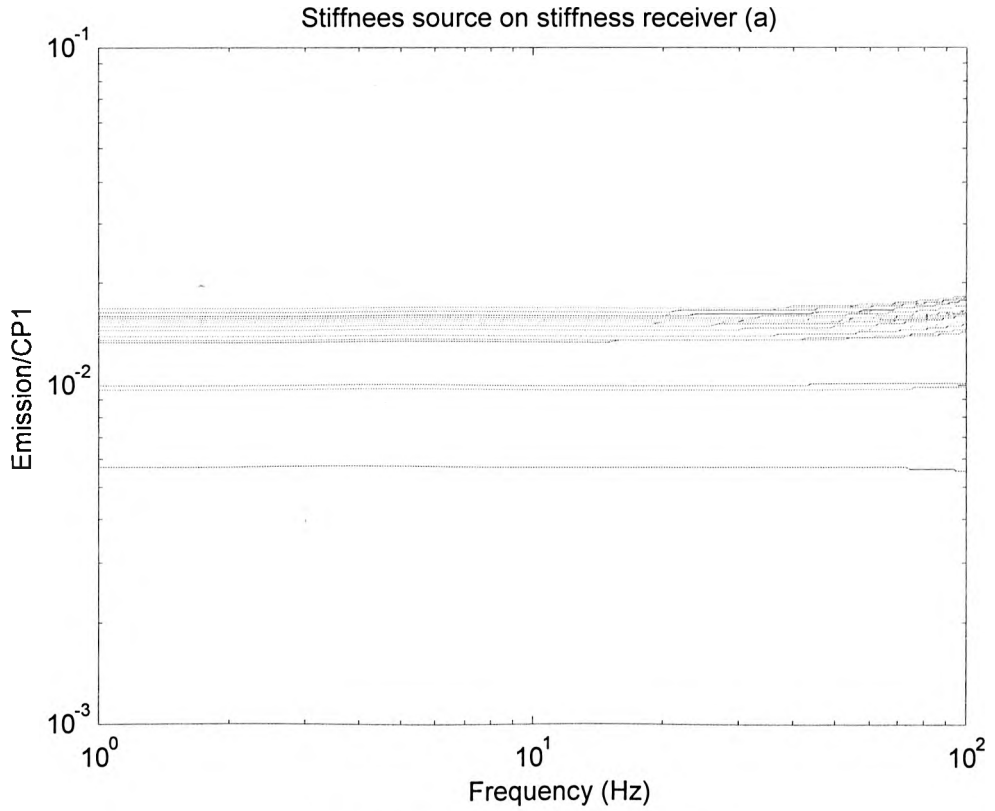
Figure 5-45 General normalised active power for CP1 (top) and CF(bottom) for a combination of a 2cm thickness plate in stiffness frequency range on another plate in stiffness frequency range. Each line correspond to a random excitation position.
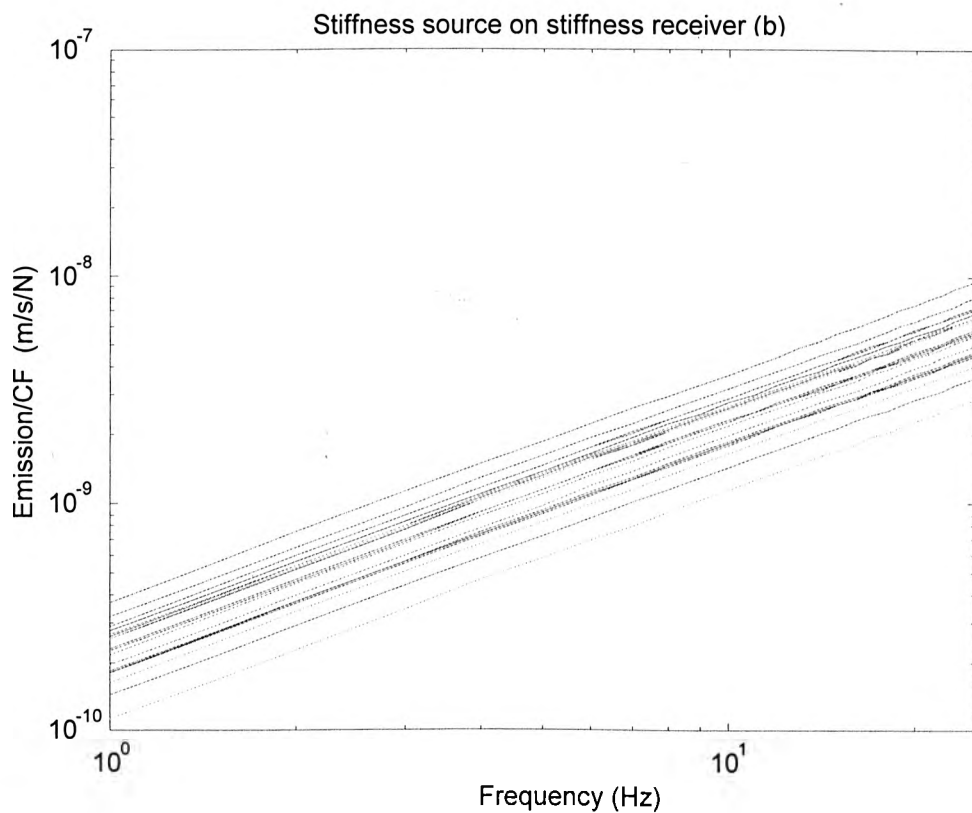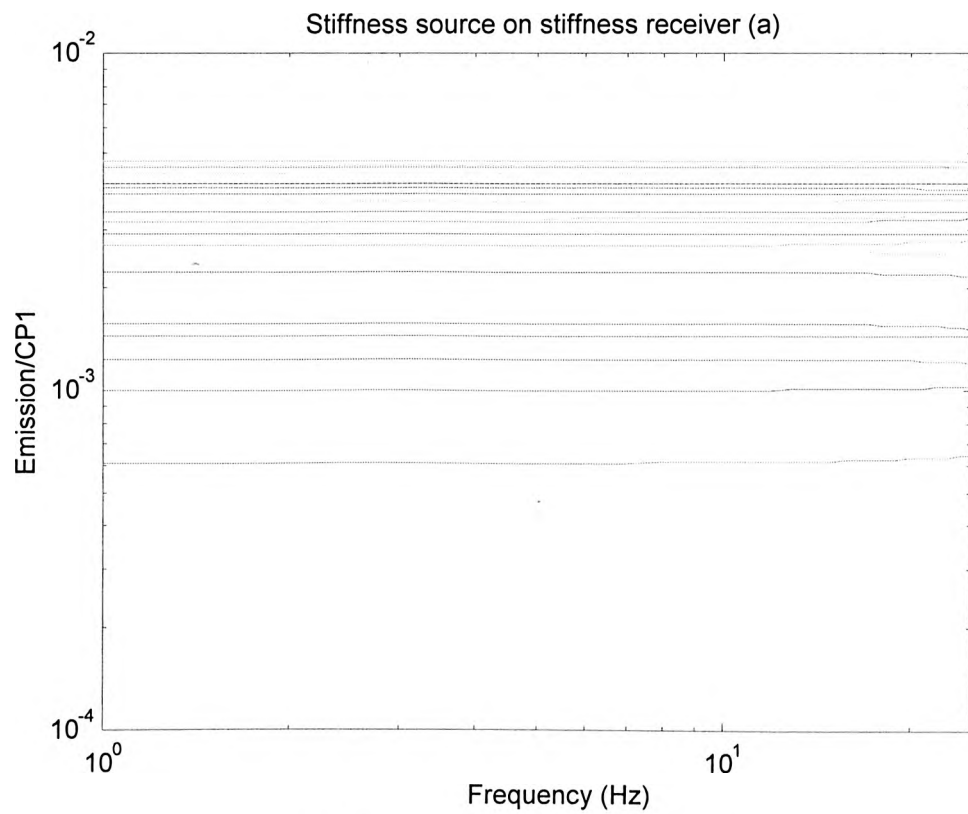
Figure 5-46 General normalised active power for CP1 (top) and CF(bottom) for a combination of a 0.5cm thickness plate in stiffness frequency range on another plate in stiffness frequency range . Each line correspond to a random excitation position.

CHAPTER 6

VALIDATION WITH REAL STRUCTURE-BORNE

SOUND SOURCES

6.1 Introduction

It can be said that most important aim of characterising a source is to enable the active power emission from source to receiver to be predicted. The question therefore arises of how to predict the active power emission by using s_1 and s_2. From chapter 5 we can see that the 'general normalised active power band' has a width, so that for given s1 and s2, the power into the receiver has a 'range'. Using the median line of the general normalised active power band to approximately predict the active power emission is proposed in this chapter. The probability that the true general normalised power lies on one side or other of the median line is fifty percent, so using the median line to predict power emission should be a good choice. (Another obvious choice would be to use the mean, but this is not discussed further).This approach, which can be applied using CF, CP1 or CP2, is here called the 'single figure' prediction method. In this chapter the 'single figure' prediction method is tested by applying it to some practical machines on various plate receivers. Some other simplified characterisations which were described in chapter 3, namely the 'poles' method and the effective mobility, are applied to the same cases to establish the relative 'cost' of various forms of simplification.

6.2 Prediction equations

Observing the general normalised power band in chapter 5, in most cases the equation for the median line can be approximately expressed in the following form:

$$\left(\frac{P}{CF}\right)_{median} \approx \overline{\sum \text{Re}(Y_{R,ii})} \frac{1}{\left|1 + (\alpha^\Sigma / \beta_1)^{\beta_2}\right|^{2\beta_3}} / \beta_4 \qquad (6\text{-}1)$$

$$\left(\frac{P}{CP1}\right)_{median} \approx \frac{\overline{\sum \mathrm{Re}(Y_{R,ii})}}{\overline{\sum |Y_{R,ii}|}} \frac{(\alpha^{\Sigma}/\beta_1)^{\beta_2}}{\left|1+(\alpha^{\Sigma}/\beta_1)^{\beta_2}\right|^{2\beta_3}}/\beta_4 \qquad (6\text{-}2a)$$

$$\left(\frac{P}{CP2}\right)_{median} \approx \frac{\overline{\sum \mathrm{Re}(Y_{R,ii})}}{\overline{\sum |Y_{R,ii}|}} \frac{(\alpha^{\Sigma}/\beta_1)^{\beta_2}}{\left|1+(\alpha^{\Sigma}/\beta_1)^{\beta_2}\right|^{2\beta_3}}/\beta_4 \qquad (6\text{-}2b)$$

Therefore, the following equations for prediction of the active power emission are proposed:

$$P \approx \overline{\sum \mathrm{Re}(Y_{R,ii})} \frac{1}{\left|1+(\alpha^{\Sigma}/\beta_1)^{\beta_2}\right|^{2\beta_3}}/\beta_4 \times CF \qquad (6\text{-}3)$$

$$P \approx \frac{\overline{\sum \mathrm{Re}(Y_{R,ii})}}{\overline{\sum |Y_{R,ii}|}} \frac{(\alpha^{\Sigma}/\beta_1)^{\beta_2}}{\left|1+(\alpha^{\Sigma}/\beta_1)^{\beta_2}\right|^{2\beta_3}}/\beta_4 \times CP1 \qquad (6\text{-}4a)$$

$$P \approx \frac{\overline{\sum \mathrm{Re}(Y_{R,ii})}}{\overline{\sum |Y_{R,ii}|}} \frac{(\alpha^{\Sigma}/\beta_1)^{\beta_2}}{\left|1+(\alpha^{\Sigma}/\beta_1)^{\beta_2}\right|^{2\beta_3}}/\beta_4 \times CP2 \qquad (6\text{-}4b)$$

where $\overline{\sum \mathrm{Re}(Y_{R,ii})}$ is the average point mobility real part, while $\overline{\sum |Y_{R,ii}|}$ is the average point mobility magnitude. Equation 6-3 can be understood as an extension of equation (2-30), while equation 6-4 is an extension of equation (2-31). For single point contact, the results of prediction by using equation (2-30) and by using equation (2-31) are the same. But for multiple points, the results of prediction by using equations 6-3 and 6-4 are different. The $\beta_i (i=1,2,3,4)$ are called the 'adjustment factors' which are obtained according to median line of the general normalised active power bands in chapter 5. For the single point case, the adjustment factor can be understood as unity.

It is noted that some information about the real part of the mobility matrix of the receiver is required.

For the limiting case $\sum \text{Re}(Y_{R,ii}) = 0$, the predicted solution by using equation 6-3 and 6-4 is zero, which agrees with the exact solution. It can be proved as follows: when $\sum \text{Re}(Y_{R,ii})$ equals zero, then we have

$$\sum \lambda_{R,i} = \sum \text{Re}(Y_{R,ii}) = 0 \quad (6\text{-}5)$$

where $\lambda_{R,i}$ are the eigenvalues of the real part of receiver matrix. All eigenvalues must be non negative, so the only possible solution to equation (6-5) is that all eigenvalues are zero (and it can be shown this means that the whole real part of the matrix equals zero). This means the active power emission equals zero, no matter what the imaginary part of the receiver mobility matrix.

6.3 Prediction for real fans on various plate receivers

Based on the above analysis, several examples are now given. The case studies presented in the rest of this chapter comprise typical practical fans upon various plate receivers. In all cases the mobilities and free velocities of the fan were obtained from archive measured data, and the mobilities of the various plate receivers were calculated using thin plate theory.

6.3.1 Fan A on various receivers

Case1: Fan A attached to a low mobility infinite plate.

In this case the infinite plate receiver has a low mobility in comparison to that of the source. The material and geometric properties of the plate are: Young's modulus

E=$2.0*10^{10}$ N/m^2, density ρ=$2.3*10^3$ kg/m^3 Poisson's ratio ν=0.3, loss factor η=0.01, and thickness 0.10m, i.e. it has the characteristics of a 100mm thick concrete plate.

The sum of the point mobility magnitudes for FanA $\sum|Y_{s,ii}|$ and for infinite plate receiver $\sum|Y_{R,ii}|$ are shown in figure 6-1a, and the average point mobility magnitude α^{Σ} in figure 6-1.b. It is suggested that the source can be considered as an off-resonant sourceover the whole frequency range: there are no significant regions of stiffness or mass behaviour, and the resonant peaks are not isolated. Even if one were to consider the peaks as 'single mode' resonance behaviour, the number of data points is statistically insignificant as a proportion of the whole frequency range.

For off-resonant sources we choose β_1=0.5 β_2=0.95 β_3=0.9 β_4=1 in expression (6-1), β_1=0.6 β_2=0.95 β_3=0.9 β_4=1 in expression (6-2a), and β_1=0.6 β_2=0.95 β_3=0.9 β_4=1.5 in expression (6.2b). These values have been obtained by substituting values into equation 6-1 and 6-2 until agreement was obtained with the median line of the appropriate general normalised active power band from Chapter 5. These values are suitable for stiffness receivers, off-resonant receivers and infinite plate receivers, in fact for all types of receiver except single mode resonant. For single mode resonant receivers we choose β_1=0.3 β_2=1 β_3=1.1 in expression (6-1) and expression (6-2), and β_4=3 in expression (6-1) and (6-2b), and β_4=3 for expression (6-2a). Figures 6-2~6-5 show a comparison of the two curves. The dark solid line is the median line from the general normalised active power band in chapter 5. The light solid line is the result of calculation based on equation 6-1 and 6-2 and using the above values.

Since the real fan is a physical structure, the eigenvalues of the real part of the mobility matrix should be positive. If the minimum eigenvalue is positive, then all others must also be positive, but if it is negative then at least one eigenvalue is negative, so the mobility data is 'unphysical'. Therefore, we can use the minimum eigenvalue of the real part of mobility to check if the mobility matrix is physical or not.

Figure 6-6 shows the minimum eigenvalues of the real part of the source mobility matrix. The value is negative over about 35 percent of the whole frequency range. This is unphysical, and is due to measurement errors, so the following study will not consider frequency ranges where the data is unphysical. Frequencies at which negative eigenvalues occur are called 'not considered frequencies', and otherwise, 'considered frequencies'.

In order to compare the results of prediction by different methods (equations), the cumulative distribution function $y= F(x)=P(X\leq x)$ is introduced. Here 'P' means probability (note the difference with italic letter 'P' used to denote power). X is defined by the following expression.

$$X = 10\log\frac{P_{prediction}}{P_{true}} \qquad (6\text{-}6)$$

Figure 6-7a shows the true active power emission together with the prediction from equation 6-3. The two curves are in close agreement. In figure6-7b the predicted active power normalised by the true power is shown. For all frequencies the error

does not exceed a factor of ±5. Ninety percent of the predicted active power lies between true+3dB and true−1.5dB.

Figure 6-8a shows the true active power emission and prediction from equation 6-4a (CP1). The two curves are not close like in figure 6-7a. For most frequencies the error does not exceed a factor ±6.5 (see figure 6-8b) and 90 % of the predicted active power lies between true+5dB and true−4.5dB (see figure6-8c).

Figure 6-9a shows the corresponding results from equation 6-4b (CP2). The agreement is similar to the above case, and 90 % of the predictions lie between true+4.5dB and true−4dB (see figure6-9c).

In Figure 6-10a are shown the true active power and that predicted from the effective mobility (only point mobility assumption). The prediction shows poor agreement with the true value, and the 90 % limits are true+5.5dB and true−8.5dB, (see figure6-10c).

Figures 6-11 are similar to 6-10, except that the unit magnitude, zero phase force ratio assumption is made for the effective mobility. The agreement is worse than any of the previous methods, with 90% limits of true+10dB and true−20dB, (figure6-11c).

Figure 6-12a shows the corresponding results for the poles method. The agreement with the true power is no better than when using CP1 and CP2 (equation 6-4) and considerably better than for the effective mobility method. The 90 % limits are true+4dB and true−7dB, (figure6-12c).

To summarise, using CF (Equation 6-3) gives the best accuracy in predicting active power out of the above six prediction methods. Effective mobility gives the worst accuracy even though more source data is required. The results of prediction by using CP1 (Equation 6-4a) and CP2 (Equation.6-4b) are similar; and their cumulative distribution functions are close, see figure 6-13a.

It was expected that the blocked force characterisation would work best in this case because the ratio of average point mobility magnitude α^Σ is less than 0.1. For such values, the general normalised active power band for CF is narrower than that of CP1 and CP2 as shown in Chapter 5, while the width for CP1 and CP2 is similar. Thus, these results were broadly expected from Chapter 5. Therefore, prediction of active power by using CF is more accurate than by using CP1 and CP2. This is different for the single point case where all three parameters give identical results.

In order to evaluate the effect of the adjustment β, Figure 6-13b lists the results of cumulative distribution functions corresponding to $\beta_1 = \beta_2 = \beta_3 = 1$. The curves for CP1 and CP2 move to the left, which means that there is a tendency for underestimation, while the curve for CF does not obviously change.

Case2: FanA attached to an infinite plate of matched mobility

This case study consists of the above fan attached to an infinite plate of matched mobility. The plate material is the same as above and the thickness is 9mm. The sum of the point mobility magnitude for FanA $\Sigma|Y_{s,ii}|$ and for the thin infinite plate receiver $\Sigma|Y_{R,ii}|$ are shown in figure 6-14a. The average point mobility magnitude α^Σ is shown in figure 6-14.b. For most frequencies α^Σ is between 0.2 and 3.

In figure 6-15a the true active power is compared to that predicted by using CF (equation 6-3). The two curves are not so close as for case 1. In figure 6-15b the prediction power normalised by the true active power is shown, and 90 % of the predicted values are between true-4.5dB and true+4.8dB (see figure6-15c).

Figure 6-16a shows the true active power and that predicted by using CP1 (equation 6-4a). The two curves are quite close, the prediction proving to be more accurate than for case 1 (see figure 6-16b). 90 % of predicted values are between true-3.0dB and true+1.5dB as shown in figure10-16c.

Again, the results obtained by using equation 6-4b (CP2) are similar to those from equation 6-4a (CP1), and only the cumulative distribution functions have been shown in figure 6-20a.

In figure 6-17 are shown corresponding results from using effective mobility (only point mobility assumption). The accuracy is better than that for case1, but is still worse than the results in figures 6-16. The 90 % margins are true-2.2dB and true+3.2dB.

Figure 6-18 shows the results from using the effective mobility (unit magnitude, zero phase force ratio assumption). The prediction is poor, with 90 % of the predicted active power between true+5dB and true–6dB.

Results from the poles method are given in Figure 6-19. The accuracy is similar to using equation 6-4 with 90% margins of true+1.8dB and true–2.8dB, see figure6-19c.

To summarise, the effective mobility (with unit magnitude, zero phase force ratio assumption) gives the worst results. The point mobility assumption gives better results, in fact better than by using CF, but the best results are from CP1 , CP2 and the poles method. As for the previous case, the results of prediction by using CP1 and CP2 are similar, the two cumulative distribution functions being close (see figure 6-20). This can be explained by the results of Chapter 5; the average point mobility magnitude ratio α^{Σ} is between 0.2 and 3. In this range, the general normalised active power bands for CP1 and CP2 are similar and narrower than that for CF, so equation 6-3 is expected to give worse results than equation 6-4.

Figure 6-20b lists the results of cumulative distribution functions corresponding to $\beta_1 = \beta_2 = \beta_3 = 1$. The curve for CP1and CP2 moves to the left, indicating a tendency for underestimation, while that for CF moves to the right, giving a tendency for overestimation.

Case3: FanA attached to a lower mobility SSSS plate

This case study is of fanA upon a lower mobility SSSS plate receiver (simply supported all round). The physical properties of the plate are the same as above and the geometric parameters are shown in figure 6-21. The sum of the point mobility magnitude for FanA ($\Sigma|Y_{s,ii}|$) and for the plate ($\Sigma|Y_{R,ii}|$) are shown in figure 6-22a, and the average point mobility magnitude ratio α^{Σ} is shown in figure 6-22b. In all the 'considered frequency range' α^{Σ} lies between 0.001and 0.1.

The true and predicted active power by using equation 6-3 is shown in figure 6-23a. The two curves are not in close agreement as was the case for a thick infinite plate receiver (case1), since here the condition number for the finite receiver mobility matrix is larger. The 90 % margins are true-4dB and true+4dB, (see figure.6-23c).

Figures 6-24 shows the results from equations 6-4a. The 90% margins are true-6.5dB, +7.0dB. The results by using equation 6-4b are similar to those from equation 6-4a, so as above only the cumulative distribution functions have been shown in figure 6-26a.

The prediction using effective mobility with unit magnitude zero phase force ratio force assumption is shown in figure 6-25. The prediction is the poorest, with 90 % margins of true-28dB, +9dB. About 12% of the predicted values are negative (shown by the dotted line). This is not physical and arises since the equation for prediction itself has a conflict. This is the main reason why these results are poor. In fact, the same problem also occurred in the two previous cases, but was not highlighted since only a few values were negative.

The prediction using the effective mobility (only point mobility assumption) is poor, while results from the poles method are not generally better than for equation 6-4.(only the cumulative distribution functions have been plotted for these two cases)

Again, using CF for predicting the active power gives the best results. Effective mobility gives poor results, while results for CP1 and CP2 are similar. The poles method is no better than that of using CP1 and CP2 in this case. The comparison of

cumulative distribution functions is shown in figure 6-26a. Figure 6-26b shows the cumulative distribution functions which correspond to $\beta_1 = \beta_2 = \beta_3 = 1$. The results are similar to case 1, and no further discussion is required here.

Case4: Fan A attached to a matched SSSS plate

This case study is the fan A upon a SSSS plate receiver whose mobility is of a similar magnitude to that of the source. The physical parameters and geometry of the SSSS plate are the same as Case 3, except that the plate thickness is 7mm. The sum of the point mobility magnitude for FanA $\sum |Y_{s,ii}|$ and for the thin SSSS plate receiver $\sum |Y_{R,ii}|$ are shown in figure 6-27a. The average point mobility magnitude ratio α^Σ is shown in figure 6-27b, showing that for most 'considered' frequencies the α^Σ are between 0.1 and 10.

Figures 6-28 to 6-31 list the results of prediction by using equations (6-3), (6-4), effective mobility and poles method. The blocked force method, (Equation 6-3) gives 90% margins of ±5.5dB. The characteristic power, CP1 gives better accuracy: –3.5dB, +2.5dB, and as before, the results from CP2 are similar, (still only cumulative distribution function have been plotted). Effective mobility (point mobility assumption) is no better than CP1 or CP2 (still only cumulative distribution function have been plotted), with 90% margins of –2.5, +4.5, while the unit magnitude, zero phase force ratio assumption, again gives the worst results, (not been plotted). The poles method gives the best results: –2.7, +2dB.

Figure6-31b shows the cumulative distribution functions corresponding to $\beta_1 = \beta_2 = \beta_3 = 1$. The conclusions are similar to case 2.

Case3 and Case 4 show again that in the case of lower mobility receivers, using CF for prediction is better than using CP1 and CP2, while in the case of matched mobility receiver the opposite is the case. These results can be explained by using the general normalised active power bands given in chapter 5. In other words, these cases provide a practical validation of the conclusions of Chapter 5 which were based on 'abstract' structures.

6.3.2 Prediction of active power from fan B into finite plate receiver.

Fan B is another typical practical fan. The sum of point mobility magnitude $\sum |Y_{s,ii}|$ is shown in figure 6-32a. The minimum eigenvalue is negative over about 50% of the whole frequency (see 6-33). Below 100Hz there are no positive eigenvalues. This is a region of mass-like behaviour, but the curve in this frequency range deviates from that of a pure mass-like source. Therefore, the data is of suspect quality in this frequency range which is not therefore considered. From 100Hz to 400Hz fan B shows stiffness-like behaviour, and above 400Hz it can be considered as an off-resonant source.

For stiffness sources the same adjustment factors are used as for off-resonant sources, except that β_1 is slightly changed to β_1=0.45. (The adjustment factors for off-resonant sources can also be used for single mode resonant sources, although no such behaviour was present in this case).

Case5 Fan B attached to a lower mobility SSSS plate

The properties of the plate assumed are as follows: Young's modulus $E=2.0*10^{10}$

N/m^2, density ρ=2.3*10^3 kg/m^3, Poisson's ratio ν=0.3, loss factor η=0.02, and the geometric parameters are shown in figure 6-34. The thickness of the plate is 0.09m. The sum of the point mobility magnitude $\sum|Y_{R,ii}|$ for the SSSS plate receiver are shown in figure 6-32a. The average point mobility magnitude ratio α^Σ is shown in figure 6-32b.

Figures 6-35 to 6-40 give the results of prediction by using expression 6-3, 6-4, effective mobility and poles method. In the stiffness range, prediction by using CF (equation 6-3) looks better than other methods, and CP1 and CP2 give similar results. These results are consistent with chapter 5. The effective mobility and poles method proved to be less accurate than CP1 and CP2 for this case. The cumulative distribution function for this frequency range was not plotted as there was insufficient data.

In the off-resonant range (above 400Hz), the prediction by using CF is still the best one with 90% probability limits of -2.5dB, +3dB, and effective mobility (unit magnitude, zero phase force ratio assumption) is still worst. Conclusions are generally consistent with case3 (see figure 6-41).

Case 6 Fan B attached to a matched SSSS plate

The SSSS plate receiver is steel with physical properties: Young's modulus E=1.8*10^{11} N/m^2 , density ρ=7.8*10^3 kg/m^3, Poisson's ratio ν=0.3, loss factor η=0.01. Geometry is shown in figure 6-42. The sum of point mobility magnitude for Fan B, $\sum|Y_{s,ii}|$ and for the thin plate receiver $\sum|Y_{R,ii}|$ are shown in figure 6-43a. The

average point mobility magnitude ratio α^Σ is shown in figure 6-43b and lies in the range 0.1~10, i.e. the structures are 'matched'.

Figures 6-44 to 6-45 give the results of prediction by using different methods. In the stiffness range the prediction by using CF (equation 6-3) is poorer than using CP1 and CP2. This is consistent with the results of chapter 5. The results by using effective mobility are not worse than that of using CP1 and CP2. In this example the relationship between points on the source in the stiffness range is relatively weak, especially for sources with flange bases [34] (like fanB). Also, for thin plate receivers the transfer mobility is less than the point mobility, and these two factors mean that the assumption of uncoupled points is likely to work reasonably well. The poles method gives better results.

However, in the off-resonant range, the prediction by using the effective mobility (unit magnitude, zero phase force ratio assumption) is still the worst, while the prediction by using CF (equ.6-3) is the next worst. The poles method is slightly better than using CP1 and CP2 (equ.6-4). In this case, prediction by using effective mobility (only point mobility assumption) is not worse than that of using CP1 and CP2.

6.3.3 Prediction for a motor on various receivers

The motor example includes regions of mass-like behaviour which has not been considered up to now. Figure 6-47 shows the sum of point mobility magnitude for typical motor in the frequency range of 10~300Hz (solid curve). From 100 Hz the solid curve begins to bend, and deviates from ideal mass behaviour (dotted line) above 150Hz. Thus, the motor can be considered as a mass source at frequencies

below 150Hz. For a mass source the real part of the mobility should be small (it is zero for an ideal mass), but in the range of 10~50Hz the real part is not small (see dashed curve) due to measurement errors (the lower the frequency the more the measurement error). Therefore we consider only the frequency range of 50~150Hz.

For a mass source we choose $\beta_1=j$ $\beta_2=1$ $\beta_3=1$ $\beta_4=1$ in expression (6-1) and (6-2) when the receiver is an infinite plate, but for other receiver types the prediction equations will be more complex. For off-resonant receivers it is seen from figures (5-12~5-12) that a sensible approximation to the median line can be made with two straight lines, that is by the following:

$$
P \approx
\begin{cases}
\overline{\sum \mathrm{Re}(Y_{R,ii})} \times CF & (\alpha^{\Sigma} < 1) \\
\overline{\sum \mathrm{Re}(Y_{R,ii})} / \left| \alpha^{\Sigma} \right|^2 \times CF & (\alpha^{\Sigma} > 1)
\end{cases}
\tag{6-7}
$$

$$
P \approx
\begin{cases}
\dfrac{\overline{\sum \mathrm{Re}(Y_{R,ii})}}{\overline{\sum |Y_{R,ii}|}} \alpha^{\Sigma} \times CP1 & (\alpha^{\Sigma} < 1) \\[4mm]
\dfrac{\overline{\sum \mathrm{Re}(Y_{R,ii})}}{\overline{\sum |Y_{R,ii}|}} / \alpha^{\Sigma} \times CP1 & (\alpha^{\Sigma} > 1)
\end{cases}
\tag{6-8a}
$$

$$
P \approx
\begin{cases}
\dfrac{\overline{\sum \mathrm{Re}(Y_{R,ii})}}{\overline{\sum |Y_{R,ii}|}} \alpha^{\Sigma} \times CP2 & \alpha^{\Sigma} < 1 \\[4mm]
\dfrac{\overline{\sum \mathrm{Re}(Y_{R,ii})}}{\overline{\sum |Y_{R,ii}|}} / \alpha^{\Sigma} \times CP2 & \alpha^{\Sigma} > 1
\end{cases}
\tag{6-8b}
$$

For stiffness receivers, equation 6-7 and 6-8 can be used in the range $\alpha^{\Sigma} < 0.1$, but in the matched case the prediction based on general normalised active power is difficult as illustrated by figures 5-2~5-4. Such predictions are also difficult for receivers for which the mobility curve displays high, sharp peaks (approximated as single mode

resonant structures), because the sharper the peak, the greater the adjustment factors β_3 and β_4.

Case 7 Motor on infinite plate

Figure 6-48 shows the prediction normalised by the true active power for the motor on an infinite plate. (The sum of the point mobility magnitude for the infinite plate receiver $\sum \left| Y_{R,ii} \right|$ are shown too in figure 6-47). The solid line (curve) was obtained using CF (equation6-3), and the dotted and dashed lines using CP1and CP2 (equation 6-4a,b) respectively. Results from all methods except the poles method show an error in the shape of the spectrum. The range of error is similar for CF, CP1 and CP2 which coincides with the properties of the corresponding general normalised active power band in chapter5, where the widths of the three bands are similar. However, CF over predicts which may possibly be explained as follows. The prediction equation is based on the median line of the corresponding general normalised active power band. However, for ideal mass sources the rank is not full, so the matrix inverse does not formally exist, and CF cannot therefore be determined for a given free velocity. To avoid this problem, the SVD method has been used to obtain CF and hence the general normalised active power band. This method effectively sets CF to a minimum solution[51]. Therefore, using the median equation may overestimate the active power from a practical mass source into a receiver. Curves from other methods give less accurate results except for the 'polar' method where the agreement is good.

In the above examples, the sources are practical machines. Although data was available for a number of cases, none has been found with sharp resonance peaks. Therefore, it has not been possible to validate the single mode resonance model. In

this case the relationships between CF, CP1, and CP2 are simple (see equation 5-17~18), and equations 6.3 and 6.4 become a single equation. For equation (6-4a) we can choose the adjustment factors $\beta_2 = \beta_3 = \beta_4 = 1$, but it is difficult to determine β_1. β_1 is highly sensitivity to receiver parameters, for example condition number. Therefore, we may expect difficulties in avoiding bias errors if this type of behaviour is prominent in other situations. However, it was found in Chapter 5 that CP1 forms an effective upper bound to the power, which may provide sufficient information in some cases.

6. 4 Conclusion

The prediction of active power from typical practical machines into various receiver types has been studied. Here, the input data to the predictions is from real structures, in contrast to Chapter 5, where 'abstract' data in the form of generic sources and receivers were used. In general, the results from real structures have been found to validate the generic results from Chapter 5 and therefore endorse the general approach used.

For practical fans, off-resonant behaviour is found to occupy most of the frequency range. Predictions based on the single figure parameters CF, CP1 and CP2 are on the whole more accurate than those based on the effective mobility method, even though the latter uses more data. The poles method gives slightly lower accuracy than CP1 and CP2 in the case of low α^{Σ}, but is slightly better in the matched case. Therefore, compared with the effective mobility method, using CP1 or CP2 combined with the average point mobility magnitude to characterise the source not only reduces the amount of data for characterisation but is also more reliable in terms of accuracy.

Compared with the poles method, using CP1 or CP2 combined with the average point mobility magnitude to characterise the source there is little 'cost' in accuracy but the characterisation is simpler. In the case of lower α^Σ the blocked force parameter CF was consistently the best characterisation. However, in the matched case it is worse than other methods except the effective mobility method with the assumption of unit magnitude, zero phase force ratios. Therefore, using three data CF, CP1 (or CP2) and average point mobility magnitude for characterisation of source will have better accuracy than using only two data.

For stiffness-like sources, the above results are still valid for lower α^Σ, while in the matched case the prediction by using CP1 or CP2 is slightly more 'costly' in accuracy compared with the poles method and is comparable for the effective mobility method.

For mass-like sources the poles method is more reliable than any of the 'single figure' prediction methods.
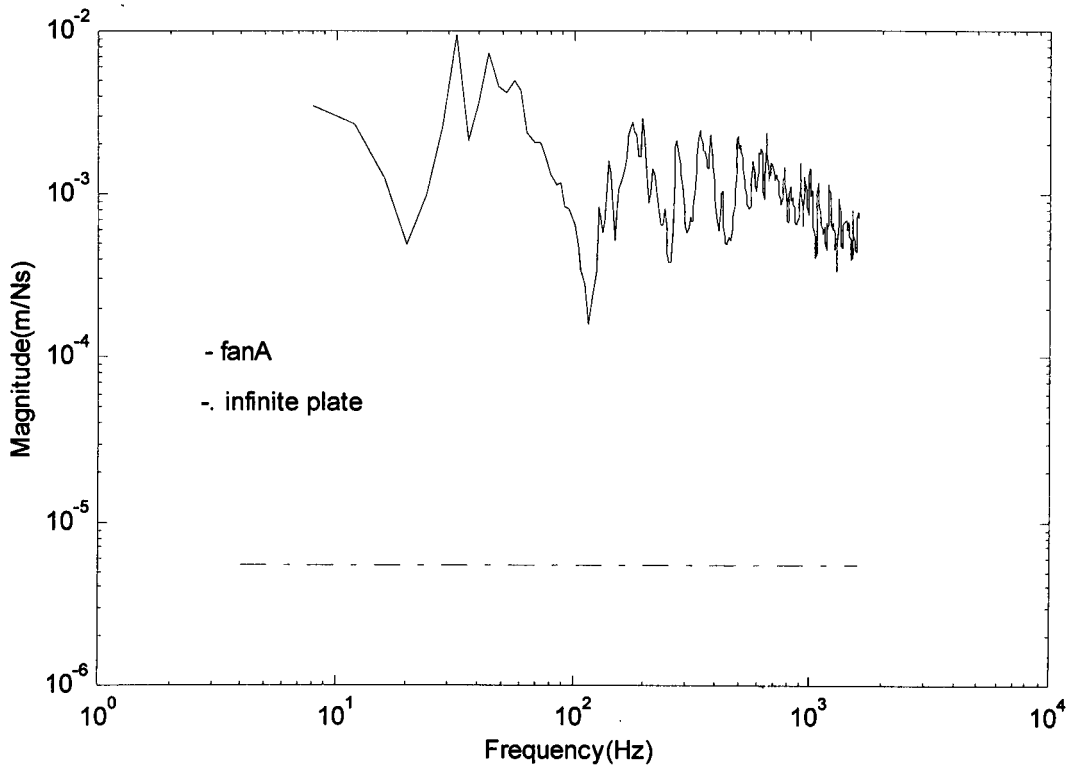
Figure 6-1a A sum of point mobility magnitude for fanA and for infinite plate
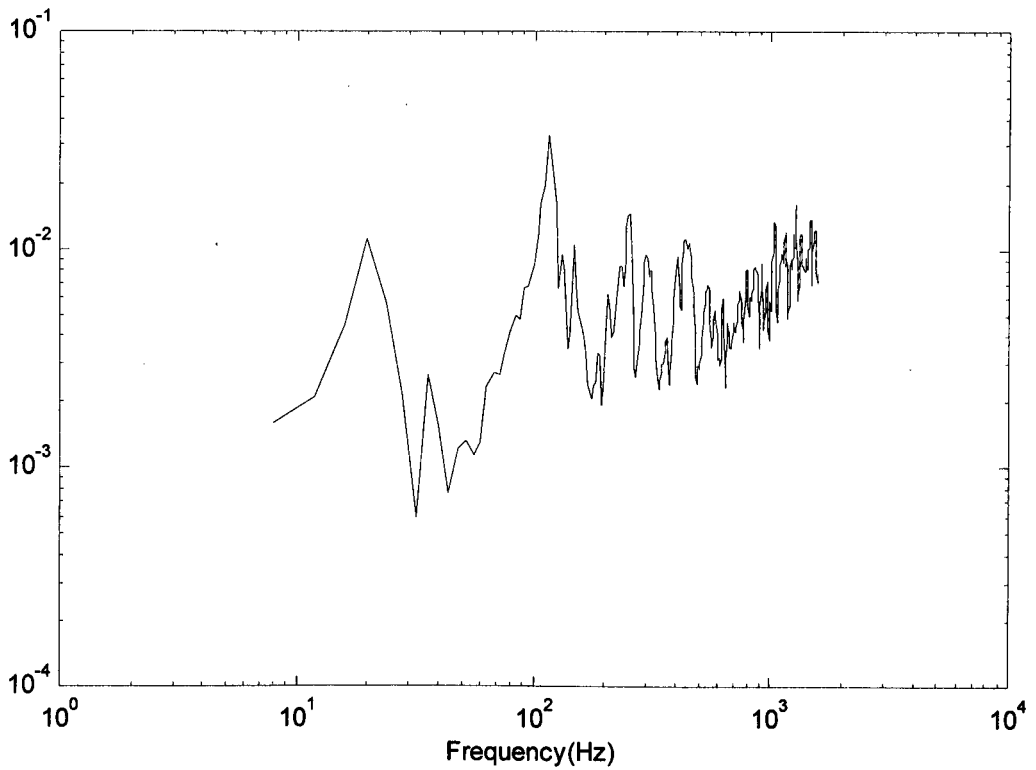
Figure 6-1b A average point mobility magnitude ratio of infinite plate to fanA
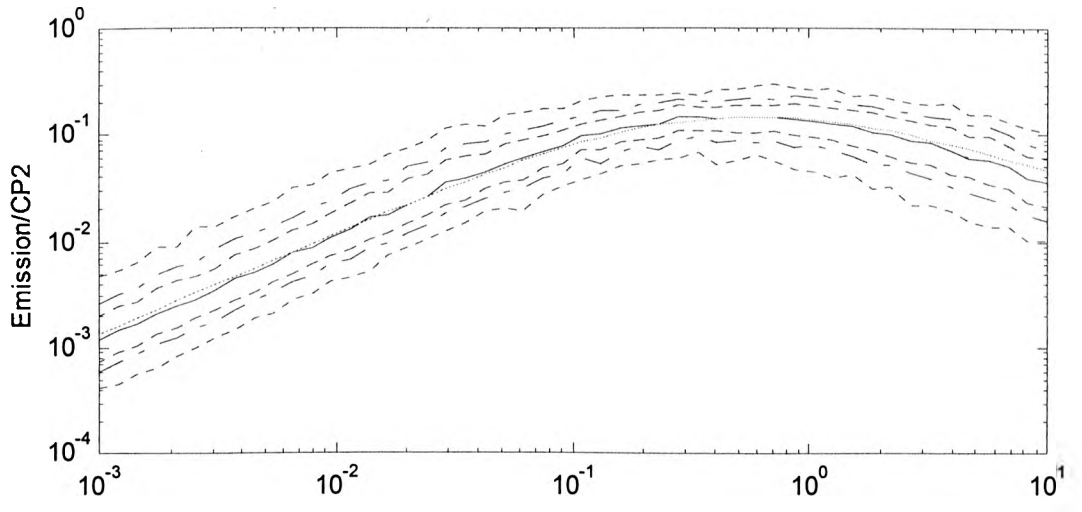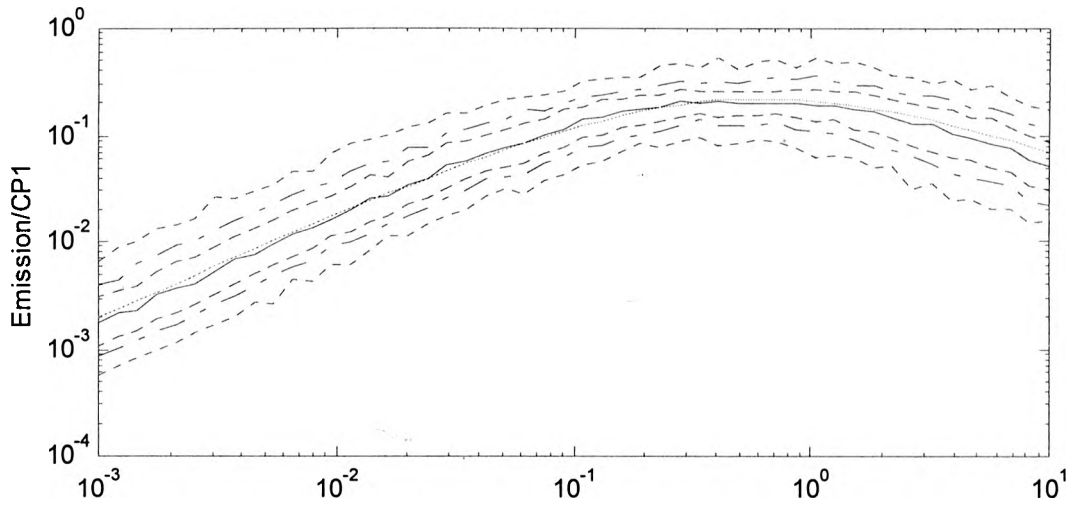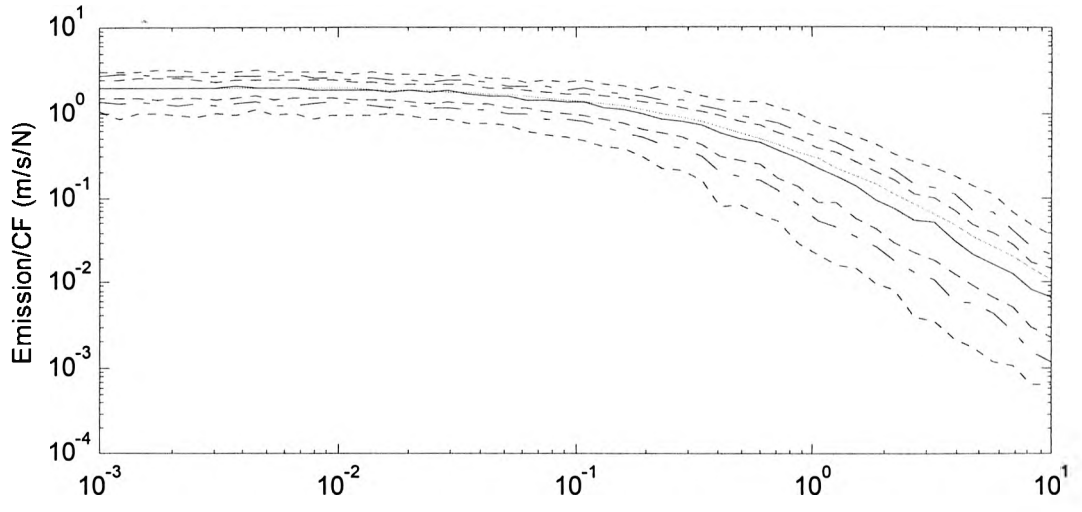
Figure 6-2 Comparison of median and calculation (off-resonant source on off-resonant receiver)
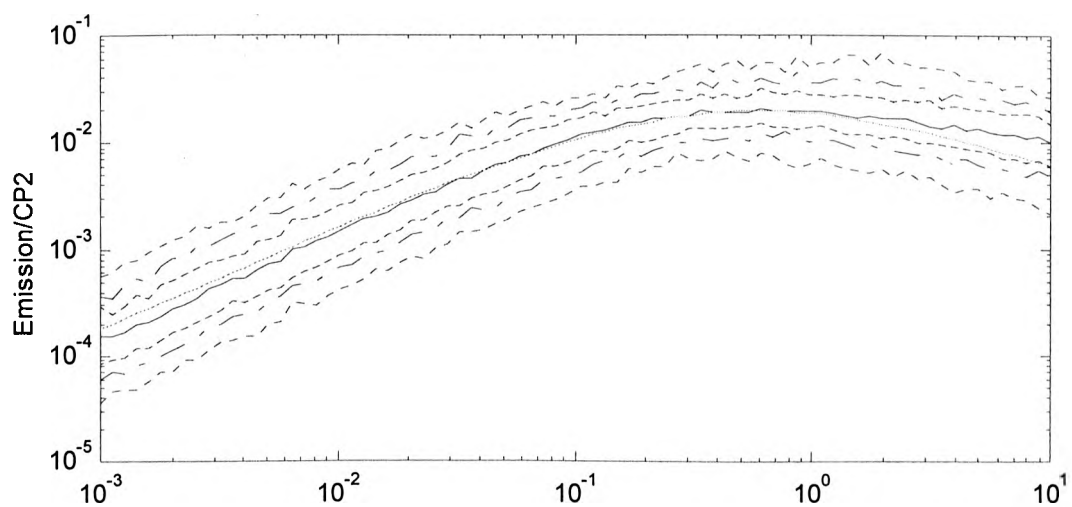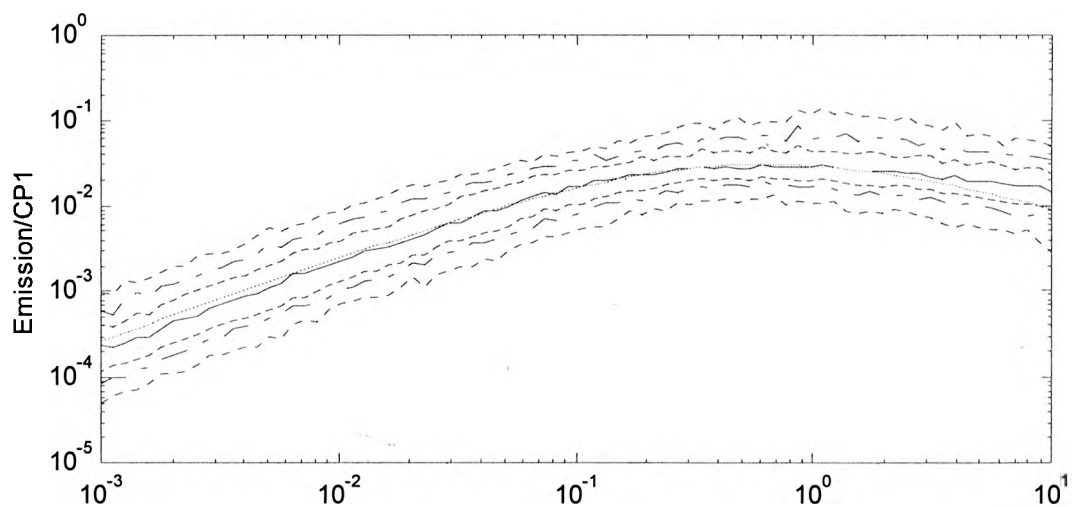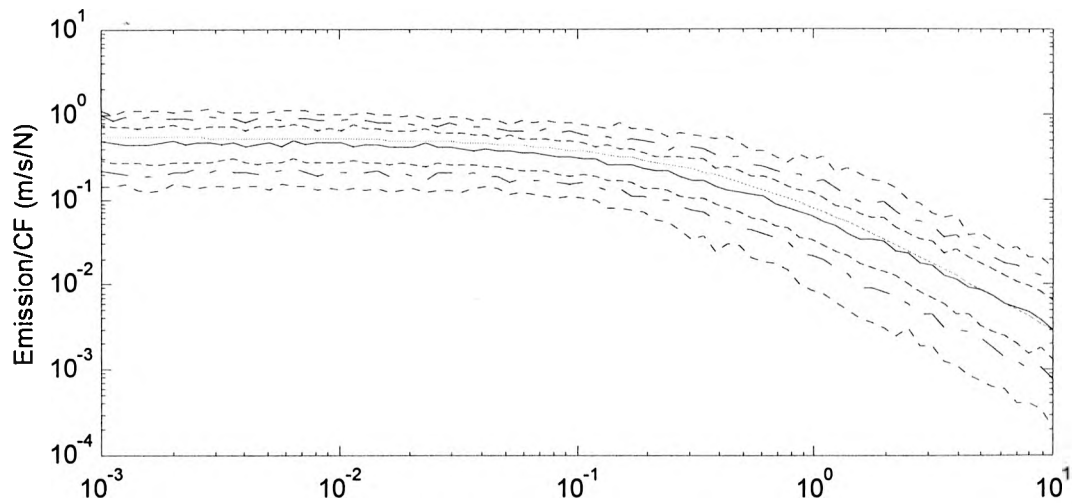
Figure 6-3 Comparison of median and calculation (off-resonant source on stiffness receiver)
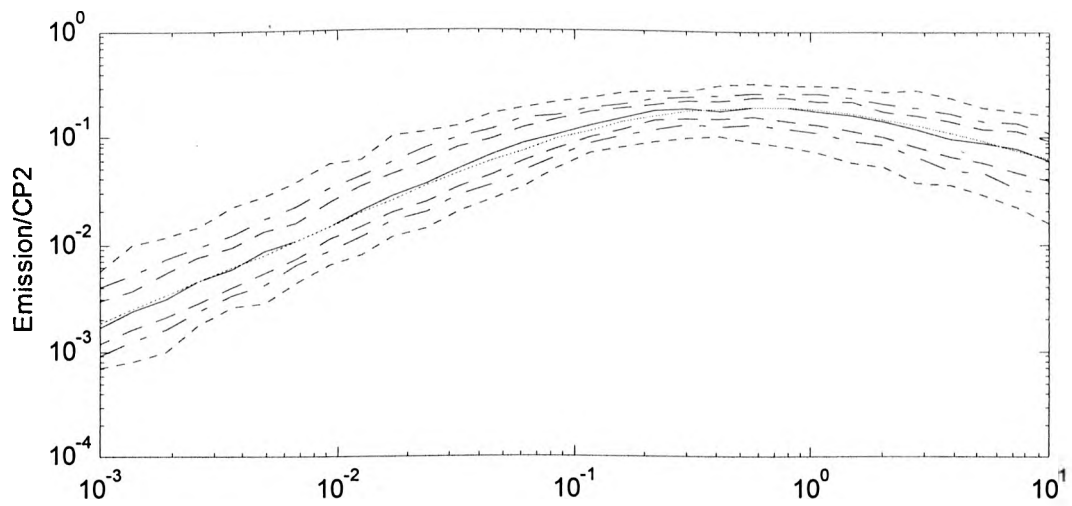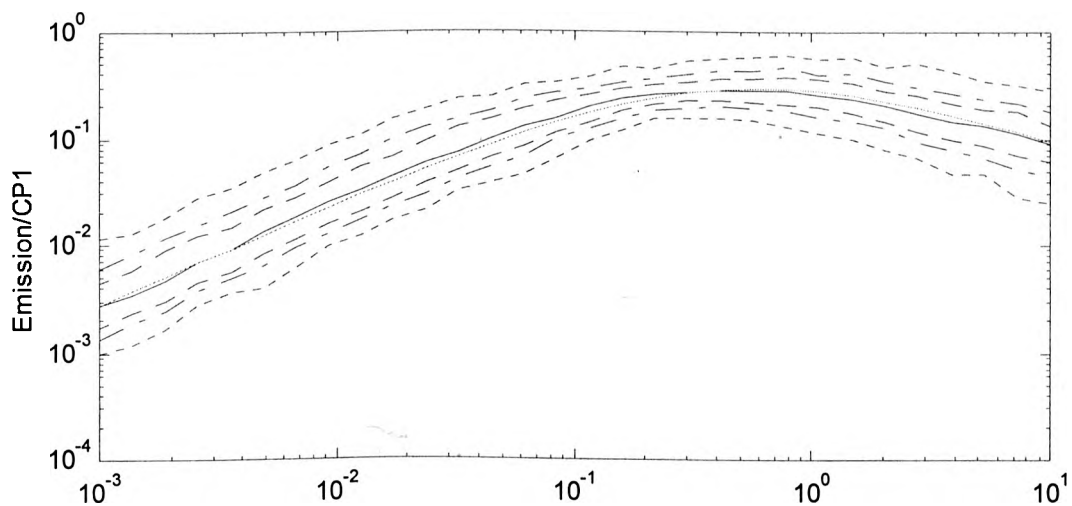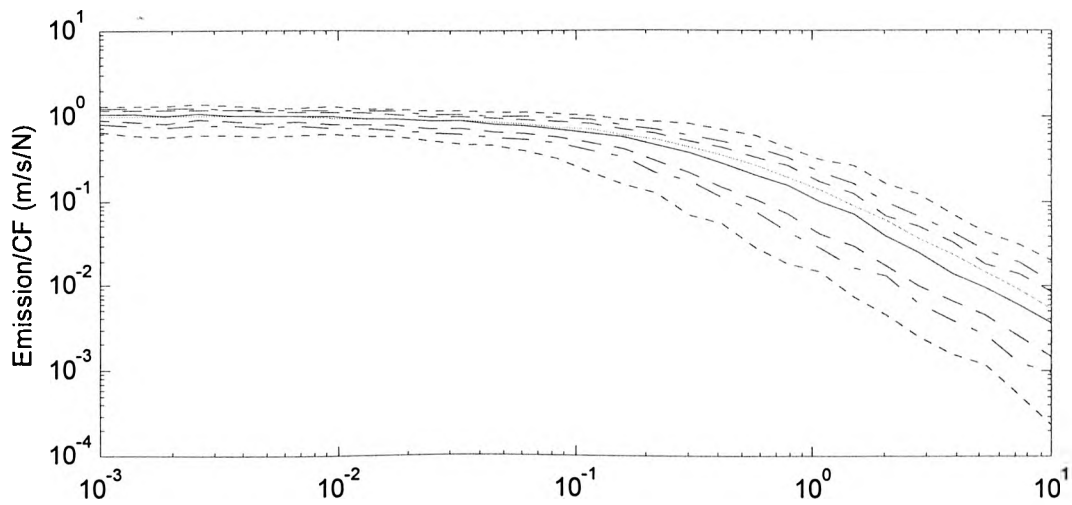
Figure 6-4 Comparison of median and calculation (off-resonant source on infinite plate)
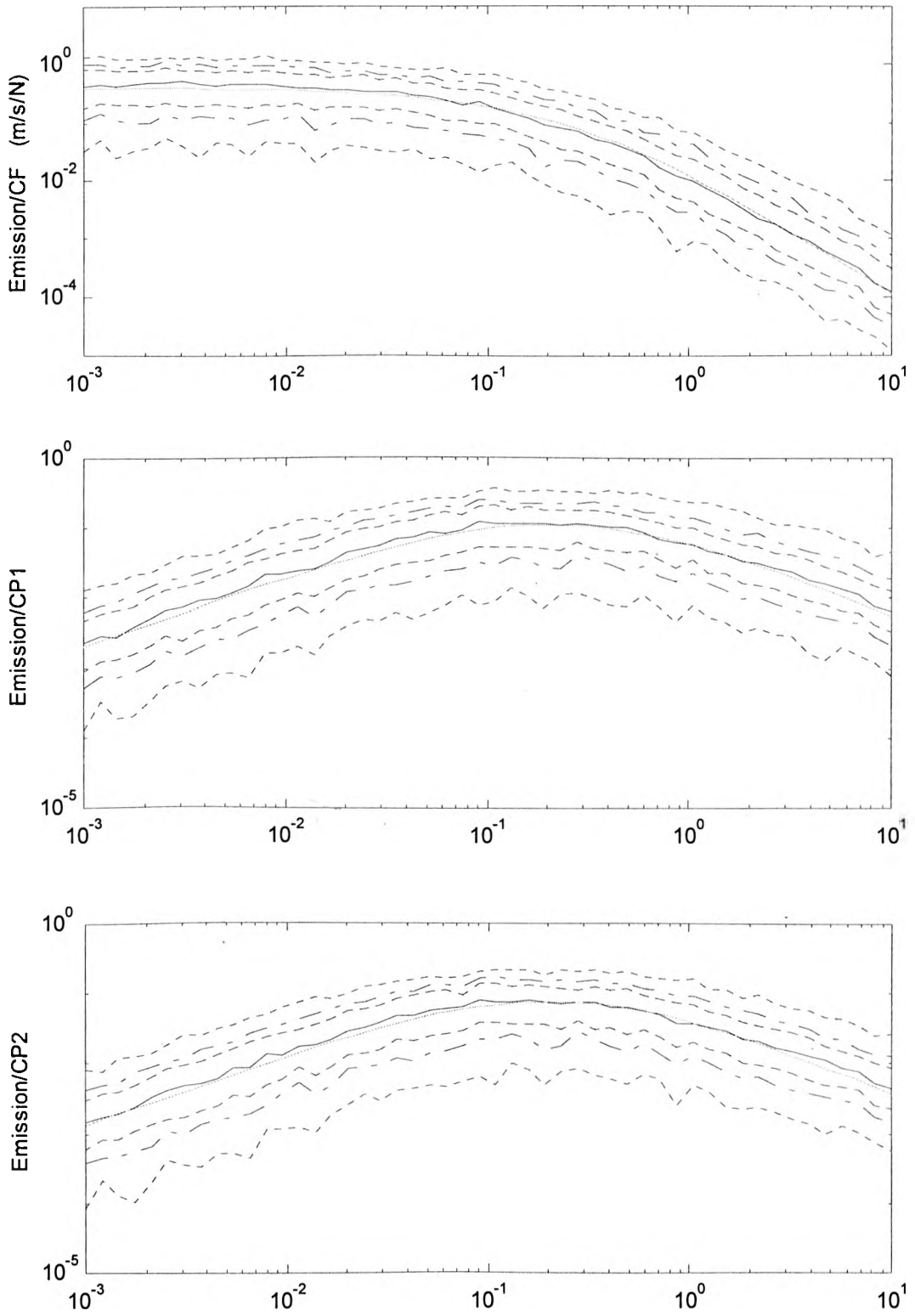
Figure 6-5 Comparison of median and calculation (off-resonant source on single mode resonant receiver)
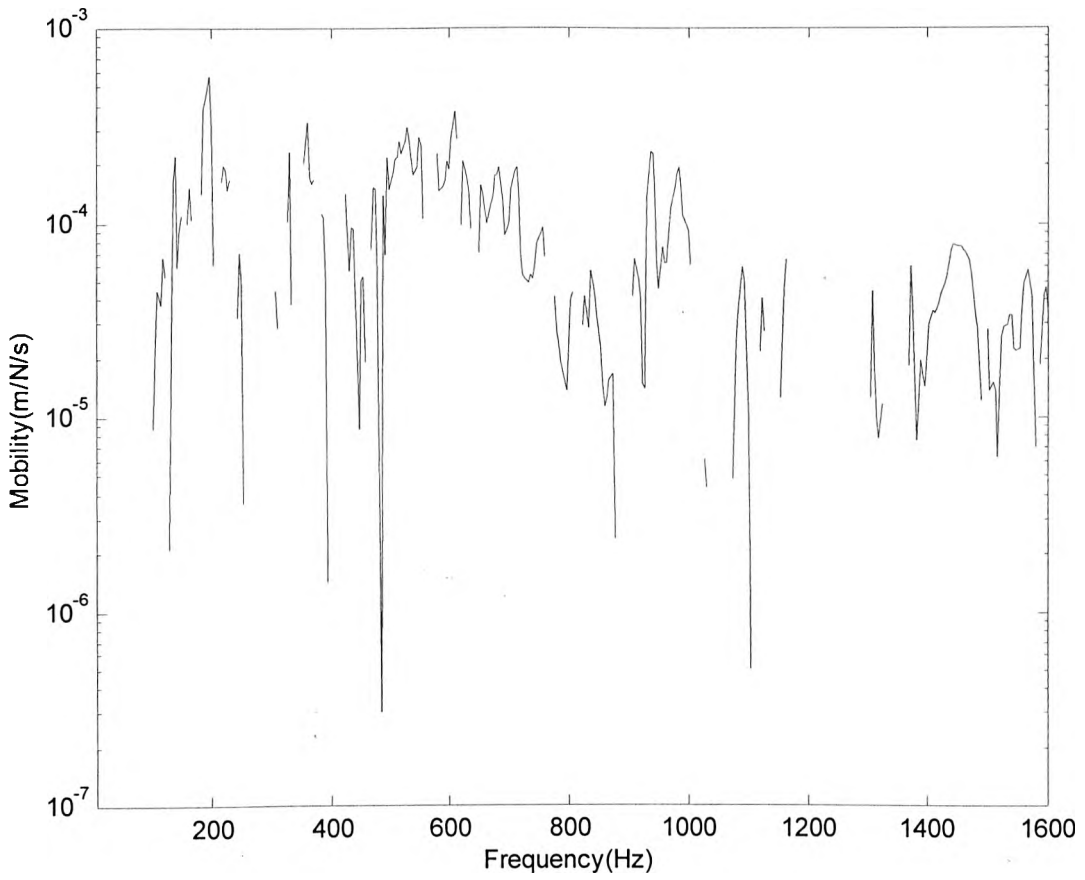
Figure 6-6 Minimum eigenvalue of real part mobility for fanA
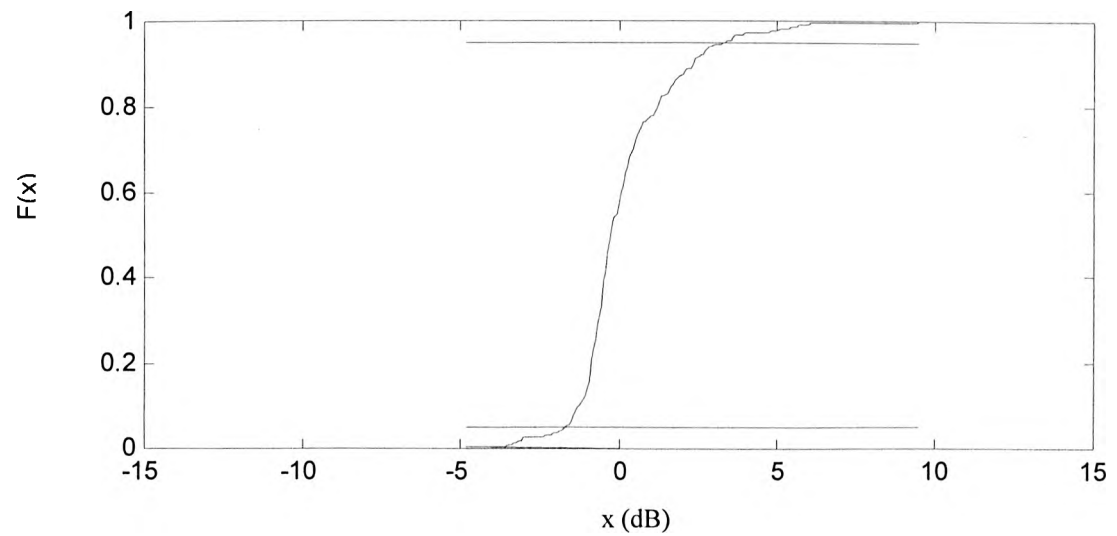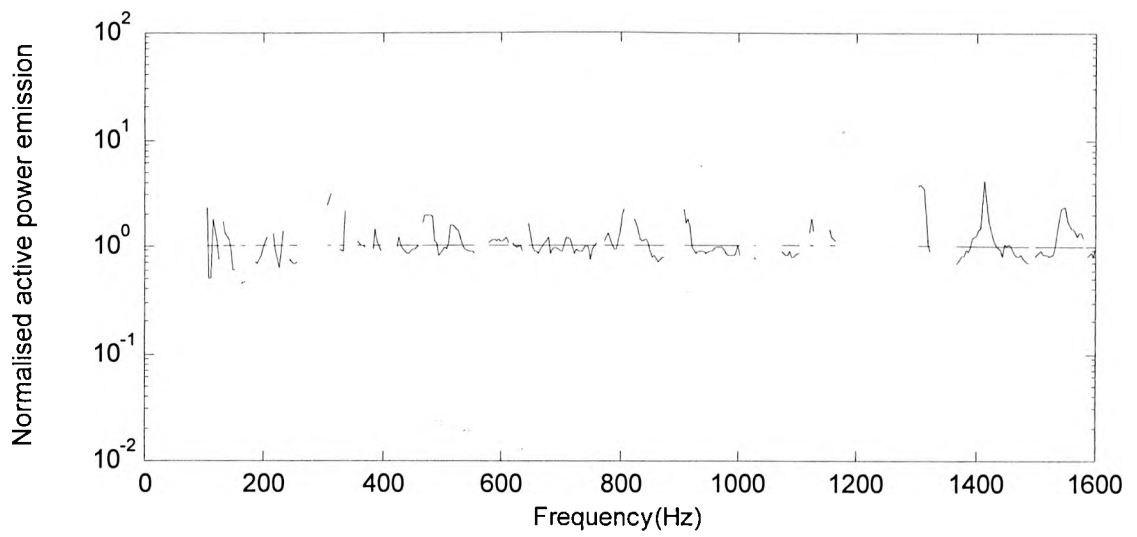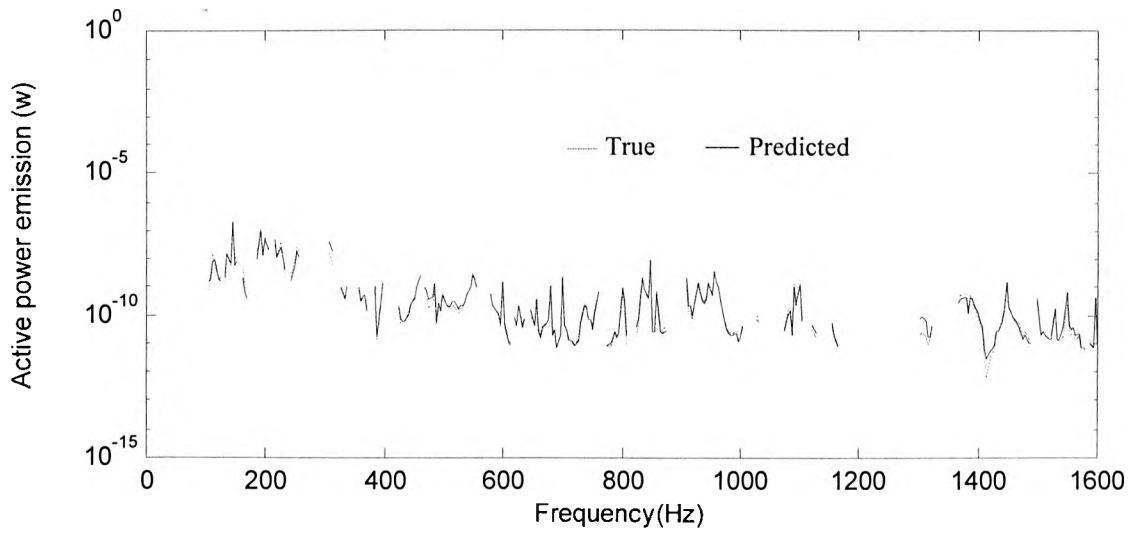
Figure 6-7a,b,c. Prediction by using CF for fan attached on lower mobility infinite plate
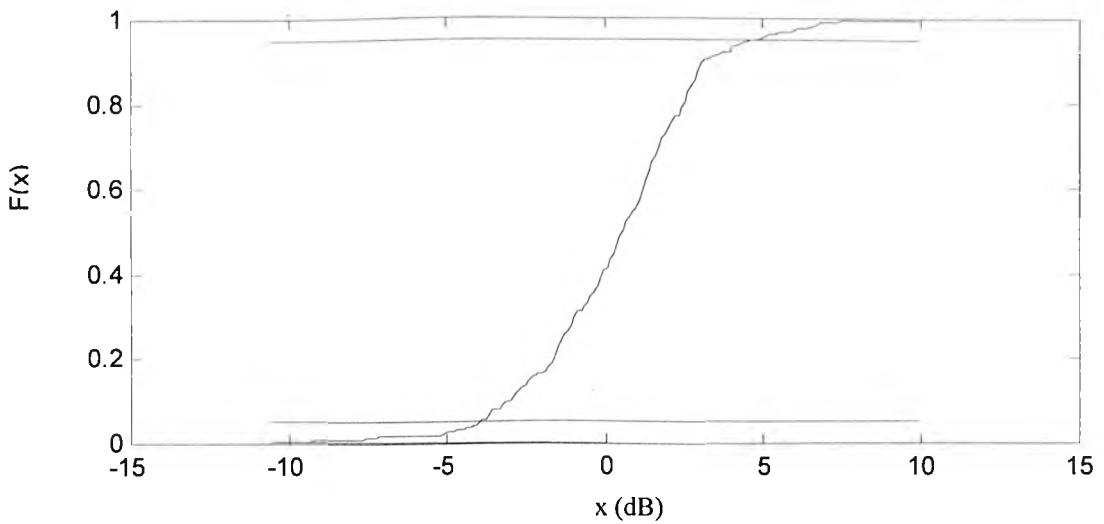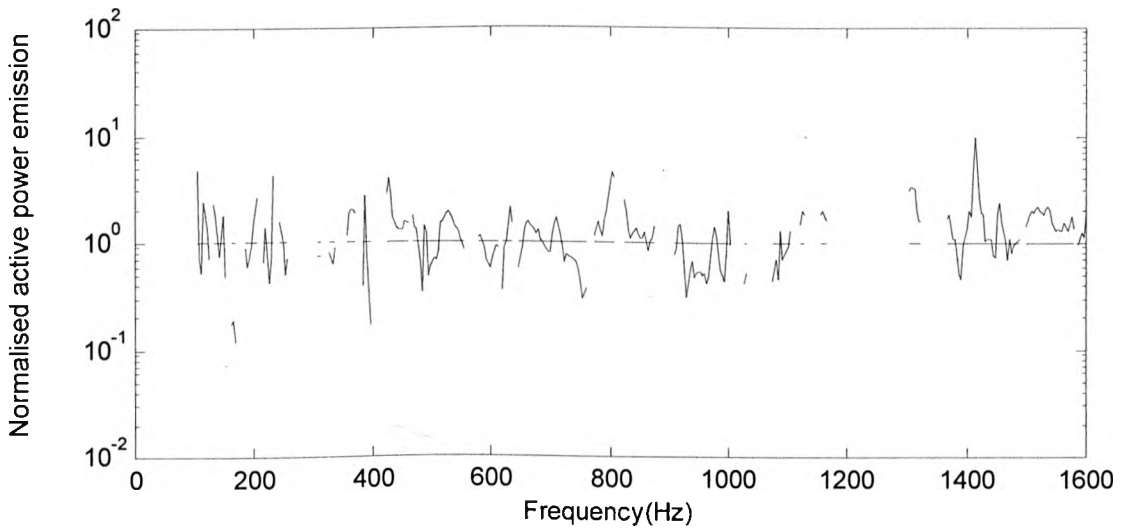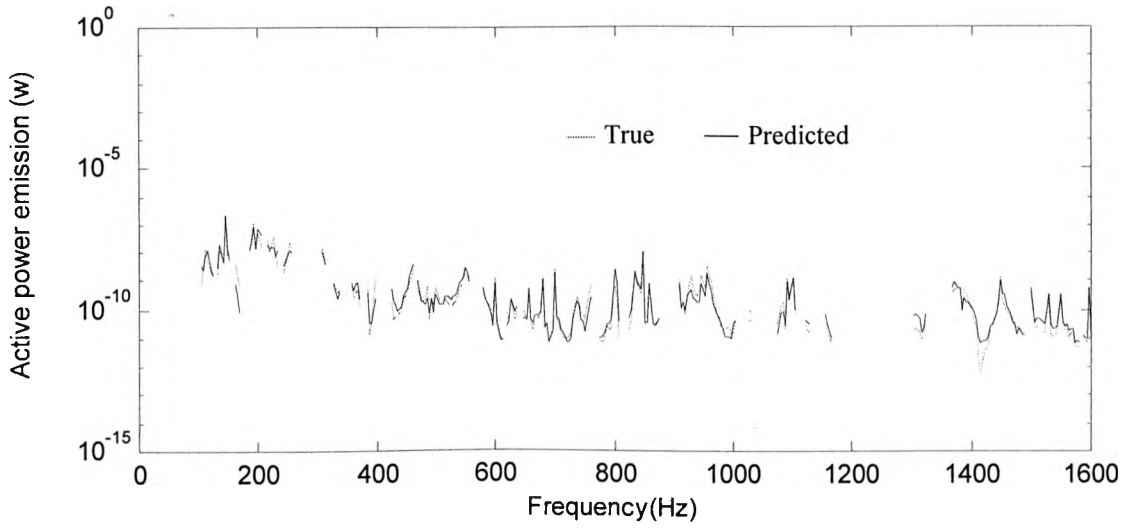
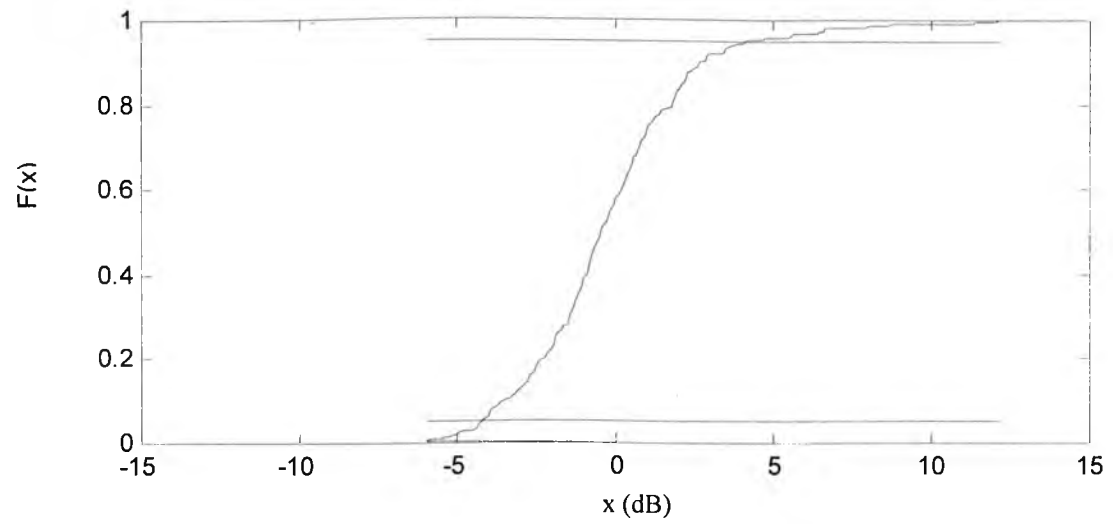**Figure 6-8a,b,c.** Prediction by using CP1 for fanA attached to a lower mobility infinite plate
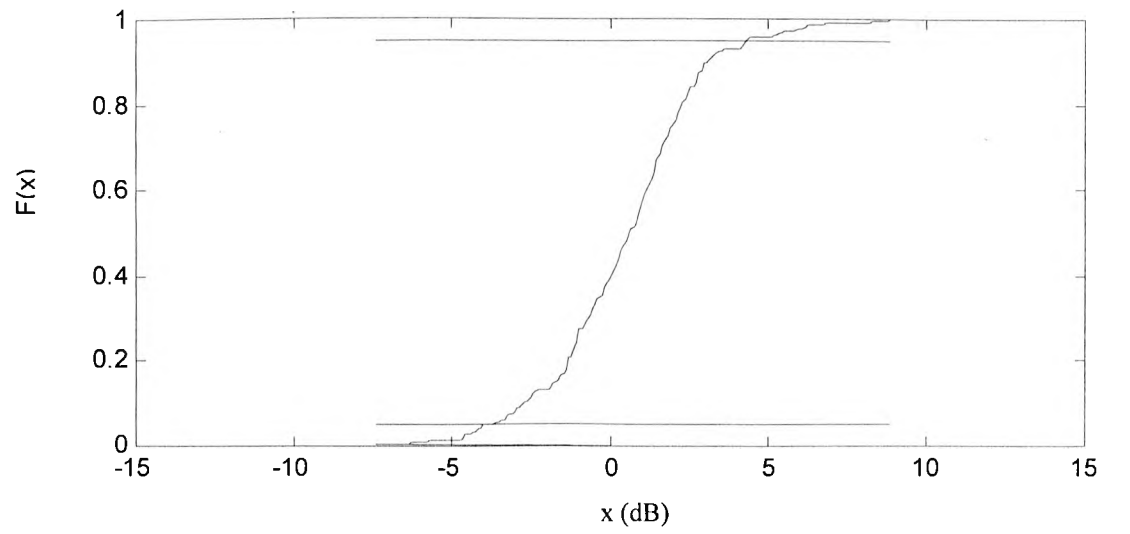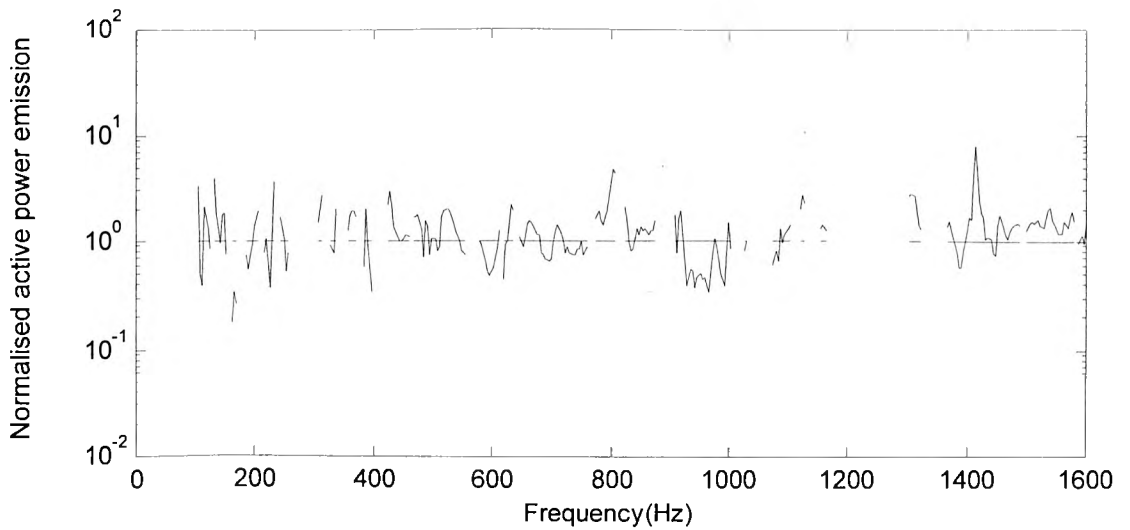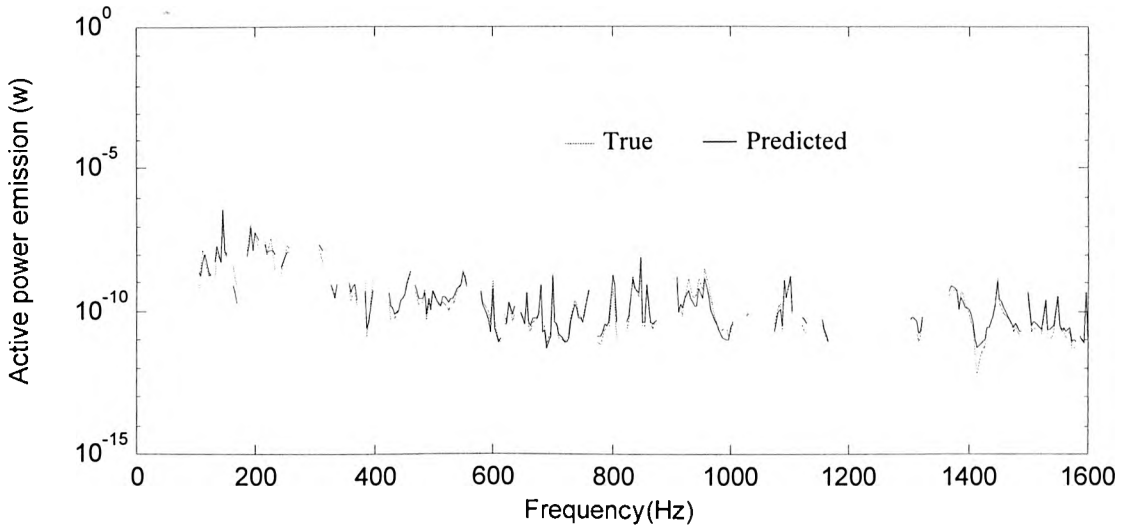
Figure 6-9a,b,c. Prediction by using CP2 for fanA attached to a lower mobility infinite plate
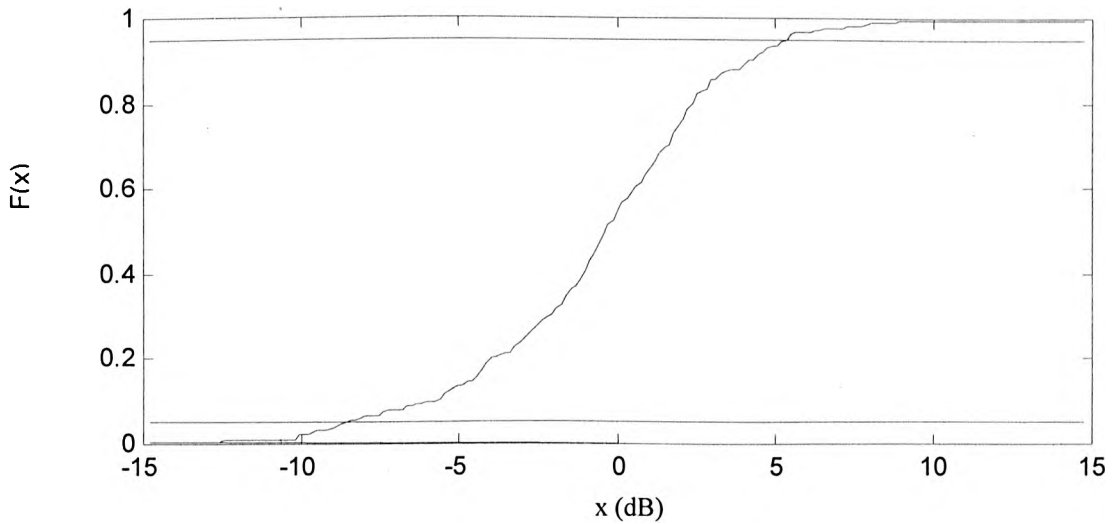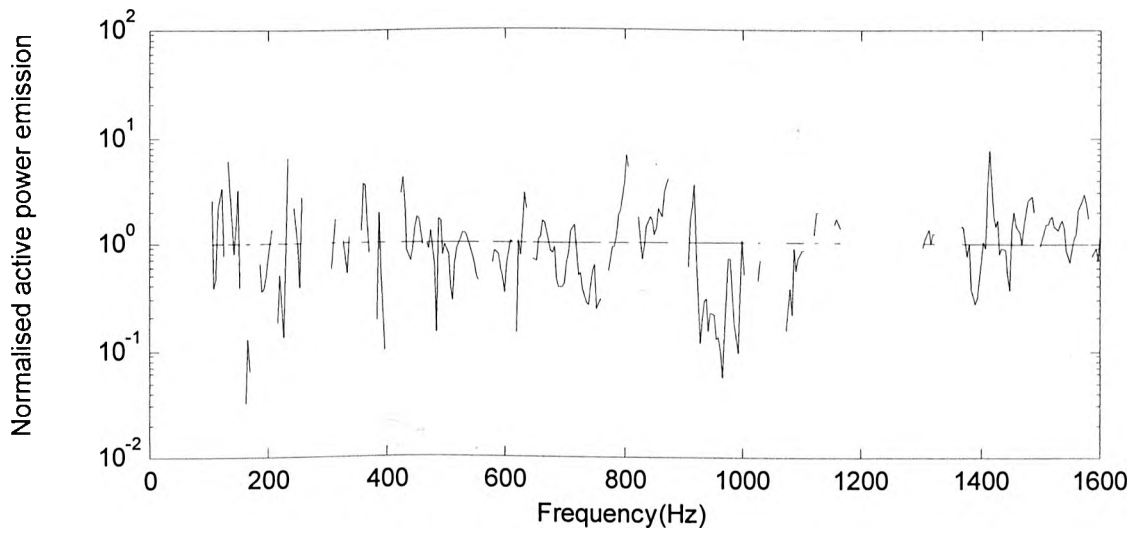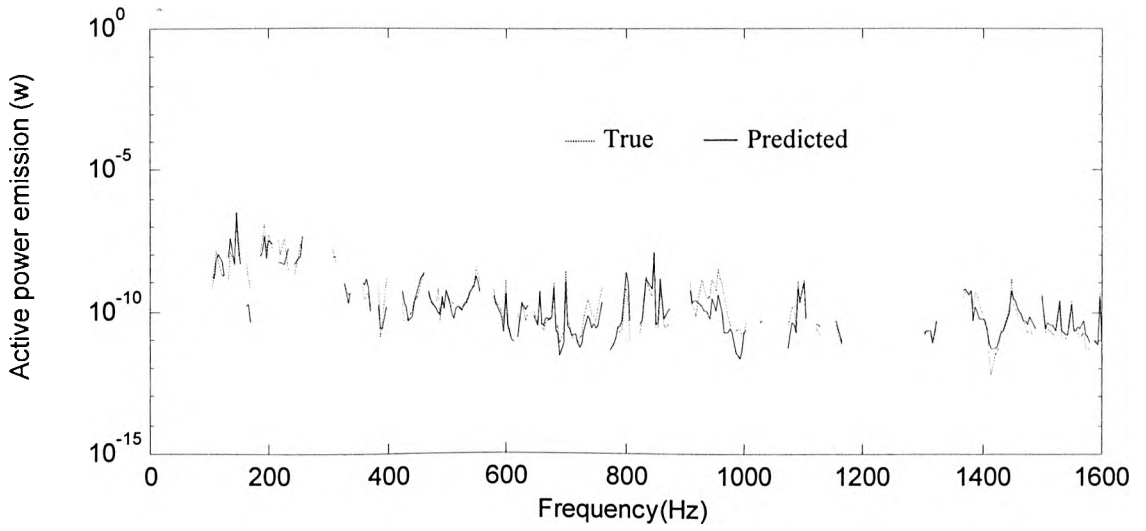
Figure 6-10a,b,c. Prediction by using effective mobility(only point mobility assumption) for fanA attached to a lower mobility infinite plate
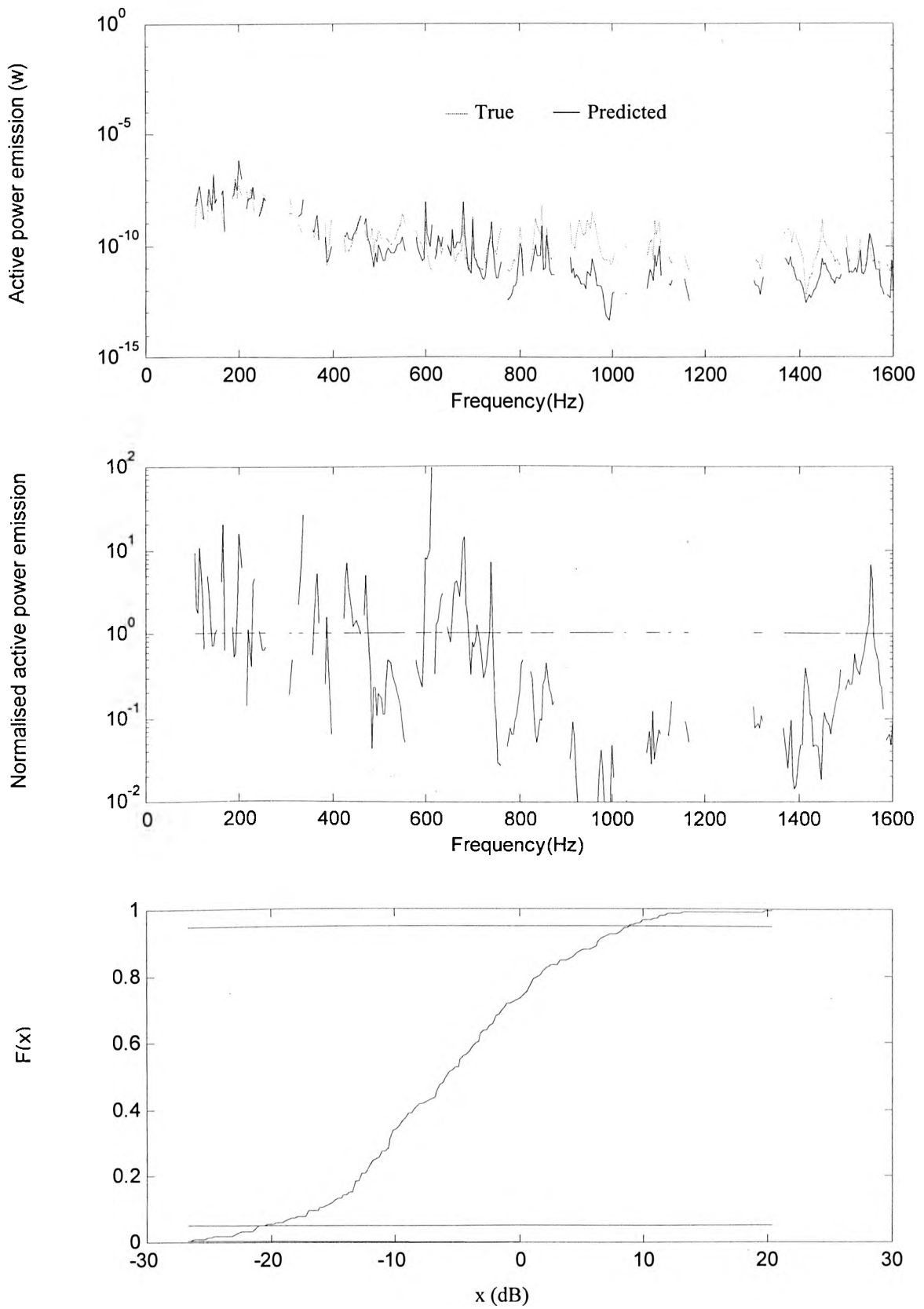
Figure 6-11a,b,c. Prediction by using effective mobility(unit magnitude, zero phase force ratios) for fanA attached to a lower mobility infinite plate
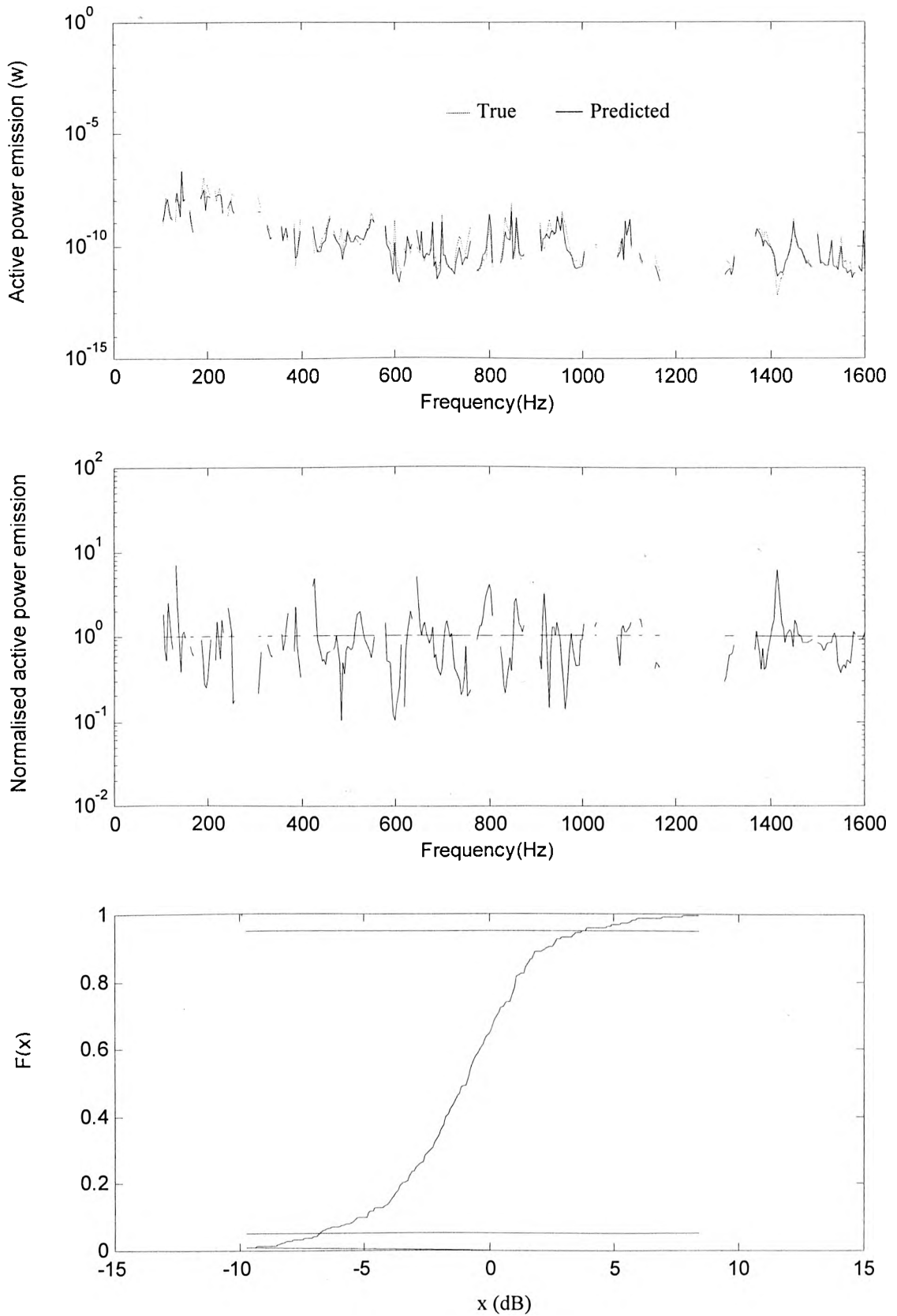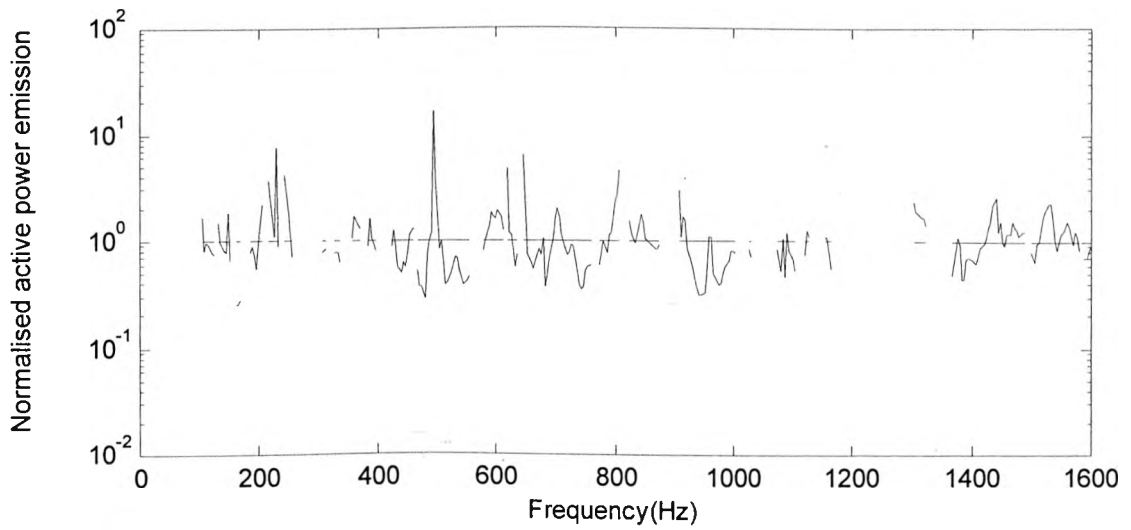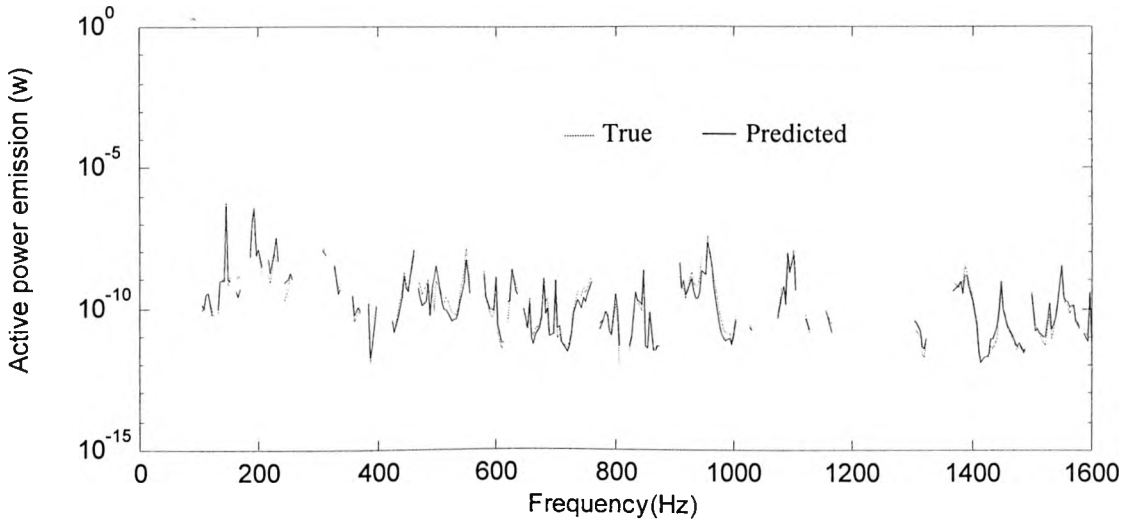
Figure 6-12a,b,c. Prediction by using poles for fanA attached to a lower mobility infinite plate
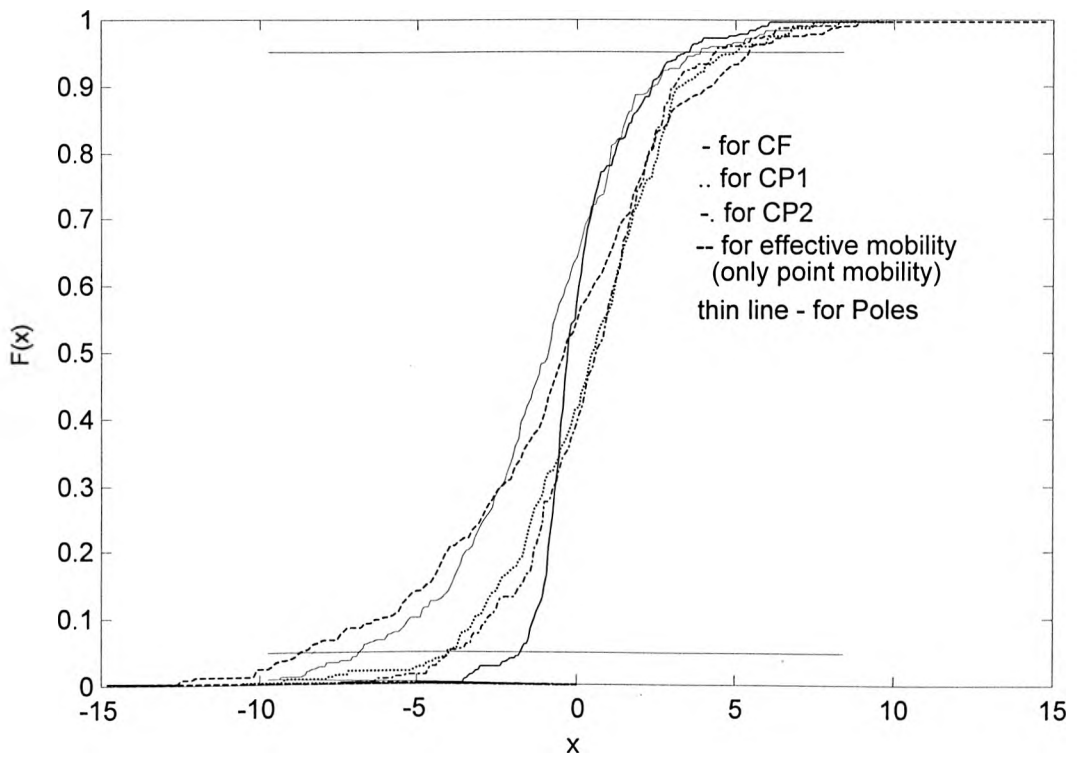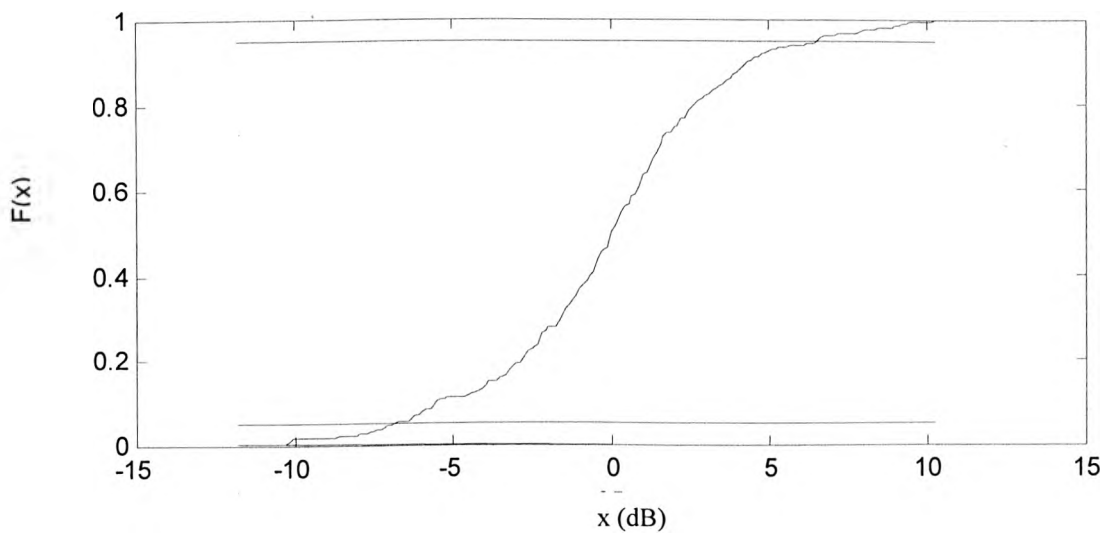
Figure 6-13a Comparison of cumulative distribution function (case1)
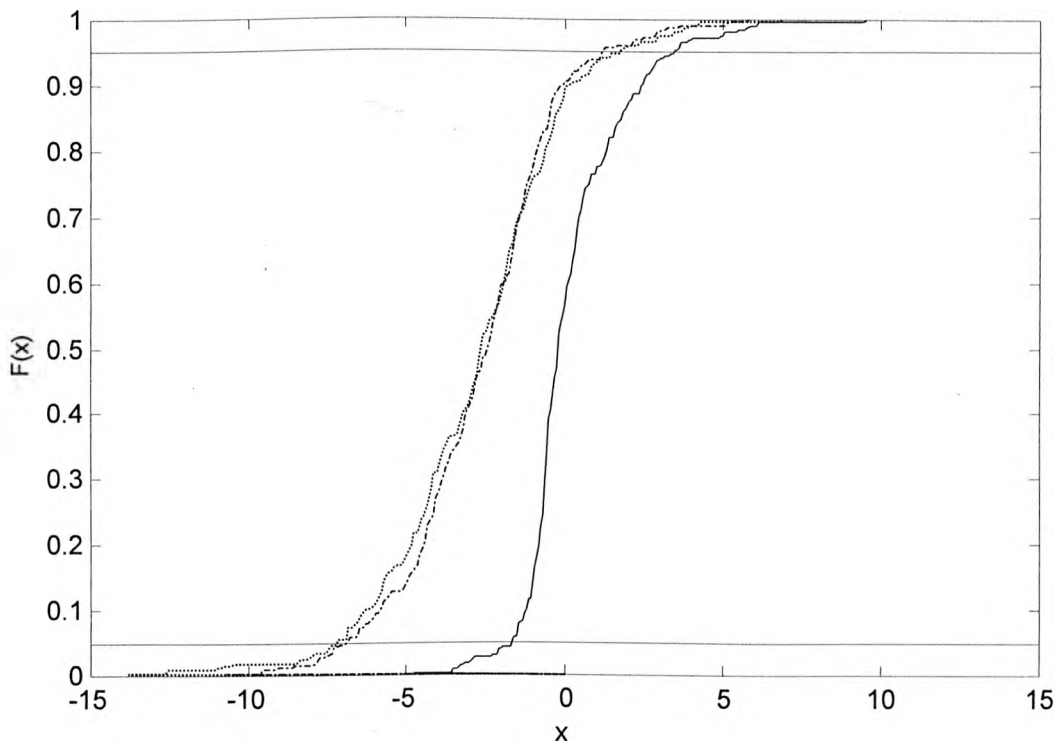
Figure 6-13b The effect of adjustment factor
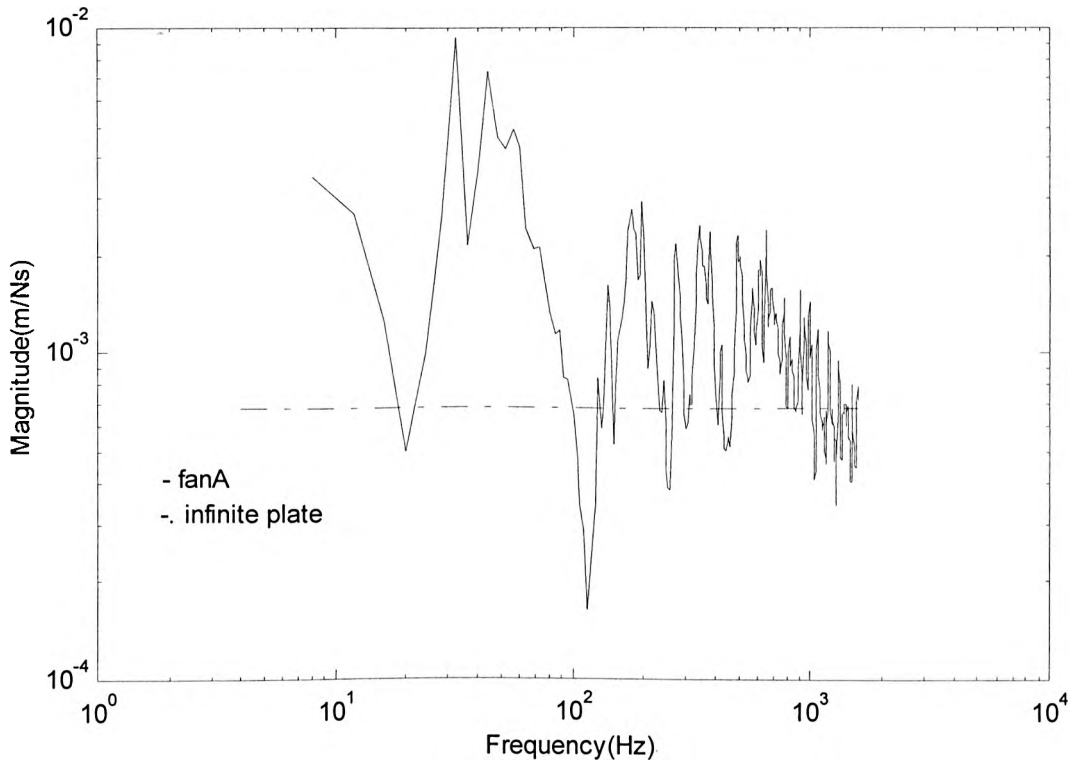
Figure 6-14a A sum of point mobility magnitude for fanA and matched mobility infinite
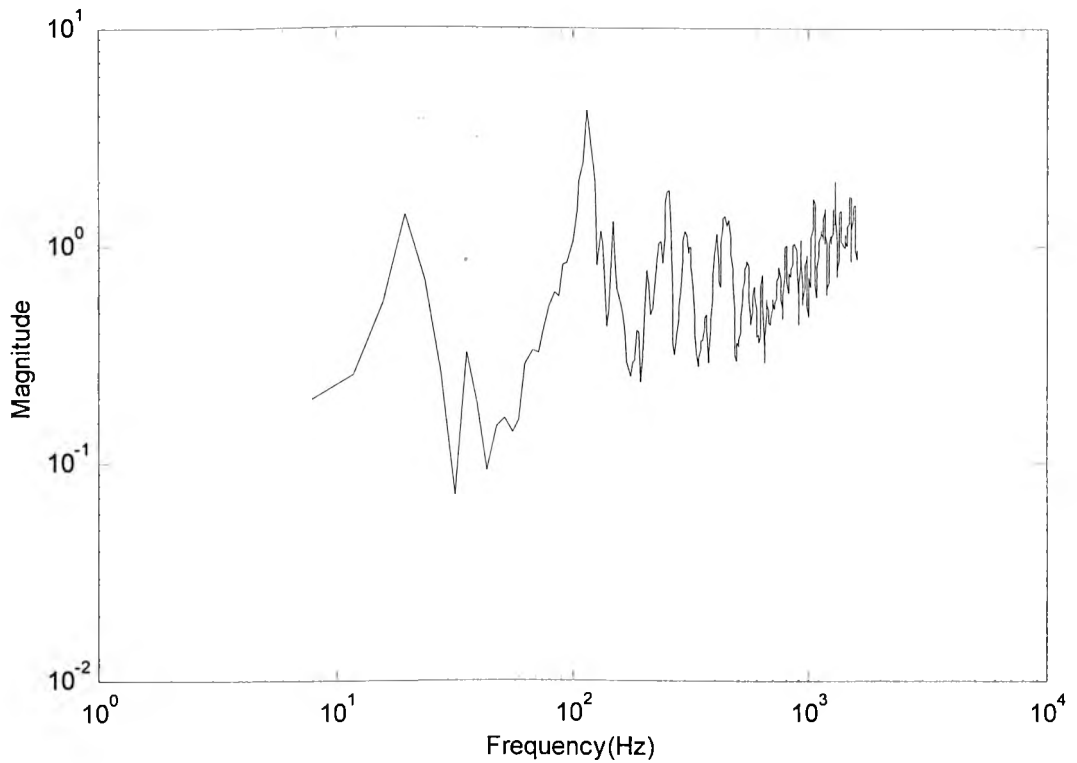
Figure 6-14b A average point mobility magnitude ratio of matched mobility infinite plate to fanA
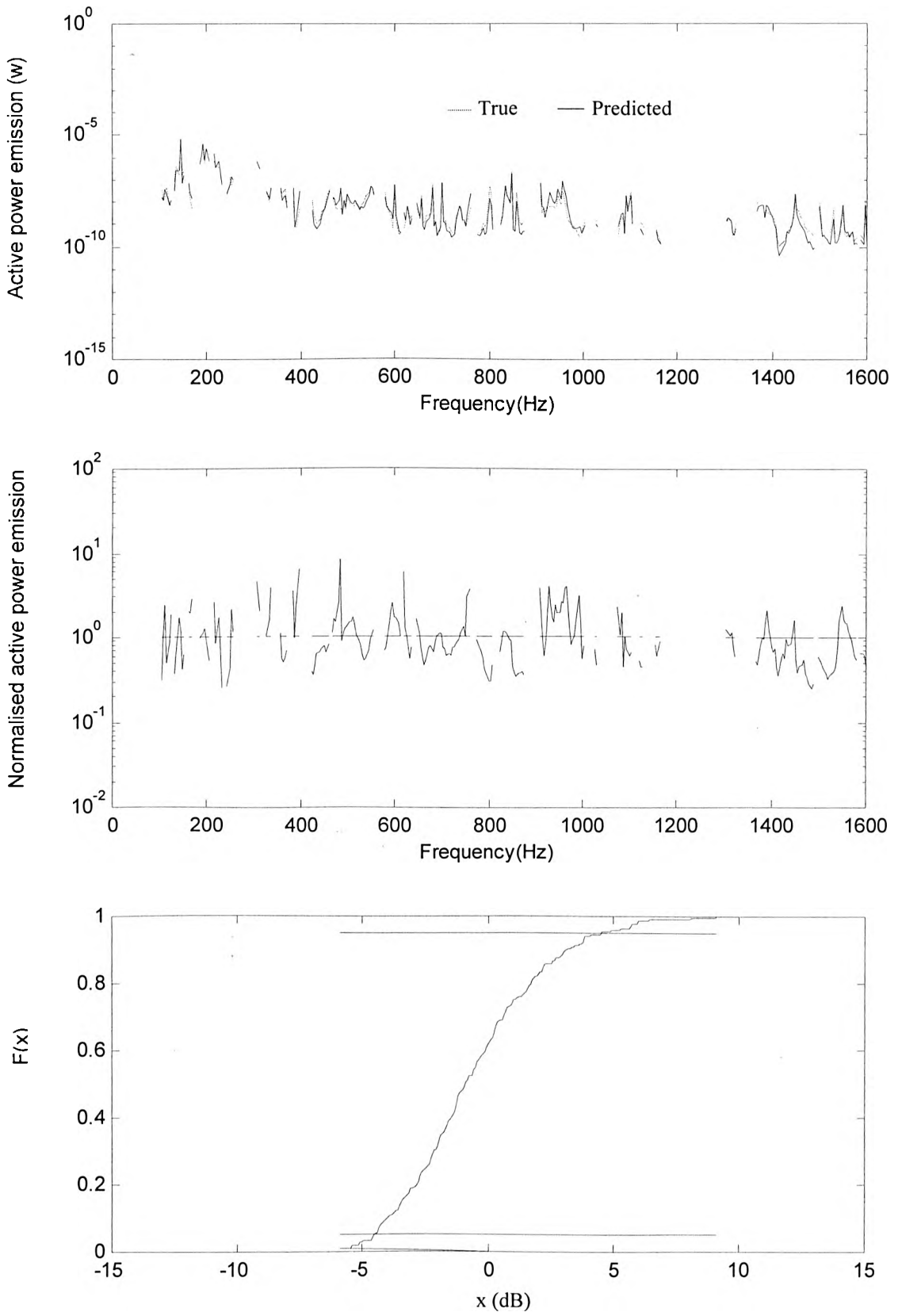
Figure 6-15a,b,c. Prediction by using CF for fanA attached to a matched mobility infinite plate
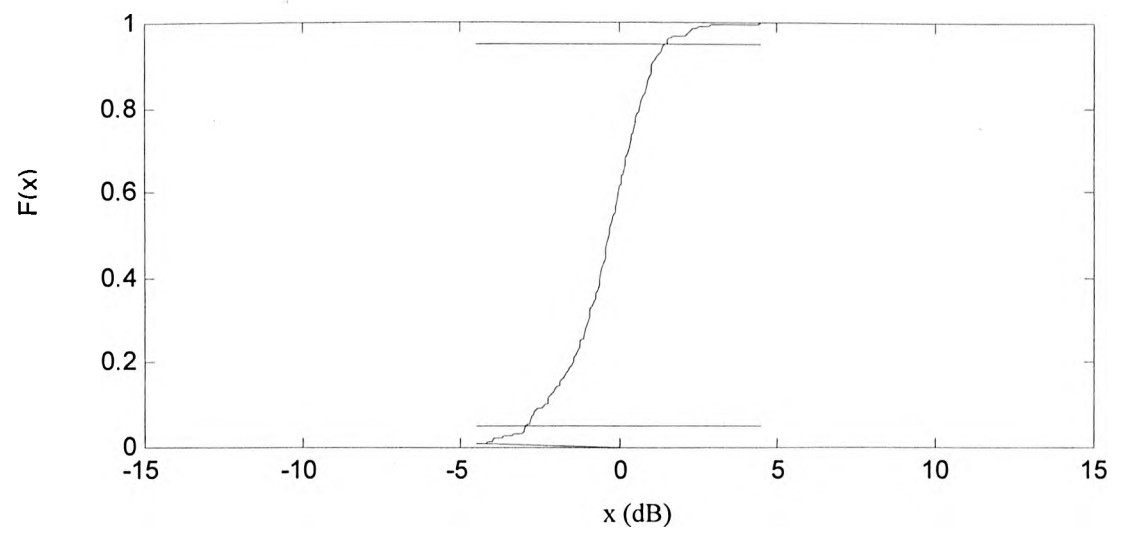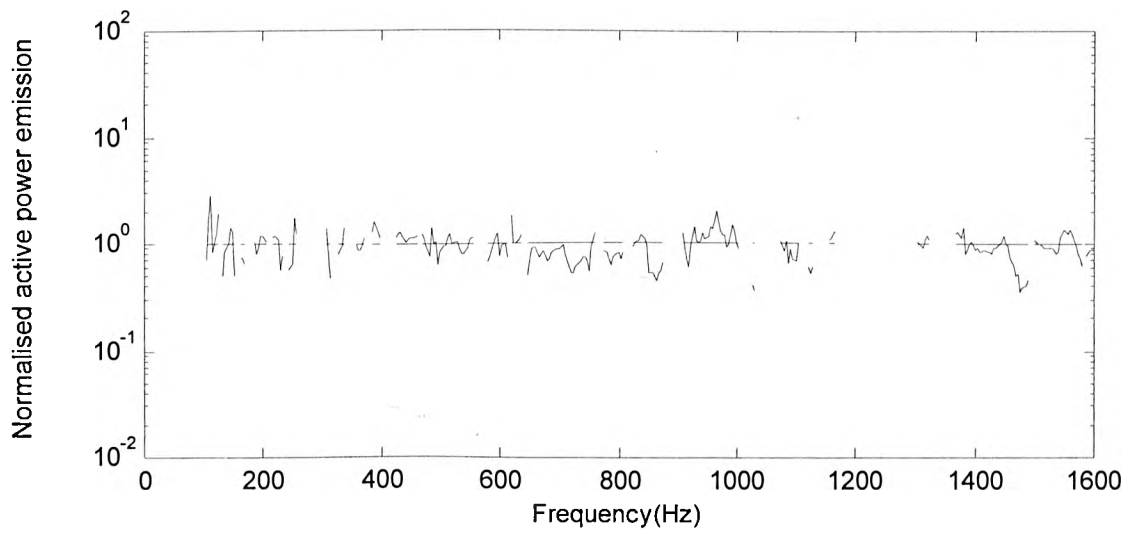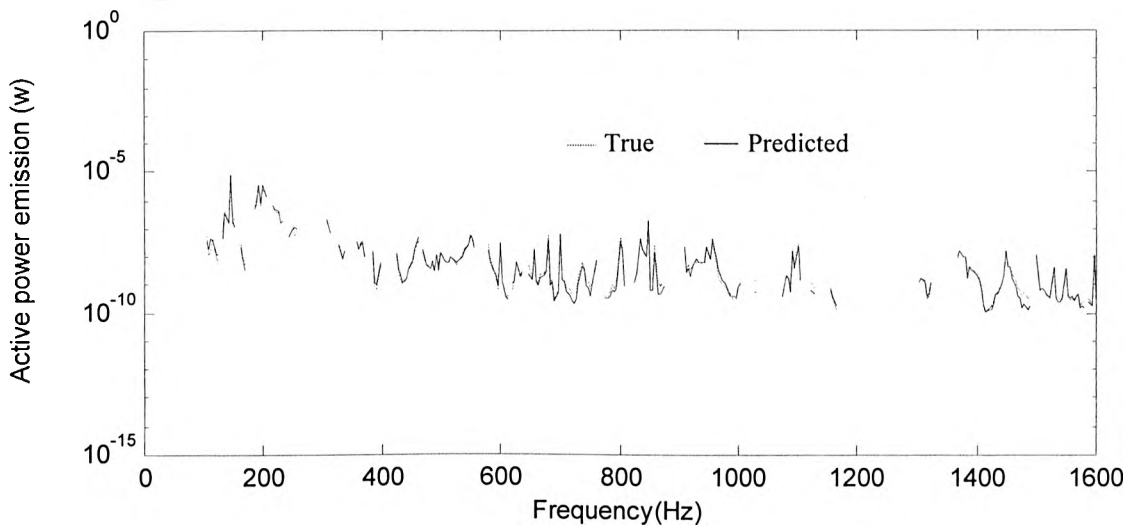
Figure 6-16a,b,c. Prediction by using CP1 for fanA attached to a matched mobility infinite plate
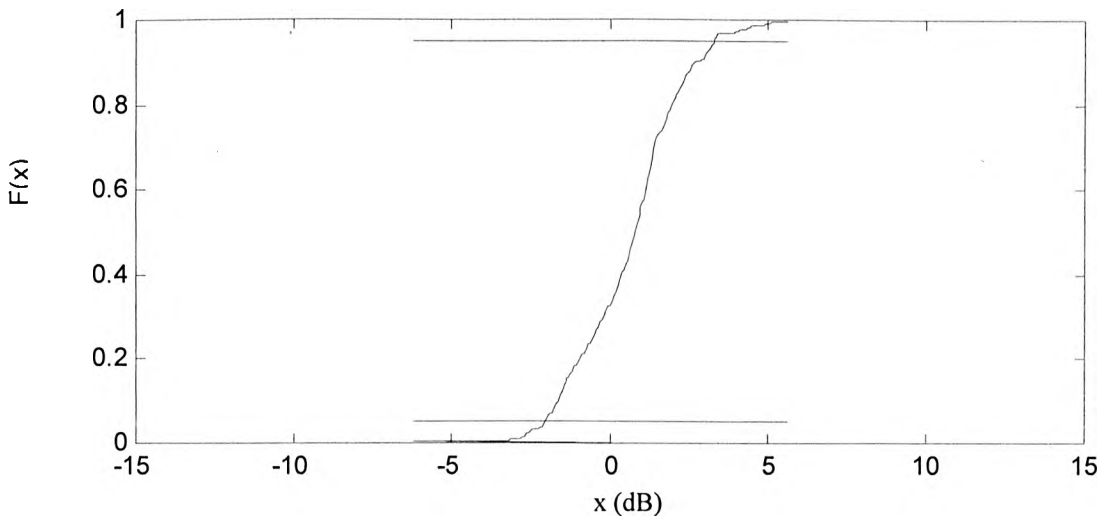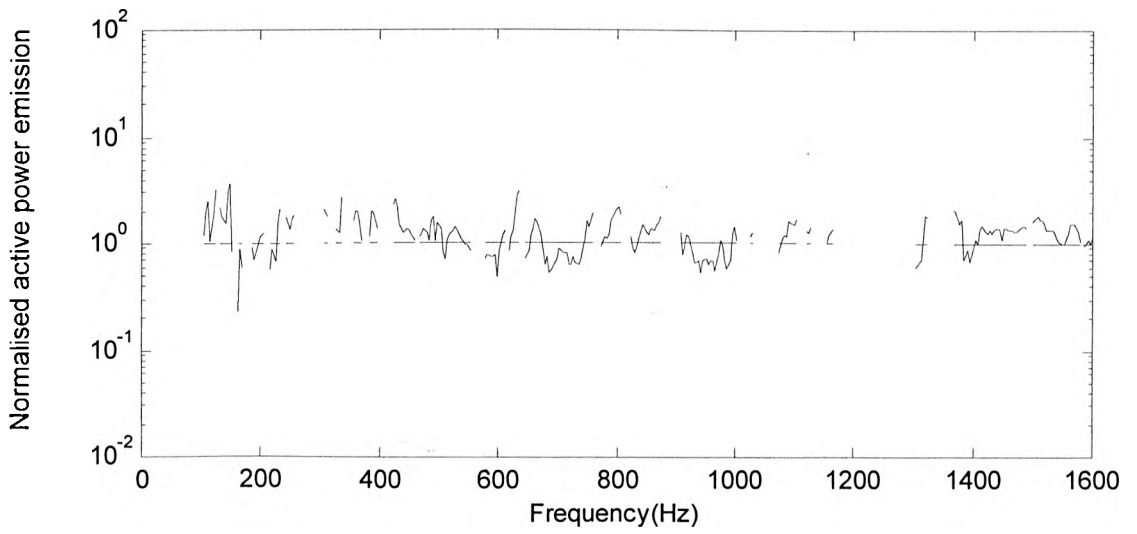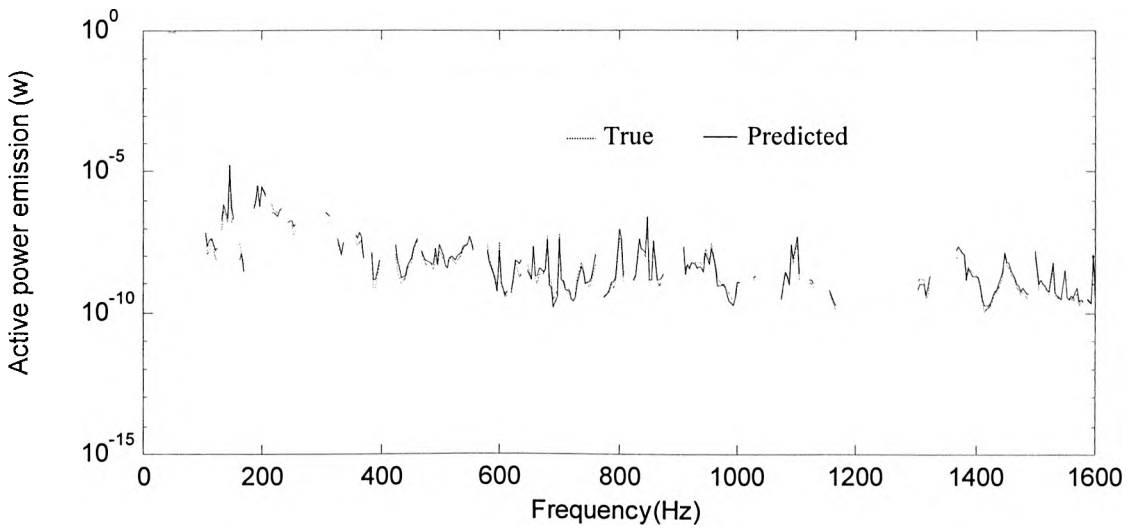
Figure 6-17a,b,c. Prediction by using effective mobility(only point mobility assumption) for fanA attached to a matched mobility infinite plate
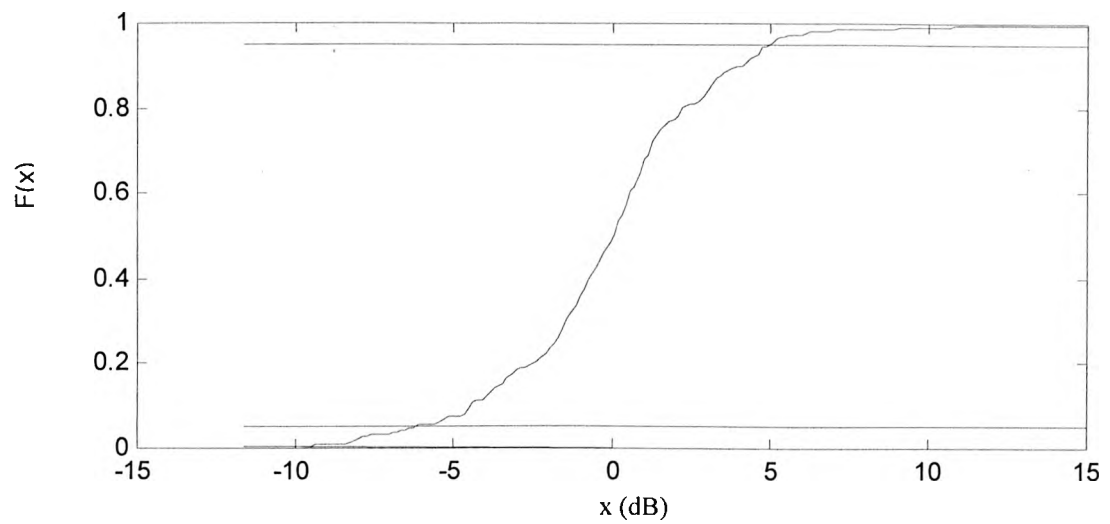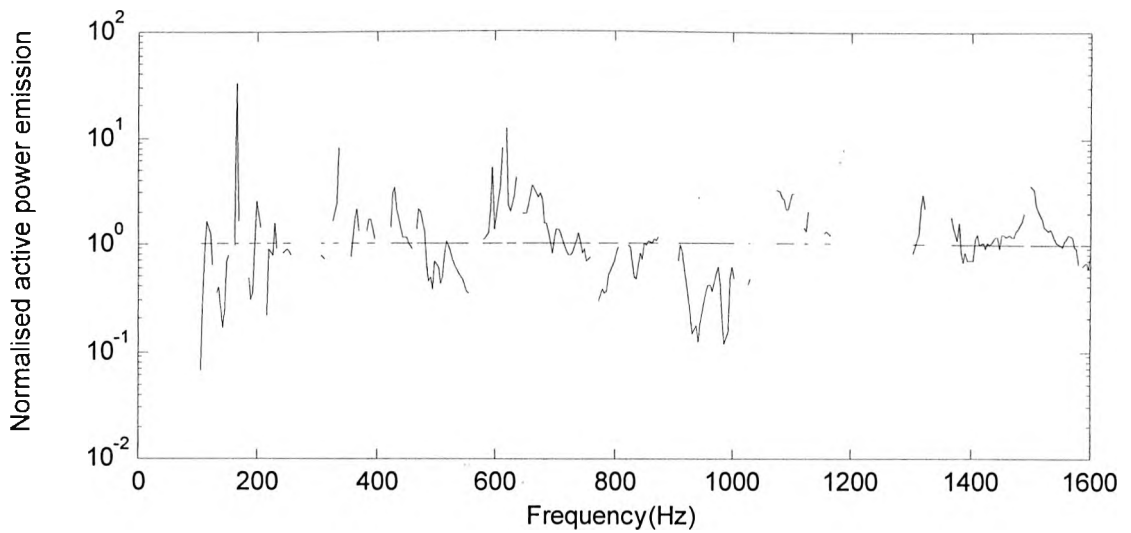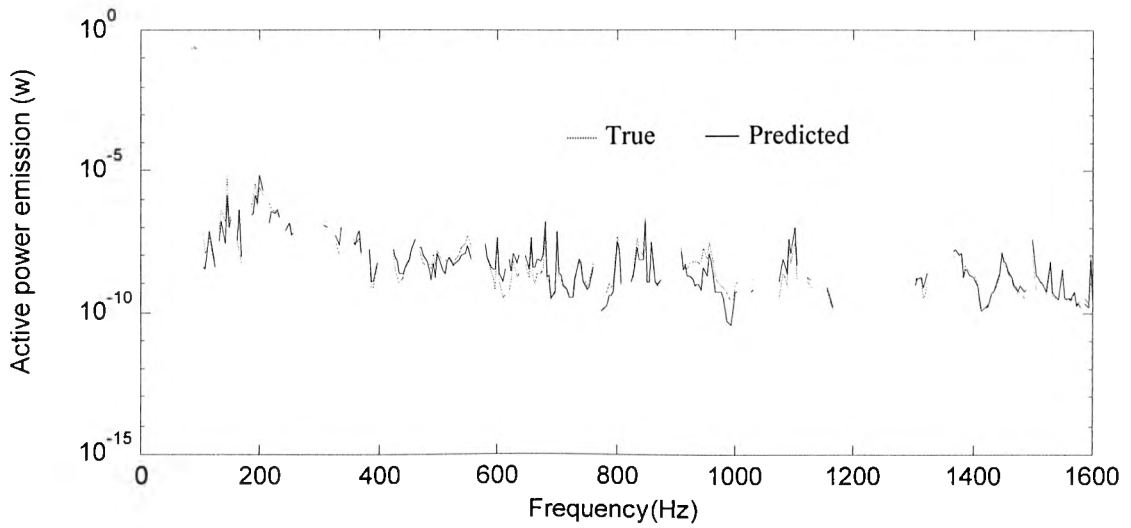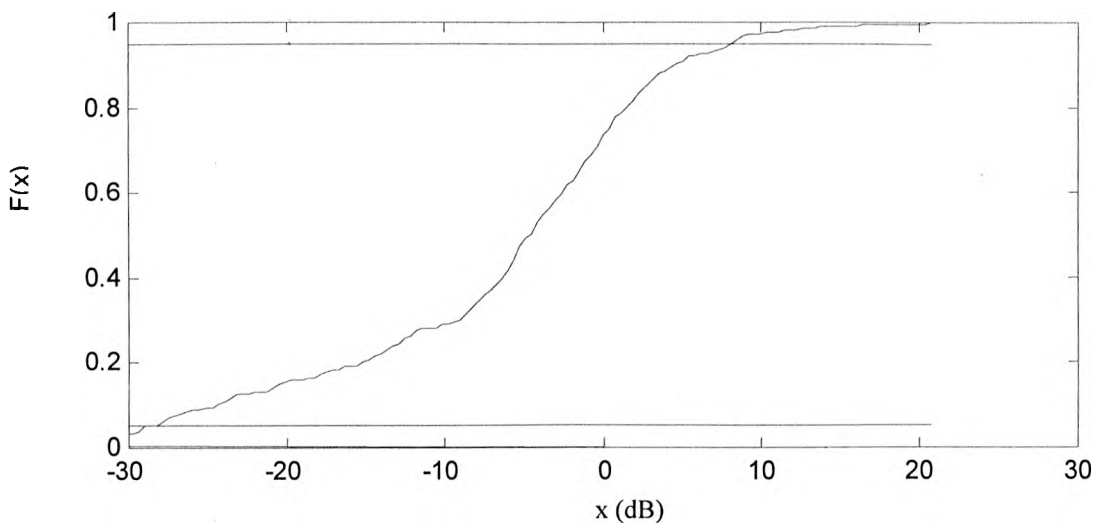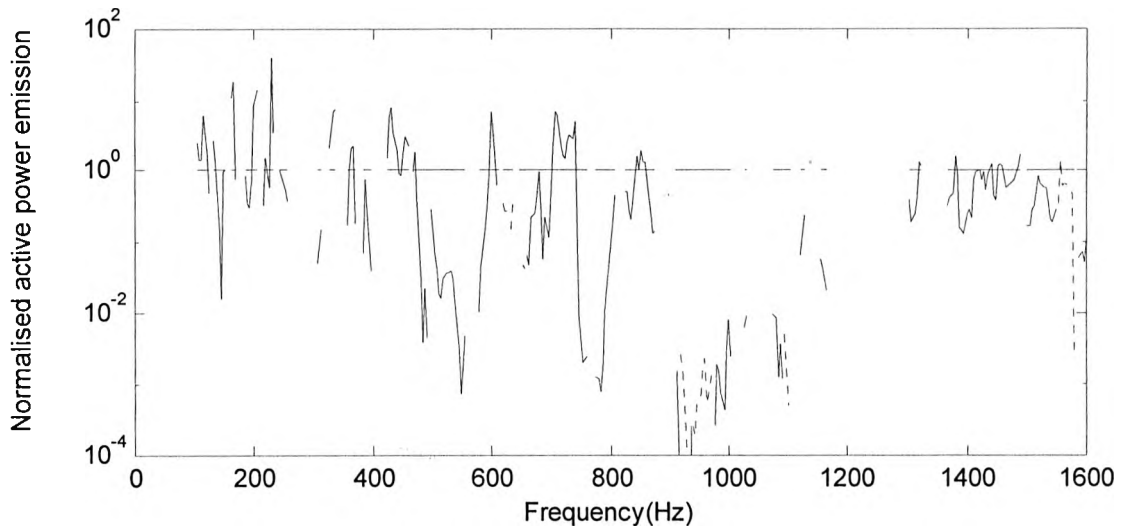
Figure 6-18a,b,c. Prediction by using effective mobility(unit magnitude zero phase force ratios) assumption) for fanA attached to a matched mobility infinite plate
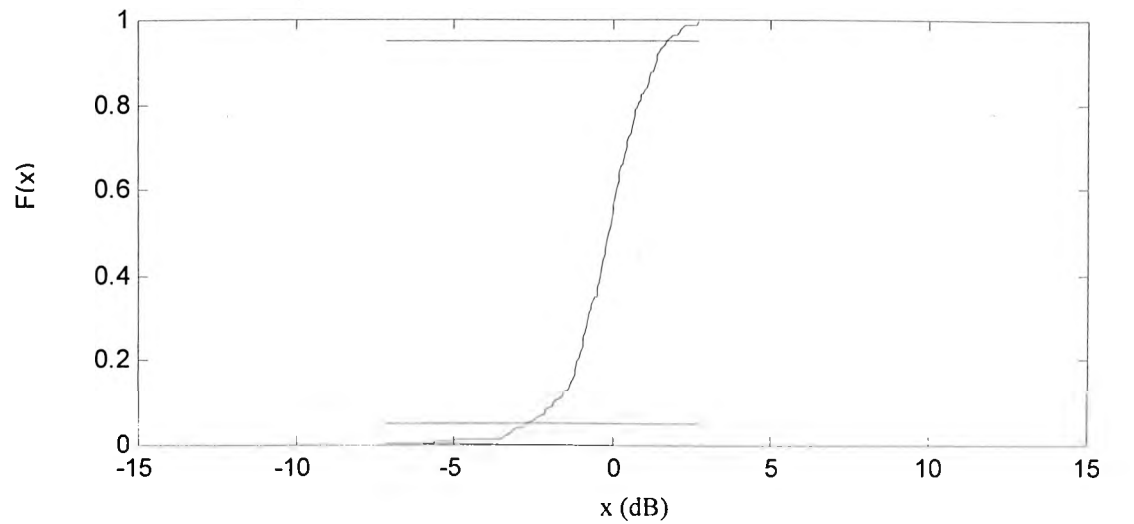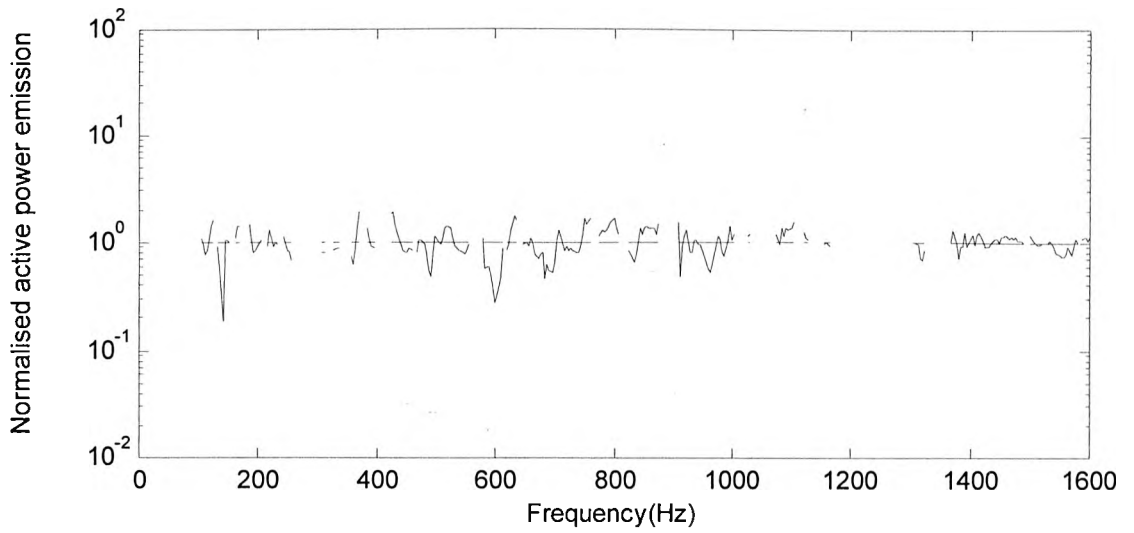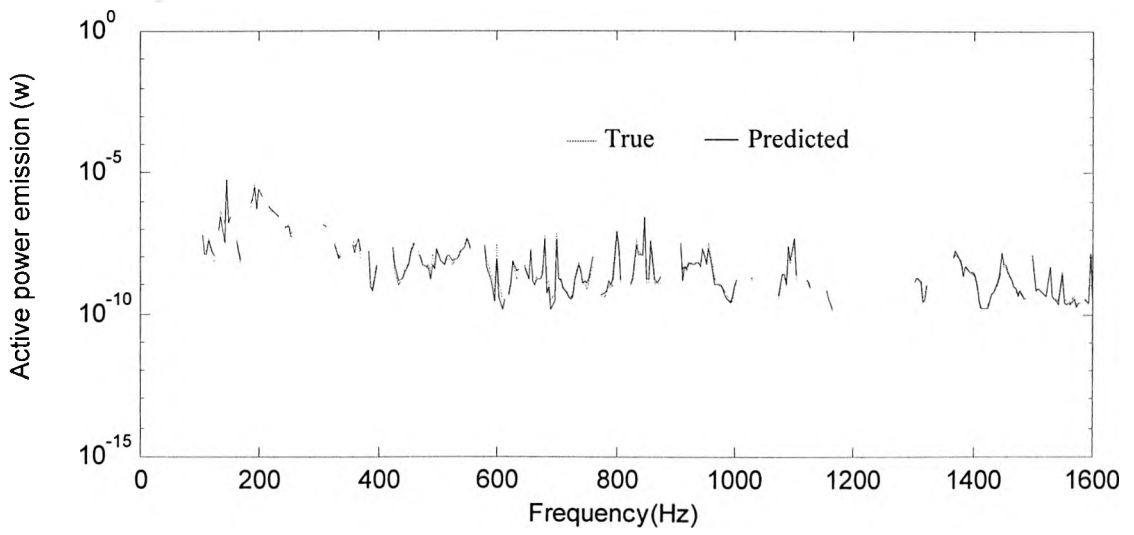
Figure 6-19a,b,c. Prediction by using poles for fanA attached to a matched mobility infinite plate
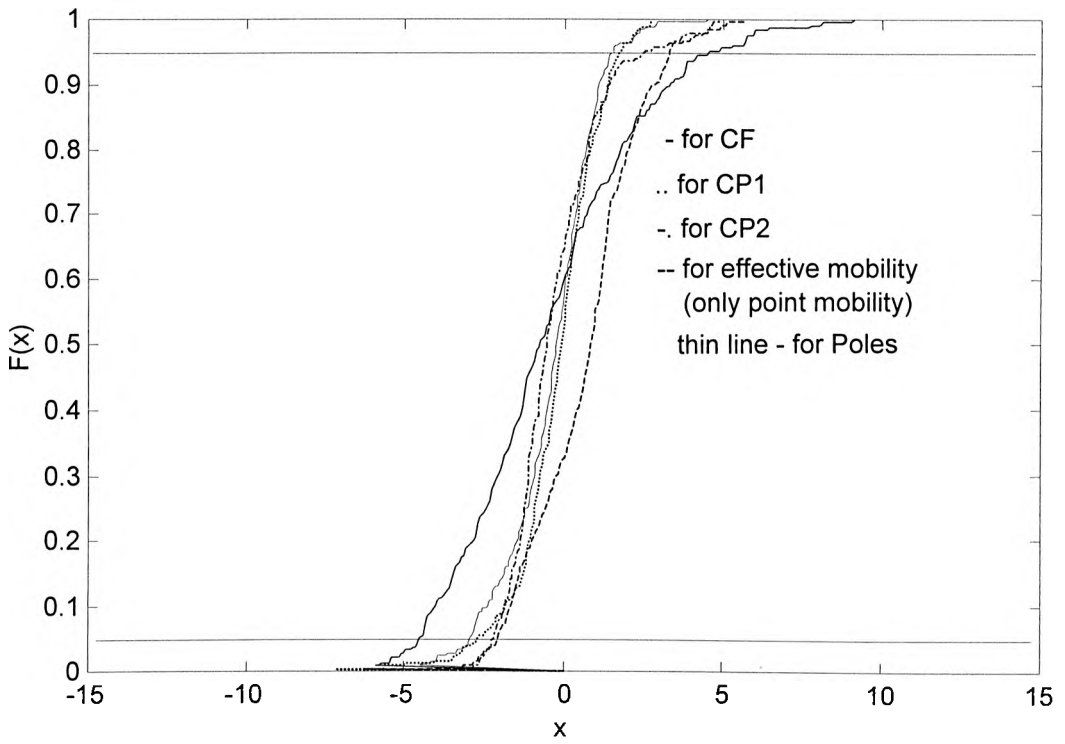
Figure 6-20a Comparison of cumulative distribution function (case2)
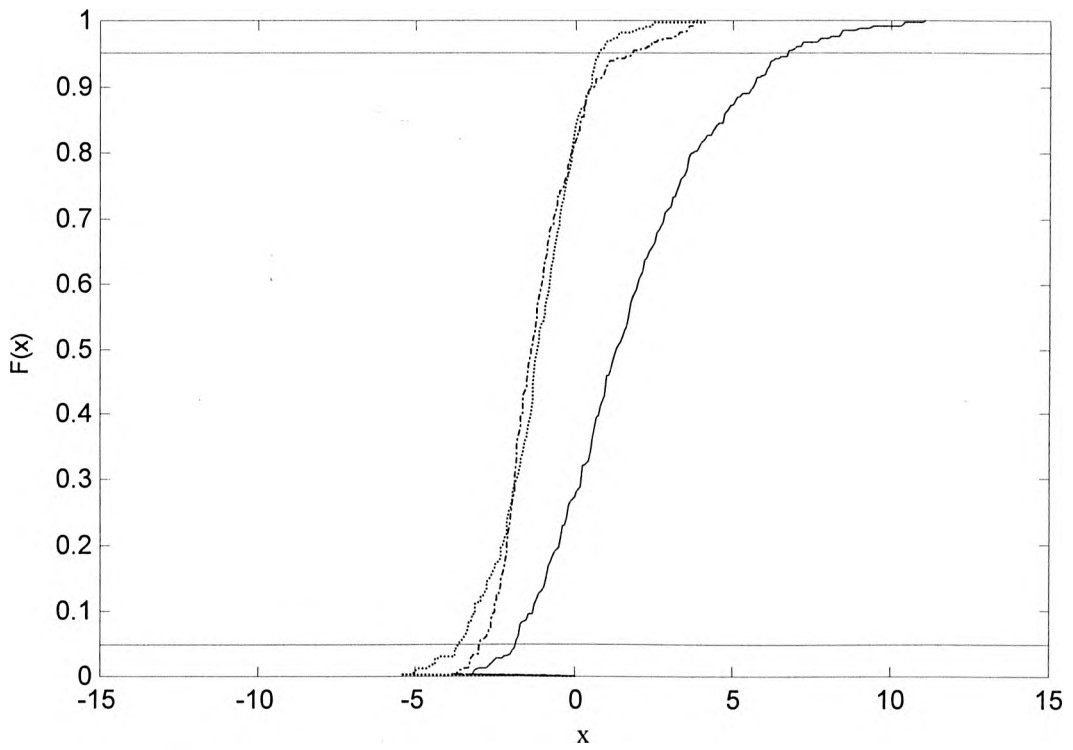
Figure 6-20b The effect of adjustment factor
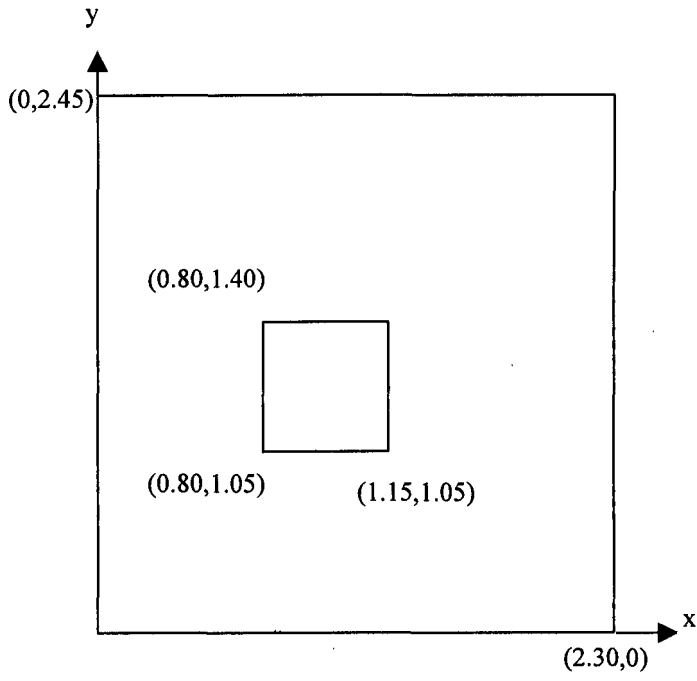
Figure 6-21 FanA on the ssss-plate
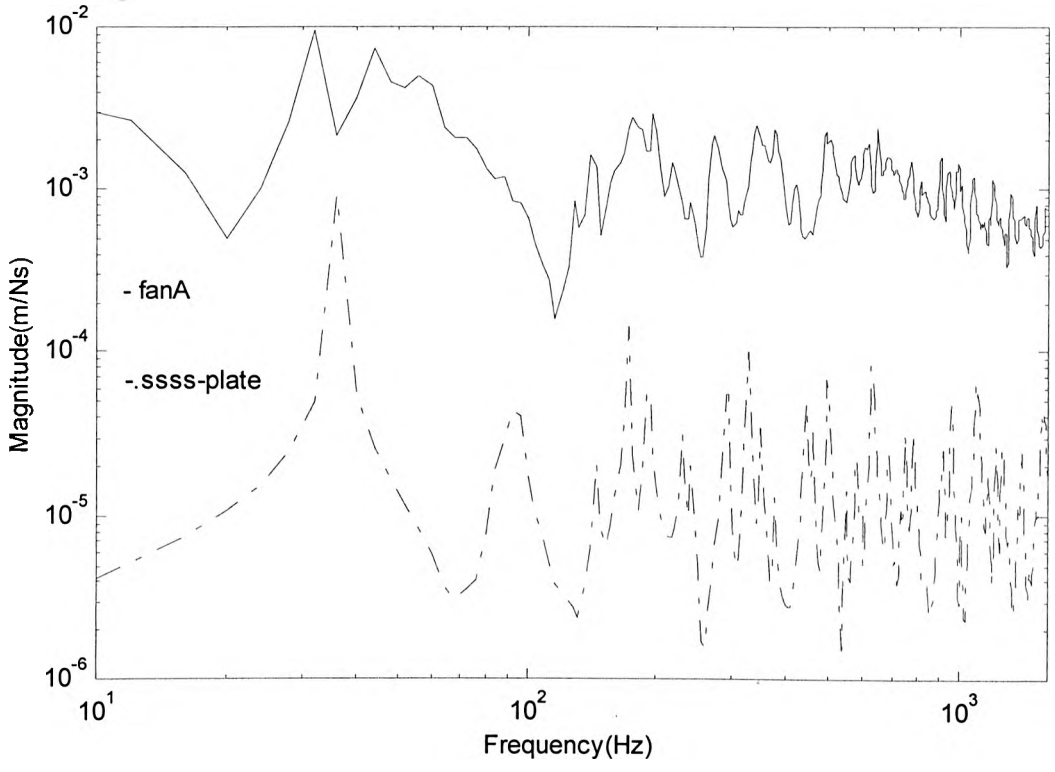
Figure 6-22a A sum of point mobility magnitude for fanA and lower ssss-plate
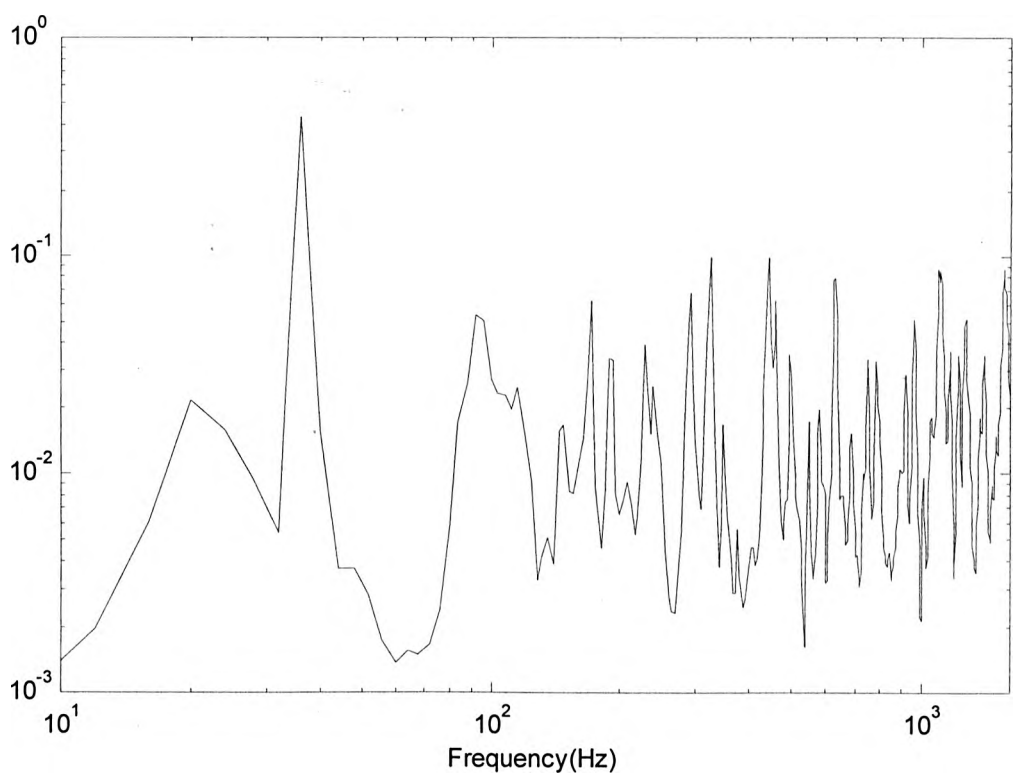
Figure 6-22b A average point mobility magnitude ratio of lower ssss-plate to fanA

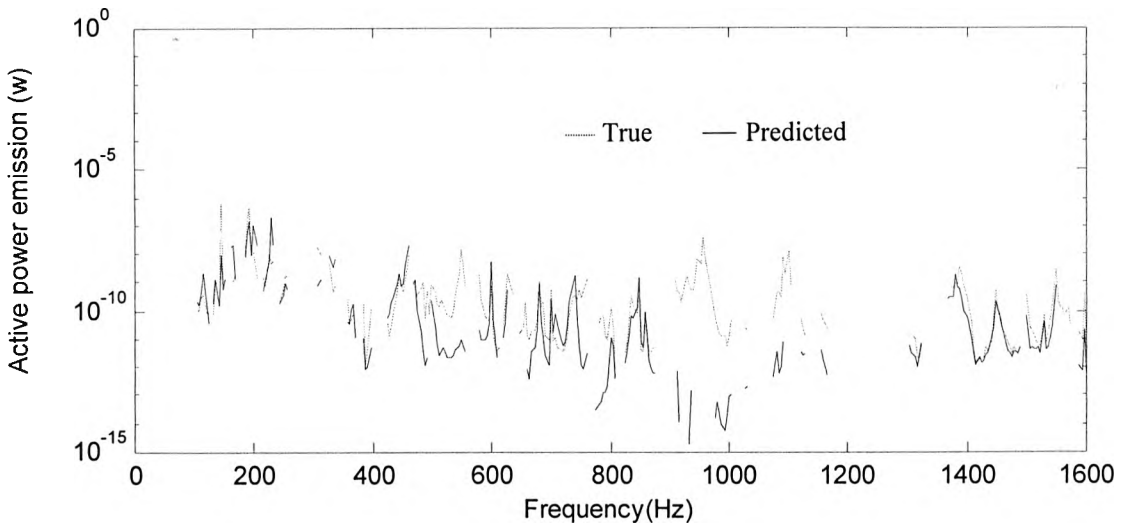**Figure 6-23a,b,c** Prediction by using CF for fanA attached to a lower mobility ssss-plate
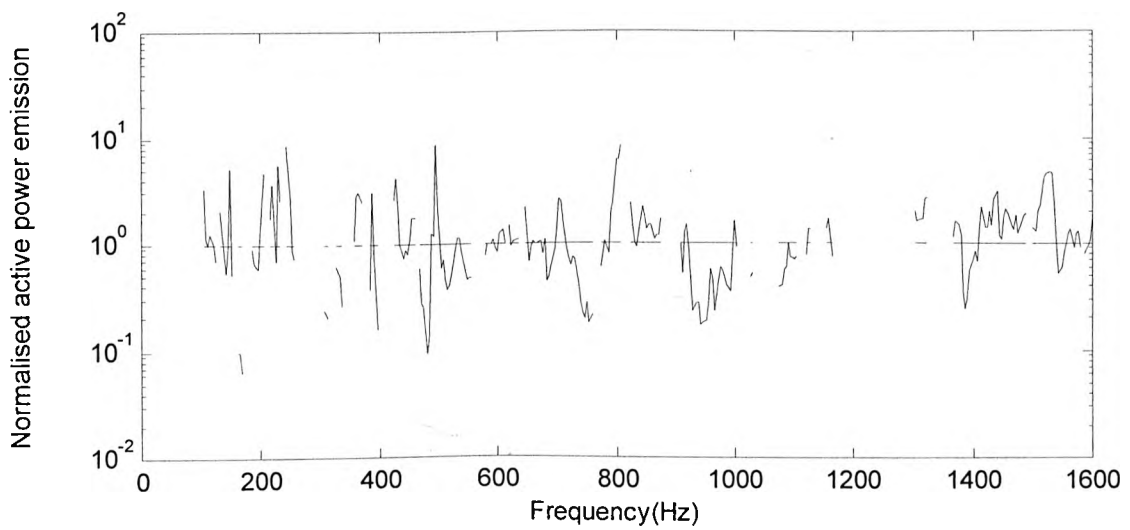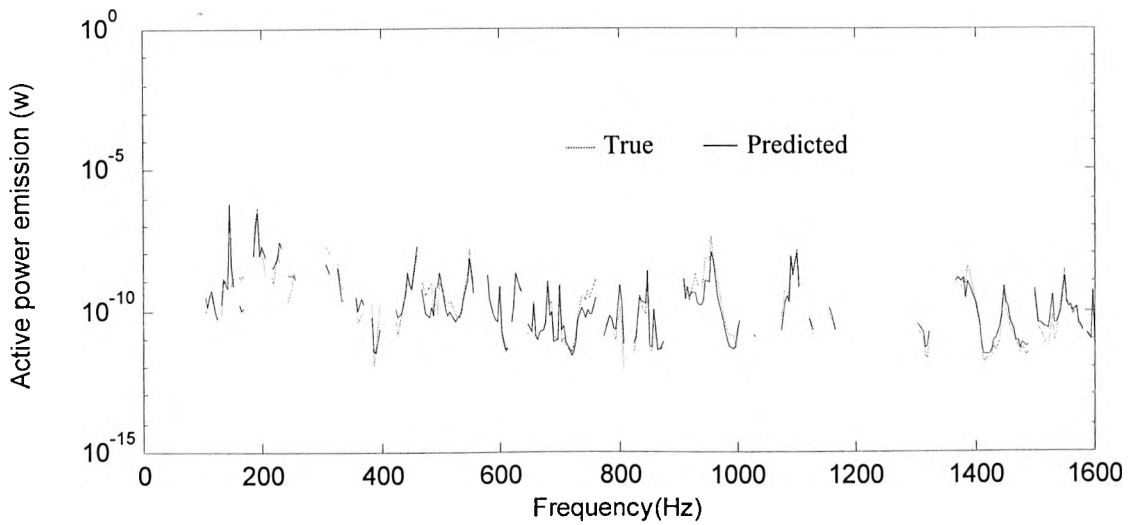
Figure 6-24a,b,c. Prediction by using CP1 for fanA attached to a lower mobility ssss- plate

Figure 6-25a,b,c. Prediction by using effective mobility(unit magnitude, zero phase force ratios) for fanA attached to a lower mobility ssss- plate
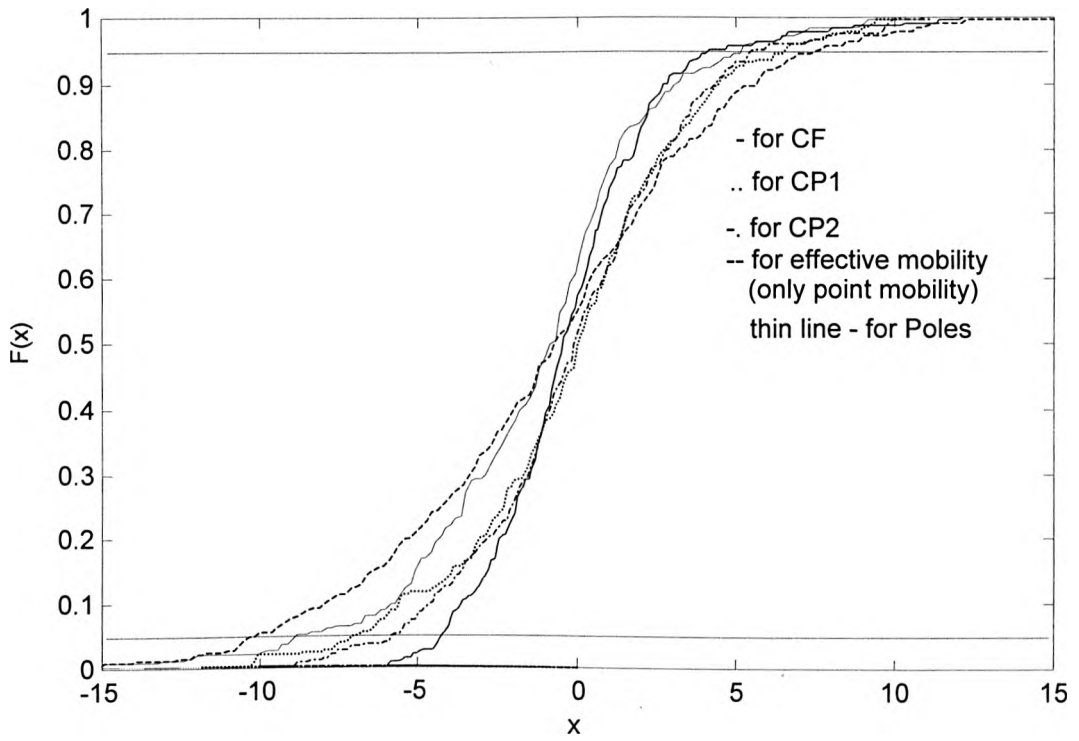
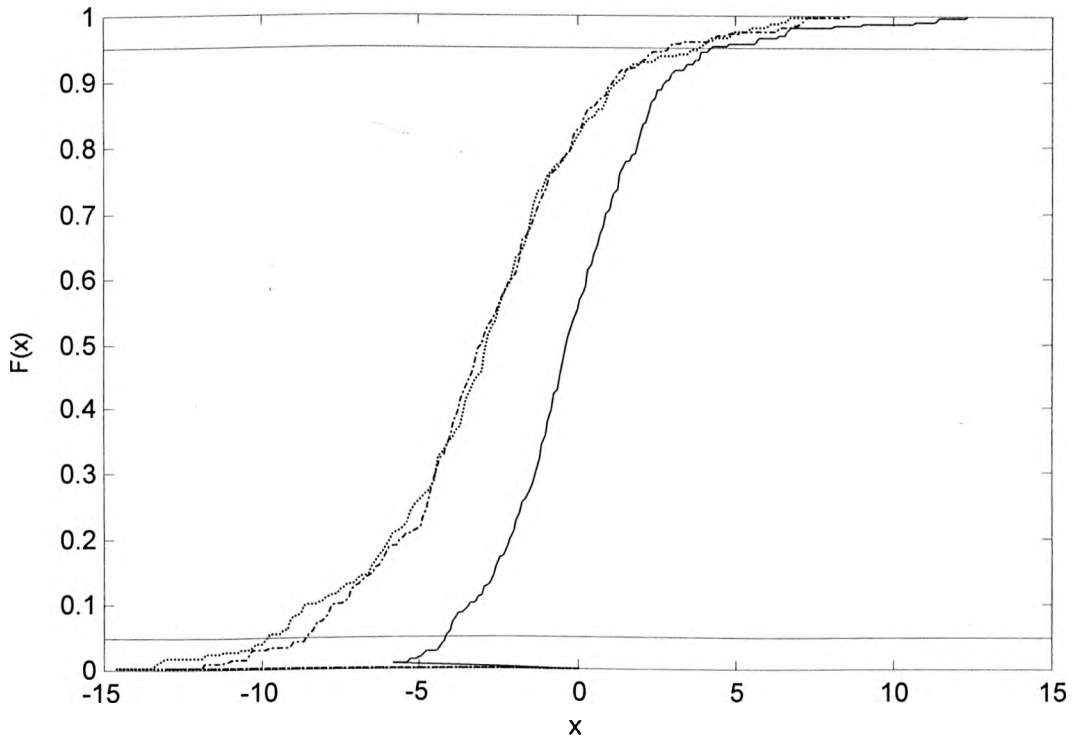**Figure 6-26a** Comparison of cumulative distribution function (case3)

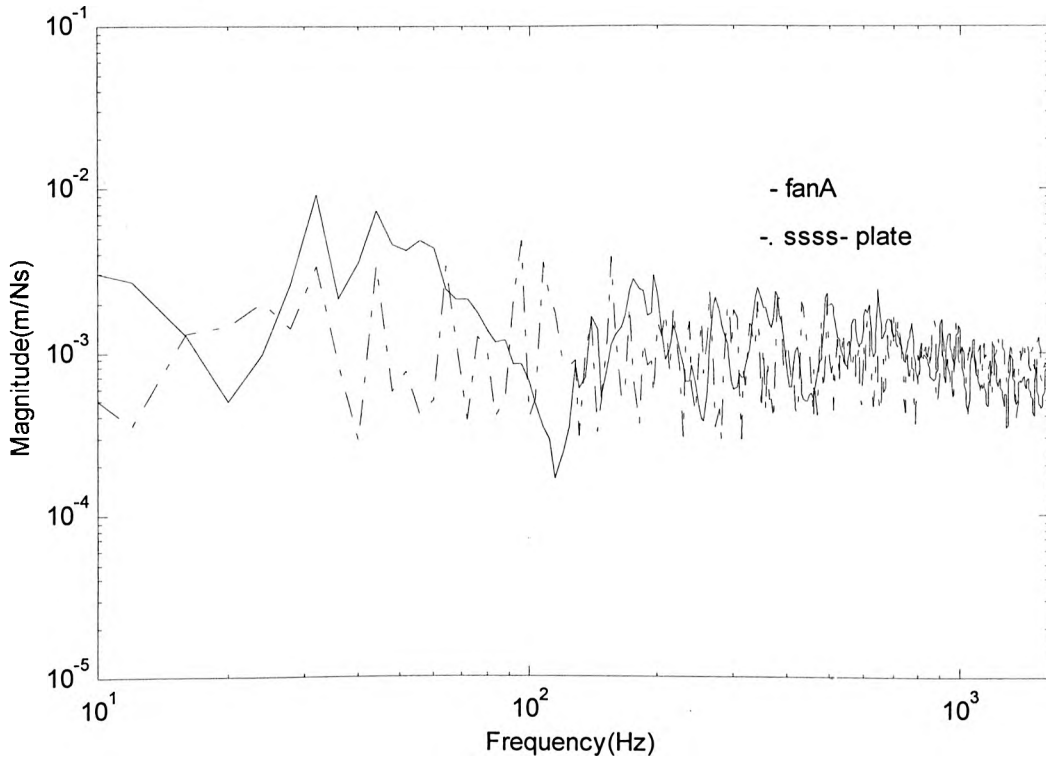**Figure 6-26b** The effect of adjustment factor

Figure 6-27a A sum of point mobility magnitude for fanA and matched ssss-plate
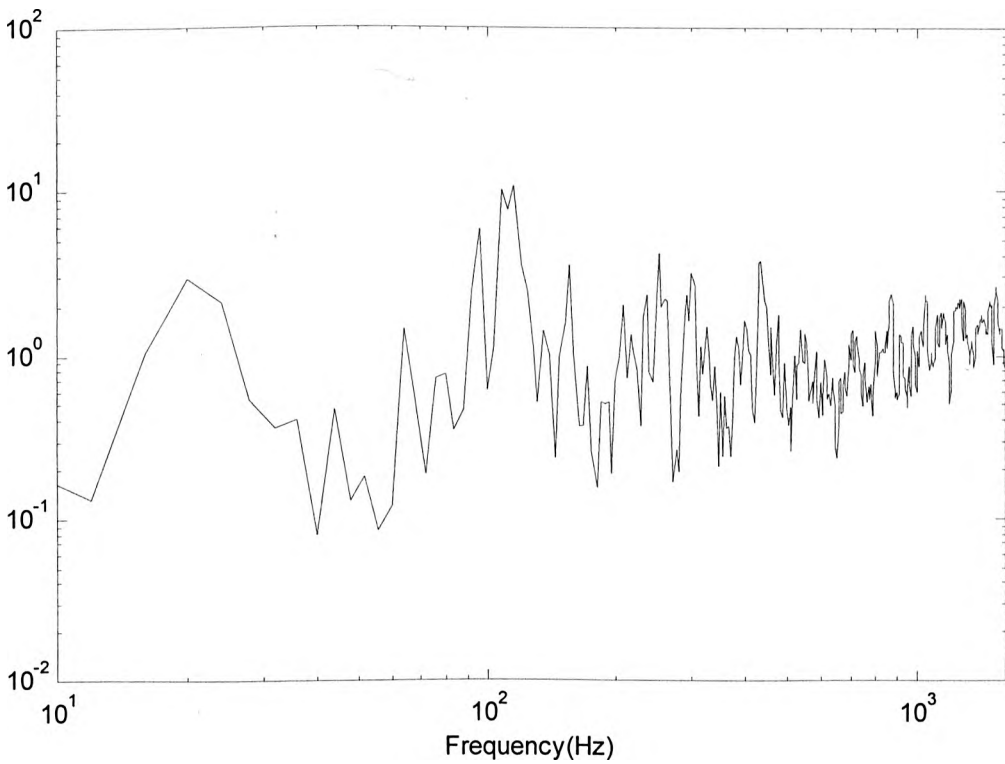

Figure 6-27b A average point mobility magnitude ratio for matched ssss-plate to fanA
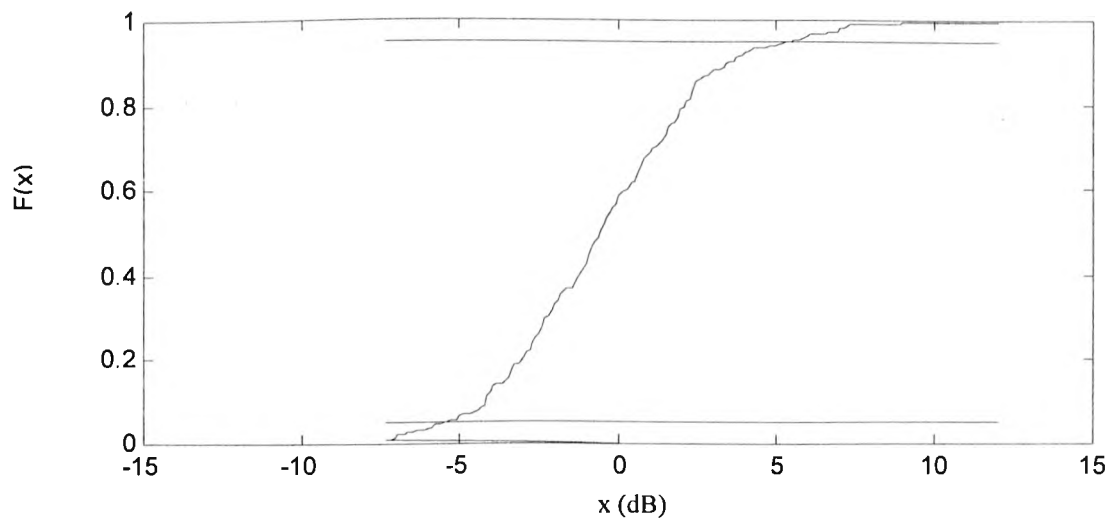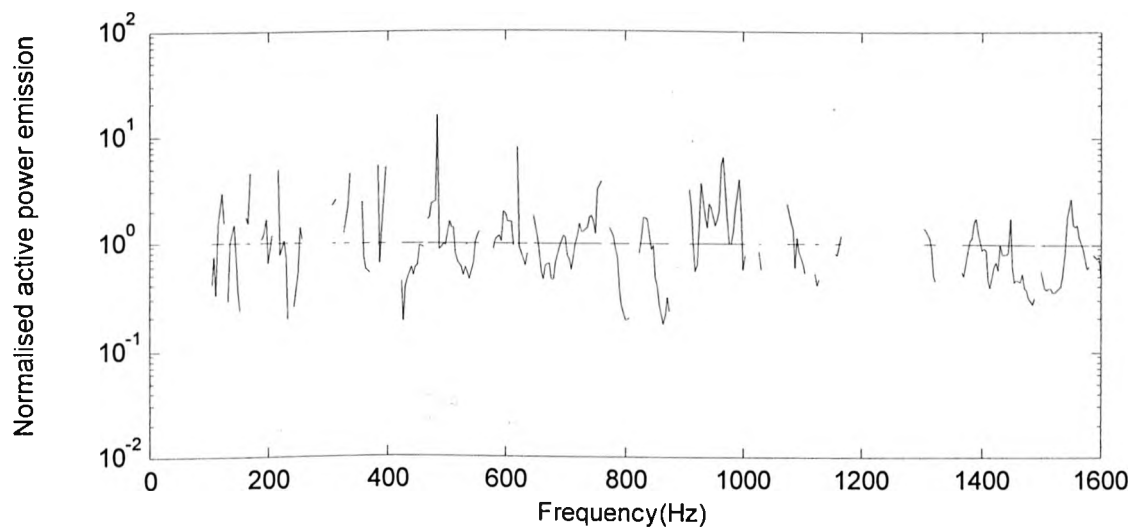
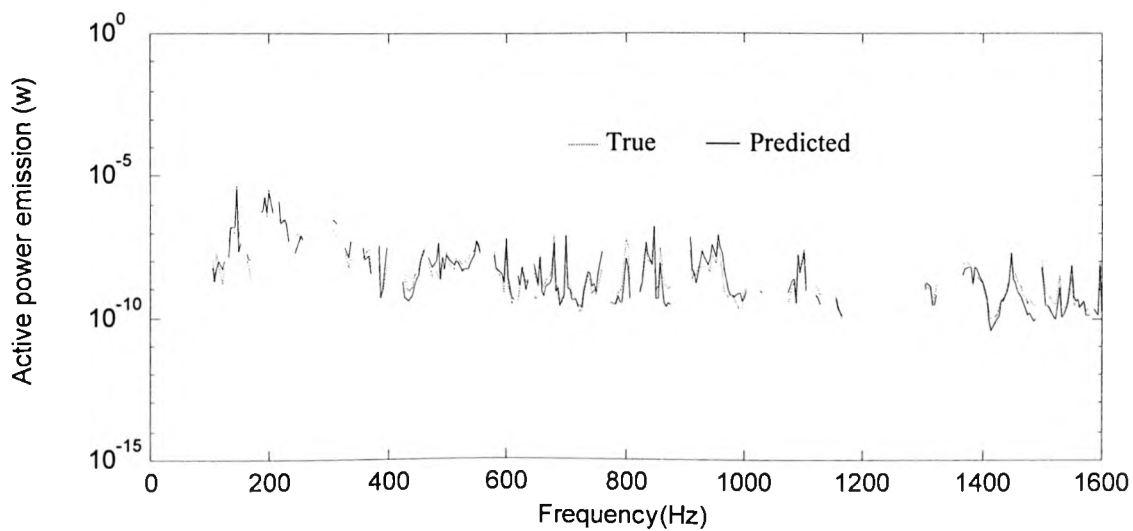**Figure 6-28a,b,c.** Prediction by using CF for fanA attached to a matched ssss- plate
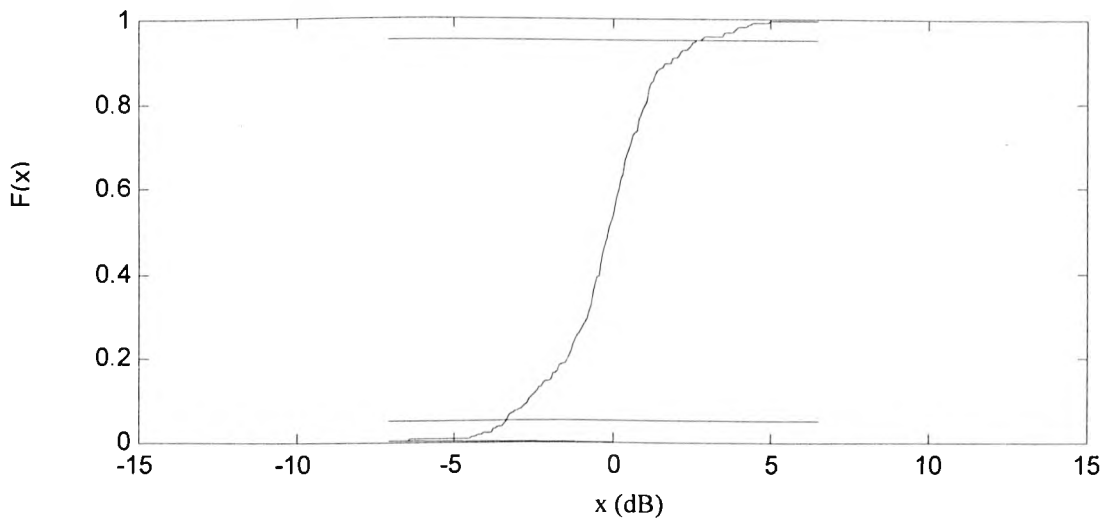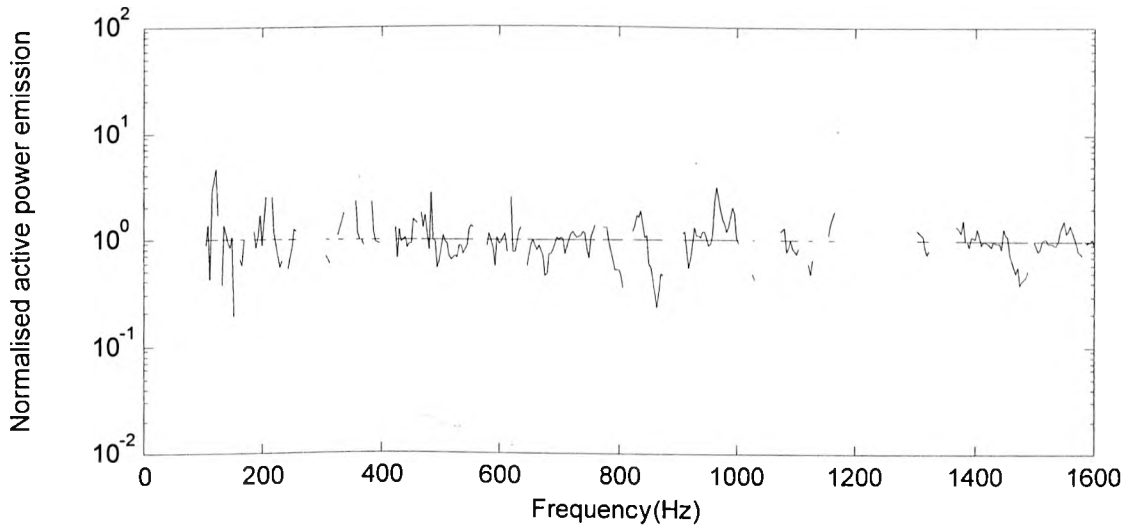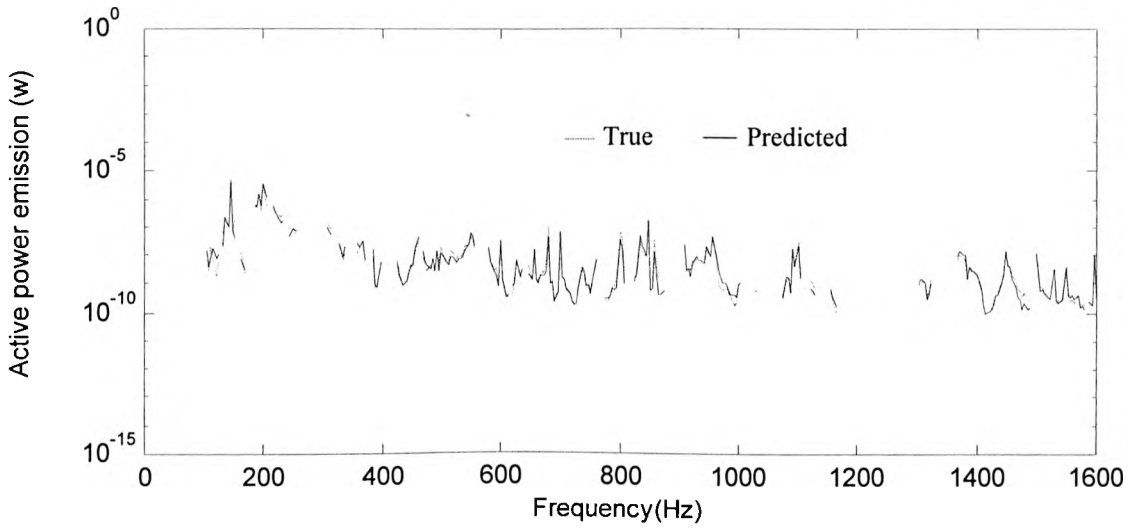
Figure 6-29a,b,c. Prediction by using CP1 for fanA attached to a matched ssss- plate
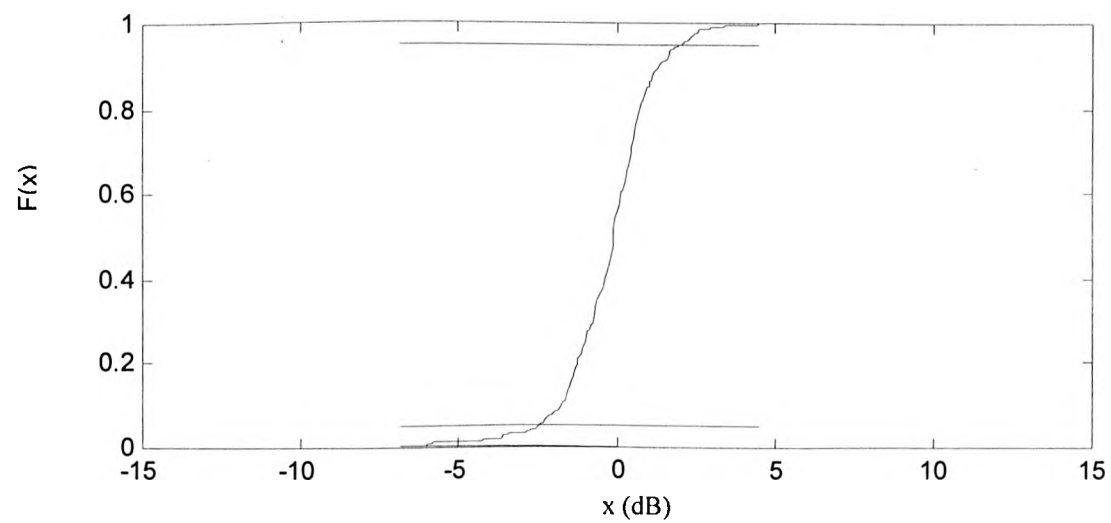
Figure 6-30a,b,c. Prediction by using poles for fanA attached to a matched ssss- plate
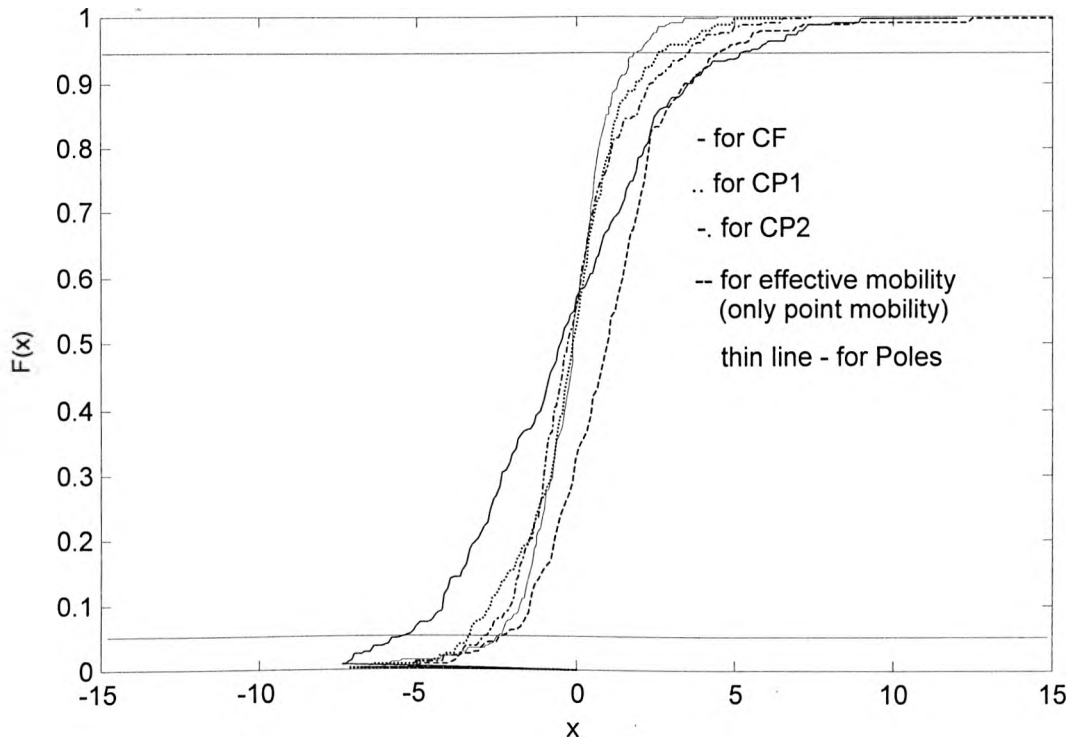
Figure 6-31a Comparison of cumulative distribution function (case4)
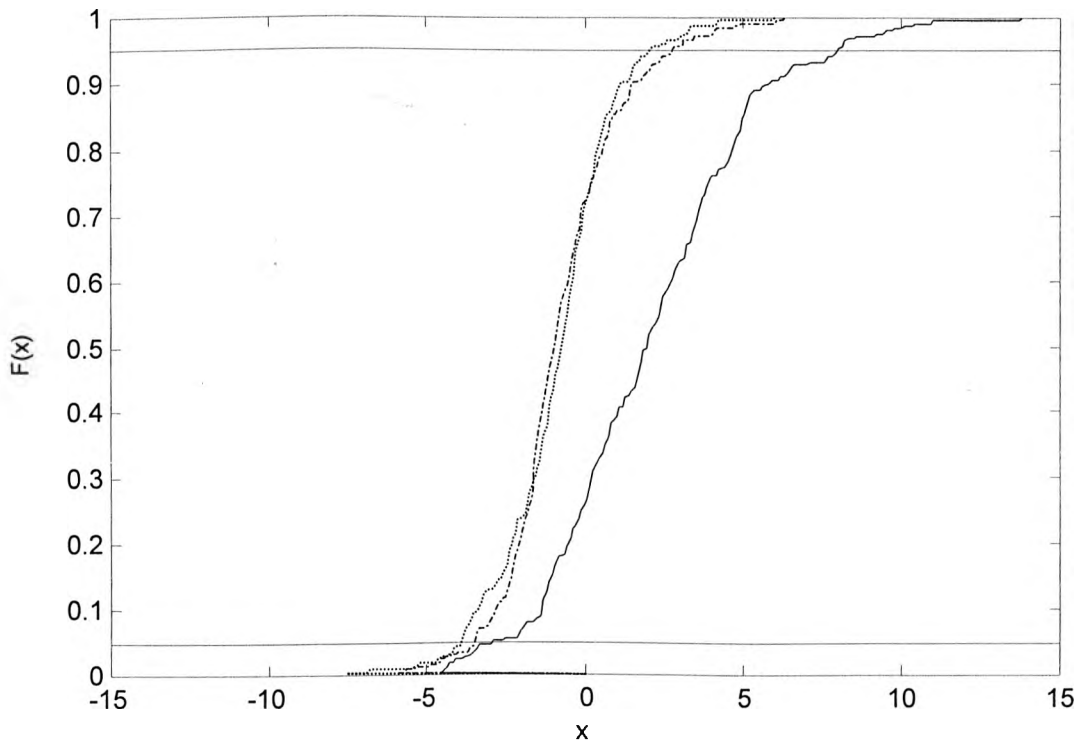
Figure 6-31b The effect of adjustment factor
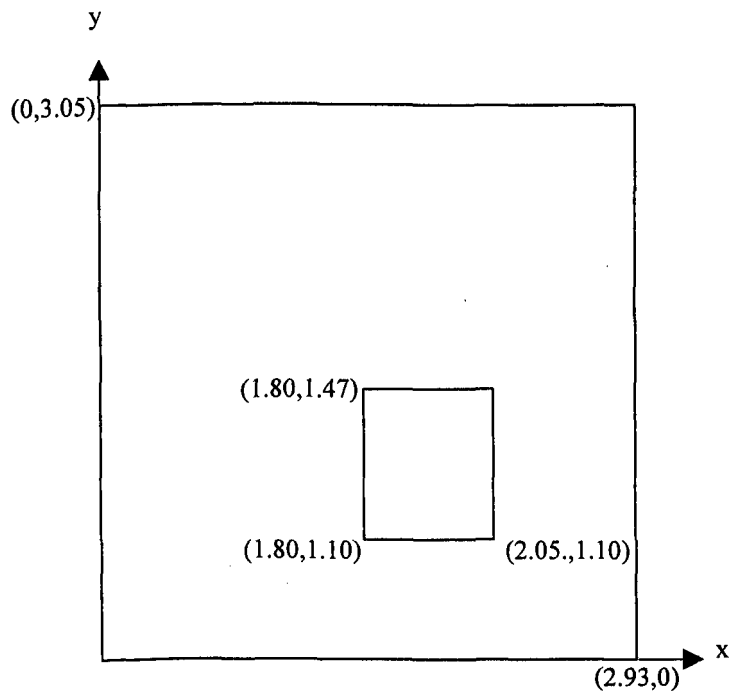
Figure 6-32 FanB on the ssss-plate (thickness is 0.09m)
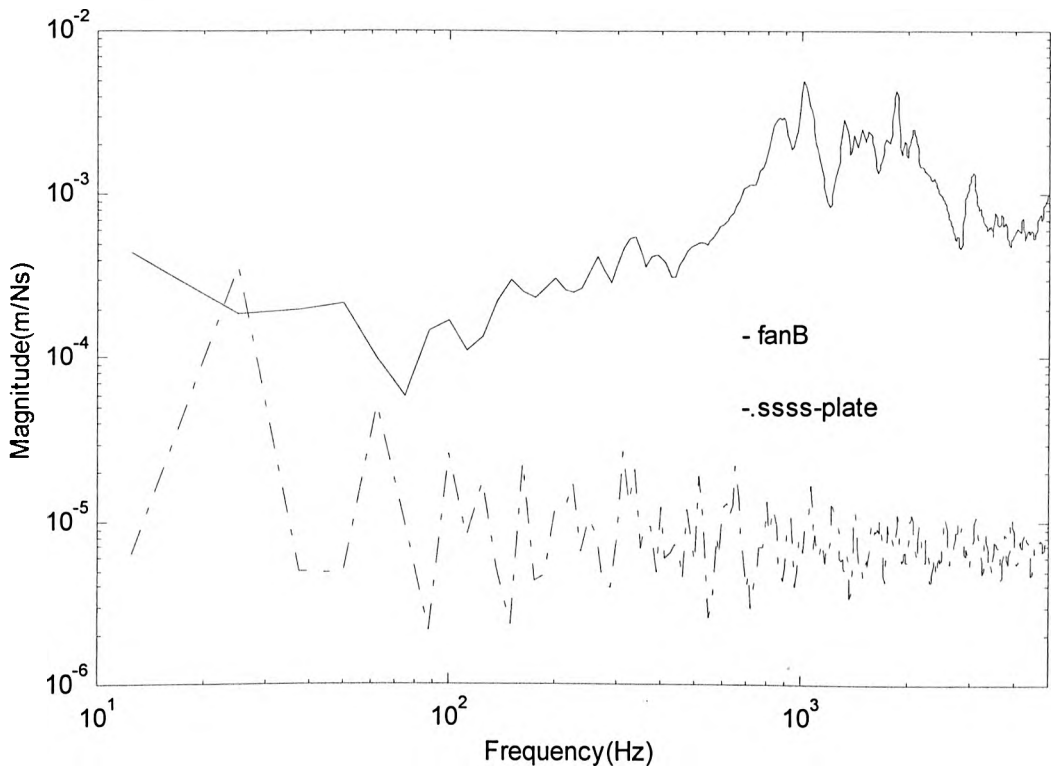
Figure 6-33a A sum of point mobility magnitude for fanB and lower mobility ssss-plate
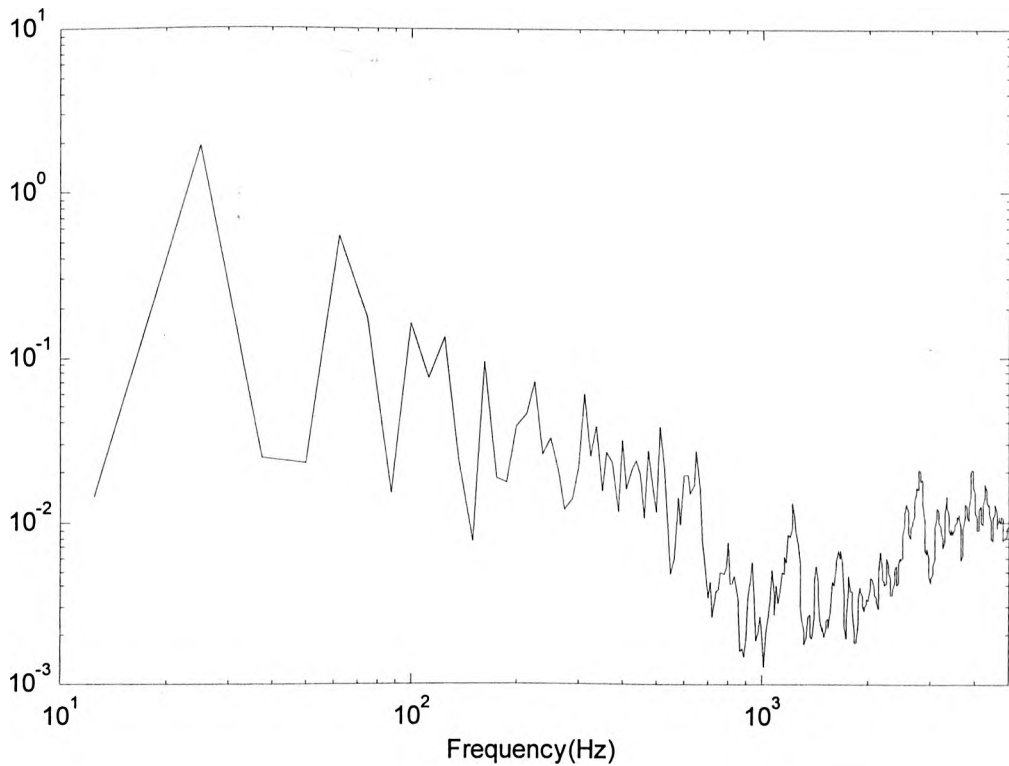
Figure 6-33b A average point mobility magnitude ratio of lower mobility ssss-plate to fanB
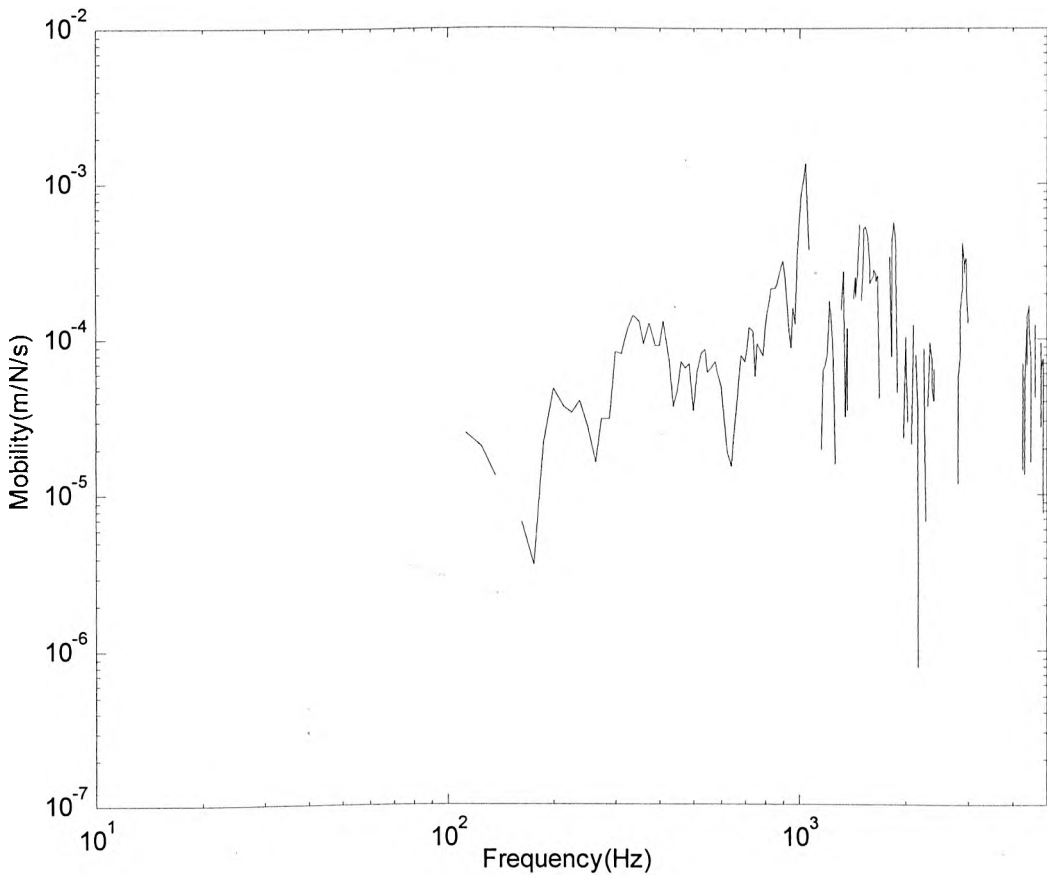
Figure 6-34 Minimum eigenvalue of real part of the mobility for fanB
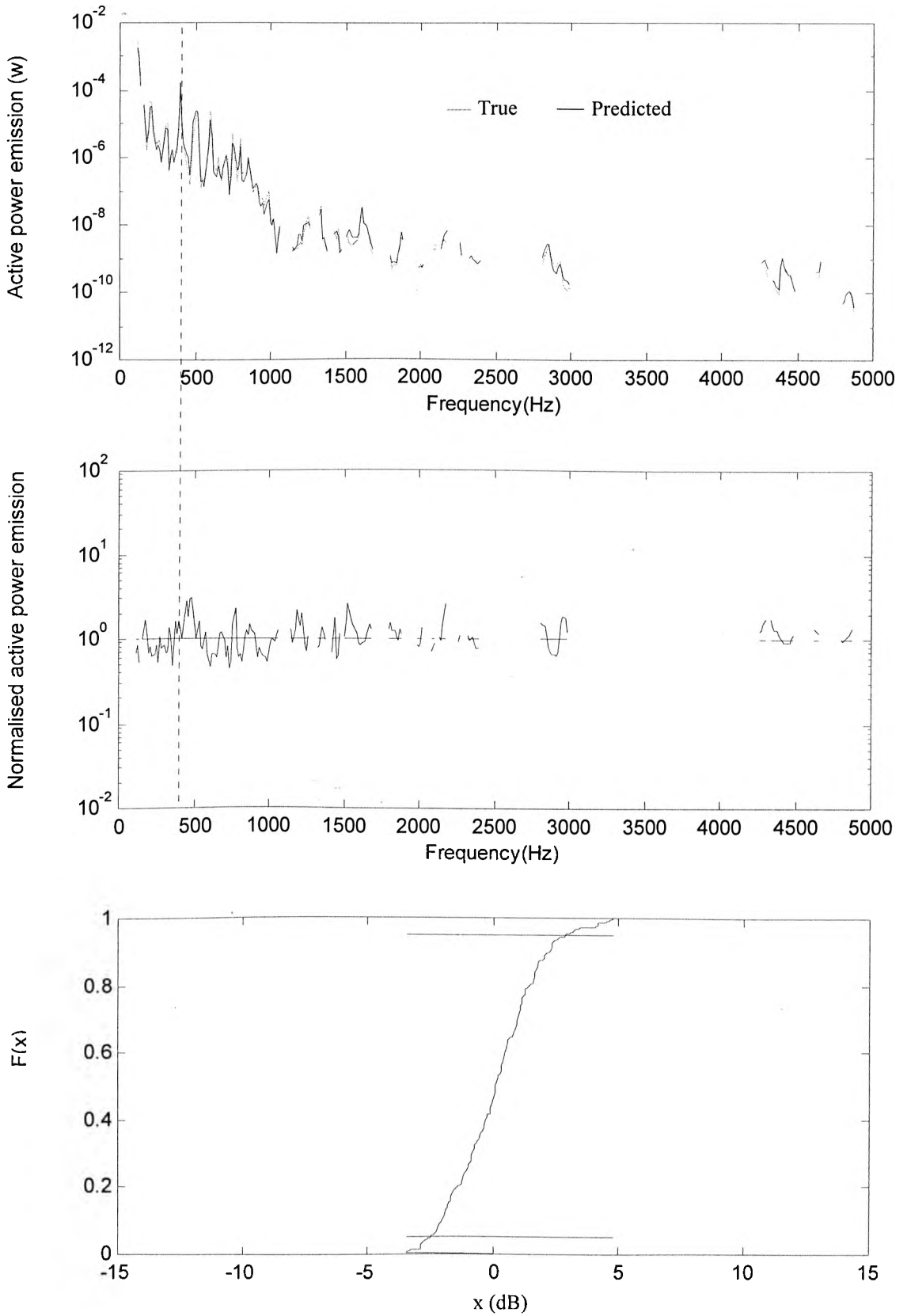
Figure 6-35a,b,c. Prediction by using CF for fanB attached to a lower mobility ssss- plate
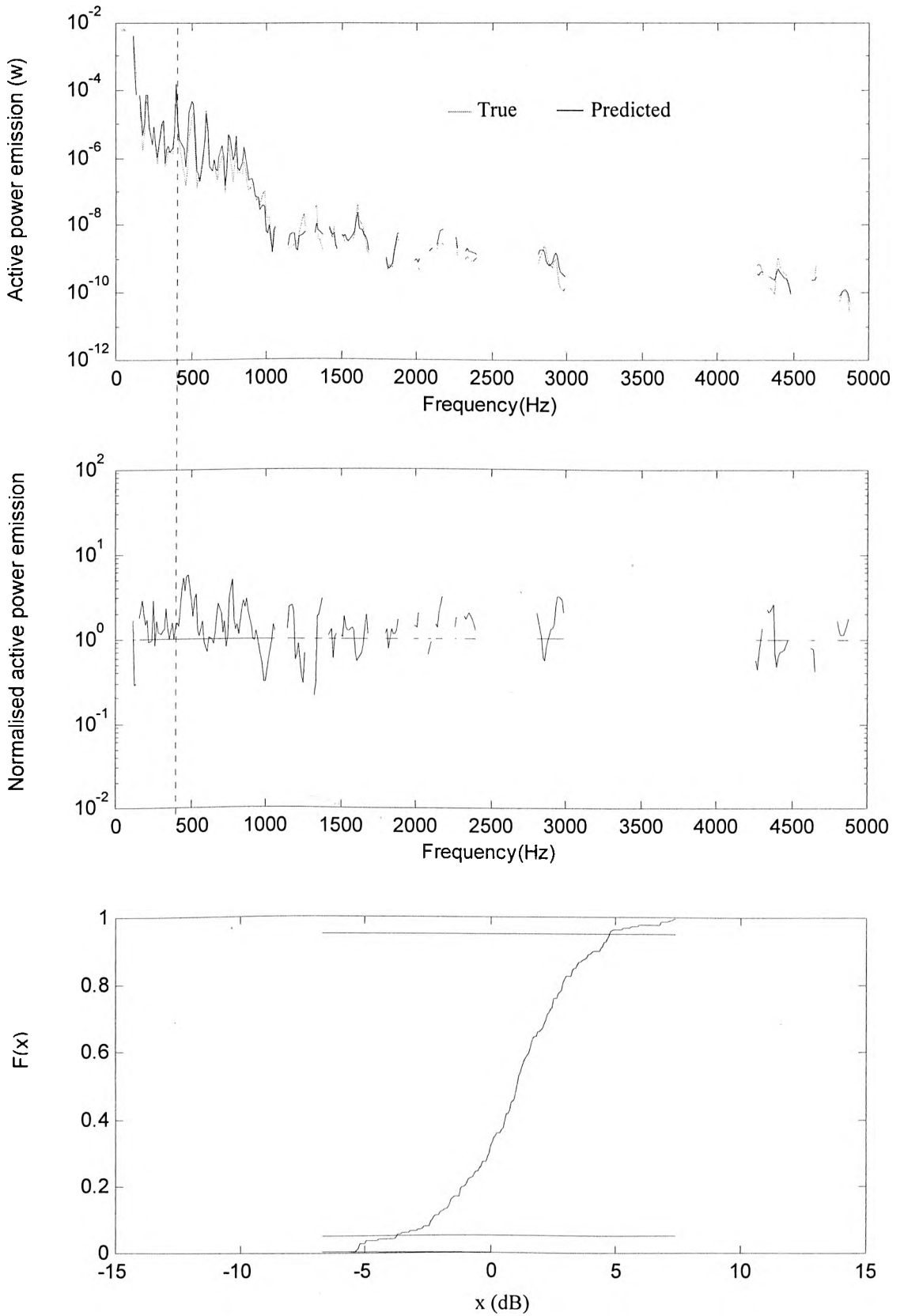
Figure 6-36a,b,c. Prediction by using CP1 for fanB attached to a lower mobility ssss- plate
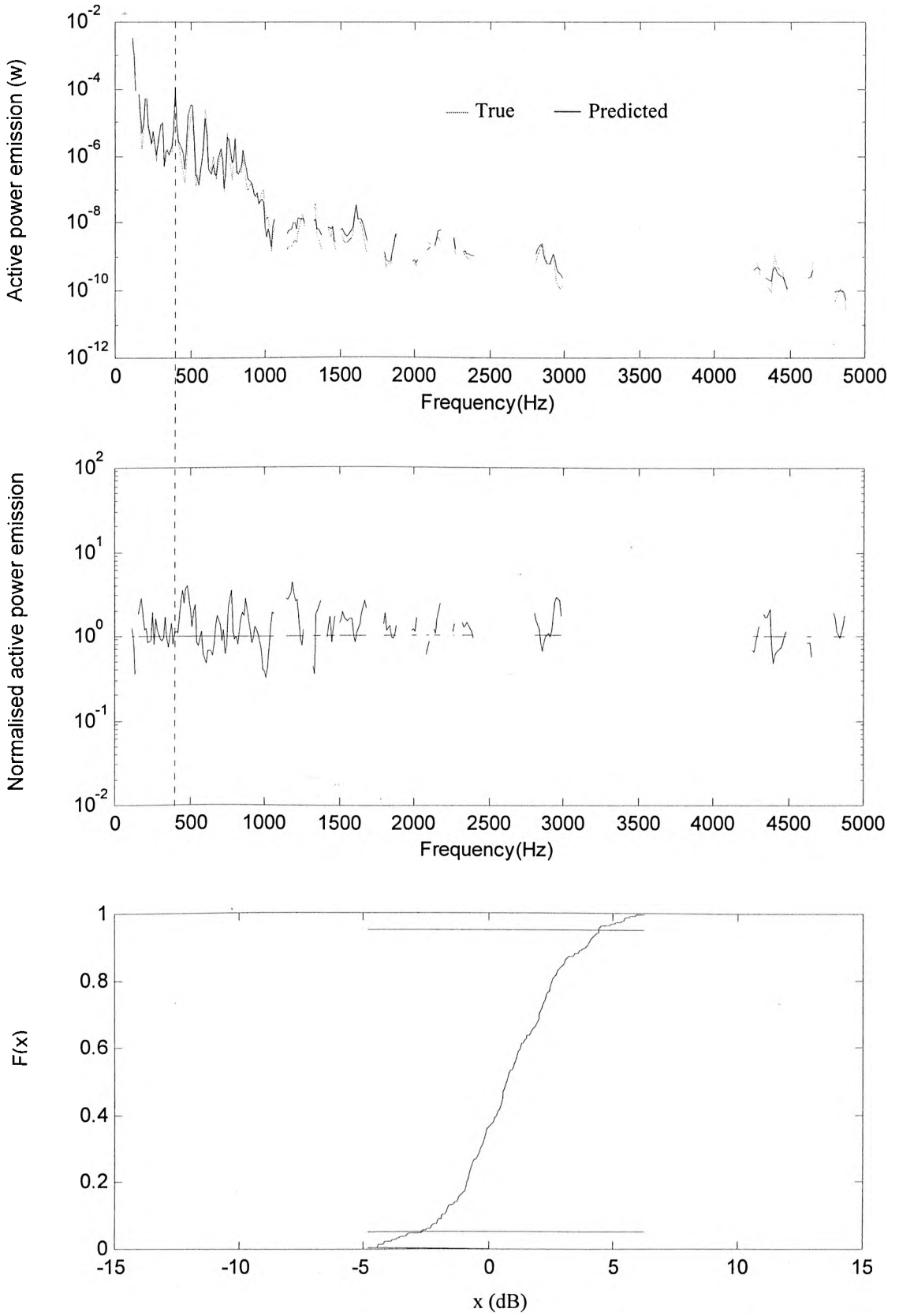
Figure 6-37a,b,c. Prediction by using CP2 for fanB attached to a lower mobility ssss- plate
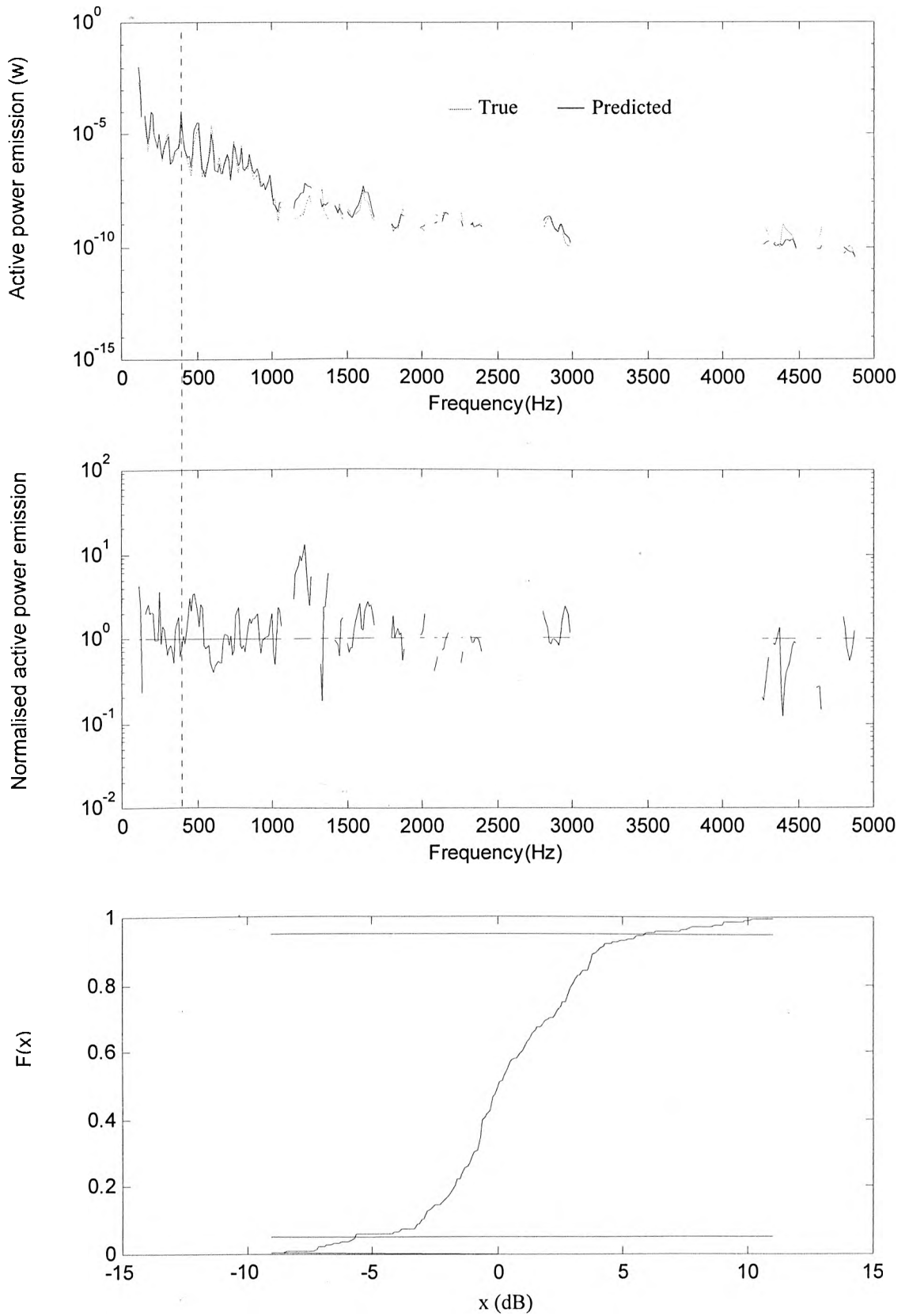
Figure 6-38a,b,c. Prediction by using effective mobility (only point mobility assumption) for fanB attached to a lower mobility ssss- plate
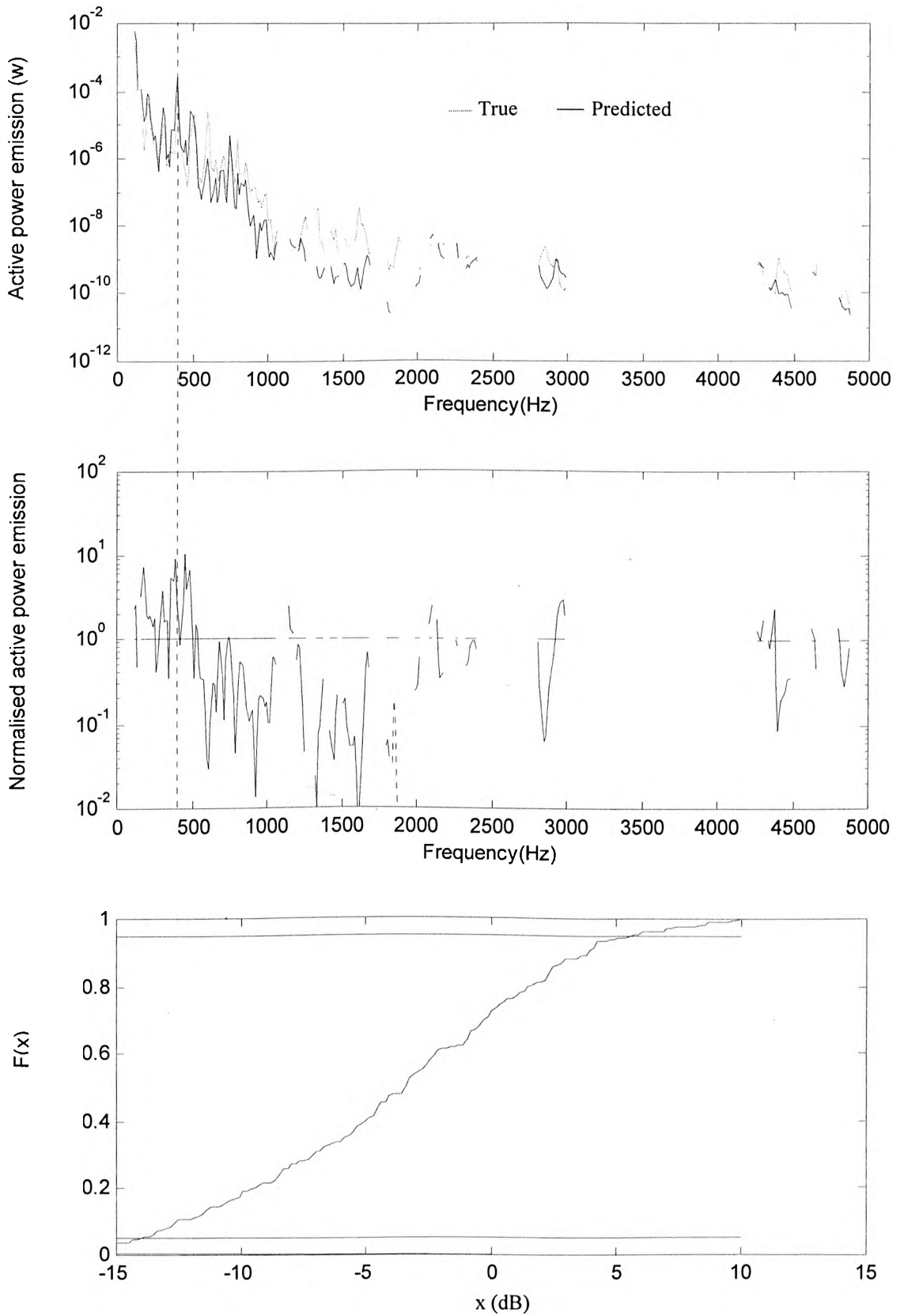
Figure 6-39a,b,c. Prediction by using effective mobility (unit magnitude, zero phase force ratios) for fanB attached to a lower mobility ssss- plate
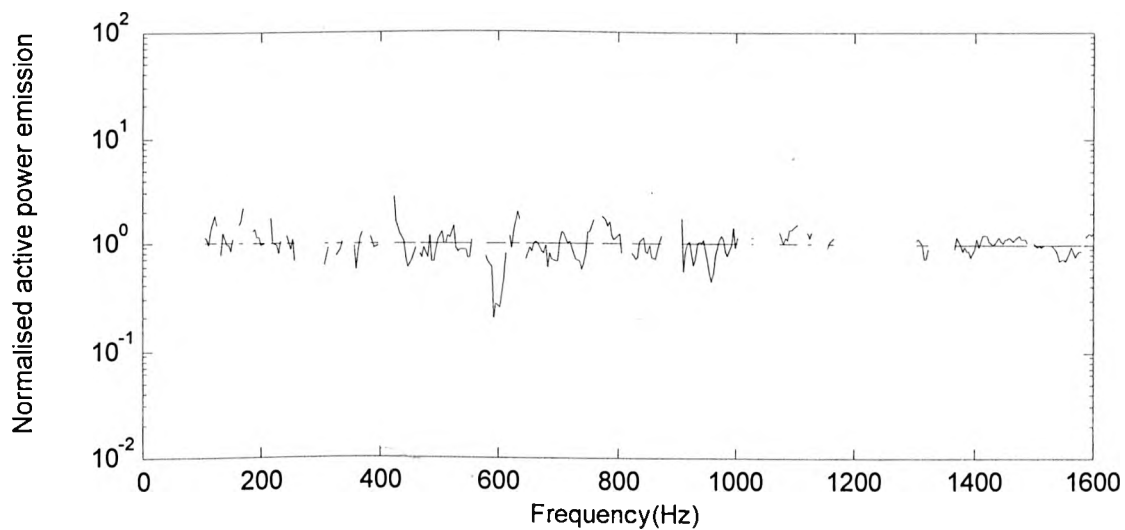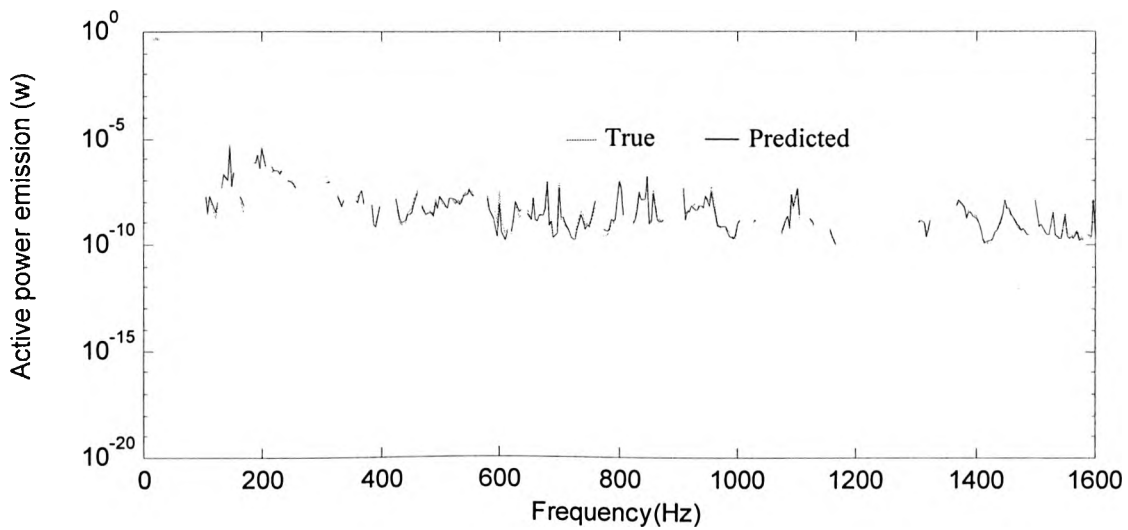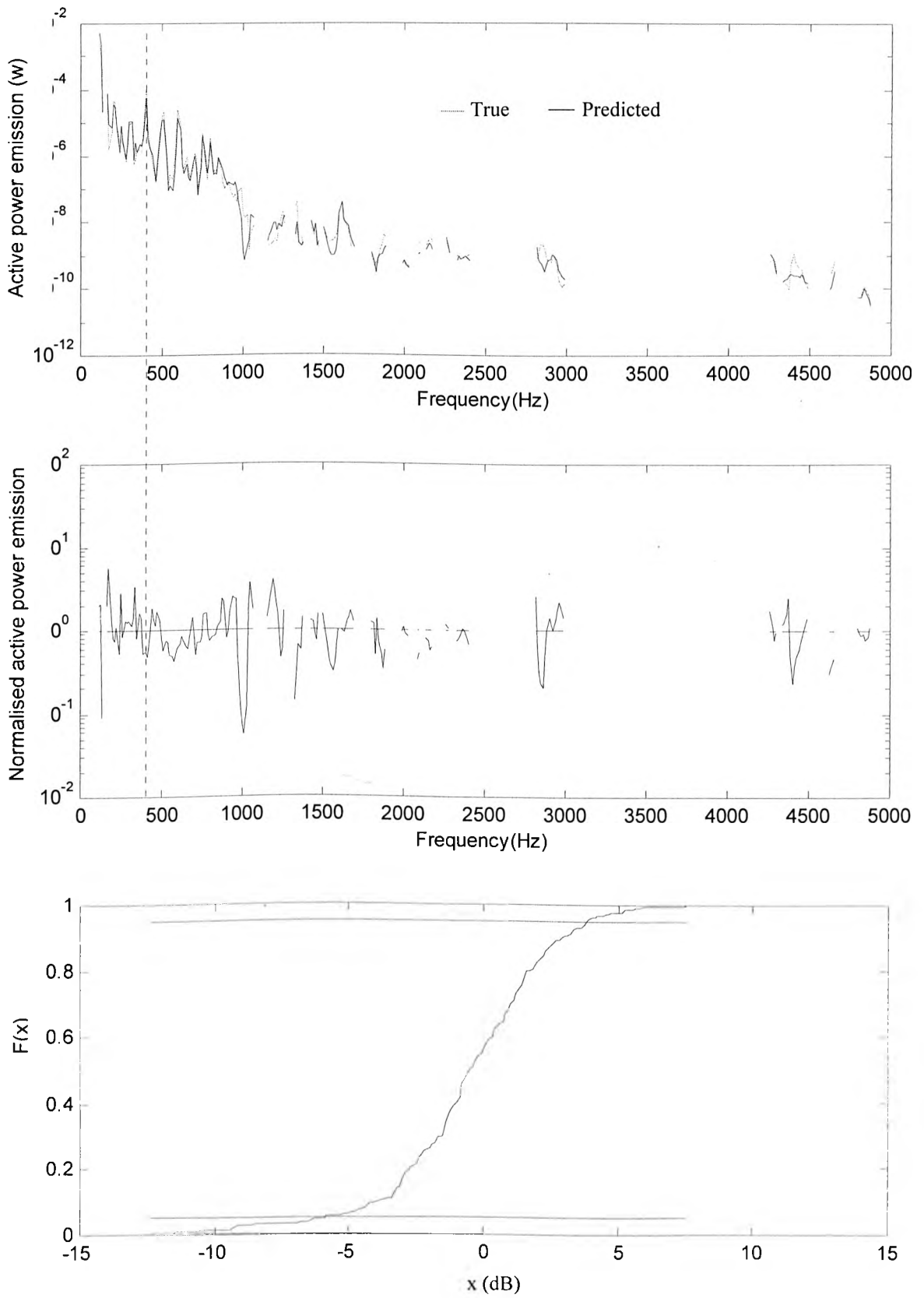
Figure 6-40a,b,c. Prediction by using poles for fanB attached to a lower mobility ssss- plate
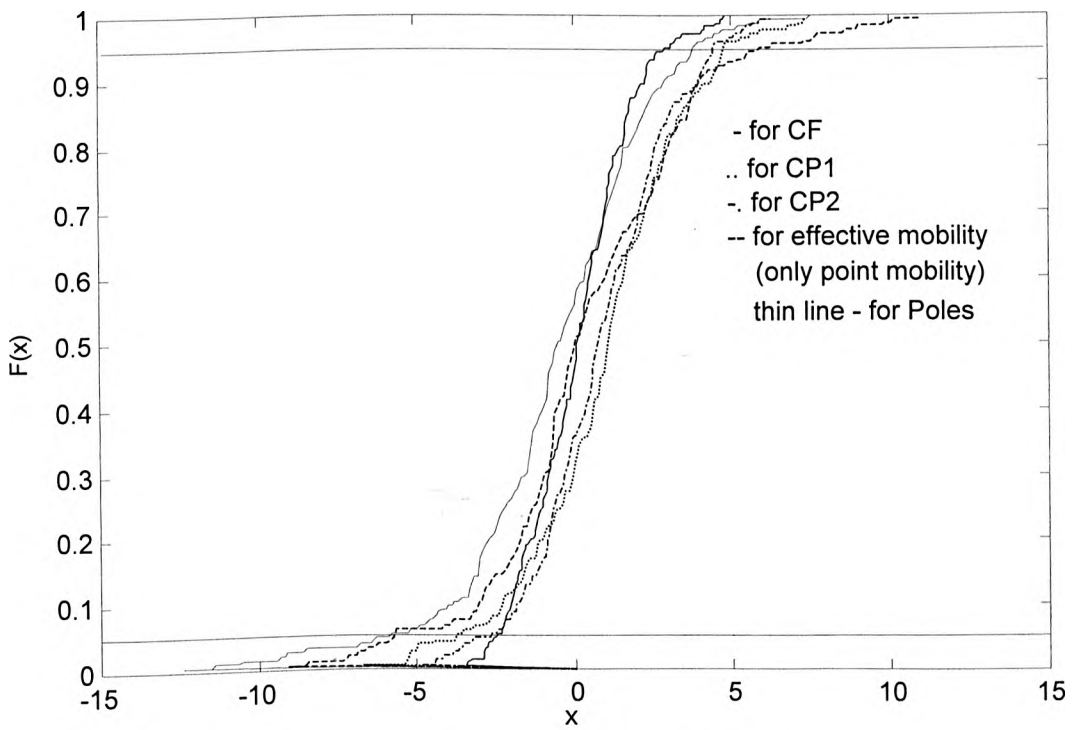
Figure 6-41a Comparison of cumulative distribution function(case5)
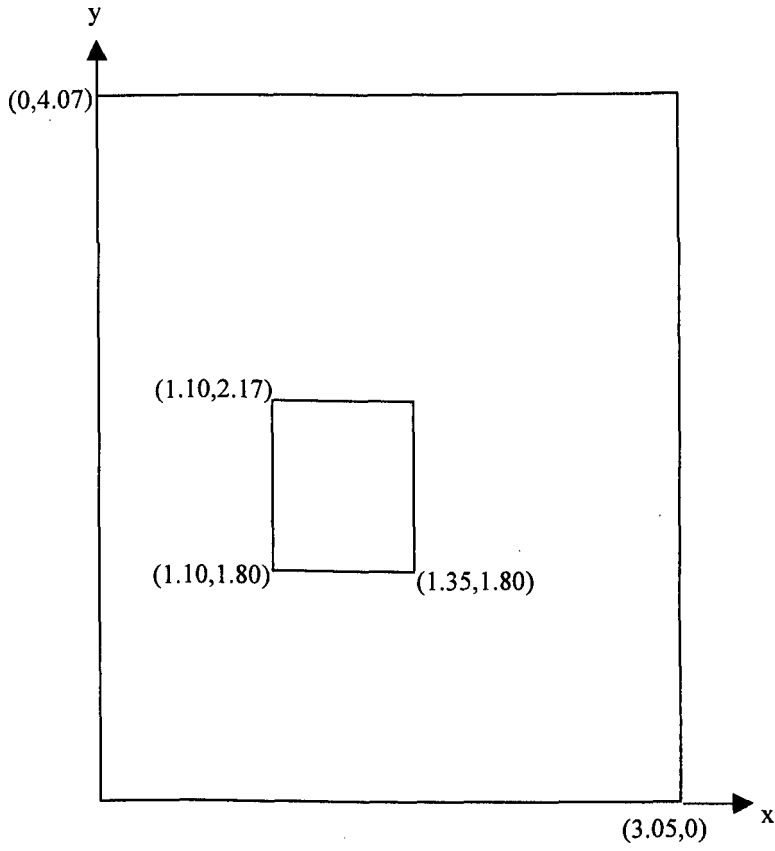
Figure 6-42 FanB on the ssss-plate (thickness is 4mm)
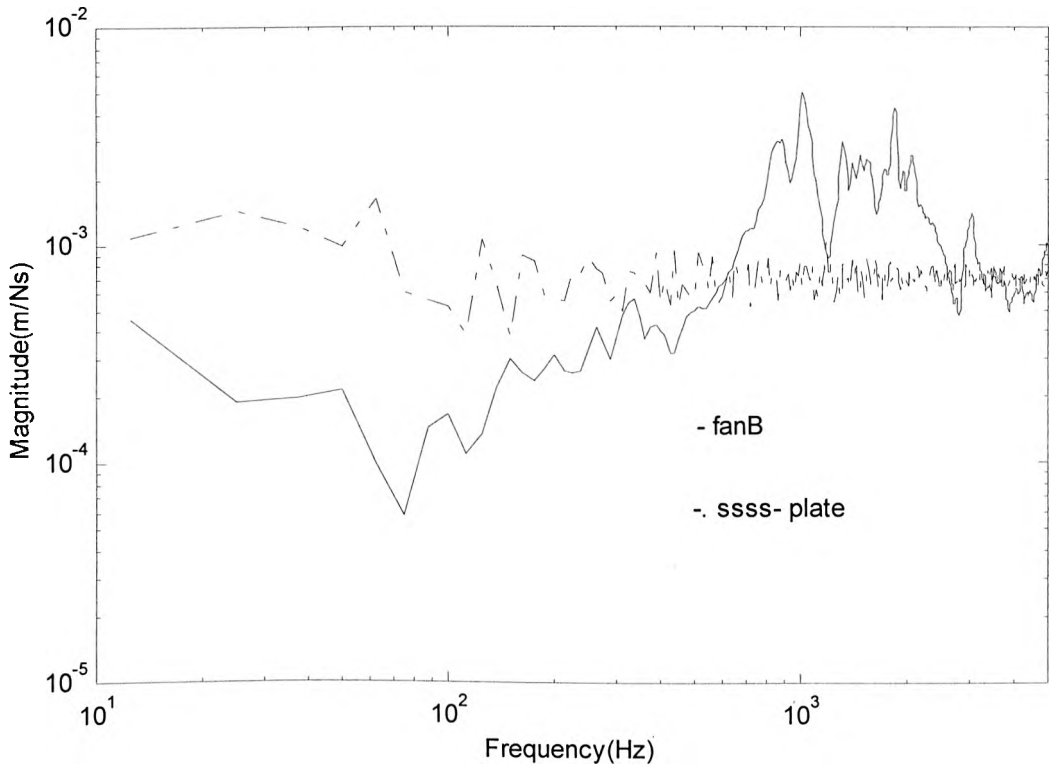
Figure 6-43a A sum of point mobility magnitude for Fan B and matched ssss-plate
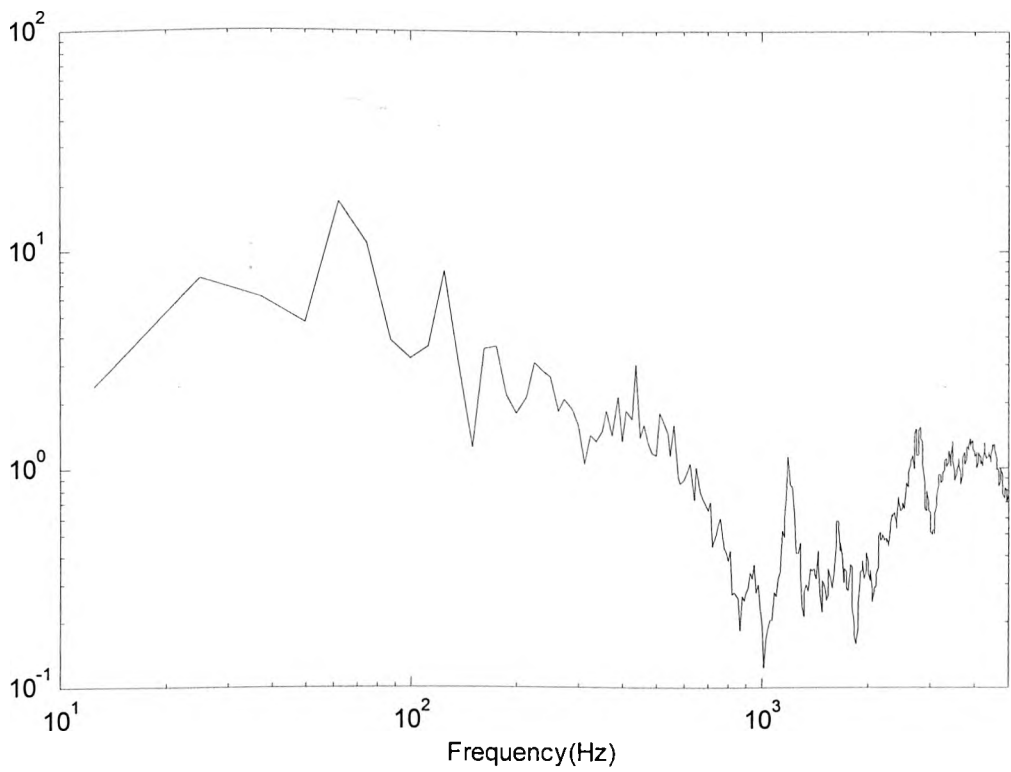
Figure 6-43b A average point mobility magnitude ratio of matched ssss-plate to fanB
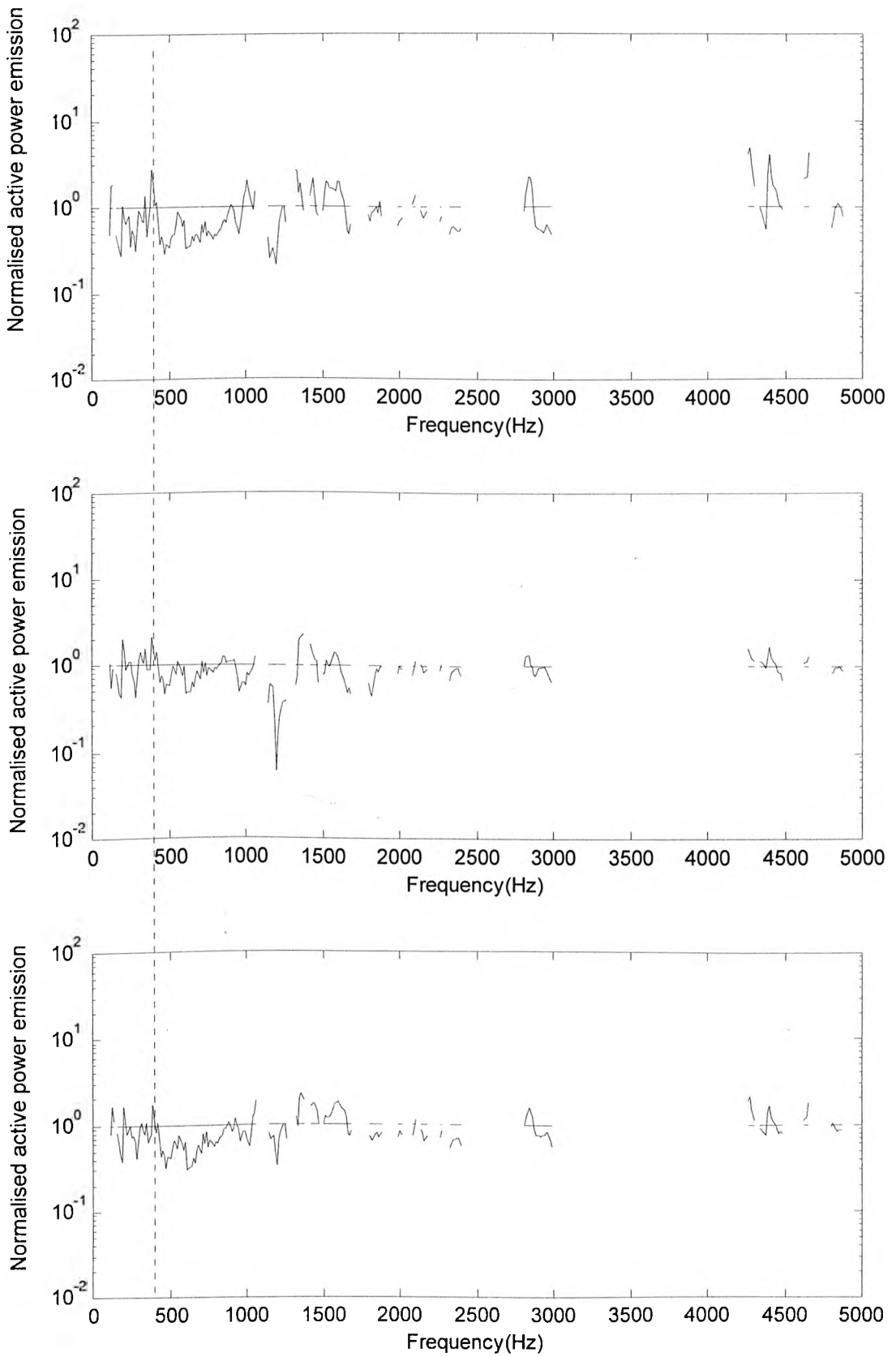
Figure 6-44 Prediction by using CF (a),CP1(b),CP2(c) for fanB attached to a lower mobility ssss- plate
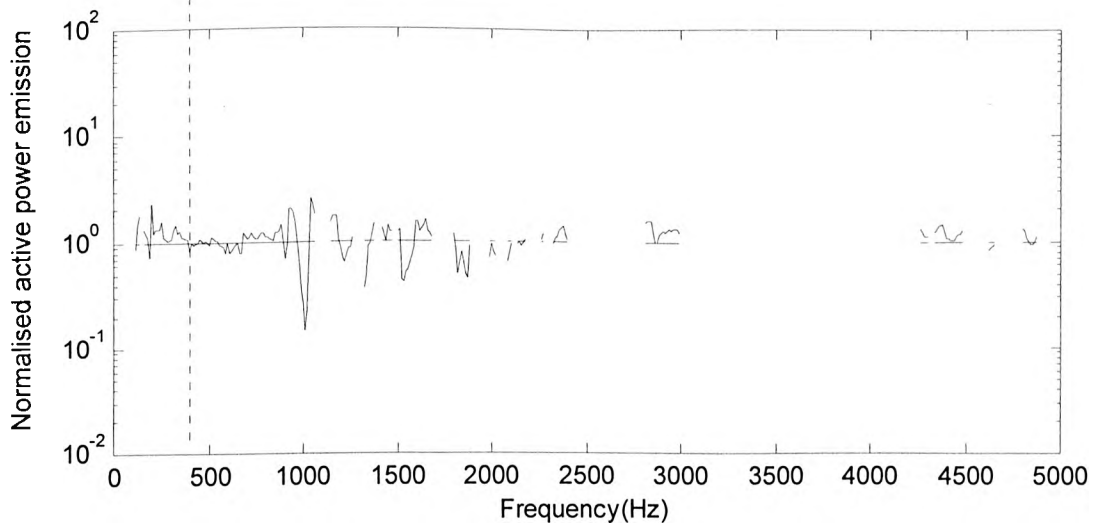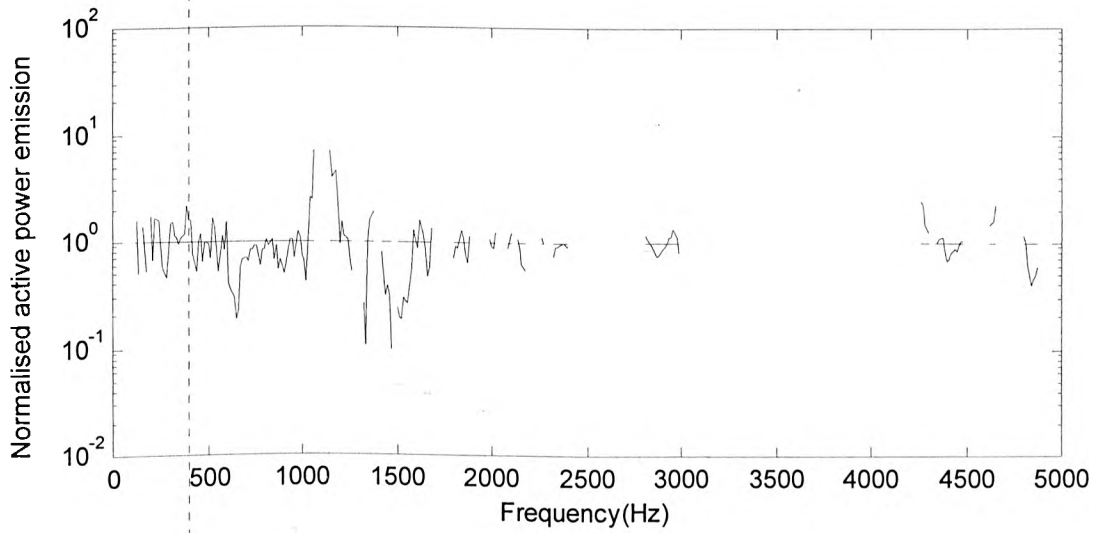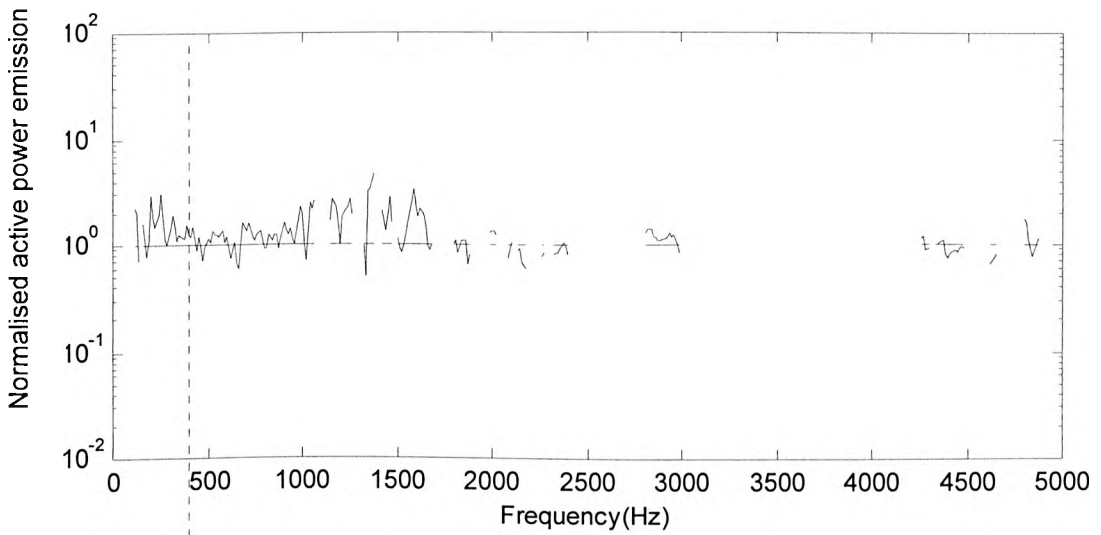
Figure 6-45 Prediction by using effective mobility (a: only point mobility assumption),(b: unit magnitude zero phase force ratio), and poles (c) for fanB attached to a matched mobility ssss- plate
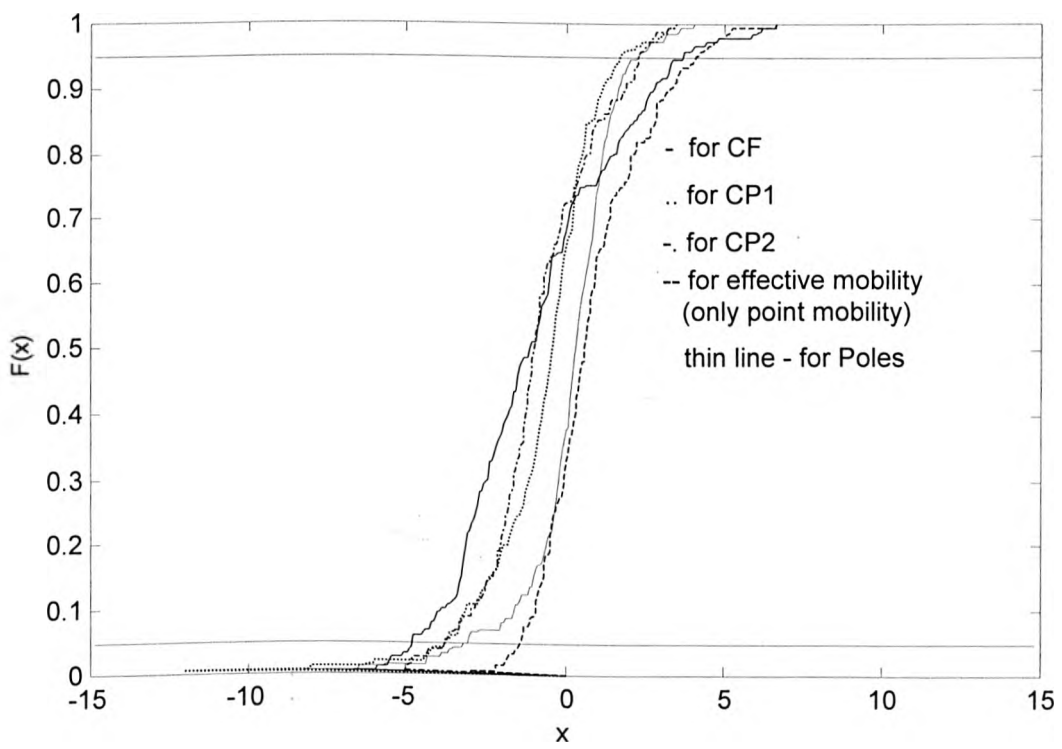
Figure 6-46a Comparison of cumulative distribution function(case6)
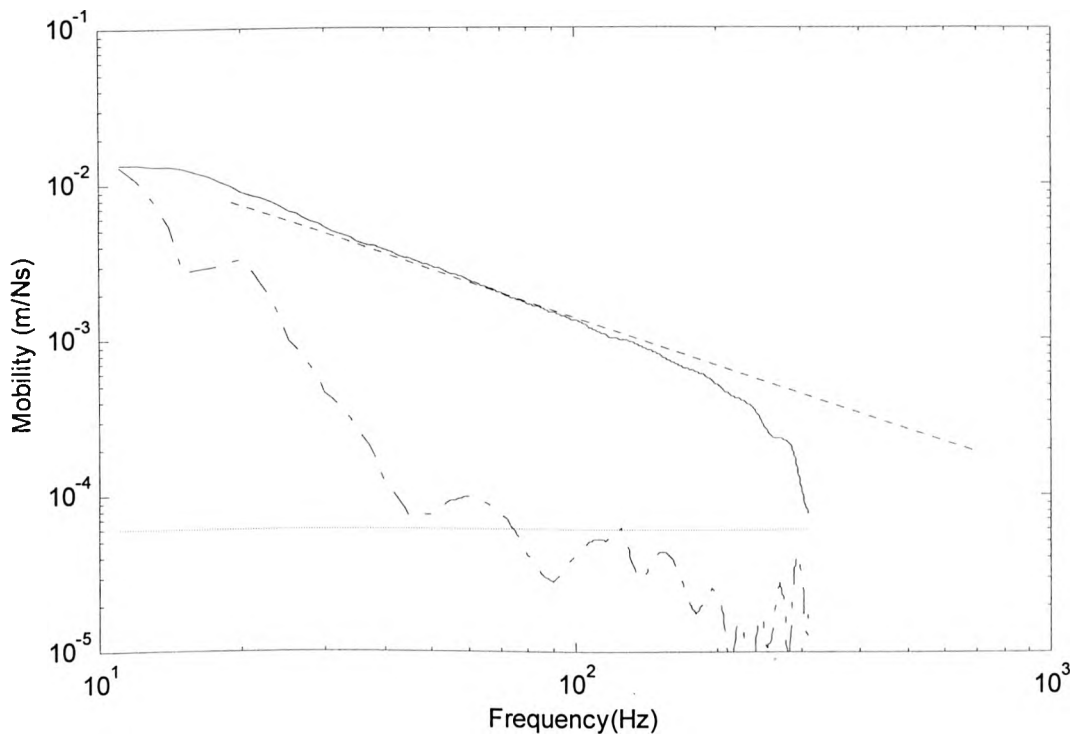
Figure 6-47 A sum of point mobility: solid line is magnitude for motor (dark) and for infinite plate (light),dashed line is real part for motor , dotted line is for a ideal rigid body.

- CF
.. CP1
-.CP2
∘∘ effective mobility(only point mobility)
∘-∘ polars
⊢⊢ effective mobility(unit magnitud,zero phase force ratios)
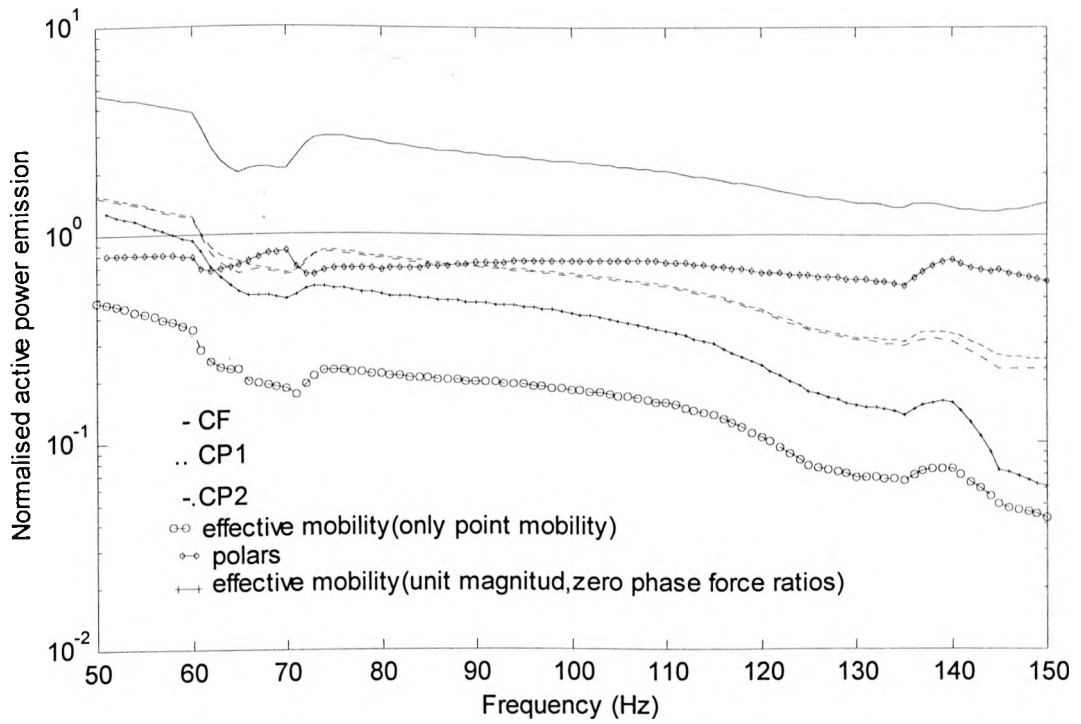
Figure6-48 Prediction for motor attached to infinite plate

CHAPTER7

CONCLUSIONS

Conclusions .

A complete characterisation for multiple-point-connected structure-borne sound sources contains too many elements (or parameters). It is not convenient for practical use. In this thesis, simplified characterisations have been researched, particularly those reduced to a single 'active' and a single 'dynamic' parameter.

The active power emission from a source into a receiver is sensitive to the receiver. This cannot be changed no matter how we choose the parameters to characterise the source. Whether the source parameters (S_c) can be used as parameters to rank a number of sources or not, depends on whether equation $L = f(r_1, r_2, ... r_m, S_c)$ can be satisfied. (This equation can be interpreted as stating that a higher value of (S_c) always leads to a higher value of the target quantity for sources installed on the same receiver)

Both the 'active' and dynamic parameters strongly influence the active power from a source into a receiver, so it is not possible to describe this influence by a single source parameter. The 'single figure' method was introduced to simplify characterisation of structure borne sources, i. e. the many elements needed for a full characterisation were collapsed into two parameters, one representing the 'active' property, which contains information about the 'strength' of the source (called 's_1') and another representing the dynamic property (called 's_2'.). In theory, there is an infinite number of pairs of valid parameters 's_1' and 's_2'. In this thesis, the average point mobility magnitude was chosen as the dynamic property parameter, while three alternative forms for the 'active' property parameter were investigated. These are 'CF' (based on blocked forces and with units of force squared), 'CP1' and 'CP2' (which are both based

around the idea of 'characteristic power', and have units of power). Whether the chosen 's_1' and 's_2' is 'good' or 'not good' has been shown in the corresponding 'general normalised active power band'. The general normalised active power band provides insight into the global behaviour of the source after knowing these two parameters (s_1 and s_2).

In order to obtain the 'general normalised active power band' a 'replacement method' has been adopted where practical structures are replaced by 'generic' structures. These generic structures are represented by randomly varied 'generic' matrices, which are based on the inherent properties of the mobility matrices and free velocity vector for different types of behaviour. This approach was necessary in order to provide sufficient data for statistical analysis of all the possible combinations of source and receiver types.

The properties of the mobility matrix and free velocity for four types of source (mass-like source, stiffness source, single mode resonant source, and off-resonant source) and four types of receiver (stiffness receiver, single mode resonant receiver, off-resonant receiver and infinite plate receiver) have been considered. For example, the imaginary part of the mobility matrix for a mass source has non-positive eigenvalues, and the free velocity vector has some relationship with the mobility matrix. For the case of a non-full rank mobility matrix, the mobility matrix ($[Y]$) and corresponding augmented matrix ($([Y, \hat{V}_{sf}])$) have the same rank. For the stiffness source and receiver, the real part and imaginary part are the same except for a constant multiplier. Matrix elements were randomly varied within these constraints in order to produce a statistical set of generic matrices. This 'generic structures' approach is one of the main

novelties of this work. The 'rules' of behaviour, formulated as a 'means to an end', can also be considered a useful outcome in that they provide some insight into the different types of behaviour.

The three kinds of 'general normalised active power bands' for combinations of different types of source and receiver have been plotted.

a) For high mobility sources, the general normalised active power band for CF are relatively flat while those for CP1 and CP2 are sloped. Furthermore, the variation for CF is significantly less than for CP1 and CP2. This means that using CF as source strength parameter will be more advantageous than using CP1 or CP2, even if each source has the same average point mobility magnitude. This phenomenon is different to the single point case where all three forms are identical, which emphasises that the choice of parameter is important for multiple point contact.

b) When the source and receiver mobilities are matched, the general normalised active power bands for CF, CP1 and CP2 are more complicated as might be expected. Overall, the power based descriptors CP1 and CP2 have advantages over CF in this case. However, the situation is less clear-cut than for the 'high mobility source' case described above. For stiffness and off-resonant sources (which applies to a large proportion of practical cases) the general normalised active power bands for CP1 and CP2 are relatively flat and narrow compared with that for CF. This means that using CP1 or CP2 as a strength parameter will be more reliable than using CF, in other words a rank ordering based on CP1 or CP2 will be more stable than one based on CF. However, for mass-like sources on

stiffness receivers, the three bands are all wide (up to 30dB) and none are flat. Thus, for mass-like sources, the single figure approach could lead to potentially large errors, and a more complete description, such as the polar mobility description is desirable.

Both CP1 or CP2 can be considered as an practical upper limit of the active power from a source into the receiver. This result is not always correct, but in most cases it will be quite reliable, unless the source is mass-like and the receiver mobility magnitude matches that of the source. This result may be useful for practical cases, particularly when it is not necessary to know the active power emission accurately, but just the approximate upper limit. The only case where this limit is exceeded is for mass sources on spring receivers. We can speculate, based on theory for a single mass-spring system, that the power will not exceed $CP1/\eta$, where η is the loss factor of the receiver. This appears to agree with results of Chapter 5, although further work would be required to confirm this.

Some examples have been shown of using the general normalised active band power band ('single figure' prediction method) to predict the active power emission from practical machines into plate receivers. Compared with the effective mobility method, the 'single figure' prediction method achieves a better effect in accuracy, whilst requiring less data. Compared with the polar mobility method the 'single figure' prediction method pays a slight 'cost' in terms of uncertainty in matched cases, particularly for mass-like sources. However, perhaps surprisingly, the uncertainty in CF is less than all other descriptors, even those using more data.

The parameters describing the activity of structure-borne sound sources has been contracted into a single data (s_1) in the 'single figure' method. In many practical cases, the source and receiver properties will be known with sufficient accuracy to place the installation in either the 'high mobility source' or the 'matched' category. For example, for building service machinery, the source is often to be installed on a concrete floor where the mobility is much smaller than that of the source, and the condition number is relatively low. In this case s_1 can be used as a source strength parameter to rank the source.

In this thesis the receiver mobilities chosen have a condition number less than 30dB, except for single mode resonance receivers. This is likely to be a 'worst case' for practical structures in which loss factors lower than 0.01 are relatively rare because of energy loss into connected structures. It is possible that condition numbers could exceed 30dB around resonant peaks for structures with lower damping (from experience this could occur if a peak in s_2 is a factor 10^2 greater than the next trough). In this case the corresponding 'normalised active power band will be slightly wider than shown in Chapter 5. However, we can conclude that the bands shown in Chapter 5 are not limited to cases of high damping, but cover most practical situations.

A final comment concerns the relative merits of simplified and full source characterisations. On one hand, more data means that less restrictive assumptions have to be made and the predicted emission should in theory be more reliable. However, on the other hand with more data there is more possibility that the data set contains errors which will lead to errors in the predicted emission. Indeed, it is often found, even in cases where a full set of measured data is available, that the errors in

the predicted power emission are significant, possibly even of similar order to those produced here with far less input data. Single figure descriptors will always give a range of uncertainty. However, their reliability is considerably increased when the likely errors are known and understood, and it is hoped that this thesis has contributed in some measure to this. Perhaps the most important advantage of the single figure approach however is that it gives some insight into the problem of structure-borne sound emission.

REFERENCES

[1] T.Kihlman, *Urgent need for structure-borne sound source data*, Inter-Noise 78, 343-347(1978).

[2] ISO/DIS 9611 *Characterisation of sources of structure-borne sound with respect to sound radiation to connected structures-Measurement of velocity at the contact points of machinery when resiliently mounted* (1996)

[3] R.J.Bernhard, *The limits of predictability due to manufacturing and environmentally induced uncertainty*, Inter-Noise96, 2867-2872(1996).

[4] Jean-louis Guyader, Morvan Ouisse, *Energy residual a tool to study dispersion of vibroacoustic performances of structures*, The 10th International Congress on Sound and Vibration (2003).

[5] M.Ohlrich, *Noise sources in ships,* NORDFORSK MILJOVARDSSENEN Publ.Chap.3,(1983)

[6] M.Ohlrich and A.Crone, *An equivalent force description of gear-box sources Applied in prediction of structural vibration in wind turbines*, Inter-Noise 88, 479-484 (1988).

[7] Jan W.Verheij, Marcel H.A.Janssens, Paul J.G,Charlier,*Using pseudo-forces for characterisation of structure –borne sound sources*, Inter-noise 95, 559-562(1995).

[8] T.ten Wolde and G.R.Gadefelt, *Development of standard measurement methods for structureborne sound emission*, Noise control Engineering Journal 28(1),5-14 (1987).

[9] J.Tourret and Leon Gavric, *Numerical study of the reverberate reception plate method for structure-borne noise characterisation of small compact machines*, Inter-Noise 94, 615-620.(1994)

[10] M.Ohlrich, *The use of surface power for characterisation of structure-borne sound sources of low modal density*, Inter-Noise 96, 1313-1318 (1996).

[11] J.W.Verheij, *Inverse and Reciprocity Methods for Machinery Noise Source Characterisation and Sound Path Quantification, Part1: Sources*, International Journal of Acoustics and Vibration, Vol. 2, No.1,11-20 (1997).

[12] G. Pavic, *Measurement of Structure-borne Wave Intensity, Part I: Formulation of the Methods*, Journal of Sound and Vibration, 49, 221-230(1976).

[13] J.W.Verheij, *Cross Spectral Density Methods for Measuring Structure-borne Power Flow on Beams and Pipes*, Journal of Sound and Vibration, 70,133-138(1976)

[14] B.M.Gibbs, *Structure-borne sound sources in Buildings*, Building Acoustics Vol.1 No.4 313-329 (1994).

[15] A.T. Moorhouse, *Structure borne emission of installed machinery in buildings*, PhD Thesis, The University of Liverpool (1989).

[16] Leissa *Vibration of Shells*, Published by Acoustical Society of America. (1993)

[17] Leissa *Vibration of Plate*, Published by Acoustical Society of America. (1993)

[18] Ewins D.J., *Modal Testing:Theory and Practice*, Research Studies Press (1984)

[19] Petyt M., *Introduction To Finite Element Vibration Analysis*, Cambridge University Press (1990).

[20] R.Brewer and J.C.Tukker, *Resilient mounting system in buildings*, Applied Acoustics,9,77-101 (1976).

[21] A.T.Moorhouse and B.M.Gibbs, *Measurement of structure–borne sound emission from resiliently mounted machines in situ*, Journal of Sound and Vibration 180(1),143-161 (1995).

[22] J.M.Mondot and B.A.T Petersson, *Characterisation of structure-borne sound source: The source descriptor and the coupling function*, Journal of Sound and Vibration 114(3), 507-518 (1987).

[23] M.Ohlrich, *Terminal Source power for predicting structure borne sound transmission from main gearbox to a helicopter fuselage*, Inter-noise 95, 555-558 (1995).

[24] R.H.Lyon and J.W.Slack, *A Review of structural Noise Transmission*, The Shock and Vibration Digest, 14, 8, (1982).

[25] L.Cremer, M.Heckl and E.E.Ungar, *Structure –Born Sound*, Springer Verslag. Berlin,1973.

[26] R.G.White and J.G.Walker, *Noise and Vibration*, Ch.26.,Ellis Horwood Limited, Chichester U.K.,(1982)

[27] R.Melzig-Thiel, *Peculiarities and Results of the Pre-Determination of the Structure–born Sound Excitation of Buildings by Machines*, Inter-Noise 79, 909-911 (1979).

[28] Su Jianxin,A.T.Moorhouse and B.M.Gibbs,*Towards a practical characterisation for structure-borne sound source based on mobility techniques*, Journal of Sound and Vibration 185(4),737-741 (1995).

[29] L.Ji, B.R.Mace, R.J.Pinnington, *A power mode technique for estimating power transmission to a Flexible receiver*, Proc.IOA Spring Conference 2002, Salford (2002)

[30] V.I.Popkov, Vibroacoustic *Diagnosis and the Reduction of the Vibration of Ship borad Machinery*, JPRS Translation No.64931,Arlington Va,1975.

[31] B.À.T Petersson and J.Plunt, *Structure-borne Sound Transmission between a Machinery and Foundation*, Department of building Acoustics, Chalmers University of Technology, Report (1980).

[32] B.A.T Petersson and J.Plunt, *On Effective mobilities in the Prediction of Structure-borne Sound Transmission between a source structure and a Receiving Structure. Part1: Theoretical Background and basic Experimental studies*, Journal of Sound and Vibration 82 , 517-529 (1982).

[33] B.A.T Petersson and J. Plunt, *On Effective mobilities in the Prediction of Structure-borne Sound Transmission between a source structure and a Receiving Structure. Part2: Procedures for the Estimation of Mobilities*, Journal of Sound and Vibration 82, 531-540 (1982).

[34] R.A. Fulford, *Structure–Borne Sound Power and Source Characterisation in Multi-Point Connected System*, PhD Thesis, The University of Liverpool (1995)

[35] R.J.Pinnington and D.C.R. Pearce, *Multipole expansion of the vibration transmission between a source and a receiver*, Journal of Sound and Vibration 142(3),461-479 (1990).

[36] R.J. Pinnington, R.A.Fulford and M.Terry, *The use of polar mobilities for predicting the coupled response of machine Mounting systems*, Inter-Noise96, 1587-1592(1996).

[37] A.T.Moorhouse, J X Su, *Statistical mobility for multiple point excited structures*, The 8th International Congress on Sound and Vibration, 1973-1980 (2001).

[38] Robert J.M.Craik, *SOUND TRANSMISSION THROUGH BUILDINGS:Using Statistical Energy Analysis*, Chap.2, Published by Gower Publishing Limited (1996).

[39] Eugen Skudrzyk, *The mean-value method of predicting the dynamic response of complex vibrators*, J.Acoust.Soc.Am.,67(4),1105-1136 (1980).

[40] A.T.Moorhouse,B.M.Gibbs, *Simplified characterisation of multiple point excited structures using mobility matrix eigenvlues and eigenvector*, Acoustics Vol. 84, 843-853 (1998).

[41] Ronald E.Walpole,Raymond H.Myers, *Probability and Statistics for Engineers and Scientists*, The Macmillan Company (1972).

[42] P.M.Morse,K.U.Ingard, *Theoretical Acoustics*, McGraw-Hill, (1968)

[43] A .T. Moorhouse, *On the Characteristic power of structure- borne sound source*, Journal of Sound and Vibration 248(3), 441-459 (2001).

[44] M.R.Spiegel, *Theory and problems of theoretical mechanics*, Published by Schaum Publishing Company (1967)

[45] Xu Zhilun, *Elastic mechanics* Vol.2, Published by High Education Publishing Company (1982) (Chinese).

[46] E.Eichler, *Plate-edge admittances*. J.Acoust.Soc.Am.36,344-348(1964).

[47] C. Kauffmman, *Input mobilities and power flows for edge-excited, semi-infinite, plates*, J.Acoust.Soc.Am.103,1874-1884(1998).

[48] J X Su, A.T. Moorhouse, *A closed form solution for the mobility of an edge-excited, semi-infinite plate*, accepted for publication in J.Acoust.Soc.Am

[49] G.L.Squires, *Practical Physics*, Cambridge University (1985).

[50] A.T.Moorhouse,B.M.Gibbs, *Measurement of the characteristic power of structure–borne sound sources*, The 6th International Congress on Sound and Vibration (1999).

[51] William H. Press ... [et al.], *Numerical recipes in Fortran 90 : the art of parallel scientific computing*, Chap.2, Published Cambridge: Cambridge University Press, c1996. Edition 2nd ed

[52] M I. Mogilevski, *Point impedance's of rectangular plates and vibration isolation of machines*, Journal of Sound and Vibration 161(2),213-225 (1993).

[53] Lars V.Ahlfors, *Complex analysis*, Chap.3 McGraw-Hill Book Company,(1979)

APPENDIX A FORCE MOBILITY OF HOMOGENEOUS BEAM

A.1 The general form force mobility solution

For a homogeneous beam (see figureA-1) the force mobility from excited point x_0 to an

arbitrary point x on beam is given by:

$$Y_{vF} = Ae^{kx} + Be^{-kx} + Ce^{jkx} + De^{-jkx} \qquad x \le x_0 \qquad \text{(A1-1)}$$

$$Y_{vF} = ae^{kx} + be^{-kx} + ce^{jkx} + de^{-jkx} \qquad x_0 \le x$$

Where $k = \sqrt{\omega}(m_0 / \overline{B})^{1/4}$ is wave number . $\overline{B} = EI$ is the bending stiffness of beam.

The eight as yet unknown quantities (A,B,C,D,a,b,c,d,) can be determined from continue

and force balance condition at the excitation point and the ends supporting boundary

conditions. Basing on the continue and force balance condition at the excitation point

the four expression for   solving unknown quantities (A,B,C,D,a,b,c,d,)was given by

following

$$A - a = \frac{-j\omega}{4\overline{B}k^3}e^{-kx_0} \qquad \text{(A1-2)}$$

$$B - b = \frac{+j\omega}{4\overline{B}k^3}e^{kx_0}$$

$$C - c = j\frac{-j\omega}{4\overline{B}k^3}e^{-jkx_0}$$

$$D - d = -j\frac{-j\omega}{4\overline{B}k^3}e^{+jkx_0}$$

Four of the remaining expressions for solving unknown quantities are dependent upon the ends boundary condition.

A.1.1 Four of the remaining expressions based on boundary condition

a) Infinite beam

$a = 0$

$c = 0$

$B = 0;$

$D = 0$

b) A semi-infinite beam with simply supported at the one end (extending from x=0 to x=+∝);

$a = 0$

$c = 0$

$A + B + C + D = 0$

$A + B - C - D = 0$

c) A semi-infinite beam with guided supported at one end(extending from x=0 to x=+∝);

$a = 0$

$c = 0$

$A - B + jC - jD = 0$

$A - B - jC + jD = 0$

d) A semi-infinite beam with free supported at one end(extending from x=0 to x=+∝);

$a = 0$

$$c = 0$$

$$A + B - C - D = 0$$

$$A - B - jC + jD = 0$$

e) A semi-infinite beam with clamped   supported at one end (extending from x=0 to

x=+∝);

$$a = 0$$

$$c = 0$$

$$A + B + C + D = 0$$

$$A - B + jC - jD = 0$$

f) A finite beam of length

For finite beam of length the four of the remaining expressions do not list

A.2 Force mobility

A.2.1 Infinite and semi infinite beam

a) Infinite beam

$$Y_{vF} = \frac{\omega}{4\overline{B}k^3}(e^{-jk|x-x_0|} - je^{-k|x-x_0|})$$

b) A Semi-infinite with simply supported at one end

$$Y_{vF} = \frac{\omega}{4\overline{B}k^3}(je^{-k(x_0+x)} - je^{-k(x_0-x)} + e^{-jk(x_0-x)} - e^{-jk(x_0+x)}) \qquad x \le x_0$$

$$Y_{vF} = \frac{\omega}{4\overline{B}k^3}(je^{-k(x_0+x)} - je^{-k(x-x_0)} + e^{-jk(x-x_0)} - e^{-jk(x_0+x)}) \qquad x_0 \le x$$

c) A Semi-infinite beam with guided supported at one end

$$Y_{vF} = \frac{\omega}{4\overline{B}k^3}(-je^{-k(x_0+x)} - je^{-k(x_0-x)} + e^{-jk(x_0-x)} + e^{-jk(x_0+x)}) \qquad x \leq x_0$$

$$Y_{vF} = \frac{\omega}{4\overline{B}k^3}(-je^{-k(x_0+x)} - je^{-k(x-x_0)} + e^{-jk(x-x_0)} + e^{-jk(x_0+x)}) \qquad x \geq x_0$$

d) A Semi-infinite beam with free supported at one end

$$Y_{vF} = \frac{\omega}{4\overline{B}k^3}(-je^{-k(x_0-x)} + e^{-k(x_0+x)} + e^{-jk(x_0-x)} - je^{-jk(x_0+x)} + (1-j)(e^{-jkx}e^{-kx_0} + e^{-jkx_0}e^{-kx})) \qquad x \leq x_0$$

$$Y_{vF} = \frac{\omega}{4\overline{B}k^3}(-je^{-k(x-x_0)} + e^{-k(x_0+x)} + e^{-jk(x-x_0)} - je^{-jk(x_0+x)} + (1-j)(e^{-jkx}e^{-kx_0} + e^{-jkx_0}e^{-kx})) \qquad x \leq x_0$$

e) A Semi-infinite beam with clamped supported at one end

$$Y_{vF} = \frac{\omega}{4\overline{B}k^3}(-je^{-k(x_0-x)} + e^{-k(x_0+x)} + e^{-jk(x_0-x)} - je^{-jk(x_0+x)} - (1-j)(e^{-jkx}e^{-kx_0} + e^{-jkx_0}e^{-kx})) \qquad x \leq x_0$$

$$Y_{vF} = \frac{\omega}{4\overline{B}k^3}(-je^{-k(x-x_0)} + e^{-k(x_0+x)} + e^{-jk(x-x_0)} - je^{-jk(x_0+x)} - (1-j)(e^{-jkx}e^{-kx_0} + e^{-jkx_0}e^{-kx})) \qquad x \leq x_0$$

A.2.2 Finite beam of length

a Simply-simply

Closed form solution

$$Y_{vF} = \frac{-j\omega}{2\overline{B}k^3}(\frac{\sinh kx \sinh k(l-x_0)}{\sinh kl} - \frac{\sin kx \sin k(l-x_0)}{\sin kl}) \qquad 0 \leq x \leq x_0$$

$$Y_{vF} = \frac{-j\omega}{2\overline{B}k^3}(\frac{\sinh kx_0 \sinh k(l-x)}{\sinh kl} - \frac{\sin kx_0 \sin k(l-x)}{\sin kl}) \qquad x_0 \leq x \leq l$$

Infinite series expressions

$$Y_{vF} = \frac{2j\omega}{M}\sum_{n=1}^{\infty}\frac{\varphi_n(x_0)\varphi_n(x)}{\omega_n^2 - \omega^2}$$

where $\varphi_n(x) = \sin\frac{\pi\beta_n}{l}x$

$$\omega_n = (\frac{\beta_n \pi}{l})^2 \sqrt{\frac{\overline{B}}{m_0}} \quad \beta_n = n$$

b Guided-guided

Closed form solution

$$Y_{vF} = \frac{-j\omega}{2\overline{B}k^3}(\frac{\cosh kx \cosh k(l - x_0)}{\sinh kl} + \frac{\cos kx \cos k(l - x_0)}{\sin kl}) \qquad 0 \le x \le x_0$$

$$Y_{vF} = \frac{-j\omega}{2\overline{B}k^3}(\frac{\cosh kx_0 \cosh k(l - x)}{\sinh kl} + \frac{\cos kx_0 \cos k(l - x)}{\sin kl}) \qquad x_0 \le x \le l$$

Infinite series expression

$$Y_{vF} = \frac{2j\omega}{M} \sum_{n=1}^{\infty} \frac{\varphi_n(x_0)\varphi_n(x)}{\omega_n^2 - \omega^2} + \frac{1}{j\omega M}$$

where $\varphi_n(x) = \cos \dfrac{\pi \beta_n}{l} x$

$$\omega_n = (\frac{\beta_n \pi}{l})^2 \sqrt{\frac{\overline{B}}{m_0}} \quad \beta_n = n$$

c Free-free

Closed form solution

$$Y_{vF} = \frac{j\omega}{2\overline{B}k^3}(f_1(x_0)g_1(x) + f_2(x_0)g_2(x)) \qquad 0 \le x \le x_0$$

$$Y_{vF} = \frac{j\omega}{2\overline{B}k^3}(f_1(x)g_1(x_0) + f_2(x)g_2(x_0)) \qquad x_0 \le x \le l$$

where

$$f_1(x) = \cosh kx - \cosh k(l - x)\cos kl - \sinh k(l - x)\sin kl$$
$$- \cos kx + \cos k(l - x)\cosh kl - \sinh kl \sin k(l - x)$$

$$f_2(x) = \sinh kx + \sinh k(l-x)\cos kl - \sin kl \cosh k(l-x)$$
$$- \sin kx + \sinh kl \cos k(l-x) - \cosh kl \sin k(l-x)$$

$$g_1(x) = -(\sin kx + \sinh kx)/2(1 - \cosh kl \cos kl)$$

$$g_2(x) = (\cos kx + \cosh kx)/2(1 - \cosh kl \cos kl)$$

Infinite series expression

$$Y_{vF} = \frac{j\omega}{M}\sum_{n=1}^{\infty}\frac{\varphi_n(x_0)\varphi_n(x)}{\omega_n^2 - \omega^2} + \frac{1}{j\omega M}(1 + \frac{2\sqrt{3}}{l}(x_0 - \frac{l}{2})\frac{2\sqrt{3}}{l}(x - \frac{l}{2}))$$

where $\varphi_n(x) = \cosh(\frac{\pi\beta_n}{l}x) + \cos(\frac{\pi\beta_n}{l}x) + b_n(\sinh(\frac{\pi\beta_n}{l}x) + \sin(\frac{\pi\beta_n}{l}x))$

$$b_n = -(\cosh(\pi\beta_n) - \cos(\pi\beta_n))/(\sinh(\pi\beta_n) - \sin(\pi\beta_n))$$

$$\omega_n = (\frac{\beta_n\pi}{l})^2\sqrt{\frac{B}{m_0}}$$

β_n is root of equation $\cosh(\beta\pi)\cos(\beta\pi) - 1 = 0$. $\beta_0 = 0$ is root of this equation too, the correspondent model solution is second term of the expression of the mobility

$$\beta_1 = 1.5056, \quad \beta_2 = 2.4997, \cdots, \beta_n \approx n + 1/2$$

d Clamp-clamp

Closed form solution

$$Y_{vF} = \frac{j\omega}{2\overline{B}k^3}(f_1(x_0)g_1(x) + f_2(x_0)g_2(x)) \qquad 0 \le x \le x_0$$

$$Y_{vF} = \frac{j\omega}{2\overline{B}k^3}(f_1(x)g_1(x_0) + f_2(x)g_2(x_0)) \qquad x_0 \le x \le l$$

where

$$f_1(x) = \cosh kx - \cosh k(l-x)\cos kl - \sinh k(l-x)\sin kl$$
$$+ \cos kx - \cos k(l-x)\cosh kl + \sinh kl \sin k(l-x)$$

$$f_2(x) = \sinh kx + \sinh k(l-x)\cos kl - \sin kl \cosh k(l-x)$$
$$+ \sin kx - \sinh kl \cos k(l-x) + \cosh kl \sin k(l-x)$$

$$g_1(x) = (\sin kx - \sinh kx)/2(1 - \cosh kl \cos kl)$$

$$g_2(x) = -(\cos kx - \cosh kx)/2(1 - \cosh kl \cos kl)$$

Infinite series expression

$$Y_{vF} = \frac{j\omega}{M} \sum_{n=1}^{\infty} \frac{\varphi_n(x_0)\varphi_n(x)}{\omega_n^2 - \omega^2}$$

where $\varphi_n(x) = \cosh(\frac{\pi\beta_n}{l}x) - \cos(\frac{\pi\beta_n}{l}x) + b_n(\sinh(\frac{\pi\beta_n}{l}x) - \sin(\frac{\pi\beta_n}{l}x))$

$$b_n = -(\cosh(\pi\beta_n) - \cos(\pi\beta_n))/(\sinh(\pi\beta_n) - \sin(\pi\beta_n))$$

$$\omega_n = (\frac{\beta_n \pi}{l})^2 \sqrt{\frac{\overline{B}}{m_0}}$$

β_n is root of equation $\cosh(\beta\pi)\cos(\beta\pi) - 1 = 0$.

$$\beta_1 = 1.5056, \quad \beta_2 = 2.4997, \cdots, \beta_n \approx n + 1/2$$

e Clamp-free

Closed form solution

$$Y_{vF} = \frac{j\omega}{2\overline{B}k^3}(f_1(x_0)g_1(x) + f_2(x_0)g_2(x)) \qquad 0 \le x \le x_0$$

$$Y_{vF} = \frac{j\omega}{2\overline{B}k^3}(f_1(x)g_1(x_0) + f_2(x)g_2(x_0)) \qquad x_0 \le x \le l$$

where

$$f_1(x) = \cosh kx + \cosh k(l-x)\cos kl + \sinh k(l-x)\sin kl$$
$$+ \cos kx + \cos k(l-x)\cosh kl - \sinh kl \sin k(l-x)$$

$$f_2(x) = \sinh kx - \sinh k(l-x)\cos kl + \sin kl \cosh k(l-x)$$
$$+ \sin kx + \sinh kl \cos k(l-x) - \cosh kl \sin k(l-x)$$

$$g_1(x) = (\sin kx - \sinh kx)/2(1 + \cosh kl \cos kl)$$

$$g_2(x) = -(\cos kx - \cosh kx)/2(1 + \cosh kl \cos kl)$$

Infinite series expression

$$Y_{vF} = \frac{j\omega}{M} \sum_{n=1}^{\infty} \frac{\varphi_n(x_0)\varphi_n(x)}{\omega_n^2 - \omega^2}$$

$$\varphi_n(x) = \cosh(\frac{\pi\beta_n}{l}x) - \cos(\frac{\pi\beta_n}{l}x) + b_n(\sinh(\frac{\pi\beta_n}{l}x) - \sin(\frac{\pi\beta_n}{l}x))$$

$$b_n = -(\cosh(\pi\beta_n) + \cos(\pi\beta_n))/(\sinh(\pi\beta_n) + \sin(\pi\beta_n))$$

$$\omega_n = (\frac{\beta_n\pi}{l})^2\sqrt{\frac{\overline{B}}{m_0}}$$

β_n is root of equation $\cosh(\beta\pi)\cos(\beta\pi) + 1 = 0$.

$$\beta_1 = 0.597, \quad \beta_2 = 1.494, \beta_n = 2.500, \cdots, \beta_n \approx n - 1/2$$

$$\varphi_n(x) = \cosh(\frac{\pi\beta_n}{l}x) - \cos(\frac{\pi\beta_n}{l}x) + b_n(\sinh(\frac{\pi\beta_n}{l}x) - \sin(\frac{\pi\beta_n}{l}x))$$

$$b_n = -(\cosh(\pi\beta_n) + \cos(\pi\beta_n))/(\sinh(\pi\beta_n) + \sin(\pi\beta_n))$$

f Clamped-simply

Closed form solution

$$Y_{vF} = \frac{j\omega}{2\overline{B}k^3}(f_1(x_0)g_1(x) + f_2(x_0)g_2(x)) \qquad 0 \leq x \leq x_0$$

$$Y_{vF} = \frac{j\omega}{2\overline{B}k^3}(f_1(x)g_1(x_0) + f_2(x)g_2(x_0)) \qquad x_0 \leq x \leq l$$

where

$$f_1(x) = \cosh kl \sin k(l-x) - \cos kl \sinh k(l-x)$$

$$f_2(x) = \sinh kl \sin k(l-x) - \sin kl \sinh k(l-x)$$

$$g_1(x) = (\sin kx - \sinh kx)/(\cosh kl \sin kl - \sinh kl \cos kl)$$

$$g_2(x) = (-\cos kx + \cosh kx)/(\cosh kl \sin kl - \sinh kl \cos kl)$$

Infinite series expression

$$Y_{vF} = \frac{j\omega}{M} \sum_{n=1}^{\infty} \frac{\varphi_n(x_0)\varphi_n(x)}{\omega_n^2 - \omega^2}$$

$$\varphi_n(x) = \cosh(\frac{\pi\beta_n}{l}x) - \cos(\frac{\pi\beta_n}{l}x) + b_n(\sinh(\frac{\pi\beta_n}{l}x) - \sin(\frac{\pi\beta_n}{l}x))$$

$$b_n = -(\cosh(\pi\beta_n) - \cos(\pi\beta_n))/(\sinh(\pi\beta_n) - \sin(\pi\beta_n))$$

$$\omega_n = (\frac{\beta_n\pi}{l})^2 \sqrt{\frac{\overline{B}}{m_0}}$$

β_n is root of equation $\cosh(\beta\pi)\sin(\beta\pi) - \sinh(\beta\pi)\cos(\beta\pi) = 0$.

$$\beta_1 = 1.249\cdots, \quad \beta_2 = 2.2500,\cdots, \beta_n \approx n+1/4$$

g Clamped-guided

Closed form solution

$$Y_{vF} = \frac{-j\omega}{2Bk^3}(f_1(x_0)g_1(x) + f_2(x_0)g_2(x)) \quad 0 \le x \le x_0 \le l$$

$$Y_{vF} = \frac{-j\omega}{2Bk^3}(f_1(x)g_1(x_0) + f_2(x)g_2(x_0)) \quad 0 \le x_0 \le x \le l$$

$$f_1(x) = \cos kl \cosh k(l-x) - \cosh kl \cos k(l-x)$$

$$f_2(x) = \sin kl \cosh k(l-x) + \sinh kl \cos k(l-x)$$

$$g_1(x) = (\cosh kx - \cos kx)/(\cos kl \sinh kl + \sin kl \cosh kl)$$

271

$$g_2(x) = (\sinh kx - \sin kx)/(\cos kl \sinh kl + \sin kl \cosh kl)$$

Infinite series expression

$$Y_{vF} = \frac{j\omega}{M} \sum_{n=1}^{\infty} \frac{\varphi_n(x_0)\varphi_n(x)}{\omega_n^2 - \omega^2}$$

$$\varphi_n(x) = \cosh(\frac{\pi\beta_n}{l}x) - \cos(\frac{\pi\beta_n}{l}x) + b_n(\sinh(\frac{\pi\beta_n}{l}x) - \sin(\frac{\pi\beta_n}{l}x))$$

$$b_n = -(\sinh(\pi\beta_n) + \sin(\pi\beta_n))/(\cosh(\pi\beta_n) - \cos(\pi\beta_n))$$

$$\omega_n = k_n^2\sqrt{\frac{B}{m_0}} = (\frac{\beta_n\pi}{l})^2\sqrt{\frac{B}{m_0}}$$

β_n is root of equation $\cosh(\beta\pi)\sin(\beta\pi) + \sinh(\beta\pi)\cos(\beta\pi) = 0$.

$$\beta_1 = 0.7528, \quad \beta_2 = 1.7500, \cdots, \beta_n \approx n - 1/4$$

h Free-guided

Closed form solution

$$Y_{vF} = \frac{-j\omega}{2Bk^3}(f_1(x_0)g_1(x) + f_2(x_0)g_2(x)) \quad 0 \le x \le x_0 \le l$$

$$Y_{vF} = \frac{-j\omega}{2Bk^3}(f_1(x)g_1(x_0) + f_2(x)g_2(x_0)) \quad 0 \le x_0 \le x \le l$$

$$f_1(x) = \cos kl \cosh k(l-x) + \cosh kl \cos k(l-x)$$

$$f_2(x) = \sin kl \cosh k(l-x) - \sinh kl \cos k(l-x)$$

$$g_1(x) = (\cosh kx + \cos kx)/(\cos kl \sinh kl + \sin kl \cosh kl)$$

$$g_2(x) = (\sinh kx + \sin kx)/(\cos kl \sinh kl + \sin kl \cosh kl)$$

Infinite series expression

$$Y_{vF} = \frac{j\omega}{M} \sum_{n=1}^{\infty} \frac{\varphi_n(x_0)\varphi_n(x)}{\omega_n^2 - \omega^2} + \frac{1}{j\omega M}$$

$$\varphi_n(x) = \cosh(\frac{\pi\beta_n}{l} x) + \cos(\frac{\pi\beta_n}{l} x) + b_n (\sinh(\frac{\pi\beta_n}{l} x) + \sin(\frac{\pi\beta_n}{l} x))$$

$$b_n = -(\sinh(\pi\beta_n) - \sin(\pi\beta_n)) / (\cosh(\pi\beta_n) + \cos(\pi\beta_n))$$

$$\omega_n = k_n^2 \sqrt{\frac{\bar{B}}{m_0}} = (\frac{\beta_n \pi}{l})^2 \sqrt{\frac{\bar{B}}{m_0}}$$

β_n is root of equation $\cosh(\beta\pi)\sin(\beta\pi) + \sinh(\beta\pi)\cos(\beta\pi) = 0$. $\beta_0 = 0$ is root of this equation too, the correspondent model solution is second term of the expression of the mobility

$$\beta_1 = 0.7528, \quad \beta_2 = 1.7500, \cdots, \beta_n \approx n - 1/4$$

i Simply-guided

$$Y_{vF} = \frac{-j\omega}{2Bk^3} (f_1(x_0)g_1(x) + f_2(x_0)g_2(x)) \quad 0 \le x \le x_0 \le l$$

$$Y_{vF} = \frac{-j\omega}{2Bk^3} (f_1(x)g_1(x_0) + f_2(x)g_2(x_0)) \quad 0 \le x_0 \le x \le l$$

$$f_1(x) = \cos kl \cosh k(l - x)$$

$$f_2(x) = \cosh kl \cos k(l - x)$$

$$g_1(x) = \sinh kx / \cos kl \cosh kl$$

$$g_2(x) = -\sin x / (\cos kl \cosh kl)$$

$$Y_{vF} = \frac{2j\omega}{M} \sum_{n=1}^{\infty} \frac{\varphi_n(x_0)\varphi_n(x)}{\omega_n^2 - \omega^2}$$

$$\varphi_n(x) = \sin(\frac{\pi \beta_n}{l} x)$$

$$\omega_n = k_n^2 \sqrt{\frac{B}{m_0}} = (\frac{\beta_n \pi}{l})^2 \sqrt{\frac{B}{m_0}}$$

β_n is root of equation $\cos(\beta \pi) = 0$ $\beta_n = n - 1/2$.

j Free-simply

Closed form solution

$$Y_{vF} = \frac{j\omega}{2Bk^3}(f_1(x_0)g_1(x) + f_2(x_0)g_2(x)) \quad 0 \le x \le x_0 \le l$$

$$Y_{vF} = \frac{j\omega}{2Bk^3}(f_1(x)g_1(x_0) + f_2(x)g_2(x_0)) \quad 0 \le x_0 \le x \le l$$

where

$$f_1(x) \triangleq \sin kl \sinh k(l-x) + \sinh kl \sin k(l-x)$$

$$f_2(x) = \cos kl \sinh k(l-x) + \cosh kl \sin k(l-x)$$

$$g_1(x) = -(\cosh kx + \cos kx)/(\cosh kl \sin kl - \sinh kl \cos kl)$$

$$g_2(x) = (\sin kx + \sinh kx)/(\cosh kl \sin kl - \sinh kl \cos kl)$$

Infinite series expression

$$Y_{vF} = \frac{j\omega}{M} \sum_{n=1}^{\infty} \frac{\varphi_n(x_0)\varphi_n(x)}{\omega_n^2 - \omega^2} + \frac{1}{jM\omega} \frac{\sqrt{3}(l-x_0)}{l} \frac{\sqrt{3}(l-x)}{l}$$

$$\varphi_n(x) = \cosh(\frac{\pi \beta_n}{l} x) + \cos(\frac{\pi \beta_n}{l} x) + b_n(\sinh(\frac{\pi \beta_n}{l} x) + \sin(\frac{\pi \beta_n}{l} x))$$

$$b_n = -(\cosh(\pi \beta_n) + \cos(\pi \beta_n))/(\sinh(\pi \beta_n) + \sin(\pi \beta_n))$$

$$\omega_n = k_n^2 \sqrt{\frac{\overline{B}}{m_0}} = (\frac{\beta_n \pi}{l})^2 \sqrt{\frac{\overline{B}}{m_0}}$$

β_n is root of equation $\cosh(\beta\pi)\sin(\beta\pi) - \sinh(\beta\pi)\cos(\beta\pi) = 0$. $\beta_0 = 0$ is root of this equation too, the correspondent model solution is second term of the expression of the mobility

$$\beta_1 = 1.249\cdots, \quad \beta_2 = 2.2500, \cdots, \beta_n \approx n + 1/4$$
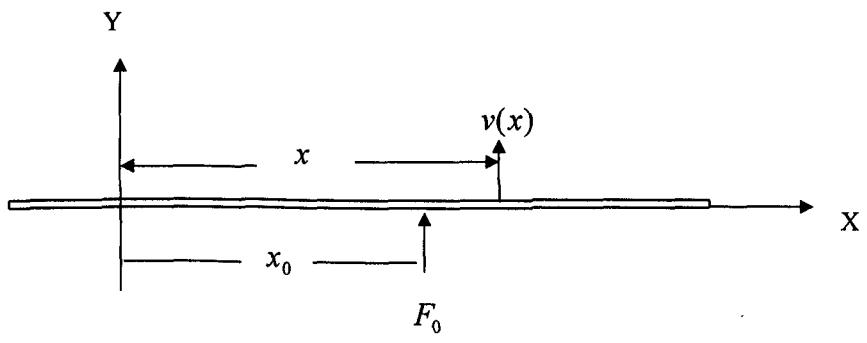
Figure A-1 A homogeneous beam excited by a transverse force

APPENDIX B A CLOSED FORM SOLUTION FOR MOBILITY OF AN EDGE-EXCITED, SEMI-INFINITE PLATE

B.1 Differential equation and boundary condition

For a thin elastic plate of constant thickness h, the transverse motion under sinusoidal excitation of angular frequency ω satisfies the following differential equation:

$$(D\nabla^4 - \omega^2 m'')w = 0 \qquad\qquad\qquad (\text{B-1})$$

where $D = Eh^3/12(1-v^2)$ is the bending stiffness, E is Young's modulus, v is Poisson's ratio, and m" is the mass per unit area. (The notation used throughout this appendix is consistent with both Eichler and Kauffmann).

Consider a semi-infinite plate (see FigureB-1). The plate occupies- $\infty<y<\infty$ x$\leq$0 with a free edge at x=0 except for the area $|y| < a$ where it is excited by an arbitrary load. The transverse force, normal and tangential moments at the edge are related to the plate displacement by the boundary conditions

$$-D\frac{\partial}{\partial x}[\frac{\partial^2}{\partial x^2}w + (2-v)\frac{\partial^2}{\partial y^2}w] = N - \frac{\partial H}{\partial y} = f(y) \qquad\qquad (\text{B-2})$$

$$-D[\frac{\partial^2}{\partial x^2}w + v\frac{\partial^2}{\partial y^2}w] = m(y) \qquad\qquad\qquad (\text{B-3})$$

where N is the distribution of the transverse force per unit length, H is the distribution of the normal moment per unit length, $f(y)$ is the externally applied force per unit length and $m(y)$ the externally applied tangential moment per unit length.

B.2 Point mobility matrix

The point mobilities at $x=0$ $y=0$ are of interest, and can be obtained by letting $f(y) = N - \partial H/\partial y = F_z \delta(y) - M_n \delta'(y)$ and $m(y) = M_t \delta(y)$ and solving for the velocity and angular velocity at $x=0$ $y=0$

$$\begin{bmatrix} \Omega_n \\ \Omega_t \\ V_z \end{bmatrix} = i\omega \begin{bmatrix} \partial w/\partial y \\ -\partial w/\partial x \\ w \end{bmatrix} = [Y] \begin{bmatrix} M_n \\ M_t \\ F_z \end{bmatrix}$$

(B-4)

where Ω_n is the normal angular velocity, Ω_t the tangential angular velocity and V_z the transverse velocity. Y is the point mobility matrix and can be expressed as:

$$Y = (m''D)^{-\frac{1}{2}} \begin{bmatrix} y_{\Omega_n M_n} k^2 & 0 & 0 \\ 0 & y_{\Omega_t M_t} k^2 & y_{\Omega_t F_z} k \\ 0 & y_{V_z M_t} k & y_{V_z F_z} \end{bmatrix}$$

(B-5)

the elements of the matrix are expressed in terms of a non-dimensional wave number p as:

$$\text{Re}(y_{\Omega_n M_n}) = \frac{2}{\pi} \int_0^1 p^2 \mu_1(p) M_+^{2}(p) \frac{dp}{Det(p)} + 2p_1^2 \frac{1}{\gamma}$$

(B-6)

$$\text{Im}(y_{\Omega_n M_n}) = \frac{2}{\pi} PV \int_1^\infty \frac{p^2 dp}{det(p)} - \frac{2}{\pi} \int_0^1 \frac{\mu_+(p) M_-^{2}(p) p^2 dp}{Det(p)}$$

(B-7)

$$\text{Re}(y_{\Omega_t M_t}) = \frac{2}{\pi} \int_0^1 \frac{\mu_1(p) \mu_+^{2}(p) M_-^{2}(p) dp}{Det(p)} + \frac{2\mu_-(p_1)\mu_+(p_1)}{\gamma}$$

(B-8)

$$\text{Im}(y_{\Omega_t M_t}) = \frac{2}{\pi}(\int_0^1 \frac{\mu_+(p)\mu_1^{2}(p) M_+^{2}(p) dp}{Det(p)} + PV \int_1^\infty \frac{\mu_-(p)\mu_+(p) dp}{det(p)})$$

(B-9)

$$\text{Re}(y_{\Omega_t F_z}) = -\frac{2}{\pi} \int_0^1 \mu_1(p)\mu_+(p) M_-(p) M_+(p) \frac{dp}{Det(p)} +$$

$$- [\mu_-(p_1) M_+(p_1) + \mu_+(p_1) M_-(p)]\frac{1}{\gamma}$$

(B-10)

278

$$\text{Im}(y_{\Omega,F_z}) = -\frac{1}{\pi}\int_0^1 [\mu_1^2(p)M_+^3(p) - \mu_+^2(p)M_-^3(p)]\frac{dp}{Det(p)}$$
$$-\frac{1}{\pi}PV\int_1^\infty \mu_+(p)M_-(p) + \mu_-(p)M_+(p)\frac{dp}{det(p)} \tag{B-11}$$

$$\text{Re}(y_{V,F_z}) = \frac{2}{\pi}\int_0^1 \mu_1(p)M_+^2(p)\frac{dp}{Det(p)} + 2\frac{1}{\gamma} \tag{B-12}$$

$$\text{Im}(y_{V,F_z}) = \frac{2}{\pi}PV\int_1^\infty \frac{dp}{det(p)} - \frac{2}{\pi}\int_0^1 \mu_+ M_-^2(p)\frac{dp}{Det(p)} \tag{B-13}$$

where $\mu_1(p) \equiv \sqrt{1-p^2}$ $\quad \mu_\pm(p) \equiv \sqrt{p^2 \pm 1}$, p should be understood as real integration variable

To be clear, here and from now on the Authors distinguish the square root symbol in the real field from square root symbols in the complex field.

'$\sqrt{}$' indicate square root in the real field , the function $\sqrt{x}$ should be understand single-value function , x must be real positive.

'$()^{1/2}$' indicate square root in the complex field , function $(w)^{1/2}$ is multiple-value function , the value of function can be determinate after choosing a single-value branch .

For example the square root of '-3 'is written as $(-3)^{1/2}$ not $\sqrt{-3}$,In this appendix $\sqrt{-3}$ should be understand as meaningless. The value of the function $(-3)^{1/2} = \sqrt{3}i$ or $(-3)^{1/2} = -\sqrt{3}i$ depends on how a single-value branch is chosen.

$$M_\pm(p) \equiv 1 \pm (1-v)p^2 \quad det(p) = \mu_-(p)M_+^2(p) - \mu_+(p)M_-^2(p) \tag{B-14}$$

$$\begin{aligned} Det(p) &= \mu_1^2(p)M_+^4(p) + \mu_+^2(p)M_-^4(p) \\ &= 2[-(3+v)(1-v)^3 p^8 + 2(1-3v)(1-v)p^4 + 1]] \\ &= -2(3+v)(1-v)^3(p^4 - p_1^4)(p_1^4 + p_2^4) \end{aligned} \tag{B-15}$$

$$p_1 = \left| (1-3v + 2\sqrt{v^2 + (1-v)^2})/(1-v)^2(3+v) \right|^{1/4} \tag{B-16}$$

$$p_2 = \left| \left(3v + 2\sqrt{v^2 + (1-v)^2} - 1\right) \middle/ (1-v)^2 (3+v) \right|^{1/4}$$ (B-17)

p_1 is one root of $\det(p)$ on the real axis and lies between 1 and $[4(2\sqrt{2}-1)/7]^{1/4}$ for $0 \le v \le 0.5$ [47].

The integration variable, p should be understood as a real integration variable and PV stands for principle value in Eqs.(B-7),(B-9),(B-11),(B-13) (there is one simple pole at $p = p_1$ between 1 and ∞ on the real axis). $1/\gamma$ is the residue of the function $1/\det(p)$ at the simple pole $p = p_1$. It can be expressed as:

$$\frac{1}{\gamma} = \lim_{p \to p_1} \frac{p - p_1}{\det(p)} = \frac{\mu_-(p_1)M_+^2(p_1) + \mu_+(p_1)M_-^2(p_1)}{8(3+v)(1-v)^3 p_1^3 (p_1^4 + p_2^4)}$$ (B-18)

The second form on the right hand side of Eq. 18 differs from Kauffmann's (although it is still equivalent) and is used in the following proofs. Expressions (B-6)–(B-13) can be obtained directly from Eq.s (47)-(52) of Kaufmann's paper[47] or from Eq.s (18)-(25) of Eichler's paper[46] in the case of ka→0, but are repeated here for completeness.

Eichler and Kaufmann both evaluated numerical results for the point mobility but Kaufmann's, with greater computing power available, are more accurate[47]. From his numerical results for Poisson's ratio $v = 0.3$, he conjectured that following relations might be satisfied for all values of Poisson's ratio, $(0 < v < 0.5.)$

$\text{Im}(y_{V_z F_z}) = 0$, $\text{Re}(y_{\Omega_t F_z}) = \text{Im}(y_{\Omega_t F_z})$, $\text{Re}(y_{\Omega_n M_n}) = \text{Re}(y_{\Omega_t M_t})$

These relations are formally proved in the following section.

B.3 Proof for the conjectures and closed form expressions point mobility

It will now be shown that the above conjectures can be proved and most elements of the point

mobility matrix can be expressed by closed form expressions instead of integration formulae.

Some definition of symbols is needed before completion of the proof.

$\int_\Gamma F(z)dz$ stands for integration on the complex plane z, the real and imaginary axes of which

are denoted x and y. $z \equiv x+yi$ is a complex integration variable, and x and y real integration

variables. Γ is the contour of integration on the complex plane z.

a. Proof of $\text{Im}(y_{V_iF_i}) = 0$

To prove that Eq. (B-13) is equal to zero we consider the following integral around a closed

contour Γ:

$$\int_\Gamma \frac{dp}{\det(z)}, \quad \widetilde{\det}(z) \equiv \widetilde{\mu}_-(z)M_+^{\ 2}(z) - \widetilde{\mu}_+(z)M_-^{\ 2}(z) \tag{B-19}$$

where $M_\pm(z) \equiv 1 \pm (1-v)z^2$ and $\widetilde{\mu}_\pm(z)$ is a single-valued branch formed by the square root

with a positive real part of the multiple-valued function $(z^2 \pm 1)^{1/2}$ [52]. The contour of

integration Γ is shown in FigureB-2 in which Γ_{c1} and Γ_{c2} are semi-circles of radius ε. The

integrand is analytic within Γ, so the integral should be zero .i.e

$$\int_\Gamma \frac{dz}{\widetilde{\det}(z)} = 0 \tag{B-20}$$

and this integration can be rewritten as:

$$\int_{\Gamma} \frac{1}{\det(z)} dz = \int_{\Gamma_1} + \int_{\Gamma_{c1}} + \int_{\Gamma_2} + \int_{\Gamma_{CR}} + \int_{\Gamma_3} + \int_{\Gamma_{c2}} + \int_{\Gamma_4} \frac{1}{\det(z)} dz = I_1 + I_{c1} + I_2 + I_{CR} + I_3 + I_{c2} + I_4$$

(B-21)

The sub integrals in (21) are now evaluated. To evaluate I_1, we rewrite in terms of $Det(x)$:

$$I_1 = i \int_0^1 \frac{\mu_1(x) M_+^{\ 2}(x) dx}{-Det(x)} + \int_0^1 \frac{\mu_+(x) M_-^{\ 2}(x) dx}{-Det(x)} + \int_1^{p_1-\varepsilon} \frac{dx}{\det(x)} \qquad , (B-22)$$

$$\mu_1(x) \equiv \sqrt{1-x^2} \quad \mu_{\pm}(x) \equiv \sqrt{x^2 \pm 1}$$

$M_{\pm}(x) = 1 \pm (1-v)x^2$ and $\det(x) = \mu_-(x) M_+^{\ 2}(x) - \mu_+(x) M_-^{\ 2}(x)$

$$I_2 = \int_{p_1+\varepsilon}^R \frac{dx}{\det(x)}$$

(B-23)

To evaluate I$_3$ let iy replace z so that we have

$$I_3 = \int_{iR}^{i(p_1+\varepsilon)} \frac{dz}{\widetilde{\det}(z)} = \int_{p_1+\varepsilon}^R \frac{dy}{\det(y)} = I_2$$

(B-24)

$$I_4 = \int_{i(p_1-\varepsilon)}^0 \frac{dz}{\widetilde{\det}(z)} = i \int_0^1 \frac{\mu_1(y) M_+^{\ 2}(y) dy}{Det(y)} + \int_0^1 \frac{\mu_+(y) M_-^{\ 2}(y) dy}{-Det(y)} + \int_1^{p_1-\varepsilon} \frac{dy}{\det(y)}$$

(B-25)

while

$$\lim_{\varepsilon \to 0}(I_{c1} + I_{c2}) = -\pi i (\text{Res} \frac{1}{\widetilde{\det}(p_1)} + \text{Res} \frac{1}{\widetilde{\det}(ip_1)}) = 0$$

(B-26)

$$\lim_{R \to \infty} I_{CR} = 0$$

(B-27)

because: if $R > \max(1, 1/(1-v), \frac{3|2(1-3v)(1-v)|}{(3+v)(1-v)^3})^{1/4}, (\frac{1}{(3+v)(1-v)^3})^{1/8})$

$$\left| \int_{\Gamma_{CR}} \frac{1}{\det(z)} \right| \le \frac{24\sqrt{2}}{2|(3+v)(1-v)^3||R|^2} \frac{\pi R}{2R}$$

(B-28)

so adding the non-zero integrals, I_1, I_2, I_3, I_4 some terms cancel leaving

$$\lim_{\substack{R \to \infty \\ \varepsilon \to 0}} \int_\Gamma \frac{1}{\widetilde{\det}(z)} dz = 2(PV \int_1^\infty \frac{dx}{\det(x)} - \int_0^1 \frac{\mu_+(x) M_-^2(x) dx}{Det(x)}) = 0 \qquad \text{(B-29)}$$

Comparing Eq.s (B-29) and (B-13) shows that the imaginary part of the point mobility is identically zero, in other words that edge mobilities, like the point mobility of an infinite plate, are pure real.

b Proof of $\mathrm{Re}(y_{\Omega_i F_z}) = \mathrm{Im}(y_{\Omega_i F_z})$

The proof follows similar lines to the above and proceeds by considering the integral:

$$\int_\Gamma F(z) dz = \int_\Gamma \frac{\widetilde{\mu}_-(z) M_+(z) + \widetilde{\mu}_+(z) M_-(z) \, dz}{\widetilde{\det}(z)} \qquad \text{(B-30)}$$

The single valued branch and contour of integration is selected as above. Again, according to the residue theorem, this integral is zero around the contour and can be expressed as a sum of integrals (denoted by the same symbols as above for simplicity) i.e.

$$0 = \int_{\Gamma_1} + \int_{\Gamma_{c1}} + \int_{\Gamma_2} + \int_{\Gamma_{CR}} + \int_{\Gamma_3} + \int_{\Gamma_{c2}} + \int_{\Gamma_4} F(z) dz = I_1 + I_{c1} + I_2 + I_{CR} + I_3 + I_{c2} + I_4 \quad \text{(B-31)}$$

By rewriting the integrand of (B-30) in terms of Det(z) we get

$$I_1 = \int_0^1 \frac{\mu_1^2(x) M_+^3(x) - \mu_+^2(x) M_-^3(x)}{Det(x)} dx - i \int_0^1 \frac{2\mu_1(x) M_+(x)\mu_+(x) M_-(x)}{Det(x)} dx + \int_1^{p_1-\varepsilon} \frac{\mu_-(x) M_+(x) + \mu_+(x) M_-(x)}{\det(x)} dx$$
$$\text{(B-32)}$$

$$I_2 = \int_{p_1+\varepsilon}^R \frac{\mu_-(x) M_+(x) + \mu_+(x) M_-(x)}{\det(x)} dx \qquad \text{(B-33)}$$

To evaluate I_3 let iy replace z giving

$$I_3 = i \int_{p_1+\varepsilon}^R \frac{\mu_-(y) M_+(y) + \mu_+(y) M_-(y)}{\det(y)} dy = i I_2 \qquad \text{(B-34)}$$

$$I_4 = -\int_0^1 \frac{2\mu_1(y)M_+(y)\mu_+(y)M_-(y)}{Det(y)}dy +$$

$$i\int_0^1 \frac{\mu_1^2(y)M_+^3(y) - \mu_+^2(y)M_-^3(y)}{Det(y)}dy + i\int_1^{p_1-\varepsilon}\frac{\mu_-(y)M_+(y) + \mu_+(y)M_-(y)}{det(y)}dy \qquad \text{(B-35)}$$

while $\lim\limits_{R\to\infty} I_{\Gamma_{CR}} = 0$ \hfill (B-36)

$$\lim\limits_{\varepsilon\to 0} I_{\Gamma_{c1}} = -\pi i\,\frac{\mu_-(p_1)M_+(p_1) + \mu_+(p_1)M_-(p_1)}{\gamma} \qquad \text{(B-37)}$$

$$\lim\limits_{\varepsilon\to 0} I_{\Gamma_{c2}} = -\pi\,\frac{\mu_-(p_1)M_+(p_1) + \mu_+(p_1)M_-(p_1)}{\gamma} \qquad \text{(B-38)}$$

so

$$\lim\limits_{\substack{R\to\infty \\ \varepsilon\to 0}} \int_\Gamma F(z)dz = (1+i)\int_0^1 \frac{\mu_1^2(x)M_+^3(x) - \mu_+^2(x)M_-^3(x) - 2\mu_1(x)M_+(x)\mu_+(x)M_-(x)}{Det(x)}dx +$$

$$(1+i)PV\int_1^\infty \frac{\mu_-(x)M_+(x) + \mu_+(x)M_-(x)}{det(x)}dx - \pi(1+i)[\mu_+(p_1)M_-(p_1) + \mu_-(p_1)M_+(p_1)]\frac{1}{\gamma} = 0$$

$$\text{(B-39)}$$

Multiplying both sides of Eq. (B-39) by factor $1/\pi(1+i)$ shows that the difference of Eq.s (B-10) and (B-11) is zero, thereby proving that the phase of the cross mobility is constant at $\pi/4$ irrespective of the Poisson's ratio.

c . Real part of point force mobility

To evaluate the real part of the point mobility we proceed by considering the integral:

$$\int_\Gamma F(z)dz = \int_\Gamma \frac{\tilde{\mu}_-(z)f(z)dz}{Det(z)}, \quad f_1(z) \equiv ((1+(1-v)z^2)^2 \qquad \text{(B-40)}$$

where $\tilde{\mu}_-(\dot{z})$ is a single-valued branch formed by the square root with a positive **imaginary part** of the multiple-valued function $(z^2 - 1)^{1/2}$.

The contour of integration Γ is shown in FigureB-3. The integrand is analytic within Γ except at three simple poles: $(z_1 = ip_1 \quad z_2 = p_2 e^{\pi i/4} \quad z_3 = p_2 e^{3\pi i/4})$, where p_2 is defined in Eq.s (B-17).

Expression (B-40) can be rewritten as

$$\int_\Gamma F(z)dz = \int_{\Gamma_1} + \int_{\Gamma_{c2}} + \int_{\Gamma_2} + \int_{\Gamma_3} + \int_{\Gamma_{c1}} + \int_{\Gamma_4} + \int_{\Gamma_{CR}} F(z)dz = I_1 + I_{c2} + I_2 + I_3 + I_{c1} + I_4 + I_{CR} \qquad (B-41)$$

$$I_1 = \int_{-R}^{-(p_1+\varepsilon)} \frac{-\mu_-(x)M_+^{\,2}(x)}{Det(x)} dx = \int_{p_1+\varepsilon}^{R} \frac{-\mu_-(x)M_+^{\,2}(x)}{Det(x)} dx \qquad (B-42)$$

$$I_2 = \int_{-p_1+\varepsilon}^{-1} \frac{-\mu_-(x)M_+^{\,2}(x)}{Det(x)} dx + i\int_{-1}^{0} \frac{\mu_1(x)M_+(x)}{Det(x)} dx = $$
$$i\int_0^1 \frac{\mu_1(x)M_+(x)}{Det(x)} dx - \int_1^{p_1-\varepsilon} \frac{\mu_-(x)M_+^{\,2}(x)}{Det(x)} dx \qquad (B-43)$$

$$I_3 = i\int_0^1 \frac{\mu_1(x)M_+(x)}{Det(x)} dx + \int_1^{p_1-\varepsilon} \frac{\mu_-(x)M_+^{\,2}(x)}{Det(x)} dx = -I_2^* \qquad (B-44)$$

where '$*$' mean complex conjugate

$$I_4 = \int_{p_1+\varepsilon}^{R} \frac{\mu_-(x)M_+^{\,2}(x)}{Det(x)} dx = -I_1 \qquad (B-45)$$

while $\lim\limits_{\varepsilon \to 0} I_{c2} = \pi i \mu_-(p_1)M_+^{\,2}(p_1)/4\Lambda_1 \qquad (B-46)$

$\Lambda_1 \equiv 2(3+v)(1-v)^3 p_1^{\,3}(p_1^{\,4} + p_2^{\,4}) \qquad (B-47)$

$\lim\limits_{\varepsilon \to 0} I_{c1} = \pi i \mu_-(p_1)M_+^{\,2}(p_1)/4\Lambda_1 \qquad (B-48)$

$\lim\limits_{R \to \infty} I_{CR} = 0 \qquad (B-49)$

According to the residue theorem the value of the integral is given by the sum of the residues of the poles with .

$$\int_\Gamma F(z)dz = 2\pi i(\text{Res}F(z_1) + \text{Res}F(z_2) + \text{Res}F(z_3)) \tag{B-50}$$

$$\text{Res}F(z_1) = \mu_+(p_1)M_-^{\ 2}(p_1)/4\Lambda_1 \tag{B-51}$$

$$\text{Res}F(z_2) = (\alpha + \beta i)(1 + i(1-\nu)p_2^{\ 2})^2 e^{-\pi 3/4}/4\Lambda_2 \tag{B-52}$$

$$\Lambda_2 \equiv 2(3+\nu)(1-\nu)p_2^{\ 3}(p_1^{\ 4} + p_2^{\ 4}) \tag{B-53}$$

where $\alpha = (\sqrt{\sqrt{1+p_2^{\ 4}}-1})\sqrt{2}/2$, $\beta = (\sqrt{\sqrt{1+p_2^{\ 4}}+1})\sqrt{2}/2$ are the real and imaginary parts of $(p_2^{\ 2}i-1)^{1/2}$ respectively

$$\text{Res}F(z_3) = -(-\alpha + \beta i)(1 - i(1-\nu)p_2^{\ 2})^2 e^{\pi 3/4}/4\Lambda_2 \tag{B-54}$$

Note that $\text{Res}F(z_2)$ is the complex conjugate of $\text{Res}F(z_3)$

Finally, we obtain

$$\frac{2}{\pi}\int_0^1 \frac{\mu_1(x)M_+^{\ 2}(x)}{Det(x)}dx = \frac{\sqrt{2}}{2}\text{Re}(\beta - \alpha + (\beta + \alpha)i)f_1(p_2 e^{3\pi/4})/\Lambda_2) + (\mu_+(p_1)f_1(ip_1) - \mu_-(p_1)f_1(p_1)/2\Lambda_1 \tag{B-55}$$

The second term of Eq. (B-55) is zero since p_1 is a root of $det(p)$, so that substitution of Eq.(B-55) into Eq. (B-12) yields:

$$\text{Re}(y_{V_zF_z}) = \frac{\sqrt{2}}{2}\text{Re}(\beta - \alpha + (\beta + \alpha)i)f_1(p_2 e^{3\pi/4})/\Lambda_2) + \frac{2}{\gamma} \tag{B-56}$$

Thus, the real part of the force mobility at an edge varies from the infinite plate value by a simple function of Poisson's ratio.

d Real part of the point normal moment mobility

First we must rewrite the first term in Eq.(B-6):

$$\int_0^1 \frac{x^2 \mu_1(x) M_+^2(x) dx}{Det(x)} = \int_0^1 \frac{(1-v)^2 \mu_1(x) x^2 dx}{-2(3+v)(1-v)^3(x^4 - p_1^4)}$$

$$+ \int_0^1 \frac{\mu_1(x)[(1-(1-v)^2 p_2^4)x^2 + 2(1-v)x^4]dx}{Det(x)} \tag{B-57}$$

The first term on the right hand side of Eq. (B-57) can be obtained directly:

$$\int_0^1 \frac{(1-v)^2 \sqrt{1-x^2} x^2 dx}{-2(3+v)(1-v)^3(x^4 - p_1^4)} = \frac{(1-v)^2}{4(3+v)(1-v)^3} (2 - \frac{\mu_-(p_1)}{p_1} - \frac{\mu_+(p_1)}{p_1}) \frac{\pi}{2} \tag{B-58}$$

The second term can be obtained using the same method as described above for the real part

of the force mobility and is given by:

$$\frac{\sqrt{2}}{2} \mathrm{Re}[(\beta - \alpha + (\beta + \alpha)i)f_2(p_2 e^{3\pi i/4})/\Lambda_2] + [\mu_+(p_1)f_2(ip_1) - \mu_-(p_1)f_2(p_1)]/2\Lambda_1 \tag{B-59}$$

Where $f_2(z) \equiv [1 - (1-v)^2 p_2^4]z^2 + 2(1-v)z^4$ \tag{B-60}

It is noted that p_2 satisfies the following expression

$$[-(3+v)(1-v)^3(-p_2^4)^2 + 2((1-3v)(1-v)(-p_2^4)) + 1] = 0 \quad (\text{see Eq.(B-15)}) \tag{B-61}$$

From Eq. (B-61) we have one of the following two relationships:

$$[1 - (1-v)^2 p_2^4](\beta + \alpha) = 2(1-v)p_2^2(\beta - \alpha) \tag{B-62}$$

$$[1 - (1-v)^2 p_2^4](\beta - \alpha) = -2(1-v)p^2(\alpha + \beta) \tag{B-63}$$

For the case $0 \le v \le 0.5$, $(1 - (1-v)^2 p_2^4) > 0$ while $2(1-v)p_2^2 > 0$ and $\alpha + \beta > 0$, $\beta - \alpha > 0$

so only relationship (B-62) is correct. Hence, the first term of Eq. (B-59) is zero. The

remaining second term of Eq. (B-59) together with Eq. (B-58) are substituted into (B-57), and the resulting expression into Eq.(B-6) to give:

$$\text{Re}(y_{\Omega_m M_n}) = \frac{\mu_+(p_1)f_2(ip_1) - \mu_-(p_1)f_2(p_1)}{2\Lambda_1} + \frac{(1-v)^2}{4(3+v)(1-v)^3}(2 - \frac{\mu_-(p_1)}{p_1} - \frac{\mu_+(p_1)}{p_1}) + 2p_1^2\frac{1}{\gamma}$$

(B-64)

Again, the mobility at an edge varies from the infinite plate value by a closed form function of Poisson's ratio.

e. Proof of $\text{Re}(y_{\Omega_n M_n}) = \text{Re}(y_{\Omega_l M_l})$

We proceed by taking the difference between Eq.s (B-6) and (B-8):

$$\text{Re}(y_{\Omega_l M_l}) - \text{Re}(y_{\Omega_n M_n}) = \frac{2}{\pi}\int_0^1 \frac{\mu_1(x)(M_-^2(x) - 4(1-v)x^4)dx}{Det(x)} + 2\mu_-(p_1)\mu_+(p_1)\frac{1}{\gamma} - 2p_1^2\frac{1}{\gamma}$$

(B-65)

the first term of Eq. (B-65) is :

$$\frac{\sqrt{2}}{2}\text{Re}[(\beta - \alpha + (\beta + \alpha)i)f_3(p_2 e^{3\pi i/4})/\Lambda_2] + [\mu_+(p_1)f_3(ip_1) - \mu_-(p_1)f_3(p_1)]/2\Lambda_1 \quad (B-66)$$

where $f_3(z) = [1 - (1-v)z^2]^2 - 4(1-v)z^4$ (B-67)

Inserting (B-67) into (B-66) then into (B-65) and using the formulation (B-18) for $1/\gamma$, only one term remains:

$$\frac{\sqrt{2}}{2}\text{Re}[(\beta - \alpha) + (\beta + \alpha)i)f_3(p_2 e^{3\pi i/4})/\Lambda_2] \quad (B-68)$$

We now prove that this remaining term is zero. Evaluating Eq. (B-68) gives:

$$\frac{\sqrt{2}}{2}\operatorname{Re}\left((\beta-\alpha)+(\beta+\alpha)i)(1+i(1-v)p_2{}^2)^2+4(1-v)p_2{}^4\right)/\Lambda_2$$

$$=\frac{\sqrt{2}}{2}(\beta-\alpha)[1-(1-v)^2 p_2{}^4-2\frac{(\beta+\alpha)}{(\beta-\alpha)}(1-v)p_2{}^2+4(1-v)p_2{}^4]/\Lambda_2 \qquad (B-69)$$

Using Eq. (B-62) and rearranging, the numerator of Eq.(B- 69) is rewritten:

$$\frac{\sqrt{2}}{2}\frac{(\beta-\alpha)}{1-(1-v)^2 p_2{}^4}[-(3+v)(1-v)^3(-p_2{}^4)^2+2((1-3v)(1-v)(-p_2{}^4)+1]=0 \qquad (B-70)$$

Note that Eq. (B-61) is used again. The results follows:

$$\operatorname{Re}(y_{\Omega_n M_n})=\operatorname{Re}(y_{\Omega_t M_t}) \qquad (B-71)$$

This proves that the real parts of the normal and tangential moment mobility are equal. This would be expected for an infinite plate because of circular symmetry but why it should be so for an edge-excited plate is not clear. It should be noted that the imaginary parts of the normal and tangential mobility are not identical (proof not given), even though they both numerically tend to infinity.

B.4 Comparison of exact value with published numerical values

Point mobilities have been evaluated from Eq.s (B-29) (B-56) (B-64) and (B-71), and are compared with Kauffmann's numerical values in Table 1.

Table I Comparison of point mobility for edge-excited semi-infinite plates, $v=0.3$

	Realpart	Imaginary part
	Kauffmann)/(this paper)	Kauffmann/this paper
$y_{\Omega_n M_n}$	0.21644 / 0.21645	∞/∞
$y_{\Omega_t M_t}$	0.21644 / 0.21645	∞/∞
$y_{V_z F_z}$	0.46196/0.46198	-5.97×10^{-7} / 0

It is seen that Kauffmann's numerical results agree closely with the exact values. According to Eq. (B-5) the force point mobility was given by

$$Y_{VF} = 8Y_{VF}^{\infty} y_{V_z F_z} = \sqrt{12}(m'' Eh^3)^{-1/2} \sqrt{1-v^2} y_{V_z F_z}] \tag{B-72}$$

Figure4. a shows the edge mobility normalized by the infinite plate mobility

$g = Y_{VF}/Y_{VF}^{\infty} = 8y_{V_z F_z}$ versus Poisson's ratio v. This curve corresponds to that from Figure 2 of reference[53] for $\gamma_1 = 1$, and the shapes of both curves are almost the same. The normalized mobility is a monotonically increasing function of the Poisson's ratio v, but the range of possible values is relatively narrow. The mobility at a free edge of a plate is therefore a factor of between 3.2 and 4.2 higher than that at an interal point far from any edges. The corresponding factor for a beam is 4.

FigureB-4.b shows the mobility normalized by $Y_0 = \sqrt{12}(m'' Eh^3)^{-1/2}$

$g_1 = \sqrt{1-v^2} y_{V_z F_z}$ versus Poisson's ratio v. It is seen to increase with the increase of Poisson's ration v.This is unexpected .because one would expect bending stiffness to increase with Poisson's ratio v, and hence mobility to decrease as for an infinite plate. Here the opposite is the case which is a result of using boundary conditions Eq. (B-2).
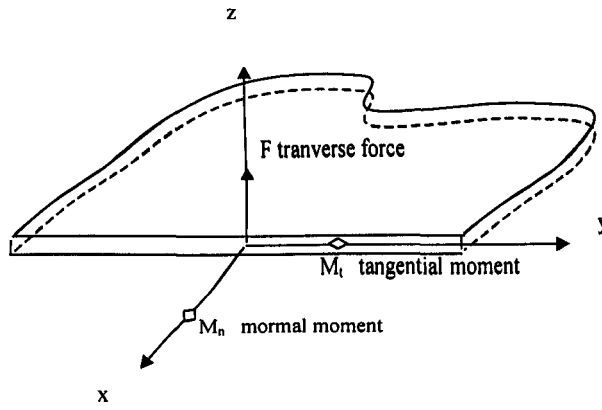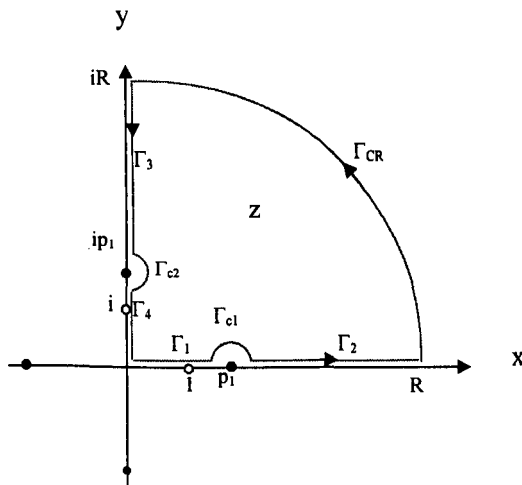
Figure B-1 Semi-infinite plate

Figure B-2 Contour of integration for evaluation of the imaginary part of the point force mobility
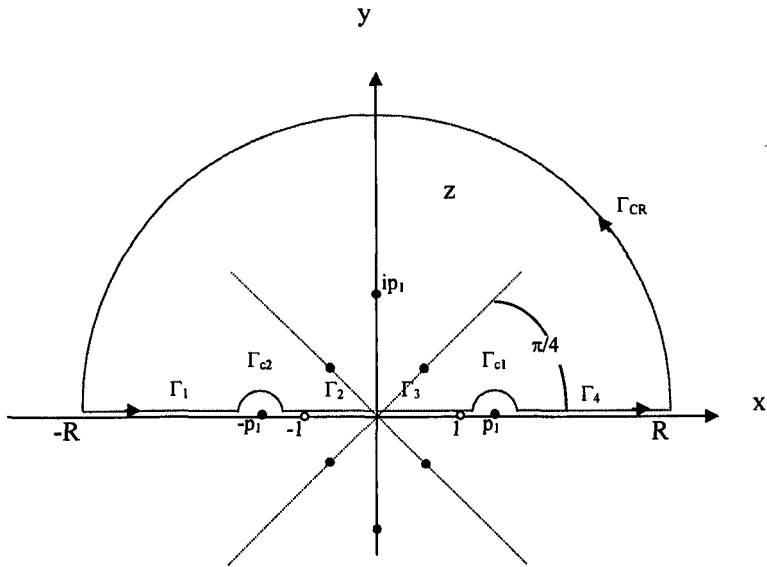
Figure B-3 Contour of integration for evaluation of the real part of the point force
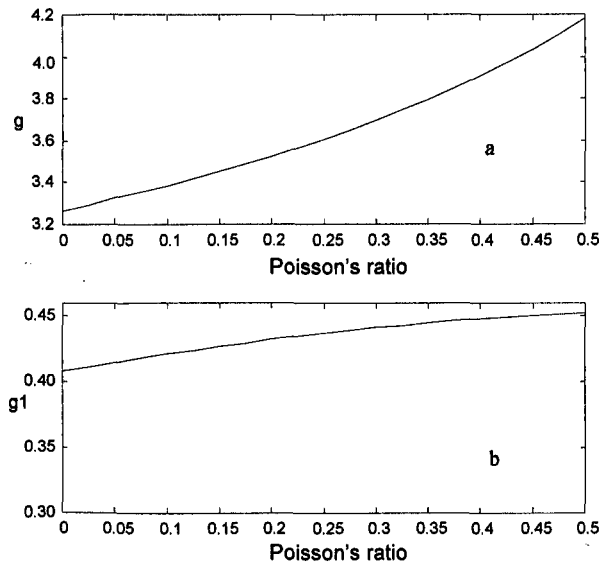
mobility

Figure B-4 The mobility normalised (a) by infinite plate (b)by Y_0